DEVELOPMENT OF THIN FILM COMPOSITE MEMBRANES FOR OSMOTICALLY DRIVEN MEMBRANE PROCESSES

by

Myoung Jun Park

A Thesis submitted in fulfilment for the degree of
Doctoral of Philosophy

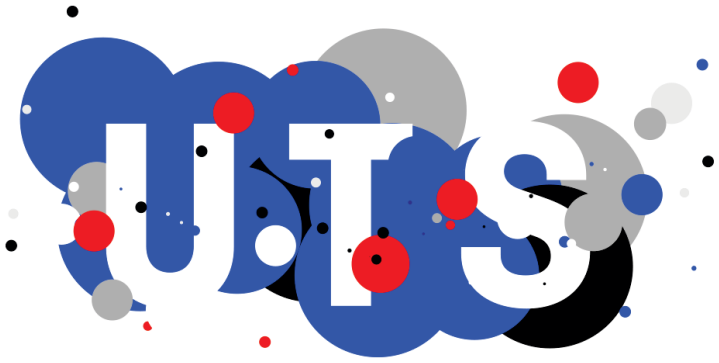

School of Civil and Environmental Engineering
Faculty of Engineering and Information Technology
University of Technology Sydney (UTS),
New South Wales, Australia

October 2018

CERTIFICATE OF AUTHORSHIP/ORIGINALITY

I certify that this thesis has not previously been submitted for a degree nor has it been submitted as part of requirements for a degree except as fully acknowledge within the text.

I also certify that the thesis has been written by me. Any help that I have received in my research work and the preparation of the thesis itself has been acknowledged. In addition, I certify that all information sources and literature used are indicated in the thesis.

Signature of candidate

Myoung Jun Park

Production Note:
Signature removed prior to publication.

ACKNOWLEDGMENTS

The success and final outcome of this thesis required a lot of guidance and assistance from many people and I am extremely fortunate to have got this all along the completion of my study.

I wish to express my deepest appreciation and gratitude to my principal supervisor Prof. Ho Kyong Shon and my co-supervisor Dr. Sherub Phuntsho, for their invaluable guidance and encouragement throughout the entire course of the PhD degree.

I would also like to extend my sincere appreciation to research staff, Dr. Leonard Tijing and Dr. Laura Chekli, and a laboratory manager Dr. Mohammed Johir for their great supports. Besides, I appreciate the assistance, cooperation and friendship of all the following colleagues and friends at UTS, Sungil Lim, Ralph Rolly Gonzales, Nawshad Akther, Van Huy Tran, Soleyman Sahebi, Yunchul Woo, Fouzy Lotfi, Syed Muztuza Ali, Federico Volpin, David Inhyuk Kim, Yunju Jo, Youngkwon Choi, Dr. Youngjin Kim, Minwei Yao, Ugyen Dorji, Nirenkumar Pathak, Pema Dorji, and Jiawei Ren.

I am extremely thankful to Dr. Grace M. Nisola, Prof. Wook-Jin Chung, and Prof. Hern Kim at Myongji University, South Korea, for their academic support and advise to accomplish this task. I would also like to thank Prof. Tao He and Prof. Xue-Mei Li at Shanghai Advanced Research Institute (SARI), and Prof. Tai-Shung (Neal) Chung at National University of Singapore (NUS), who gave me a chance to get training opportunity in membrane fabrications. The support extended by Dr. Gang Chen and Ms. Mengxi Zhang at SARI and Dr. Peng Na and Dr. Gang Han at NUS during my stay is also highly appreciated for their kind support and help.

I also want to acknowledge other external collaborators and advisors, Dr. Jihye Kim at K-water, Dr. Donghan Seo at CSIRO, Dr. Masafumi Shibuya and Prof. Hideto Matsuyama at Kobe University, and Prof. Ahmed Abdel-Wahab and Dr. Song Suk Han at Texas A&M University at Qatar.

Last but not the least, I would like to thank my family members, especially my mother Sunbun Kim, wife Jungeun Kim, father in law Seokdong Kim, mother in law Jaeim Woo, and others who did not mentioned here, for their constant encouragement and support during my PhD study.

JOURNAL ARTICLES PUBLISHED OR SUBMITTED**

1. *M. Shibuya†, **M. J. Park**†, S. Lim, S. Phuntsho, H. Matsuyama, H. K. Shon, Novel CA/PVDF nanofiber supports strategically designed via coaxial electrospinning for high performance thin-film composite forward osmosis membranes for desalination, *Desalination*, 445 (2018) 63-74
2. R. Gonzales, **M. J. Park**, L. Tijing, D. S. Han, S. Phuntsho, H.K. Shon, Modification of nanofiber support layer for thin film composite forward osmosis membranes via layer-by-layer polyelectrolyte deposition, *Membranes*, 8 (2018) 70
3. S. Lim, **M. J. Park**, S. Phuntsho, A. M-Prochnow, A. B. Murphy, D. Seo, H. K. Shon, Dual-layered nanocomposite membrane incorporating graphene oxide and halloysite nanotube for high osmotic power density and fouling resistance, *Journal of Membrane Science*, 564 (2018) 382-393
4. H. G. Zeweldi, L. A. Limjuco, A. P. Bendoy, H. -S. Kim, **M. J. Park**, H. K. Shon, E. M. Johnson, H. Lee, W. –J. Chung, G. M. Nisola, The potential of monocationic imidazolium-, phosphonium-, and ammonium- based hydrophilic ionic liquids as draw solutes for forward osmosis, *Desalination*, 444 (2018) 94-106
5. D. H. Seo, S. Pineda, Y. C. Woo, M. Xie, A. Murdock, E. Ang, Y. Jiao, **M. J. Park**, S. I. Lim, M. Lawn, F. Borghi, Z. J. Han, S. Gray, G. Millar, A. Du, H. K. Shon, T. Y. Ng, and K. Ostrikov, Anti-fouling graphene-based membranes for effective water desalination, *Nature communications*, 9 (2018) 683
6. ***M. J. Park**, R. R. Gonzales, A. Abdel-Wahab, S. Phuntsho, H. K. Shon, Hydrophilic polyvinyl alcohol coating on hydrophobic electrospun nanofiber membrane for high performance thin film composite forward osmosis membrane, *Desalination*, 426 (2018) 50-59
7. S. Lim, **M. J. Park**, S. Phuntsho, L. D. Tijing, G. M. Nisola, W. –G. Shim, W. –J. Chung, H. K. Shon, Dual-layered nanocomposite substrate membrane based on polysulfone/graphene oxide for mitigating internal concentration polarization in forward osmosis, *Polymer*, 110 (2017) 36-48
8. W. –J. Chung, R. E. C. Torrejos, **M. J. Park**, E. L. Vivas, L. A. Limjuco, C. P. Lawagon, K. J. Parohinog, S. –P. Lee, H. K. Shon, H. Kim, G. M. Nisola, Continuous lithium mining from aqueous resources by an adsorbent filter with a

3D polymeric nanofiber network infused with ion sieves, *Chemical Engineering Journal*, 309 (2017) 49-62

9. Y. C. Woo, L. D. Tijing, **M. J. Park**, M. Yao, J. –S. Choi, S. Lee, S. –H. Kim, K. –J. An, H. K. Shon, Electrospun dual-layer nonwoven membrane for desalination by air gap membrane distillation, *Desalination*, 403 (2017) 187-198
10. **M. J. Park**, G. M. Nisola, E. L. Vivas, L. A. Limjuco, C. P. Lawagon, J. G. Seo, H. Kim, H. K. Shon, W. –J. Chung, Mixed matrix nanofiber as a flow-through membrane adsorber for continuous Li^+ recovery from seawater, *Journal of Membrane Science*, 510 (2016) 141-154
11. J. Kim, **M. J. Park**, M. Park, H. K. Shon, S. –H. Kim, J. H. Kim, Influence of colloidal fouling on pressure retarded osmosis, *Desalination*, 389 (2016) 207-214
12. S. Sahebi, S. Phuntsho, Y. C. Woo, **M. J. Park**, L. D. Tijing, S. Hong, H. K. Shon, Effect of sulphonated polyethersulfone substrate for thin film composite forward osmosis membrane, *Desalination*, 389 (2016) 129-136
13. M. Zhang, R. Liu, Z. Wang, B. Zhao, J. Song, **M. J. Park**, H. K. Shon, X. –M. Li, T. He, Dehydration of forward osmosis membranes in treating high salinity wastewaters: Performance and implications, *Journal of Membrane Science*, 498 (2016) 365-373
14. ***M. J. Park**, S. Phuntsho, T. He, G. M. Nisola, L. D. Tijing, X. –M. Li, G. Chen, W. –J. Chung, H. K. Shon, Graphene oxide incorporated polysulfone substrate for the fabrication of flat-sheet thin-film composite forward osmosis membranes, *Journal of Membrane Science*, 493 (2015) 496-507
15. R. E. C. Torrejos, G. M. Nisola, **M. J. Park**, H. K. Shon, J. G. Seo, S. Koo, W. -J. Chung, Synthesis and characterization of multi-walled carbon nanotubes-supported dibenzo-14-crown-4 ether with proton ionizable carboxyl sidearm as Li+ adsorbents, *Chemical Engineering Journal*, 264 (2015) 89-98
16. G. M. Nisola, L. A. Limjuco, E. L. Vivas, C. P. Lawagon, **M. J. Park**, H. K. Shon, N. Mittal, I. W. Nah, H. Kim, W. -J. Chung, Macroporous flexible polyvinyl alcohol lithium adsorbent foam composite prepared via surfactant blending and cryo-desiccation, *Chemical Engineering Journal*, 280, (2015) 536-548

17. J. Kim, K. Jeong, **M. J. Park**, H. K. Shon, J. H. Kim, Recent Advances in Osmotic Energy Generation via Pressure-Retarded Osmosis (PRO): A Review, *Energies*, 9 (2015) 11821-11845

**Publications made during the PhD candidature including articles not entirely related to the Thesis. *Articles related to the Thesis.

CONFERENCE PAPERS AND PRESENTATIONS

1. Sungil Lim, **Myoung Jun Park**, Sherub Phuntsho, Ho kyong Shon, Preparation of dual-layered nanocomposite membranes using graphene oxide and halloysite nanotubes for enhancing membrane performance in osmotically driven processes, 2017 International Congress on Membranes and Membrane Processes (ICOM2017), 29 July – 4 August, 2017, San Francisco, USA
2. **Myoung Jun Park**, Sungil Lim, Sherub Phuntsho, and Ho Kyong Shon, Development of Pressure Retarded Osmosis (PRO) hollow fiber membrane modified with graphene oxide (GO), International Forward Osmosis Summit (IFOS), 2-4 December, 2016, University of Technology Sydney, Sydney, Australia
3. **Myoung Jun Park**, Sherub Phunstho, Ho Kyong Shon, Development of thin-film composite membranes modified by nanomaterials for forward osmosis, 2015 International Environmental Engineering Conference (IEEC2015), 28-30 October, 2015, Busan, South Korea
4. **Myoung Jun Park**, Sherub Phuntsho, Tao He, Grace M. Nisola, Leonard D. Tijing, Xue-Mei Li, Gang Chen, Wook-Jin Chung, Ho Kyong Shon, Graphene oxide incorporated polysulfone substrate for the fabrication of flat-sheet thin-film composite forward osmosis membranes, 2nd International Conference on Desalination using Membrane Technology, 26-29 July, 2015, Singapore, ***Awarded the best poster presentation***

Presentations made during the Ph.D. candidature including oral and poster presentations.

LIST OF ABBREVIATIONS

APTMS	Aminopropyltrimethoxy silane
FTIR	Fourier transform infrared spectroscopy
BDSA	Benzidinedisulfonic acid
BTEC	Biphenyl tetra-acyl chloride
CA	Cellulose acetate
CAB	Cellulose acetate butyrate
CAIP	Co-solvent assisted IP
CAP	Cellulose acetate propionate
CECP	Cake-enhanced concentration polarization
CNT_S	carbon nanotubes
CP	Concentration polarization
CTA	Cellulose triacetate
DAT	Diaminotoluene
DFBP	Difluorobenzophenone
DI	Deionised
DI water	Deionized water
DMAc	*N,N*-Dimethylacetamide
DMAPS	Dimethyl-(3-sulfopropyl)ammonium hydroxide
DMSO	Dimethyl sulfone
DS	Draw solution
ECP	External concentration polarisation
ED	Electrodialysis
FE-SEM	field emission scanning electron microscope
FO	Forward osmosis
FS	Feed solution
GO	Graphene oxide
GOTMS	3-glycidyloxypropyltrimethoxysilane
HF	Hollow fiber
HTI	Hydration technology innovations
ICP	Internal concentration polarisation
ID	Inner diameter
IP	Interfacial polymerization
IPC	Isophthaloyl chloride
LbL	Layer-by-layer
MEL	Metacryloyloxyethyl lipoate
MF	Microfiltration
MOF	Metal-organic frameworks
MPC	methacryloyloxyethyl phosphorylcholine
MPD	*m*-phenylenediamine
MW	Molecular weight
NIPS	Non-solvent induced phase separation
OD	Outer diameter
PA	Polyamide
PAA	Polyacrylic acid
PAI	Polyamide-imide
PAN	Polyacrylonitrile

PAO	Pressure assisted osmosis
PBI	Polybenzimidazole
Pei	Polyetherimide
PEI	Polyethyleneimine
Pei	Polyetherimide
PES	Polyethersulfone
PET	Polyethylene terephthalate
PIP	Piperazine
POSS	Polyhedral oligomeric silsesquioxane
PPD	*p*-phenylenediamine
PPO	Poly(phenylene oxide)
PPSU	polyphenylsulfone
PRO	Pressure retarded osmosis
PSf	Polysulfone
PSS	Polystyrene sulfonate sodium
PVA	Polyvinyl alcohol
PVDF	Polyvinylidene fluoride
PVP	polyvinylpyrrolidone
rGO	Reduced graphene oxide
RO	Reverse osmosis
RSF	Reverse solute flux
sDCDPS	3,3'-di-sodiumdisulfate-4,4'-dichlorphenyl sulfone
SDS	Sodium dodecyl sulfate
SPEK	Sulfonated poly(ether ketone)
sPPSU	Sulfonated polyphenylenesulfone
SRSF	Specific reverse solute flux
TEOS	Tetraethylorthosilicate
TFC	Thin-film composite
TFN	thin film nanocomposite
TMC	Trimesoyl chloride
TPC	Terephthaloyl chloride
UF	Ultrafiltration
XPS	X-ray photoelectron spectroscopy

LIST OF SYMBOLS

A	Pure water permeability coefficient (L m^{-2} h^{-1} bar^{-1} or LMH/bar)
B	Salt permeability coefficient (ms^{-1})
C	Molar solute concentration (Moles or M)
D	Solute diffusivity (m^2s^{-1})
d_h	Hydraulic diameter (m)
J_s	Reverse salt flux (g m^{-2} h^{-1} or mmoles m^{-2} h^{-1} or gMH)
J_v *or* J_w	Water flux (L m^{-2} h^{-1} or LMH)
k	Mass transfer coefficient
K	Solute resistivity (sm^{-1})
L	Length of channel (m)
M	Molar concentration of the solution (Moles or M)
M_w	Molecular weight (Mole/g)
P	Applied pressure (bar)
Re	Reynolds number
R	Salt rejection (%)
Sc	Schmidt number
Sh	Sherwood number
π	Osmotic pressure (bar)
S	Structural parameter (M)
X_A	Mole fraction of the solvent (Moles or M)
$\Delta\mu^*_A$	Chemical potential of the pure solvent
$\Delta\mu_A$	Chemical potential of the solvent in solution
n	Amount of solute molecules
V_m	Volume of the solvent (L or ml)
T	Temperature (°C)
n	Amount of solute molecules
R	Ideal gas constant (L atm mol^{-1} $K^{-1)}$
i	Van't Hoff factor
C_s	Solute concentration (Moles or M)
R_s	Salt rejection coefficient (%)
C_f	Feed solute concentrations (Moles or M)
C_d	Draw solute concentrations (Moles or M)
x or t_s	Thickness (m)
τ	Tortuosity
φ or ε	Porosity
σ	Reflection coefficient
S_m	Effective membrane surface area
$\pi_{D,b}$	Osmotic pressures of the bulk draw solution (bar)
$\pi_{F,m}$	Osmotic pressures of the bulk feed solution (bar)
R_a	Mean roughness (μm)
R_{ms}	Root mean square of z values (μm)
R_{max}	Maximum vertical distance between the highest data points (μm)
d_p	Solute diameter (m)
μ_p	Mean effective pore size (nm)
σ_p	Geometric standard deviation

TABLE CONTENTS

LIST OF TABLES

LIST OF FIGURES

ABSTRACT

Rapid population growth and continuous economic development have resulted in a significant increase in the demand and accessibility of clean water energy resources. To solve these issues, osmotically driven processes including forward osmosis (FO) and pressure retarded osmosis (PRO) are hold some of the greatest potential in providing sustainable solutions for the global needs of both clean water and clean energy. Basically, both FO and PRO processes utilize feed solution (FS) with low salt concentration and draw solution (DS) with high salt concentration, which can drive the high osmotic pressure difference through the semi-permeable membrane to extract clean water and to produce clean energy. However, due to the poor membrane performances of commercially available membranes, properly designed high performance FO and PRO membranes need to be developed for viable applications.

Polymeric membranes for FO and PRO processes can be fabricated through a variety of methods, which include phase inversion, electrospinning, and hollow fiber spinning. FO and PRO membranes are typically made of a thin film composite (TFC). TFC membranes have a porous membrane support layer which facilitates convenient water transport while a thin active layer (i.e. polyamide) is responsible for high salt rejection. Due to their higher water permeability and lower reverse solute permeability as compared to the commercial cellulose triacetate (CTA, Hydration Technology Innovations, Inc. USA), in this study, development of high performance TFC membranes have been subjected to modifying membrane support layers using various fabrication techniques and approaches including physical and chemical modifications.

TFC-FO and -PRO membranes were newly designed and fabricated by incorporating hydrophilic graphene oxide (GO) nanomaterials into membrane support layer for improved membrane performance. In the case of TFC-FO membrane development, different amounts of GO nanosheets were incorporated in the polysulfone (PSf) to obtain PSf/GO composite flat-sheet membrane supports via a phase separation technique. Results reveal that at an optimal amount of GO addition, a PSf/GO composite support layer with favourable structural property measured in terms of thickness, porosity and pore size can be achieved due to the effect of hydrophilic GO. The optimum incorporation of GO in the PSf support layer not only significantly improved water permeability but

also allowed effective polyamide (PA) layer formation, by comparison to that of a pure PSf support layer which had much lower water permeability. Thus, a TFC-FO membrane with high water flux (19.77 LMH against 6.08 LMH for pure PSf) and reverse flux selectivity (5.75 Lg^{-1} against 3.36 Lg^{-1} for pure PSf) was obtained under the active layer facing the feed solution (AL-FS). Besides the improved structural properties (reduced structural parameter, *S*) of the support layer, enhanced support hydrophilicity also contributed to the improved water permeability of the membrane. Therefore, the GO modification of membrane supports for TFC-FO membranes showed a promising technique to improve the FO performance.

With the similar concept and perspectives of the GO effect on FO membrane performance, TFC-PRO hollow fiber membranes were also fabricated with incorporating GO into the hollow fiber membrane supports via a hollow fiber spinning device. Polyethersulfone (PES) was selected as membrane material due to its good chemical resistance, high mechanical properties, and easy in membrane fabrication. The hollow fiber membrane, fabricated by incorporation with small amounts of GO into the PES support layer, revealed the improvement in membrane porosity, hydrophilicity and pure water permeability without compromising mechanical properties when compared to the pure PES support layer. Therefore, the TFC hollow fiber PES/GO membrane showed significantly high PRO flux while maintaining the low reverse salt flux (*RSF*) at higher hydraulic pressures, resulting in high power density of 14.6 W m^{-2} at the highest applied pressure of 16.5 bar. Experimental results showed that optimum concentration of GO can be adapted as a filler of hollow fiber membranes for the TFC-PRO membrane for enhancing PRO performance without hampering its mechanical properties.

Fabrication of electrospun nanofiber support membranes for TFC-FO membrane via the electrospinning technique have drawn attention in recent years due to their high porosity, interconnected pore structure, high strength to weight ratio, low tortuosity, and ease in controlling membrane thickness (deposition time by electrospinning). Therefore, a novel electrospun nanofiber support for a high performance TFC-FO membrane was fabricated via coaxial electrospinning. This method produces a dual layer core/sheath polyvinylidene fluoride (PVDF)/cellulose acetate (CA) composite nanofiber support, prior to interfacial polymerization (IP) to produce the selective PA layer. The electrospun

nanofiber support was expected to exhibit hydrophilicity at the sheath side due to CA, and mechanical stability at the core side due to PVDF, both of which properties are preferred for TFC-FO membranes. The physical and morphological properties of composite TFC-FO membranes were characterized and the membrane performance was evaluated during FO tests, and compared with single CA, single PVDF and blend (CA/PVDF) nanofiber membranes. The composite CA/PVDF support prepared via coaxial electrospinning showed marked significant improvement in hydrophilicity due to the presence of CA on the sheath side of nanofibers, while PVDF at the core side of nanofibers retained the mechanical strength comparable to the pure PVDF nanofiber support. In the FO test result using 0.5 M NaCl as a draw solution and DI water as a feed solution, the composite CA/PVDF TFC-FO membrane achieved high FO flux (31.2 LMH) and remarkably low specific reverse salt flux (*SRSF*, 0.03 g/L) with a low structural parameter (190 μm).

In spite of many advantageous characteristics of nanofiber supports for an FO membrane, there is a membrane swelling issue with nanofiber support fabricated by hydrophilic polymers which weaken the mechanical properties since they are wetted in liquids. In addition, although it was found that the FO performance improved with composite CA/PVDF nanofiber substrate, overall mechanical properties of FO membrane supports which, when prepared by electrospinning, still seem to be one of the major obstacles for practical applications. To overcome these issues, mechanically stable hydrophobic PVDF nanofiber support was treated by heat press near the melting point (170°C) of PVDF and then hydrophilic polyvinyl alcohol (PVA) was utilized to improve the hydrophilicity as well as mechanical strength for TFC-FO membranes. The PVDF nanofiber support was modified with PVA via dip coating and acid-catalyzed crosslinking with glutaraldehyde (GA) prior to the formation of the PA active layer on the support via IP. The influence of PVA modification on the morphology and physical properties of PVDF support was evaluated through several characterization techniques while the flux performance was assessed using a lab-scale FO membrane unit. The fabricated PVA-modified TFC FO membranes exhibited high hydrophilicity, porosity, and mechanical strength, therefore resulting in excellent FO performance (24.8 LMH using 0.5 M NaCl and DI water as draw and feed solution, respectively). Dip coating of the nanofiber support in PVA is therefore a simple and effective method for the improvement of PVDF support with high

mechanical properties as well as hydrophilicity to fabricate high performance TFC FO membranes.

In this study, high performance engineered osmosis membranes were successfully developed through the membrane substrate modifications either by GO incorporation or hydrophilic surface modifications. Membrane substrates incorporated with small loadings of GO (≤ 0.25 wt%) exhibited significantly improved membrane performance for both FO and PRO applications via enhanced hydrophilicity and membrane porosity without deterioration of mechanical properties. For further improvement of FO flux, porous and a low tortuous electrospun nanofiber supports were used as FO membrane supports and additionally modified the nanofibers via coaxial electrospinning or hydrophilic PVA dip-coating for having both hydrophilic and mechanically stable properties. Therefore, a hydrophilic modification of membrane substrates without consideration of type of substrates for engineered osmosis has high potential to improve the membrane performance.

CHAPTER 1

INTRODUCTION

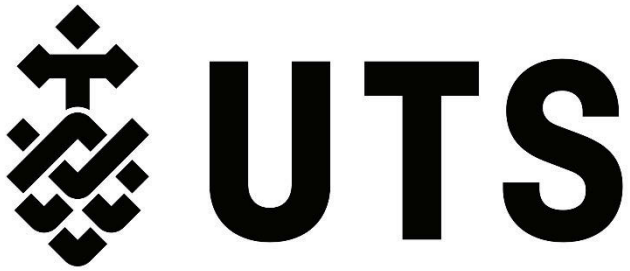

1.1. Introduction

Increasing water and energy demands have become serious problems globally due to rapid population growth and economic development (Cath et al. 2005, Chung et al. 2012a, Chung et al. 2012b, Geise et al. 2010b, Holloway et al. 2007b, Shannon et al. 2008b). Therefore, exploring new environment-friendly technologies and processes to resolve these emerging problems is an essential requirement. Osmotically driven processes including forward osmosis (FO) and pressure retarded osmosis (PRO), are emerging technologies in recent years and it is expected that these might provide sustainable solutions for the global demands of both clean water and energy.

Seawater desalination is one of the most promising solutions to supply alternative clean and drinking water resources (Chung et al. 2012b, Geise et al. 2010b, Shannon et al. 2008b). The reverse osmosis (RO) process is the most common membrane-based separation process for seawater desalination; however, RO technology faces major challenges due to its high energy cost and frequent membrane scaling and fouling problems (Greenlee et al. 2009). Unlike the typical membrane processes utilizing hydraulic pressure for separation to obtain clean water such as the RO process, FO is an osmotically driven process. This process utilizes a feed solution (FS) with low salt concentration and draw solution (DS) with high salt concentration, which can then drive a high osmotic pressure difference through a semi-permeable membrane which extracts fresh water from FS to DS. Therefore, FO requires low energy in operating a hydraulic pump with high pressure to allow water to pass throughout the semi-permeable membrane, making it highly beneficial in terms of energy consumption, as compared to the RO process. Therefore, FO can be utilized for various applications including desalination (Chung et al. 2012a), wastewater treatment (Cath et al. 2005, Holloway et al. 2007a), osmotic power generation (Achilli et al. 2010, Chung et al. 2012b, She et al. 2012, Yip et al. 2011b), pharmaceutical industry (Yang et al. 2009b), direct irrigation (Kim et al. 2013a) and food processing (Garcia-Castello et al. 2011). However, there are still several problems with the FO process for viable application in various fields, such as poor membrane performance (i.e. water flux and salt selectivity) and ease of recovery of DS, for viable application in various fields (Chekli et al. 2016). It is therefore imperative for high performance FO membranes to be further developed.

Current research has focused on developing thin film composite (TFC) FO membranes, which exhibit higher water permeability and lower reverse solute permeability, especially when compared to the commercially available cellulose triacetate (CTA) FO membranes (Hydration Technology Innovations Inc., HTI Co., USA) (Puguan et al. 2014, Wei et al. 2011). A TFC-FO membrane is typically composed of a (1) thin active layer (i.e. polyamide) responsible for high salt rejection, and (2) subjacent porous structure as a mechanical support layer, for convenient water transport (Bui et al. 2011, Bui et al. 2013b, Emadzadeh et al. 2014c, Han et al. 2012c, Wang et al. 2015, Wei et al. 2011, Widjojo et al. 2013). Considering these TFC membrane components, a more industrially-viable FO system can be attained by further improving the membrane capacity. One way to achieve this is through structural manipulation of the support layer. The traditional TFC membranes are usually fabricated with the porous membrane supports prepared via a phase separation technique for flat-sheet or hollow fiber membranes, and the PA active layer is deposited on the surface of membrane supports by the interfacial polymerization (IP) process (Alsvik et al. 2013b). For the development of desired TFC-FO membranes, membrane supports should have highly porous structure and hydrophilic property for easier and faster water permeability, but should also be mechanically stable and selective with the PA active layer (Bui et al. 2011, Bui et al. 2013b, Emadzadeh et al. 2014c, Han et al. 2012c, Wang et al. 2015, Wei et al. 2011, Widjojo et al. 2013). One of the main issues in the FO process is severe internal concentration polarization (ICP) occurring in membrane support layers, which effectively reduces the FO flux. ICP is mainly due to the thick and dense support structures, poor porosity, and hydrophobicity of the support layer. Thus, it is necessary to design the support layer of the TFC-FO membrane carefully for high porosity, hydrophilic property and low tortuosity to mitigate ICP and improve the FO performance.

A number of recent studies have focused on developing FO membranes with various approaches to designing the membrane support layer to obtain the desirable structure, as well as the physical and chemical properties. Some studies focused on modifying the membrane support layer for the TFC-FO membrane via incorporating hydrophilic nanomaterials such as graphene oxide (Lim et al. 2017), titanium dioxide (TiO_2) (Emadzadeh et al. 2014c), silica nanoparticles (Bui et al. 2016, Obaid et al. 2016a, Tian

et al. 2017), porous zeolite nanoparticles (Ma et al. 2013) and metal-organic frameworks (Lee et al. 2015a) into the membrane support, resulting in reducing ICP in the FO process with low membrane structural parameters (S) (Bui et al. 2013b, Han et al. 2012a, Huang et al. 2014, Puguan et al. 2014, Tian et al. 2014b, Yasukawa et al. 2015a). Other studies improved the FO performance fabricating FO membrane supports using hydrophilic polymers such as sulfonated polysulfone (Sahebi et al. 2016, Widjojo et al. 2011b), hydrophilic cellulose acetate propionate (Li et al. 2012b), sulfonated polyether ketone (Han et al. 2012a), and polyketone (Shibuya et al. 2017, Yasukawa et al. 2015a). These studies show that the membrane fabrication and modification with hydrophilic materials for TFC-FO membranes are promising approaches to improve the FO performance.

Meanwhile, PRO uses similar physical principles and process components compared to FO, however it is very different from an application perspective. (Klaysom et al. 2013a). Similarly with FO, PRO also utilizes the osmotic pressure difference between two solutions of different salinity, but FS faces the membrane support layer while DS faces the membrane active layer (PRO mode), which is opposite to that of FO mode (active layer facing FS and support layer facing DS). PRO facilitates the conversion of osmotic pressure difference to hydraulic pressure, hence enabling the generation of electric power when releasing the hydraulic pressure through a turbine or other devices (Achilli et al. 2010). Although the theoretical concept of harnessing the energy by the mixing of low-saline and high-saline water first was discovered in the early 1950s, the specific mechanism was proposed by Loeb in the 1970s. Based on recent advances in the technological and economic improvement of membrane technologies, PRO has re-emerged as a potentially viable energy option, and lab-scale to pilot-scale demonstrations have actively been conducted. For example, the first PRO pilot plant was constructed by Statkraft in Norway in 2009, and since then several PRO and PRO-hybrid pilot plants have been built or are under construction (Skilhagen et al. 2008). However, despite this increasing attention and the rapid advancements of the PRO process, several challenges remained for PRO commercialisation, such as the lack of suitable membranes for the PRO process, among others.

In recent years, many studies have been focused on developing high performance PRO membranes for viable application. PRO membranes have very similar characteristics with FO membranes, requiring high water flux, low concentration polarization (CP) in the

support layer, high porosity, hydrophilicity, thin film selective layer, and low *S* value. However, PRO membrane additionally requires high mechanical properties which will allow it to withstand high hydraulic pressures during the PRO operation (Zhang et al. 2014). For the fabrication of high performance PRO membranes, in the previous studies, various types of membrane support for TFC-PRO membranes were introduced such as electrospun nanofiber membrane (Song et al. 2013, Tian et al. 2015a), flat-sheet membrane (Han et al. 2013c, Yip et al. 2011b) and hollow fiber membrane (Chou et al. 2013, Han et al. 2013b, Zhang et al. 2014). These studies have successfully prepared and developed PRO membranes which achieved high power density (W m^{-2}).

1.2. Research motivation

Since the osmotically driven processes including FO and PRO are emerging technologies with high potential for real application and eco-friendliness, there is a higher demand for more suitable membranes with high performance developed for specific applications. However, the currently available commercial HTI CTA membrane exhibits low water permeability and high reverse salt flux, which are unfavourable for FO and PRO applications. One of the most heavily considered factors affecting membrane performance is ICP occurring within the membrane support layers, which decreases the effective osmotic pressure gradient across the membrane between FS and DS. As a result, the water flux dramatically decreases due to dilutive ICP for FO and concentrative ICP for PRO. The severe ICP for FO and PRO is usually observed in the membrane support layers with poor membrane porosity, high thickness and hydrophobic property, which consequently reduces the solute diffusivity in the support layer. Hence, both FO and PRO membranes are required to have thin membrane support layers with high porosity and hydrophilicity.

Many studies have recently focused on developing TFC membranes for the osmotically driven process because TFC membranes can be specifically designed and optimized separately for each thin-film PA layer as an active layer with high selectivity and of porous, mechanically stable and hydrophilic substrate as a support layer with a low S value. The design of the membrane support layer for high performance TFC membranes is one of the most important parameters in FO and PRO membranes development.

Therefore, the studies have focused on developing and modifying membrane substrates of TFC membranes via various approaches to improve the performances required to achieve the aims of viable application of FO and PRO.

1.3. Objectives and the research scope

For wide and practical applications of osmotically driven membranes, the studies have focused on developing high performance TFC membranes. In recent years, TFC membranes for FO and PRO were developed and commercialized by several companies and these were mostly fabricated using typical polysulfone or polyethersulfone polymeric membrane supports via phase separation techniques. Although their membranes showed much higher membrane performance when compared to a HTI-CTA membrane which is composed of single polymeric material, high performance TFC membranes seem to remain developed in terms of water flux and salt selectivity for wider applications. For example, FO membranes for desalination require high salt selectivity to obtain high quality of pure water. The main objective of this study is therefore to develop novel TFC membranes not only with high water flux but also with high salt selectivity. To achieve these goals, the membrane supports were prepared and modified using various approaches with new ideas thus the new membrane fabrication technique can provide a tip for industrial applications. In addition, the fabricated membranes will be thoroughly investigated and characterized using various tools to academically understand the effect of membrane modifications. The following are the specific objectives of this particular study:

- Investigate the effect of hydrophilic nanomaterials as a filler of membrane substrates for TFC-FO membranes to improve FO performance.
- Develop TFC-PRO hollow fiber membranes with mechanically stable and high PRO performance via incorporating hydrophilic nanomaterials in hollow fiber membrane supports.
- Improve the FO performance by designing a new type of electrospun nanofiber support for TFC-FO membrane via coaxial electrospinning to simultaneously produce a dual-layer core/sheath hydrophobic-hydrophilic composite nanofiber support.

- Modify the hydrophobic nanofiber support for TFC-FO membrane via dip-coating of hydrophilic polymers and its crosslinking to enhance hydrophilicity and mechanical properties of the membrane.

1.4. Structure of the Study

The outline of the thesis which consists of eight chapters is as follows:

Chapter 1 as an introduction chapter includes the background, research motivation and objectives of the study.

Chapter 2 provides a comprehensive review on the current state of osmotically driven membrane fabrications and its applications. Chapter 3 presents the brief experimental methods in membrane preparation, and characterization and evaluation of membrane performance. However, more specific information can be found in their respective chapters.

Hydrophilic graphene oxide incorporated in polysulfone substrate for TFC-FO membranes prepared via a phase inversion to enhance the FO performance is introduced in Chapter 4.

Chapter 5 investigates the effect of graphene oxide addition in hollow fiber support membranes for improvement of PRO performance in terms of mechanical stability, salt selectivity and water flux.

Chapter 6 presents the novel approach to design the cellulose acetate/polyvinylidene fluoride dual-layered composite nanofiber membrane via coaxial electrospinning as a support layer of the TFC-FO membrane.

Chapter 7 presents the high performance TFC-FO membrane prepared via hydrophilic polyvinyl alcohol coating on hydrophobic electrospun nanofiber substrate.

Conclusions obtained from this study and recommendations for future studies are presented in Chapter 8.

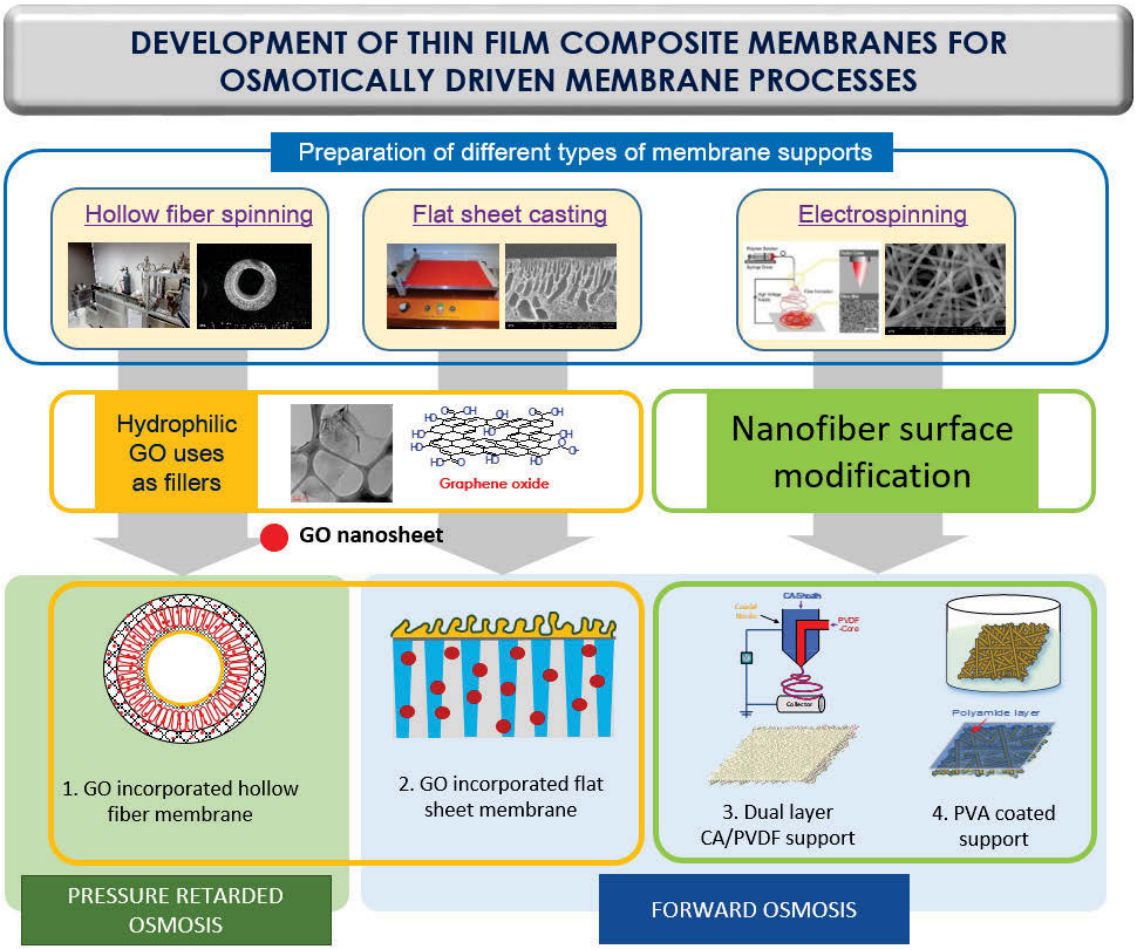

Figure 1 - 1. Schematic diagram of the study.

CHAPTER 2

LITERATURE REVIEW

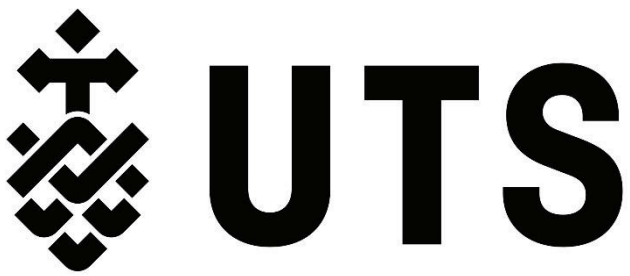

2.1. Introduction

Exponential world population growth and rapid economic development have significantly increased the demand for accessible clean water (Shannon et al. 2008a). In order to address the water scarcity crisis, water conservation, water infrastructure development, and water distribution improvements are undertaken in scientific research and implemented by government units. In addition, wastewater reuse and seawater desalination are mostly practised to provide a fresh and clean water supply. There is an immensely urgent need to find sustainable and efficient solutions to water scarcity. Specifically, in arid regions thermal desalination of seawater is carried out due to the lack of freshwater resources. Due to the expensive cost of thermal desalination processes, other processes have been exploited, especially in the field of filtration and membrane.

During the last 50 years, membrane has been an integral part of scientific research, especially in the field of water resources and water reuse. Membrane technology is a widely accepted field in production of potable water quality from various sources: surface runoff, aquifers, brackish, and seawater. It is widely used in industrial processes, as well as in municipal wastewater treatment (Nicolaisen 2003). Membrane technology has evolved consistently throughout the years, making it highly possible to manage all the water resources, particularly in areas where water scarcity is a huge problem. As research and industrial applications on membranes have thrived, advanced materials and methods have also increased, making membrane technology a continuously evolving field of study. New membranes with better chemical and thermal stability and transport properties are continuously being prepared and developed for the improvement of current technology and the potential use of membrane technology in many other applications.

Membrane processes are mostly utilised in any of the following main areas: separation of substances, controlled release, energy storage, and membrane reactors. This chapter, however, focuses entirely on water separation. Membranes have been widely used for water technology, specifically purification and desalination, to obtain clean, usable, and/or drinkable water. Membranes are primarily characterized according to their mechanical, chemical, and thermal stability, as wells as selectivity and permeability (Strathmann 2001). It is highly important to consider the propensity of the membrane to fouling, compatibility with the environment, ease of preparation, and cost.

This chapter provides a brief introduction to the following: current water treatment technologies, engineered osmosis, membrane materials, and fabrication techniques. Fundamental aspects of water treatment technologies, membranes, membrane technology, and engineered osmosis will be further explained, as the potential and further research developments in these fields are enumerated and assessed.

2.2. Current technologies for water treatment

Currently, technologies for water treatment should be able to remove salts or impurities from the source water, without the expenditure of excessive amounts of energy and resources. These efficient separation and water purification processes by membrane technology can be categorized as follows: 1) microfiltration (Alzahrani et al. 2014), 2) ultrafiltration (Wolf et al. 2005), 3) nanofiltration (Elimelech et al. 2011), 4) membrane distillation (Tijing et al. 2014), 5) capacitive deionization (Oren 2008), 6) electrodialysis (Banasiak et al. 2007), 7) pervaporation (Yan et al. 2015a), and 8) engineered osmosis (Chanukya et al. 2013).

The driving force of most membrane processes is the difference in the properties of the system components. Gradients in chemical potential, electrical potential, and pressure are able to drive the transport of ions and molecules across membranes (Strathmann 2001). Transport modes can be any of the following: convection, diffusion, or migration, as shown in Table 2.1. For all membrane-based processes, the permeability of any component is a function of its concentration and mobility through the membrane.

Table 2 - 1. Driving forces and transport modes of selected membrane processes (Strathmann 2001).

Process	Driving force	Transport mode
Microfiltration	Pressure difference	Convection
Nanofiltration	Pressure difference	Convection
Dialysis	Concentration difference	Diffusion
Gas separation	Pressure difference	Diffusion
Pervaporation	Pressure difference	Diffusion
Electrodialysis	Electrical potential difference	Migration
Engineered osmosis	Pressure/chemical potential difference	Diffusion

2.3. Engineered osmosis

Osmosis is the transport of water from a region of lower solute (feed solution) to a region with higher solute concentration (draw solution) through a selectively permeable membrane (Chung et al. 2012a). The selectively permeable membrane should be able to allow water to pass through and reject most solute molecules or ions. The main driving force of osmosis is the osmotic pressure (π) difference between the two solutions, allowing the natural movement of water from the region with higher water chemical potential to the one with less. The chemical potential of the pure solvent ($\Delta\mu^*_A$) is equal to the chemical potential of the solvent in solution ($\Delta\mu_A$) in equilibrium (Alsvik et al. 2013a), as given by Eq. 2-1:

$$\mu_A^*(P) = \mu_A(X_A P + \pi) \tag{2-1}$$

where X_A, P, and π are the mole fraction of the solvent, applied force, and osmotic pressure, respectively.

Water transport in engineered osmosis is described by Eq. 2-2:

$$J_w = A(\sigma\Delta\pi - \Delta P) \tag{2-2}$$

where J_w, A, σ, $\Delta\pi$, and ΔP are water flux, water permeability constant of the membrane, reflection coefficient, osmotic pressure difference and applied pressure, respectively (Cath et al. 2006). The osmotic pressure of a solution is the function of the amount of solute molecules (n), volume of the solvent (V_m), and temperature (T), given by Eq. 2-3:

$$\pi = \frac{n}{V_m} iRT \tag{2-3}$$

where R is the ideal gas constant and i is the dimensionless Van't Hoff factor.

Membrane processes can either be pressure-driven or osmotically-driven, depending on the amount of applied pressure on the system. A pressure-driven membrane process occurs when the applied pressure is higher than the net osmotic pressure between the two solutions. The increased pressure beyond the net osmotic pressure will then allow water flow toward the opposite direction, i.e. from the more concentrated draw solution (DS) to the less concentrated feed solution (FS), as in the case of reverse osmosis (RO) (Xie et al. 2015). RO is one of the most popular and developed water treatment and desalination processes both in academic research and industrial applications. A disadvantage of RO is the limitation in its efficiency and practicality due to intensive energy use and high operating cost. On the other hand, osmotically-driven membrane processes utilize either no applied pressure or pressure less than the net osmotic pressure between the FS and DS. Generally, the osmotically-driven membrane processes are forward osmosis, pressure retarded osmosis, and pressure assisted osmosis. A comparison of the schematic representations of these processes is shown in Figure 2-1. Basically, the low concentrated FS transports to the high concentrated DS through a semi-permeable membrane due to its osmotic differences for osmotic processes such as forward osmosis (FO), pressure assisted osmosis (PAO) and pressure retarded osmosis (PRO). However, the RO process requires a hydraulic pressure beyond the osmotic pressure of FS (i.e. seawater) to obtain the fresh water. PRO process is similar in principal with FO, however the pressure is applied on the DS side ($\Delta P < \Delta\pi$) opposite to the osmotic gradient that partially retards the water crossing the membrane driven by the osmotic force. Therefore, PRO membrane unlike to the FO, demanded the high mechanical property of membrane material (i.e. membrane support layer) to withstand high hydraulic pressures, in which, the optimal pressures are 50% of the osmotic pressure of DS. For example, when the seawater is used

as DS and fresh water as FS, a theoretical osmotic pressure of DS is ≈ 27 bar and an half of that pressure (13~14 bar) required to apply at DS side to achieve the maximum power density. Meanwhile, the hydraulic pressure is applied on the active layer of membrane that facing the FS to generates the ΔP for PAO process. Therefore, this process can be presented as an in-situ combination of RO and FO processes. The osmotic pressure therefore on the DS side is combined with the ΔP applied on the DS side to have synergic effect on the permeate side.

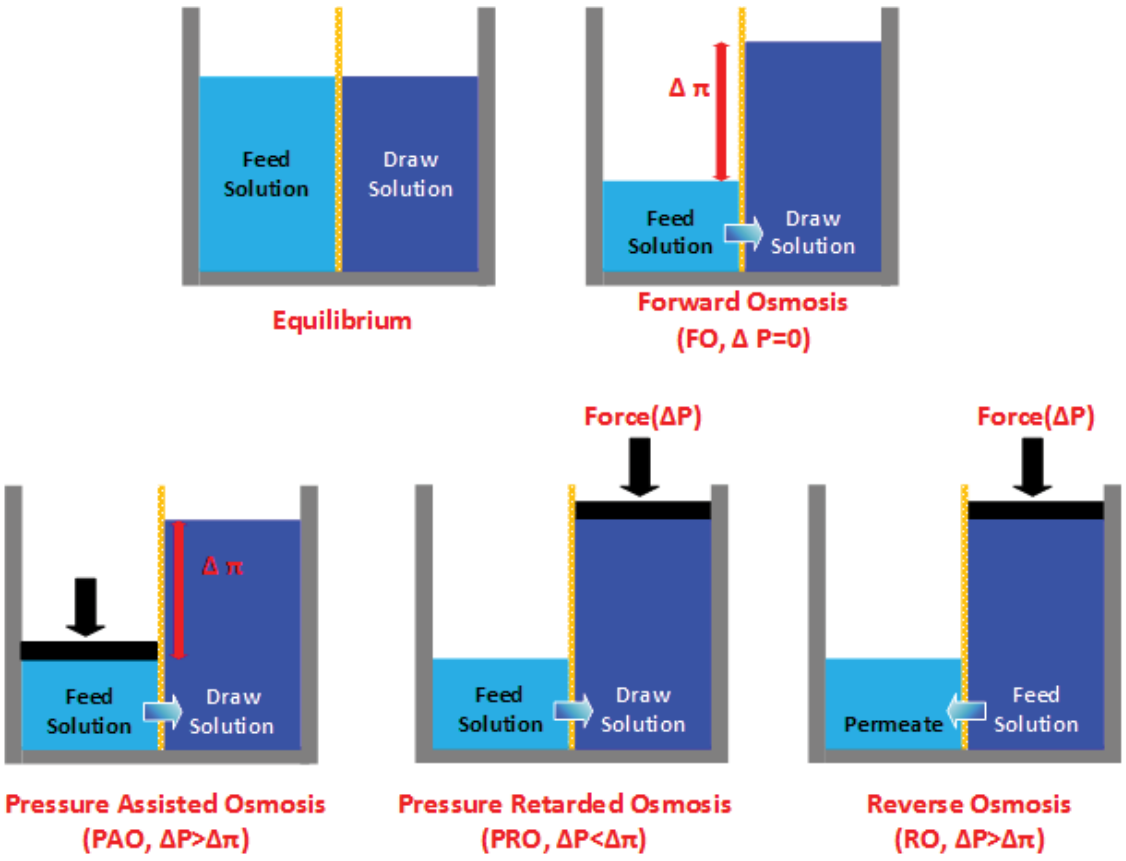

Figure 2 - 1. Comparison of the osmotic processes.

2.3.1. Forward osmosis (FO)

FO is a naturally-occurring physical phenomenon which utilizes the osmotic pressure difference between two solutions of different salinity. Unlike RO, FO does not require an external transmembrane pressure to proceed. FO has a number of applications, which include wastewater treatment, seawater and brackish water desalination, food processing, drug delivery, anti-microbial application, and power generation (Cath et al. 2006). During the application of FO for water treatment and desalination, water is generated from the

diluted DS through a suitable separation and regeneration downstream process (Chekli et al. 2012, Zhao et al. 2012), allowing higher recovery of fresh water compared to RO (Cath et al. 2006). A typical FO system is shown in Figure 2-2.

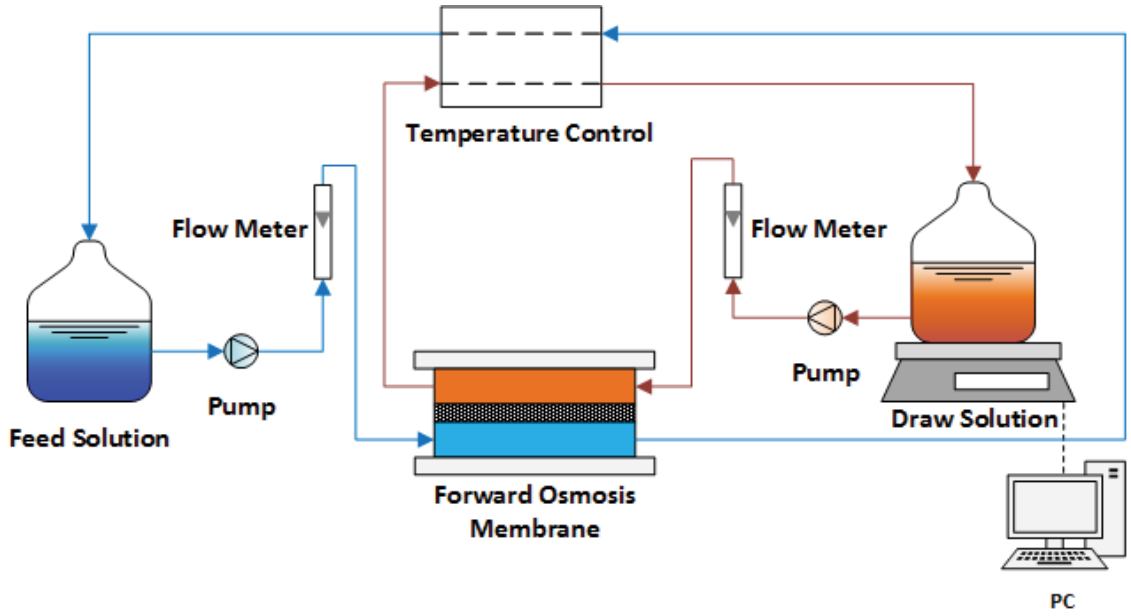

Figure 2 - 2. A schematic representation of a conventional lab-scale FO system.

2.3.2. Pressure retarded osmosis (PRO)

PRO utilizes the osmotic pressure difference between two solutions of different salinity, where water from the solution of less concentration passes through a selectively permeable membrane to the concentrated solution by osmosis (Mehta et al. 1978). The salinity gradient energy resulting from the salt concentration difference of the solutions produces power. Furthermore, PRO has a characteristic of high power density, which allows it to efficiently draw free energy from the high salinity gradient (Han et al. 2015, Yip et al. 2014). It is currently one of the alternative applications in harvesting renewable energy. The conventional PRO process is represented in Figure 2 - 3. The seawater draw solution is initially pressurized by a pressure exchanger and delivered to the semi-permeable membrane by a low pressure pump, approaching the membrane selective layer. Freshwater feed stream was likewise delivered to the semi-permeable membrane, the stream facing the porous supporting layer. Freshwater permeates from the feed solution side through the membrane towards the draw side, thereby diluting seawater, which is

then recirculated using a circulation pump and passes through the pressure exchanger for depressurization and conversion of hydraulic energy into energy by means of the hydroturbine and generator.

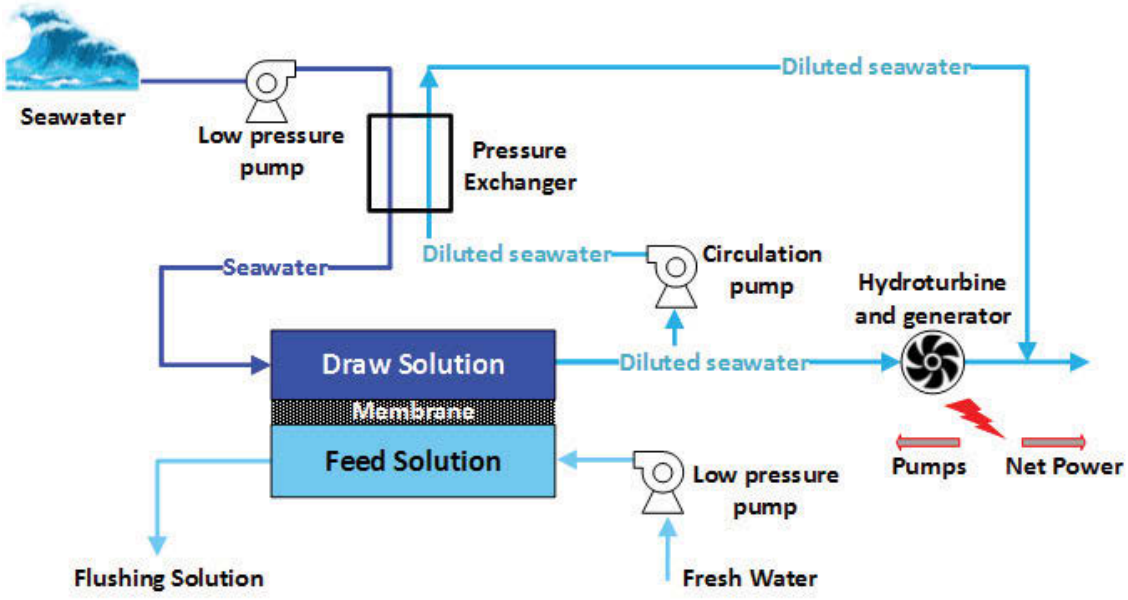

Figure 2 - 3. A schematic representation of a conventional PRO process.

While one may argue that since PRO applies minimal force, it should be regarded as a pressure-driven process, the operational concept of PRO basically works like that of FO. In a PRO process, the solvent permeates spontaneously through a selectively permeable membrane from the less concentrated FS towards the pressurized more concentrated DS (Han et al. 2015). The water flux from the diluted solution to the concentrated solution was prevented by application of pressure on the concentrated solution, hereby decreasing the quantity of water transferred, hence the process is deemed retarded by pressure. Currently, a special interest in PRO has emerged significantly due to the current focus on finding renewable energy sources. PRO only utilizes the salinity gradient energy resulting from the solute concentration difference to produce power, thus making PRO a viable

solution to significantly reduce the world's dependency on fossil fuel for energy and the carbon footprint associated with fossil fuels.

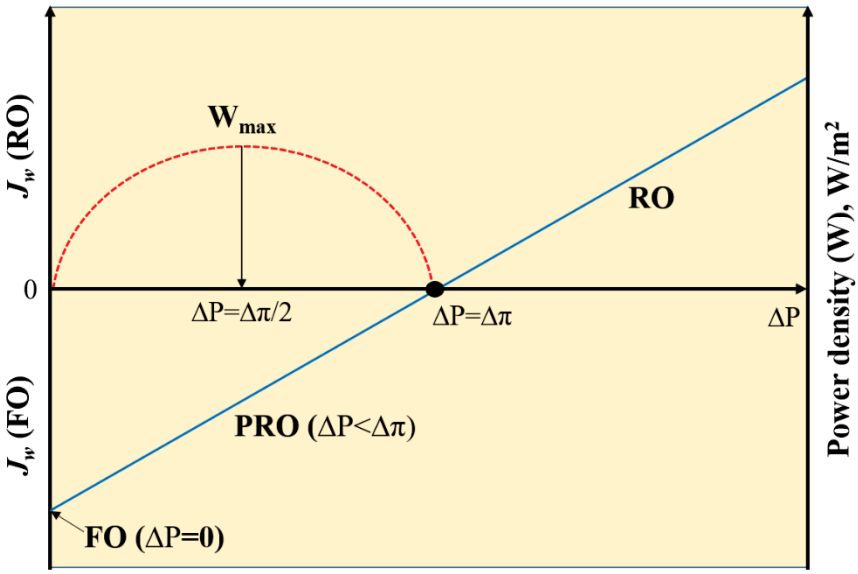

Figure 2 - 4. Water flux (J_w) and applied pressure (ΔP) relationship in FO, PRO and PRO processes. Power density (W) curve for PRO as a function of ΔP and Maximum power density (W_{max}) were also indicated.

Figure 2 – 4 shows the relationship of water flux (J_w) and applied hydraulic pressure (ΔP) in FO, RO, and PRO processes. These processes can be differentiated by the magnitude of ΔP applied in the system, i.e. $\Delta P=0$, $\Delta P<\Delta\pi$, and $\Delta P>\Delta\pi$ correspond to FO, PRO, and RO, respectively. During the FO process ($\Delta P=0$), the osmotic pressure difference across the semi-permeable is the only driving force for the water flux towards the direction where higher osmotic pressure is present. The water flux in the FO process is the product of the osmotic pressure difference across the membrane and the membrane pure water permeability coefficient (A value). Upon the application of hydraulic pressure less than the osmotic pressure difference ($\Delta P<\Delta\pi$), the process is known to be PRO. Since ΔP is lower than $\Delta\pi$, the direction of the water flux is still toward the direction of higher osmotic pressure. Due to the application of hydraulic pressure, water flux during PRO is retarded

(thus, the name of the process) and is lower than that during FO, until J_w=0 when ΔP=Δπ. Increasing hydraulic pressure applied further (ΔP>Δπ) leads to RO process operation, which causes the flow of water to change its direction from the more concentrated draw stream side to the less concentrated feed stream side. The water flux of the PRO and RO processes can be calculated as the product of the A value and the difference between the osmotic pressure difference and the applied hydraulic pressure. Figure 2 – 4 also describes the power density (W) for PRO operation as a function of ΔP. W is the product of water flux and the applied hydraulic pressure ($W = J_w \Delta P$). The power density has been known to reach a maximum theoretical value (W_{max}) when the applied hydraulic pressure is equal to half of the osmotic pressure difference across the membrane ($\Delta P = \frac{\Delta \pi}{2}$). At $\Delta P > \frac{\Delta \pi}{2}$, water flux decreases significantly that the PRO process cannot generate more power.

2.3.3. Pressure assisted osmosis (PAO)

PAO is an engineered osmotic process which incorporates both FO and RO. During PAO operation, hydraulic pressure is applied on the FS region to increase the driving force for water transport, on top of the osmotic pressure driving force already originating from the solute concentration difference of the DS and FS (Oh et al. 2014, Yun et al. 2014). Hydraulic pressure is applied not only to increase water permeability, but also to mitigate back-diffusion of salt. An advantage of PAO is the applied pressure does not need to overcome the osmotic pressure difference of the FS and DS, thus it can pose less energy requirements than RO.

It can be assumed that due to the applied hydraulic pressure, the water flux in PAO must be significantly higher than that of FO or PRO, since it is both influenced by osmotic gradient and hydraulic pressure. However, the application of hydraulic pressure also results to dilutive internal concentration polarization (which will be discussed later), resulting in the reduction of effective osmotic pressure (Blandin et al. 2015, Oh et al. 2014).

2.4. Issues for engineered osmosis membranes

There are no perfect semi-permeable membranes for engineered osmosis and this is the reason why a number of considerations must be achieved to be able to maximize water flux and process performance. These issues are concentration polarization, the membrane intrinsic properties, reverse salt flux, and fouling.

2.4.1. Concentration polarization

Concentration polarization is a phenomenon exclusively observed in osmotically-driven processes, which can either be internal or external. Concentration polarization effectively decreases the effective osmotic pressure gradient across the membrane between the FS and DS. As a result, the water flux dramatically decreases due to concentration polarization.

2.4.1.1. Internal concentration polarization

Internal concentration polarization (ICP) occurs within the porous support layer of the membrane in either one of these two situations: (1) the active layer of the membrane is facing the DS, solute inside the membrane support is concentrated as water permeates through the membrane causing concentrative ICP, or (2) the active layer is facing the FS, dilution of DS in the support layer through permeating water from feed side to draw side causing dilutive ICP.

During concentrative ICP, the solutes of the DS accumulate at the interface between the active and support layers, due to the inability of the solute particles to penetrate the active layer of the membrane (Zhou et al. 2014). This will then effectively reduce the osmotic flow of the solvent permeating through the membrane (McCutcheon et al. 2006). Concentrative ICP is mostly observed when the membrane orientation is active layer facing DS (AL-DS or PRO mode). An immobile area is formed within the porous membrane support layer, hereby decreasing the osmotic driving force (Tow et al. 2015). On the other hand, during dilutive ICP, excessive water flux from the feed passes through

the membrane, resulting in dilution of the DS, hereby decreasing the transmembrane osmotic pressure (McCutcheon et al. 2006). Dilute ICP is mostly observed at an active layer facing FS (AL-FS or FO mode) orientation of the membrane, mostly depending on the nature of the components in the FS.

Generally, ICP phenomenon is more easily observed when the draw solutes contained large solute molecules. These large solute particles cannot pass through the membrane easily and will simply tend to accumulate on the membrane and reduce the osmotic flow. Consequently, ICP is closely related to the diffusivity and molecular size of the solute, as well as the solute diffusivity and morphology of the membrane. Furthermore, ICP is more observed also during the FO processes, due to lack of applied pressure onto the system (Gray et al. 2006). It cannot be easily mitigated by increasing the feed flow rate across the membrane surface, since concentration polarization happens inside the porous membrane substrate. Therefore, hydrodynamic flow conditions cannot be performed to control ICP occurrence.

2.4.1.2. External concentration polarization

Unlike ICP, external concentration polarization (ECP) occurs at the surface of the active layer and it is mostly observed when the membrane orientation is AL-DS. ECP occurs when the salt concentration at the interface of the FS and the membrane is higher than the concentration of the FS, due to water depletion and reverse salt diffusion (to be discussed later) (Mehta et al. 1978). As a result of the constant pressure and solute rejection by the membrane, the osmotic pressure near the membrane surface increases. However, this pressure near the membrane surface is still less than the actual osmotic pressure, causing a decrease in effective water flux (Hoek et al. 2003, Sahebi 2015).

Concentrative ECP occurs when the orientation of the dense membrane active layer is facing FS, but this type of ECP is not normally observed. On the other hand, dilutive ECP occurs due to the diffusion of water from the feed to DS when the membrane orientation is AL-DS (Puguan et al. 2014).

Compared to ICP, the detrimental effects of ECP are less, even when the membrane support layer is thick, since ECP simply reduces the osmotic driving force. A method to

mitigate ECP is to simply increase the feed flow rates on the external surface of the membrane (Han et al. 2015). It is also observed in various studies that the detrimental effects of ECP on water flux and power density (in PRO processes) are less pronounced than those of ICP, especially at higher DS concentrations (Lee et al. 1981).

2.4.2. Water permeability coefficient, solute permeability coefficient, and structure parameter

The water permeability coefficient (*A*, also the hydrodynamic permeability coefficient), the solute permeability coefficient (*B*), and the structure parameter (*S*) describe the inherent properties of an osmotic membrane. Osmotically-driven membrane processes should have high water flux and low reverse solute flux (Phillip et al. 2010). The structure parameter describes the pathway of the water through the membrane (Alsvik et al. 2013a). Minimization of the structure parameter of the membrane mitigates the occurrence of ICP.

Water transport in an osmotically-driven membrane process is given by Eq. 2-4:

$$J_w = A(\Delta\pi - \Delta P) \tag{2-4}$$

where J_w and A are the water flux and water permeability coefficient, respectively. A is the function of the distribution coefficient, or solubility, and the diffusivity.
Solute flux (J_s) can be described by Eq. 2-5:

$$J_s = B\Delta C_s \tag{2-5}$$

where ΔC_s is the solute concentration difference across the membrane and B is the solute permeability coefficient, described by Eq. 2-6 (Tiraferri et al. 2011b):

$$B = J_w \left(\frac{1-R}{R}\right) exp\left(-\frac{J_w}{k}\right) \tag{2-6}$$

where R and k are the rejection coefficient and mass transfer coefficient, respectively. The rejection coefficient determines the selectivity of the membrane for a given solute, given by Eq. 2-7 (Tiraferri et al. 2011):

$$R = \frac{C_f - C_d}{C_f} = 1 - \frac{C_d}{C_f} \quad (2\text{-}7)$$

where C_f and C_d are the solute concentrations of the FS and DS, respectively.

The membrane support layer is then described by S, given by Eq. 2-8 (Gerstandt et al. 2008):

$$S = \frac{x\tau}{\varphi} \quad (2\text{-}8)$$

where x, τ, and φ are thickness, tortuosity, and porosity of the support layer, respectively.

The value of A should ideally be as high as possible to allow maximum permeability of water, while B is preferred to be as small as possible to prevent back-diffusion of solute particles (Han et al. 2015). It is therefore imperative to find the best combination of A and B to maximize FO performance and power density in the PRO processes. As mentioned earlier, the value of S must be small to minimize ICP effects. It is therefore suggested that the hydrophilic membrane support layer should have reduced thickness, high porosity, and low tortuosity. However, due to these requirements, mechanical properties, tensile strength, and elasticity of the membranes may also be sacrificed. This may lead to membrane breakage, especially at high-pressure PRO processes (Li et al. 2013c).

2.4.3. Reverse salt flux

Reverse salt flux (*RSF,* J_s) is the transport of the solute particles from the draw to the FS across the semipermeable membrane. This transport follows the same basic principle of osmosis, wherein the movement of solute is from the region with higher concentration toward the region with a lower one. The reverse permeation of solutes from the DS into the FS through the selectively permeable membrane decreases the total osmotic driving force and the membrane efficiency for all osmotically-driven processes (Alsvik et al. 2013a, Hancock et al. 2009). Salts inevitably will diffuse back into the membrane substrate because of the concentration gradient, and this will prove to be detrimental to water flux and osmotic performance due to ICP.

Reverse flux selectivity is independent on the structure parameter, S; it is dependent on the selectivity of the active layer of the membrane (Phillip et al. 2010). The selectivity of the active layer is highly important due to factors, such as size exclusion and electrostatic interactions, which control the permeability of the solute molecules across the membrane (Hancock et al. 2009, Hancock et al. 2011). Due to these factors, divalent ions with large radii, such as Mg^{2+}, Ca^{2+}, and Ba^{2+}, are not able to permeate through membranes, as compared to monovalent or neutral ions with smaller radii. In order to minimize *RSF*, DSs with multivalent ions are then preferred for these ions' lower diffusion coefficients than monovalent ions (Cath et al. 2006). However, solute particles of larger radii and lower diffusion coefficients will then result to ICP and increase the fouling within the membrane (Zhao et al. 2011a). The relationship between *RSF* and ICP was also established for commercial membranes (Shibuya et al. 2015).

A selectively permeable membrane should be able to allow water molecules to pass through from the FS to the DS and reject salt particles passing through in an opposite direction. This can be evaluated by another parameter to more effectively describe membrane selectivity, the specific reverse salt flux (*SRSF,* J_w/J_s), which is defined as the ratio of the J_s and J_w (Hancock et al. 2009, Phillip et al. 2010). It is currently the most widely used parameter to determine efficiency of FO membrane performance. The *SRSF* value is preferred to be as low as possible, i.e. high J_w and low J_s. A high *SRSF* value then is obtained when the membrane selectivity is poor, leading to an also poor FO performance (Phillip et al. 2010). *SRSF* is not dependent on the DS concentration in the membrane support later but only on the membrane active layer selectivity.

Selectivity of the membrane active layer is not only dependent on the size and charge of the solute ions, but also on the nature of the draw solutes. It was observed that the use of neutral draw solutes, such as ethylene glycol and urea, resulted in an increase in solute permeability and decrease in water flux (Yong et al. 2012). This phenomenon can be explained by the ability of the active layer of the membrane to preferentially allow the permeation of the solvent over the solute, a parameter known as the reflection coefficient, σ (Yong et al. 2012). The osmotic reaction coefficient parameter is described in Eq. 2-9 (Bhalla et al. 2009):

$$v = K(\Delta P - \sigma\Delta\Pi) \quad (2\text{-}9)$$

where v and K are transmembrane volume flux (or superficial fluid velocity) and hydraulic permeability, respectively. The v is related to the mechanical (ΔP) and osmotic ($\Delta\Pi$) pressure differences when a single solute is present. Alternatively, the reflection coefficient can be determined by the ratio of the experimental water flux and the theoretical water flux (Yong et al. 2012). A highly selective membrane would have a reflection coefficient of 1, thus being able to allow solvent to pass, but not the solute. Neutral draw solutes ethylene glycol and urea were observed to have reflection coefficients of 0.69 and 0.67, respectively, thus the actual experimental water flux values were lower than the theoretical values (Yong et al. 2012).

Not only is the *RSF* dependent only on the membrane selectivity, it is also highly dependent on the membrane orientation. RSF was found to be less when the membrane active layer is facing the FS than when the membrane active layer is facing the DS (Kong et al. 2014). This is because the membrane active layer is expected to have smaller porosity than its support layer, thus solute particles will not be able to back-diffuse and simply accumulate on the interface between the support and active layers. While it was established earlier that the concentration of the DS does not play a huge impact on SRSF, it is a factor for RSF. A previous study was performed wherein the DS concentration was doubled, resulting in an increase in *RSF* for both AL-DS and AL-FS membrane orientations (Kim et al. 2012).

2.4.4. Fouling

Fouling is the phenomenon observed when matter, such as particles, colloids, molecules, etc., are retained and deposited on the surface or in between the interfaces and pores of the membrane (Alsvik et al. 2013a). There are four general types of fouling: colloidal, inorganic (or scaling), organic, and biofouling (Amy 2008). During the occurrence of fouling, membrane water flux is effectively reduced either temporarily or permanently. At certain instances, the interaction between the foulants and the membrane surfaces can possibly cause chemical degradation of the membrane surface (Rana et al. 2010).

Chemical degradation of the membrane surface and decreased efficiency of osmotic processes caused by fouling result in economical and practical limitations of osmotically-driven membrane processes. Fouling mechanism may be dependent on a number of factors, including, but not limited to, membrane surface, system design, flow rate, water quality, temperature, etc. Modification of the surface, fabrication methods and conditions, process design, and osmotic process operation conditions may be performed to mitigate membrane fouling. Membrane fouling is also dependent on the membrane orientation. In FO mode, wherein the active layer is facing the DS, foulants are deposited on the surface of the active layer. Meanwhile in PRO mode, wherein the active layer is facing the FS, foulants are deposited on the support layer (Rana et al. 2010). Thus, for PRO processes, fouling on the support layer is the greatest issue which must be mitigated. The interactions among the molecules of the foulants result in accumulation on the surface, thus intermolecular forces of attraction among the foulants are highly correlated with fouling (Mi et al. 2010). Membrane resistance to fouling may be improved by modification of the membrane active layer and/or the support layer to mitigate fouling on both sides of the membrane.

Fouling phenomena in osmotically-driven processes are known to be different than those occurring in RO, a pressure-driven process. The applied hydraulic pressure in RO results in a more compact deposition of foulant, thus it is less reversible than the fouling in FO or PRO, which are osmotically-driven processes (Lee et al. 2010, Mi et al. 2010). Due to the less compact nature of fouling in engineered osmotic processes, physical cleaning may be performed and the use of chemical reagents may be avoided (Lee et al. 2010). Physical cleaning of membranes for engineered osmosis only requires osmotic backwashing, thus membranes used for these processes tend to have longer operational life. As a result, membranes used for osmotically driven process are not required to be replaced frequently, thereby decreasing capital and operational costs. The membranes are simply needed to be cleaned regularly to avoid long term operational drawbacks due to scaling and organic fouling.

As mentioned earlier, there is a relationship between *RSF* and fouling when multivalent ion draw solutes with lower diffusion coefficients are used to mitigate RSF for osmotic

applications requiring high salt rejection (Cath et al. 2006, Hancock et al. 2009). The relationships between ICP, *RSF*, and fouling is shown in Figure 2-4. Since multivalent ions have a larger ionic size than monovalent ions, they cause more serious ICP (Zhao et al. 2011b). As they accumulate within the membrane and possibly interfere with the foulants present in the FS, multivalent ions aggravate fouling (Zou et al. 2011). The increased fouling on the membrane surface caused by the accumulation of the ions enhances their passage through the membrane therefore inducing lower rejection values in a phenomenon known as cake-enhanced concentration polarization (CECP) (Hoek et al. 2003).

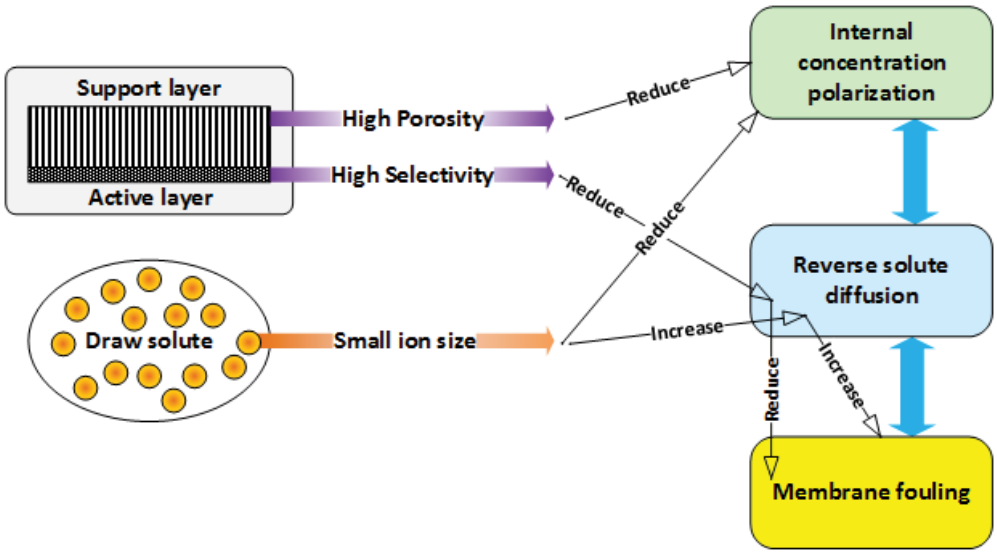

Figure 2 - 5. Relationships between internal concentration polarization, reverse salt flux, and membrane fouling in engineered osmosis processes.

Among various types of membrane fouling, biofouling is the most difficult one to control and mitigate. Unlike inorganic and organic fouling, biofouling cannot simply be cleaned by simple osmotic backwashing. The bacterial adhesion on the membrane surface associated with biofouling is difficult to remove, especially when extracellular polymeric substances (EPS) are present. The development of the bacterial adhesion and presence of EPS effectively reduces the membrane surface area, leading to a reduction in water flux. Due to the difficulty in removal of biofouling, chemical cleaning was deemed necessary. Chemical cleaning agents, such as chlorine, may be used to eliminate fouling, after several washings (Yoon et al. 2013). Another method to mitigate biofouling is the preparation of anti-microbial membranes. Graphene oxide is a nanomaterial obtained

from graphite, which was found to have anti-microbial properties (Lee et al. 2013, Perreault et al. 2014). Graphene oxide was incorporated in the preparation of membranes to functionalize the membrane's surface in order to inhibit biofouling (Perreault et al. 2014). The presence of graphene oxide inactivated E. coli by about 65% after one hour of direct contact after this study. Silver nanoparticles were also found to be significantly useful in preventing biofouling. Membranes coated with Ag/TiO_2 for functionalization were prepared and upon testing for FO, bacterial growth on the functionalized membranes showed almost 11 times reduction of biofouling, as compared to uncoated membranes (Nguyen et al. 2014).

2.4.5. Porosity

Membrane pore distribution and pore size are highly integral for engineered osmosis membranes. Thus, these should be carefully considered in membrane fabrication. Both properties can be controlled by the variation of polymer concentration and the incorporation of additives which form pores, such as polyethylene glycol, ethylene glycol, and $LiCl_3$ (Yip et al. 2010). Higher polymer concentration results in a dense membrane while lower polymer concentration producing macrovoids and finger-like morphology (Wang et al. 2012a). Additives can be added to produce micro- and nano-sized pores on the membrane support layer.

2.5. Membranes for engineered osmosis

Preparation of membranes for engineered osmosis is a relatively new area in the field of membrane science and technology. The first membranes used in osmotic processes were made from plant and animal residues. An ideal selectively permeable membrane allows the solvent molecules to pass but not the solutes. A selectively permeable asymmetric cellulose acetate membrane was prepared by Sidney Loeb and Srinivasa Sourirajan in 1963, providing a breakthrough in reverse osmosis processes and membrane science. These membranes exhibited poor water flux, though, even with the development of thin film composite membranes by John Cadotte. Interfacial polymerization (IP) of an amine solution and an acid halide may result in the formation of a polyamide (PA) on top of RO membranes (Cadotte et al. 1980). However, membranes were fabricated more for

application to RO rather than FO and PRO. Initially, membranes for RO, MF, NF, and UF were used since these membranes were more commercially-available (Akther et al. 2015). These membranes were employed for engineered osmosis because only semi-permeable membranes were thought to be required for these processes. However, these membranes were deemed unsuitable for engineered osmotic processes, primarily due to their membrane support layer thickness and dense hydrophobic support layer, leading to ICP (Sahebi 2015). Not only do these membranes limit water and solute permeability, the thickness of these membranes effectively reduce the osmotic pressure across the membranes (Lee et al. 1981). Due to the thickness of conventional water treatment membranes, severe ICP was found to occur inside the membranes. ICP present in the membranes then effectively reduces the osmotic pressure across the membranes, affecting water flux and reverse salt flux (Lee et al. 1981). Another early strategy in preparation of FO membranes is the modification of RO membranes. The modification mostly focused on making the membrane support layer more hydrophilic, to make up for the thickness. Any of the following methods were investigated to improve the hydrophilicity of the commercial RO membranes: treatment with polydopamine, polyethylene glycol, and sulfonating agents (Sahebi 2015). These membranes, however, did not produce promising results at that time.

In general, engineered osmosis membranes are highly similar to typical water treatment membranes. Unlike these conventional membranes, an FO membrane should be fabricated while keeping in mind that there are four flow connections during the FO process application: feed in, feed out, draw in, and draw out (Cath et al. 2006). A number of materials and methods can be examined in fabrication of membranes for engineered osmosis, thus interest in osmotic processes and the fabrication of FO and PRO membranes has dramatically increased. Since then, fabrication of membranes for engineered osmosis, specifically for FO, has emerged as a very promising area of study, with the primary focus on the preparation of thin support layers to improve water permeability, minimize ICP, and reduce transport resistance.

Performance of engineered osmosis processes is mainly affected by internal dilutive concentration polarization within the porous support layer. This is the reason why, during fabrication of engineered osmosis membranes, the membrane should be as thin as

possible, while maintaining porosity and low tortuosity. Thin membrane thickness ensures that the structural parameter is much smaller. An ideal membrane for engineered osmosis should have high water flux, low salt reverse flux, and minimal ICP (Chung et al. 2012a, Klaysom et al. 2013b).

The main goal of most recent membrane studies, especially for FO, is to maintain a relatively small structural parameter, while enhancing water permeability during the formation of the PA layer and other post-treatment methods (Han et al. 2015). However, enhancement of water permeability often enhances salt permeability as well; therefore, a balance between the two membrane parameters must be achieved. A number of studies have also investigated enhancing the membrane hydrophilicity to enhance water flux and reduce membrane fouling. Membranes especially for PRO and PAO are then required to have sufficient mechanical strength to withstand applied hydraulic pressure.

2.5.1. Membrane structure

Membranes can either have symmetric or asymmetric structures. A comparison of these two are shown in Figure 2-5.

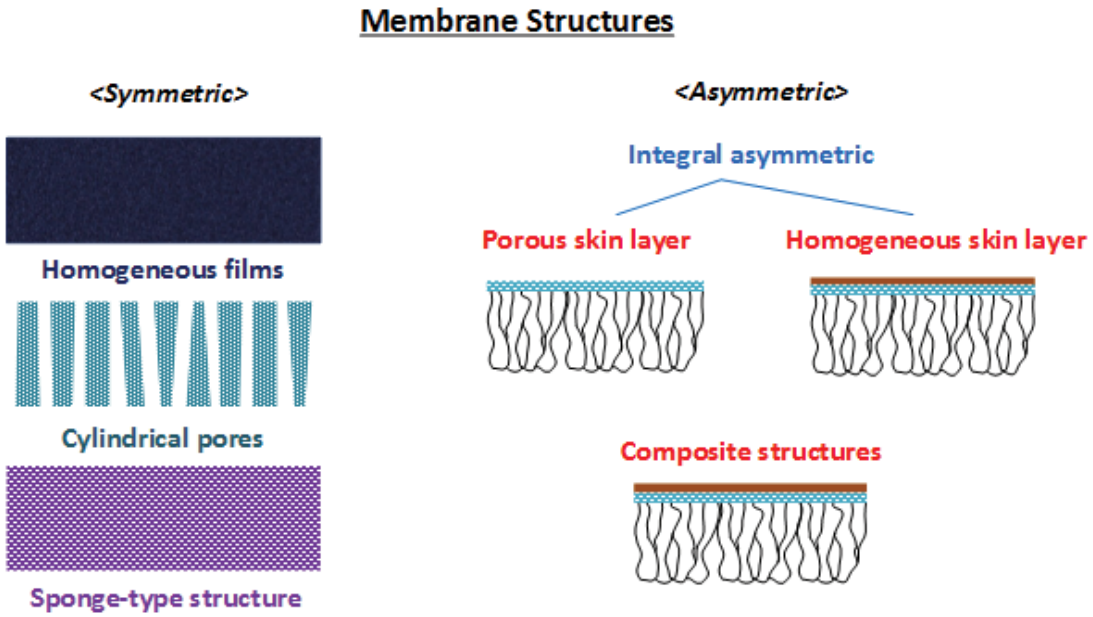

Figure 2 - 6. Comparison of symmetric and asymmetric membranes.

2.5.1.1. Symmetric membranes

Symmetric membranes are those with uniform structure and morphology. Due to the uniformity in their structure and morphology, asymmetric membranes are usually considered to be microporous and/or dense. As a consequence of the density and thickness of most symmetric membranes, water flux is highly limited (Sahebi 2015).

2.5.1.2. Asymmetric membranes

Fabrication of asymmetric membranes was a huge breakthrough in membrane technology when Loeb and Sourirajan prepared an asymmetric cellulose acetate membrane in 1963. These membranes are characteristically non-uniform in structure and morphology, with a porous support and a thin active (skin) layer on top.

2.5.2. Materials for membrane fabrication

Synthetic materials have been of special interest for fabrication of membranes of osmosis since the 1960s. However, cellulose, a natural polymer which is a structural component of cell walls or plant, is the most abundantly available polymer, and among the most widely used polymers for membrane fabrication. Aside from cellulose, there are countless other synthetic materials for membrane fabrication.

Cellulose acetate (CA) and cellulose triacetate (CTA) are important synthetic esters of cellulose, formed after the reaction of cellulose with acid anhydride. These polymeric derivatives of cellulose are known for their smoothness and strength, making both cellulose acetate and cellulose triacetate suitable engineered osmosis membrane materials (Alsvik et al. 2013a). Furthermore, cellulose-based polymers are known to have good mechanical strength, high water permeability, low fouling propensity, and high chemical resistance (Geise et al. 2010a, Zhang et al. 2010, Zhang et al. 2011). CA- and CTA-based membranes are among the most investigated membranes for FO and PRO (Gerstandt et al. 2008, Li et al. 2013a, Nguyen et al. 2013, Ong et al. 2012, Sairam et al. 2011). Phase inversion of cellulosic polymers can be carried out to fabricate either flat sheet (Wang et

al. 2010a, Zhang et al. 2010) or hollow fiber membranes (Su et al. 2012, Su et al. 2010). These polymers can even be used as nanofibrous substrates for thin film composite (TFC) membranes after electrospinning (Bui et al. 2013a). When compared with CTA, CA has less acetylate. Low acetylation of the former results in a higher hydrophilicity compared to the latter. High hydrophilicity is required for membranes in osmotically driven membrane processes, since hydrophilic membranes increase water flux and reduce the ICP (McCutcheon et al. 2008). The hydrophilicity of both CTA and CA results in better wetting. However, it was noted in various research that FO and PRO membranes derived from cellulose-based polymers have low intrinsic water permeability and high salt permeability, resulting in low water flux and high reverse salt flux (Achilli et al. 2009, Bui et al. 2014, Kim et al. 2013b, She et al. 2012). CTA was used as the material for the currently most popular commercial FO membrane, which is manufactured by Hydration Technology Innovations (HTI). This commercial FO membrane is thin (90 μm) and CTA was embedded on a woven polyester fabric. This membrane, however, is found to exhibit low water flux, low rejection, and poor resistance. Other cellulose esters, such as cellulose acetate butyrate (CAB) and cellulose acetate propionate (CAP), can also be used as the polymer in fabrication of flat sheet FO membranes (Li et al. 2012a, Ong et al. 2015, Wei et al. 2015, Zhang et al. 2011).

Sulfur-containing polymers are also popularly used for membrane fabrication. Polysulfone (PSf) is a synthetic polymer containing the aryl-C_3H_6-aryl-SO_2-aryl subunit. Polyethersulfone (PES), on the other hand, is composed of aryl-SO_2-aryl subunits. Both polymers have good chemical resistance and strength. Due to these properties, resistance to oxidation and hydrolysis, and hydrophobicity, both PSf and PES are used as support materials for most TFC membranes. These two materials, however, show poor water permeability, thus, novel approaches on modification of the PSf and PES membrane supports have been performed in a number of studies (Lay et al. 2012, Morales-Torres et al. 2016) and another previous study mixed together PSf and PES to make a high flux TFC membrane (Sun et al. 2014).

Aside from sulfur-containing polymers, nitrogen-containing polymers are also widely used for membrane fabrication. Polybenzimidazole (PBI), whose linear formula is $(C_{20}H_{12}N_4)_n$, is a polymer whose mechanical strength and stability are excellent, despite

being at elevated temperatures. This polymer can withstand prolonged heating up to 250°C, with little to no change in properties. PBI is known to produce robust nanofiltration membranes, due to its high mechanical strength and chemical stability, in addition to satisfactory water flux and salt rejection (Wang et al. 2007). Polyacrylonitrile (PAN), whose linear formula is $(C_3H_3N)_n$, is another polymeric material with high thermal stability, strength, and elasticity. Its tensile strength and tensile modulus make it a suitable material for membranes and fibers (Klaysom et al. 2013c, Makaremi et al. 2015). Another nitrogen-containing polymer is polyamide-imide (PAI), which is among the mechanically-strongest commercial polymers available (Jang et al. 2013). This membrane is capable of crosslinking with other materials for further modification.

Lastly, polymers containing halogens are also commonly used in fabrication of membranes. Among the most popular halogen-containing polymers is polyvinylidene fluoride (PVDF). It has a high chemical resistance, as well as low density and high tensile strength, making it a suitable material for membranes (Tian et al. 2013).

A huge issue in the preparation of membranes for engineered osmosis is mechanical stability. This is the reason why most membranes prepared in scientific research utilize backing fabric to strengthen the support layer for easier modulation. The fabric can either be woven or nonwoven, and is mostly made up of polymers such as polyester and polyethylene terephthalate. For commercial membrane fabrications, woven backing fabric is preferred since it has a large open area, sufficient mechanical strength, and high porosity which minimize the water transport resistance as compared with nonwoven fabrics. (Sahebi 2015).

A wide variety of membranes have been fabricated in the last few years, and these membranes for engineered osmosis are generally classified into any of these categories: phase inversion, IP, chemically-modified, nanofiber-supported, or biomimetic membranes (Zhao et al. 2012). Aside from the various methods, a number of membrane configurations, such as flat sheet, hollow fiber, nanofiber, and tubular, can also be designed. Each configuration normally requires a specific fabrication method. Over the years, IP technique has also been developed as an efficient method to produce a very thin

active layer on a support membrane, to fabricate thin film composite membranes. A summary of various fabricated membranes in literature is listed in Table 2.2.

2.5.3. Preparation of membrane substrates and TFC membranes for engineered osmosis

There are several techniques or methods in terms of membrane preparations, such as flat-sheet and hollow fiber membranes fabricated via phase inversion technique, and nanofiber membranes by electrospinning. Phase inversion is currently the most widely used method in membrane fabrication, especially for osmotically-driven processes.

2.5.3.1. Flat-sheet membrane

When fabrication of flat-sheet membranes first emerged, phase inversion was the method performed, both in research and industry. Commercially-available membranes have been made available through phase inversion by Hydration Technologies, Inc. (Ontario, Canada). Phase inversion is known to be the most-known route of fabrication of support layers of FO and PRO membranes (Han et al. 2015). This technique is known to be very convenient and versatile, due to the various configurations and morphologies which can be obtained from this method.

During fabrication of phase inversion flat sheet membranes, polymeric dope solutions are cast on a flat surface and exposed in a non-solvent substance (e.g. water for hydrophobic polymers) to form integrally-skinned flat-sheet membranes, as shown in Figure 2-6. This method is integral to the fabrication of TFC membranes since the morphology and the mechanical properties of the substrate determine the quality of the PA layer formed during IP, as well as osmotic parameters, such as ICP and structural parameter (Ghosh et al. 2009, Han et al. 2015, Kong et al. 2010, Li et al. 2013a). The polymer solution is precipitated into both the solid phase, which consists mainly of polymers forming the substrate, and the liquid phase, which facilitates pore formation.

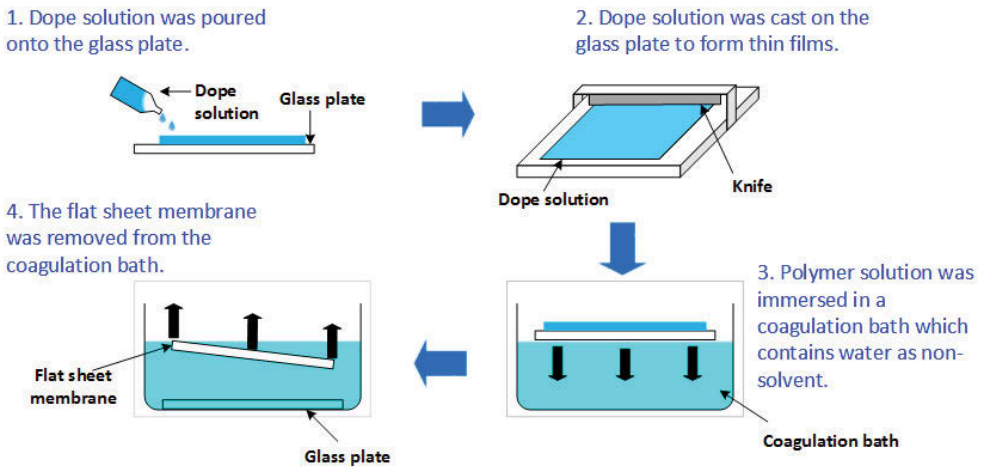

Figure 2 - 7. A typical flat sheet membrane casting process. The polymer solution is poured onto a glass plate and the casting knife spreads it evenly. The glass plate is afterwards submerged in water to facilitate the phase inversion.

Pore size and porosity of the membrane are determined by the polymer concentration, presence of additives, and the interaction of solvent and non-solvent. For example, decrease in polymer concentration or increase in non-solvent content of the casting solution enhances porosity. It is highly important that the non-solvent is incompatible with the polymer to facilitate complete phase inversion. Membrane fabrications with flat-sheet membrane for osmotically-driven applications are presented in Table 2-2.

Table 2 - 2. Flat-sheet membrane substrates prepared via phase separation for FO and PRO applications

Osmotic Process	Materials	Fabrication Method	Reference
FO	Cellulose acetate (CA)	Phase inversion & thermal annealing at 80-95°C	(Gerstandt et al. 2008)
FO	Polyacrylonitrile (PAN), aluminium terephthalate, copper benzene-1,3,5-tricarboxylate, & iron benzene-1,3,5-tricarboxylate	Phase inversion & chemical modification	(Lee et al. 2015a)
FO	CA or cellulose triacetate (CTA)	Phase inversion	(Li et al. 2013a, Nguyen et al. 2013)
FO	CTA	Phase inversion	(Ong et al. 2012)
FO	CA	Phase inversion	(Wang et al. 2010a, Zhang et al. 2010)
FO	Cellulose acetate butyrate (CAB) or cellulose acetate propionate (CAP)	Phase inversion	(Zhang et al. 2011)
FO	Polyethersulfone (PES), 1,3-dioxolane, & polyvinyl pyrrolidone (PVP)	Phase inversion & chemical modification	(Yu et al. 2011)
FO	CA on nylon fabric	Phase inversion	(Sairam et al. 2011)
FO	Polysulfone (PSf), dimethyl sulfone (DMSO), bis(4-hydroxy-3,5-dimethyl-phenyl)methane (TMBPF), 4,4'-difluorobenzophenone (DFBP), & *m*-phenylenediamine (MPD)/ trimesoyl chloride (TMC) polyamide	Phase inversion, chemical modification, & IP	(Han et al. 2012b)
FO	PSf, dopamine hydrochloride, & MPD/TMC polyamide	Phase inversion, chemical modification, & IP	(Lay et al. 2012)
FO	Sulfonated polyphenylenesulfone (sPPSU) on polyethylene terephthalate (PET) mesh & MPD/TMC polyamide	Non-solvent induced phase separation (NIPS), chemical modification, & IP	(Han et al. 2016)
FO	Nylon 6,6 microfiltration (MF) membrane & MPD/ TMC polyamide	IP	(Huang et al. 2013, Huang et al. 2015)

Osmotic Process	Materials	Fabrication Method	Reference
FO	Nylon 6,6 microfiltration (MF) membrane & piperazine (PIP)/TMC polyamide	IP	(Huang et al. 2013)
FO	PAN & MPD/TMC polyamide	Phase inversion & IP	(Klaysom et al. 2013c)
FO	PSf ultrafiltration (UF) membranes & MPD/TMC polyamide	Co-solvent assisted IP (CAIP)	(Kong et al. 2010)
FO	CAP & *p*-phenylenediamine (PPD)/TMC polyamide	Phase inversion & IP	(Li et al. 2012a)
FO	Polyvinylidene fluoride (PVDF), DMSO, & MPD/TMC polyamide	Phase inversion, chemical modification, & IP	(Liang et al. 2017)
FO	PES & MPD/TMC polyamide	Phase inversion & IP	(Liu et al. 2014b)
FO	PSf, silica powder, & MPD/TMC polyamide	Phase inversion, chemical modification, & IP	(Liu et al. 2015a)
FO	CAP or CAB, & MPD/TMC polyamide	Phase inversion & IP	(Ong et al. 2015, Wei et al. 2015)
FO	PSf & MPD/TMC polyamide	Phase inversion & IP	(Ren et al. 2016, Tiraferri et al. 2011b, Wei et al. 2011, Yip et al. 2010)
FO	Sulfonated PSF & MPD/TMC polyamide	Phase inversion, chemical modification, & IP	(Ren et al. 2016, Wang et al. 2012a)
FO	PSf/PES & MPD/TMC polyamide	Phase inversion & IP	(Sun et al. 2014, Wang et al. 2012a)
FO	PES, polyphenylsulfone (PPSU), & MPD/TMC polyamide	Phase inversion, chemical modification, & IP	(Widjojo et al. 2011a)
FO	PES, PPSU, 3,3'-di-sodiumdisulfate-4,4'-dichlorphenyl sulfone (sDCDPS), & MPD/TMC polyamide	Phase inversion, chemical modification, & IP	(Widjojo et al. 2013)
FO	PSF, PEI, & MPD/TMC polyamide	Phase inversion, chemical modification, & IP	(Xiao et al. 2015)
FO	Polyketone & MPD/TMC polyamide	NIPS & IP	(Yasukawa et al. 2015a)
FO	PSf on PET fabric & MPD/TMC polyamide	Phase inversion & IP	(Yip et al. 2010)

Osmotic Process	Materials	Fabrication Method	Reference
FO	PSf, poly(phenylene oxide) (PPO), chlorosulfonic acid, & MPD/TMC polyamide	Phase inversion, chemical modification, & IP	(Zhou et al. 2014)
PRO	Polyimide & MPD/TMC polyamide	Phase inversion & IP	(Cui et al. 2014)
PRO	Polyetherimide (PEi) & MPD/TMC polyamide	Phase inversion & IP	(Li et al. 2015b)
PRO	PVDF on PET fabric & MPD/TMC polyamide	Phase inversion & IP	(She et al. 2016)
PRO	PSf on PET fabric & MPD/TMC polyamide	Phase inversion & IP	(Yip et al. 2011a)
PRO	PAN on PET fabric, NaOH, HCl, & MPD/TMC polyamide	Phase inversion, chemical modification, & IP	(Zhang et al. 2013)
PRO	PBI, PAN, & polyhedral oligomeric silsesquioxane (POSS)	Phase inversion & chemical modification	(Fu et al. 2014)

2.5.3.2. Hollow fiber membrane

A hollow fiber membrane is a tubular-shaped membrane fabricated through a non-solvent-induced phase inversion process in a hollow fiber spinning instrument, as shown in Figure 2-7. A polymer solution is pumped through a spinneret, and a bore solution fluid is pumped through the inner tube of the spinneret, causing a hole in the middle of the fiber. Afterwards, the fiber is soaked in a coagulation solution (Clausi et al. 2000). Hollow fibers have higher surface area per module, higher mechanical strength, and higher modular applicability than most flat sheet membranes (Peng et al. 2012). However, hollow fiber spinning as FO and PRO membranes fabrication methods has a number of challenges, such as limitation of polymeric materials which can be used, use of hydrophilic and robust materials, and optimization of phase inversion procedures to achieve hollow fiber membranes with improved mechanical strength, membrane permeability and selectivity, while maintaining a low structural parameter (Peng et al. 2012). Furthermore, hollow fiber modulation proves to be a challenge due to the small internal diameters of the modules, which results in fouling and clogging. Performance of hollow fiber membranes depends largely on the mechanical strength of the hollow fiber substrates and the selectivity of the active layer, for both inner- or outer-selective hollow fiber membranes. Most studies involving hollow fiber membranes make use the inner-selective hollow fiber due to ease in fabrication and modulation. Selective layers produced on inner or outer hollow fiber substrates for FO and PRO applications are presented in Table 2-3. There is a continuous struggle in the IP process to prepare outer-selective hollow fibers, due to non-uniformity of the active layer (Han et al. 2015). Another method to prepare hollow fiber membranes is dry-jet wet spinning, wherein the melted polymer is extruded at high pressure conditions, prior to coagulation. The fiber is then washed and dried before it is again heat-treated. This method is done to prevent the formation of microvoids on the fibers (Han et al. 2013a, Luo et al. 2014, Wang et al. 2009).

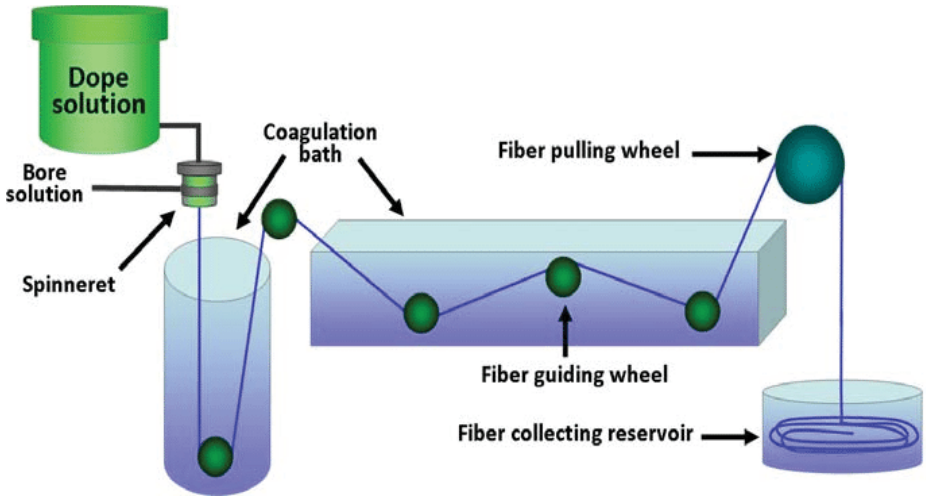

Figure 2 - 8. A schematic diagram of the phase inversion spinning process for hollow fiber membrane fabrication (Alsvik et al. 2013a)**.**

As previously mentioned, cellulose-based polymers are among the most frequently used polymers for phase inversion membranes. Cellulosic membranes have double-skin layers which are effective in the reduction of ICP within the support layer of the membrane (Zhang et al. 2010). However, performance of membranes for engineered osmosis has been largely inconsistent, since the cellulosic membrane performance is highly dependent on the interaction between the casting substrate and cellulosic polymer during the phase inversion process (Zhang et al. 2011). A previous study involving a double-skinned CA hollow fiber membrane performed thermal annealing after phase inversion, resulting in a thick outer skin, which effectively reduced concentration polarization and produced higher water flux (Su et al. 2012). One advantage of cellulosic polymeric membranes is the high biodegradability; the high biodegradability of CTA has led to reduced shelf life of CTA membranes, thereby limiting its use and applicability for long-term processes (Cath et al. 2006). Aside from the biodegradability of cellulosic polymers, specifically CTA, cellulosic membranes are highly vulnerable to biofouling and hydrolysis (Zhang et al. 2010).

Table 2 - 3. Hollow fiber supports for FO and PRO membranes using hollow fiber spinning.

Osmotic Process	Materials	Fabrication Method	Reference
FO	CA	Dry-jet wet spinning & chemical modification	(Su et al. 2012, Su et al. 2010)
FO	Polyamide-imide (PAI) & polyethyleneimine (PEI)	Phase inversion & chemical modification	(Setiawan et al. 2011)
FO	PAI, PEI, & polystyrene sulfonate sodium (PSS) salt	Phase inversion & chemical modification	(Setiawan et al. 2012)
FO	Polybenzimidazole (PBI)	Phase inversion	(Wang et al. 2007)
FO	PBI & *p*-xylylene dichloride	Dry-jet wet spinning & chemical modification	(Wang et al. 2009)
FO	PBI, PES, & PVP	Phase inversion	(Yang et al. 2009a, b)
FO	PES & MPD/TMC polyamide	Phase inversion & IP	(Chou et al. 2010, Han et al. 2017, Shi et al. 2011, Sukitpaneenit et al. 2012a, Wang et al. 2010b)
FO	PAI, PEI, & MPD/TMC polyamide	Phase inversion, chemical modification, & IP	(Fang et al. 2012)
FO	Polyimide & MPD/TMC polyamide	Dry-jet wet spinning & IP	(Luo et al. 2014)
FO	Polyketone & MPD/TMC polyamide	Phase inversion & IP	(Shibuya et al. 2017)
PRO	PES, [2-(methacryloyloxy) ethyl]dimethyl-(3-sulfopropyl)ammonium hydroxide (DMAPS), 2-methacryloyloxyethyl phosphorylcholine (MPC), & 2-metacryloyloxyethyl lipoate (MEL)	Phase inversion & chemical modification	(Cai et al. 2016)
PRO	PES & MPD/TMC polyamide	Phase inversion & IP	(Cheng et al. 2016)
PRO	PES & MPD/TMC polyamide	Phase inversion & IP	(Chou et al. 2012b)
PRO	PES & MPD/TMC polyamide	Dry-jet wet spinning & IP	(Han et al. 2013c)
PRO	PES & MPD/TMC polyamide	Phase inversion & IP	(Han et al. 2017)

Osmotic Process	Materials	Fabrication Method	Reference
PRO	PEi & MPD/TMC polyamide	Phase inversion & IP	(Le et al. 2016)
PRO	PEi, MPD/TMC polyamide, & 3-aminopropyltrimethoxy silane (APTMS)	Phase inversion, IP, & chemical modification	(Zhang et al. 2016a)

2.5.3.3. Electrospun nanofiber membrane

Electrospinning is the process of application of a polymer solution driven by electrical potential, causing the polymeric solution to form fibers which are collected on a collector of lower electrical potential (Ramakrishna et al. 2005), as shown in Figure 2-8. The nonwoven nanofiber mat produced after electrospinning should display high porosity. Electrospinning itself is a very versatile technique, and has various applications, not only in preparation of membranes for water treatment and osmotic processes, but also in medical and separation industries (Sahebi 2015). Nanofiber membranes, as the substrate of TFC membranes for both FO and PRO applications, provide remarkable benefits such as low tortuosity, high porosity with interconnected open channels, and thin membrane thickness (Kim et al. 2015).

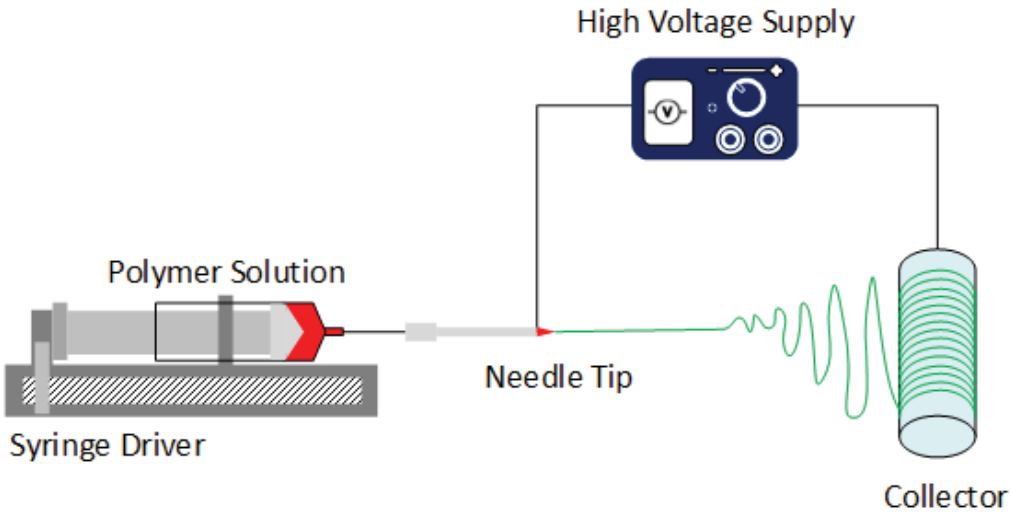

Figure 2 - 9. A schematic diagram of the electrospinning process.

2.5.3.4. TFC membranes

An important issue for preparation of membranes for engineered osmosis is the reduction of *RSF* and ICP, as well as improvement of water flux, and various methods in fabrication of phase inversion membranes have been done to address this issue. This has led to the fabrication of TFC membranes, wherein a thin active layer of the membrane is prepared on the support layer. TFC membranes are prepared by two steps: (1) the fabrication of the membrane support, and (2) formation of the active layer on top of the membrane support. Due to this, both the support and active layers can be modified and controlled separately, for more effective membrane fabrication.

TFC membranes generally show high performance; however, these membranes are susceptible to compaction due to pressure, especially for PRO and PAO. It has been observed that when higher pressures are applied, compaction occurs more often, resulting in lower porosity and performance.

TFC membranes are composed of layered materials, whose specific purpose is to improve water flux and selectivity for desalination and water purification processes. Most TFC membranes have three layers: a non-woven polyester mesh for support, on which a porous support layer was cast, and a thin PA selective layer on top (Tiraferri et al. 2011b). A combination of more than one method is conventionally investigated to fabricate composite membranes, wherein the membrane support and active layers were formed via different methods. The support layer (polymer casted on mesh) is prepared normally by phase inversion, while the selective PA layer is prepared by interfacial polymerization (Wei et al. 2011, Widjojo et al. 2013).

Hydrophilicity of the support layer is crucial in fabricating membranes for osmotic processes. Increased hydrophilicity can be achieved by the use of a hydrophilic polymer for the substrate, like PES, or by chemical modifications (Chung et al. 2015). Membrane support hydrophilicity was enhanced and higher water flux was observed (Widjojo et al. 2011a).

IP process is the coating of porous support layer with another set of polymeric substances, whose reaction happens on the interface of the support layer. It is the most common method used to fabricate TFC membranes. IP is commonly performed to produce a PA active layer, wherein two monomers are dissolved in two immiscible liquids such that the reaction between the two monomers occurs at the liquid-liquid interface (Alsvik et al. 2013a). The result is an ultrathin PA TFC membrane. In this process, the support membrane is first exposed in an aqueous amine solution. The excess amine solution is then removed by either air knife or application of pressure. The membrane is then treated with an organic acid halide solution for a short time for polymerization to occur. In previous membrane fabrication studies, the most extensively used combination of aqueous amine and organic acid halide solutions for IP is *m*-phenylenediamene (MPD) and trimesoyl chloride (TMC, or 1,3,5-benzenetricarbonyl trichloride), respectively (Wang et al. 2010a). Aside from MPD, the following can also be used as the amine for polyamide formation: *p*-phenylenediamine (PPD) (Li et al. 2012a), 2,2'-benzidinedisulfonic acid (BDSA), 2,6-diaminotoluene (2,6-DAT), and methylated MPD (Alsvik et al. 2013a). Aside from TMC, the following acid halides can be used to react with amines: 3,3,5,5-biphenyl tetra-acyl chloride (BTEC), isophthaloyl chloride (IPC), and terephthaloyl chloride (TPC) (Alsvik et al. 2013a).

The PA layer is the product of the reaction between an amine and an acid chloride. It is normally produced after IP, and is normally regarded as the active layer of most TFC membranes. The amine is usually dissolved in water while the acid chloride is dissolved in an organic solvent (Alsvik et al. 2013a). In recent studies, most PA active layers of TFC membranes are fabricated with MPD and TMC, as the amine and acid chloride, respectively (Kong et al. 2010, Sun et al. 2014). The thin film PA layer typically has a ridge and valley morphology, as shown in previous studies (Amini et al. 2013b). The surface roughness not only increases the hydrophilicity and water permeability, but also the ability for salt rejection.

PA formation via IP may be delivered onto readily available UF (Kong et al. 2010) or MF (Huang et al. 2013, Huang et al. 2015) membranes, which will then make the membranes applicable for engineered osmosis processes. However, most studies involving IP made use of phase-inversion membranes, both flat sheet (Cui et al. 2014, Klaysom et al. 2013b,

Li et al. 2015b, Liu et al. 2014b, Ong et al. 2015, Ren et al. 2016, Sahebi et al. 2017, She et al. 2016, Sun et al. 2014, Tiraferri et al. 2011b, Wang et al. 2012a, Wei et al. 2011, Wei et al. 2015, Yip et al. 2010, Yip et al. 2011a) and hollow fiber (Cheng et al. 2016, Chou et al. 2010, Chou et al. 2012b, Han et al. 2017, Le et al. 2016, Shi et al. 2011, Shibuya et al. 2017, Sukitpaneenit et al. 2012a, Wang et al. 2010b, Yasukawa et al. 2015b), as well as nanofibers (Bui et al. 2011, Huang et al. 2014, Pan et al. 2017, Puguan et al. 2014, Tian et al. 2014a, Tian et al. 2013).

2.5.3.5. Chemically-modified membranes

Chemical modification of membranes was first applied on the commercial CA FO membranes by thermal annealing (Gerstandt et al. 2008). While these membranes have better wettability due to the slight hydrophilicity of CA, and low *S* value due to thinness, they also have very low intrinsic water permeability and high salt permeability, resulting in very poor performance for engineered osmosis. Furthermore, due to the thin design of conventional FO membranes, they are easily damaged or deformed after the osmotic process performance, especially during PRO, wherein high pressure is applied. Thus, use of novel molecular designs of membrane materials and membrane morphology and modifications of the membranes are continuously performed to improve membrane strength and PRO performance. Addition of bulky polymers (Li et al. 2013b) and surfactants (Cui et al. 2014), or a molecular layer-by-layer IP approach (Choi et al. 2017), can be achieved to enhance the PA layer.

Layer-by-layer (LbL) assembly approach occurs through electrostatic forces which form covalent bonds between two materials (Johnson et al. 2012). LbL can be fabricated through numerous methods, such as dip-coating, spin-coating, or spraying. The following parameters can be controlled during LbL assembly: concentration of the polyelectrolytes, deposition time, ionic strength, and pH of the polyelectrolytes.

Another method in chemical modification of membranes is the incorporation of nanomaterials. Recent advancements in nanotechnology have showed a number of nanomaterials which can be used in preparation of novel membranes for engineered

osmosis. This has led to the development of thin film nanocomposite (TFN) membranes (Amini et al. 2013b).

2.5.3.6. Biomimetic membranes

Biomimetic membranes are membranes developed primarily to function like biological cell membranes to achieve high water permeability and specific selectivity towards water and solute particles (Shen et al. 2014). Most biomimetic membranes incorporated Aquaporins, a special type of proteins developed by Aquaporin (Denmark). The proteins are encapsulated in vesicles and are incorporated in the membrane substrate. These biomimetic membranes have shown satisfactory water flux and high salt rejection (Wang et al. 2013a, Wang et al. 2013b).

2.6. Membrane support modification for engineered osmosis

The porous membrane support layer in TFC membranes acts as the boundary layer for diffusion of water and solute particles in engineered osmotic processes. An ideal TFC membrane is semipermeable without the membrane support; however, the membrane cannot have an active layer without the membrane support. The membrane support layer provides the suitable thickness, strength and stability of the membrane, which the active layer alone cannot provide. However, the support layer may be detrimental to osmotic performance as it can potentially reduce the osmotic driving force across the membrane active layer (Yip et al. 2014). A number of porous polymeric materials can be used as a membrane support. Membrane support layers are mostly phase-inversion formed flat sheet, nanofiber, or hollow fiber, and each membrane type has its own modification procedure. Modification of the membrane support is now an important area of study in membrane fabrication, since modification can reduce the performance-retarding effects of ICP. Support layer modification is performed to reduce the limitations in the performance of engineered osmosis membranes.

The structure of an ideal support layer should be porous since it has a crucial role in the membrane's performance, especially in reduction of ICP (Wang et al. 2010a). It was also found that finger-like pores of the support layer are preferred over more commonly-

observed sponge-like pores, as it can withstand high pressures. Therefore membrane support modification is a good way to obtain the desired porosity and structure of the support layer. Also, a mixed structure support layer was found to be able to enhance FO membrane performance, in general (Tiraferri et al. 2011b). Through chemical modification, the structural characteristics of the support layer and the transport properties of the active layer can both be improved to develop and fabricate a high-performance FO TFC membrane.

Hydrophilic modification of the membrane support layer is a popular membrane modification for engineered osmosis membrane fabrications. Membrane support layer with hydrophilicity improvement was achieved by blending with hydrophilic sulphonated copolymers. The hydrophobic polymer blended with 50 wt% sulphonated polymer resulted in the formation of a fully sponge-like structure with improved hydrophilicity enhanced by the FO flux (Widjojo et al. 2011a). Furthermore, increasing the hydrophilicity of the membrane support layer is a more effective method to eliminate ICP than decreasing membrane thickness (Yu et al. 2011). As the hydrophilicity of the membrane is increased, water flux can be improved without likewise increasing *RSF*.

2.6.1. Hydrophilic nanomaterials as a filler

Incorporation of nanomaterials in polymeric membranes are one of the promising technologies to improve the membrane performances for water treatment applications which could overcome the trade-off relationship between a membrane's permeability and selectivity (Yin et al. 2015). In particular, hydrophilic nanomaterials use as a filler of membrane substrates can improve overall membrane porosity including surface and bottom open pore structures, hydrophilicity and average pore size distributions, thus improving water permeability (Yin et al. 2015). Some studies have focused on antifouling improvement with enhanced negative charge, surface roughness and hydrophilicity via the polymer solutions blended with hydrophilic nanomaterials. Figure 2-9 illustrates the nanocomposite membranes for TFC membranes modified by nanomaterials embedded in the support layer or PA active layer. The membrane supports were incorporated with various materials, such as silicon dioxide (SiO_2) (Song et al. 2013), titanium dioxide (TiO_2) nanoparticles (Emadzadeh et al. 2014b), zeolites (Ma et al. 2013), graphene oxide

(GO) (Morales-Torres et al. 2016, Wang et al. 2015), and carbon nanotubes (CNTs) (Amini et al. 2013b), to improve the structural features of the support layer thereby also decreasing S as is presented in Table 2-4. These nanomaterials are also applied in the PA selective layer which refers to thin film nanocomposite (TFN) membranes (Table 2-5). Embedding of nanomaterials in the thin film dense layer like that composed of PA improved the hydrophilicity and surface charge density as well as porosity thus resulting in enhancement of the water permeability without sacrificing the separation efficiency (Lau et al. 2015).

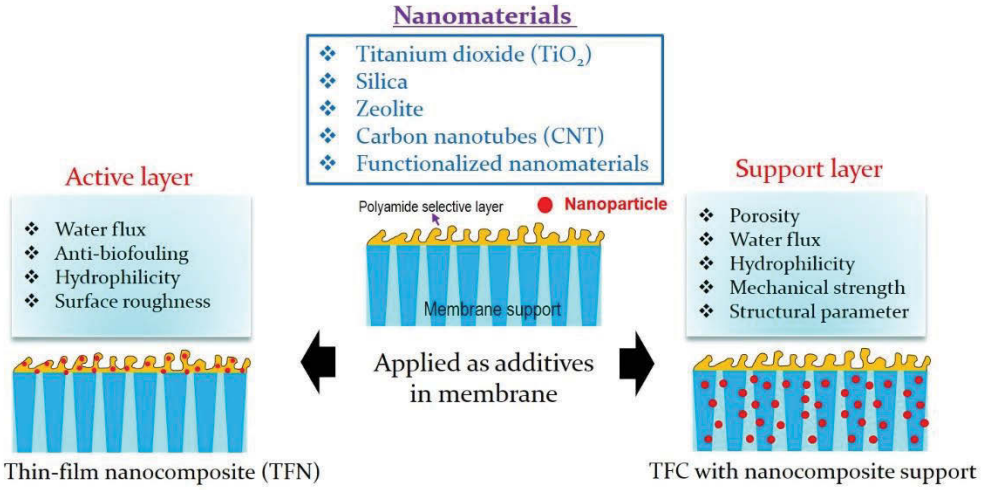

Figure 2 - 10. Nanocomposite membranes incorporated in membrane supports or in thin film layers for TFC membrane fabrications.

Table 2 - 4. TFC membranes fabricated with nanomaterials incorporated in membrane substrates.

Nanocomposite substrate		Selective layer	J_w [L m^{-2} h^{-1}]	J_s/J_w [g L^{-1}]	Orientation	Test condition	S value [μm]	Reference
Polymer	Filler/loadings							
PSf	Zeolite/0.5 wt%	PA	21	0.6	AL-FS	DS: 0.5M NaCl, FS: DI water	340	(Ma et al. 2013)
PSf	TiO_2/0.6wt%	PA	18.8	0.4	AL-FS	DS: 0.5M NaCl, FS: DI water	390	(Emadzadeh et al. 2014a)
PSf	TiO_2/0.5wt%	PA	17.1	0.17	AL-FS	DS: 0.5M NaCl, FS: 10 mM NaCl	420	(Emadzadeh et al. 2014c)
PAN	MOF_{C300}/1.0 wt%	PAH/PSS	107.4	≈0.17	AL-DS	DS: 0.5M $MgCl_2$, FS: DI water	190	(Lee et al. 2015b)
PSf	Silica	PA	31.0	0.24	AL-FS	DS: 1.0M NaCl, FS: DI water	169	(Liu et al. 2015b)
PES	CN-rGO/0.25wt%	PA	41.4	-	AL-FS	DS: 2.0M NaCl, FS: DI water	163	(Wang et al. 2015)
CA/CTA	Boehmite/0.5wt%	-	≈10	-	AL-DS	DS: 1.0M NaCl, FS: 10 mM NaCl	530	(Zirehpour et al. 2015)
PSf	HNTs/0.5wt%	PA	27.7	0.53	AL-FS	DS: 2.0M NaCl, FS: 10 mM NaCl	370	(Ghanbari et al. 2016)
PSf	$CaCO_3$/7.5wt%	PA	17.0	≈2.7	AL-FS	DS: 2.0M NaCl, FS: DI water	796	(kuang et al. 2016)
PSf	LDH-NPs/2wt%	PA	18.1	0.45	AL-FS	DS: 1.0M NaCl, FS: DI water	148	(Lu et al. 2016a)
PSf	LDH/GO/2wt%	PA	13.4	0.46	AL-FS	DS: 1.0M NaCl, FS: DI water	138	(Lu et al. 2016b)
PSf	MWf-TiO_2-M-P/0.5wt%	PA	20.3	0.66	AL-FS	DS: 2.0M NaCl, FS: DI water	-	(Morales-Torres et al. 2016)

Nanocomposite substrate		Selective layer	J_w [L m^{-2} h^{-1}]	J_s/J_w [g L^{-1}]	Orientation	Test condition	S value [µm]	Reference
Polymer	Filler/loadings							
PSf	Dual-GO/0.25wt%	PA	33.8	0.19	AL-FS	DS: 1.0M NaCl, FS: DI water	130	(Lim et al. 2017)
PES	GO/3.3 wt%	PVA	18.3	0.04	AL-FS	DS: 0.5M Na_2SO_4, FS: DI water	166	(Qin et al. 2017)

Table 2 - 5. TFN membranes fabricated via nanomaterials incorporated in selective layer.

Thin film nanocomposite		Support layer	J_w [L m^{-2} h^{-1}]	J_s/J_w [g L^{-1}]	Orientation	Test condition	Reference
Active layer	Filler/loadings						
PA	NaY zeolite/0.1wt%	PSf	30.7	≈0.2	AL-DS	DS: 1.0M NaCl, FS: 10 mM NaCl	(Ma et al. 2012)
PA	F-MWCNTs/0.1wt%	PSf	95	≈0.05	AL-DS	DS: 2.0M NaCl, FS: 10 mM NaCl	(Amini et al. 2013a)
PEI-PAI	MWCNT	PAI	12.5	0.34	AL-FS	DS: 0.5M $MgCl_2$, FS: DI water	(Goh et al. 2013)
PA	SiO_2/0.05wt%	PSf	36.5	0.04	AL-DS	DS: 2.0M NaCl, FS: 10 mM NaCl	(Emadzadeh et al. 2014a)
PA	Aquaporin/LPR 100	PES	55.2	0.08	AL-DS	DS: 0.5M NaCl, FS: DI water	(Li et al. 2015a)
PA	GO	PES	13.2	-	AL-FS	DS: 0.25M trisodium citrate, FS: DI water	(Jin et al. 2017)
PA	GO/0.1wt%	PSf	34.7	0.13	AL-DS	DS: 1.0M NaCl, FS: DI water	(Shokrgozar Eslah et al. 2017)
PA	PVP-GO/0.0175-0.02wt%	PSf	33.2	≈1.25	AL-DS	DS: 2.0M NaCl, FS: 10 mM NaCl	(Wu et al. 2017)
PA	Ag-MOF/0.04wt%	PES	82	-	AL-DS	DS: 2.0M NaCl, FS: DI water	(Zirehpour et al. 2017)

2.6.1.1. Silicon dioxide and silica

PAN mixed with tetraethylorthosilicate (TEOS) was used as the dope solution for nanofiber formation via electrospinning, with PET as the support fabric (Song et al. 2013). It was then coated with PVA, crosslinked with glutaraldehyde, and proceeded with IP. Treatment with TEOS forms silicon dioxide (SiO_2) nanoparticles mixed with the polymeric substrate. The resultant membrane was observed to have an interconnected fibrous structure, high porosity, low tortuosity, and high hydrophilicity, facilitating water permeability and avoiding ICP.

SiO_2 nanoparticles were first extracted from rice husk via a hydrothermal reaction. The extracted SiO_2 nanoparticles were then dispersed in PVDF solution. The SiO_2-incorporated PVDF solution was made into nanofibers via electrospinning and a PA active layer was formed through IP (Obaid et al. 2015a). Not only does this study show that incorporation of SiO_2 nanoparticles improves the water permeability, salt rejection, and porosity of the nanofiber-supported TFN membrane, but it also shows that this method can also be applied even with electrospinning. The same research group applied the same procedure with another polymer, PSf, in a separate study (Obaid et al. 2015b).

Commercially-available silica nanoparticles were used as a filler for polyetherimide (PEi) which was made into nanofiber support, on which PA was formed via IP (Tian et al. 2017). The resultant membrane was observed to have excellent pore size, porosity, structural parameter, water flux and mechanical strength, such that the membrane was found to have less compaction after FO operation.

2.6.1.2. Titanium dioxide

TiO_2 was mixed with PSf dope solution, which was used to produce flat sheet membranes via phase inversion, prior to IP (Emadzadeh et al. 2014a, Emadzadeh et al. 2014b). Both studies found that TiO_2 enhanced both hydrophilicity, overall porosity, and surface roughness of the membrane, resulting in an increase in water permeability. In another study, TiO_2 was also dispersed in PSf solution, which was used as the dope for electrospinning, prior to IP, to produce a nanofiber-supported TFN membrane, with

improved hydrophilicity, porosity and pore size, compared to a pristine PSf nanofiber-supported membrane (Zhang et al. 2017a).

Carbon-TiO_2 composites were synthesized by liquid phase deposition of TiO_2 onto multi-wall CNT or GO nanoparticles. The carbon-TiO_2 composites were dispersed in PSf and flat sheet membranes support was produced via the non-solvent induced phase separation (NIPS) method, prior to IP (Morales-Torres et al. 2016). Improved performance was observed due to the presence of more elongated and straight finger-like porous structure and enhanced hydrophilicity.

2.6.1.3. Zeolite

Porous zeolite nanoparticles with the size of 40-150 nm were incorporated in PSf substrate or in PA selective layer to improve FO performance by controlling ICP in FO (Ma et al. 2012, Ma et al. 2013). The addition of zeolite increased overall surface porosity and hydrophilicity, and decreased the structural parameter significantly, therefore reduced ICP in the support layer resulted in dramatically improved FO water flux. Zeolite nanoparticle as a filler in the PA selective layer for RO application has been demonstrated in previous studies. An optimal loading of zeolite in the PA layer possessed superior water permeability while maintaining salt separation ability due to the increase of PA layer porosity and hydrophilicity, which facilitated faster transport of the solvent. Likewise, zeolite embedded TFN FO membranes exhibited enhanced FO performance with high FO flux and low reverse salt flux.

2.6.1.4. Graphene oxide

GO nanosheets were synthesized by sonicating graphene oxide, and were mixed with PSf in a study which produced flat sheet membranes via phase inversion. The presence of GO showed higher water permeation and solute rejection, as well as reduction of ICP, due to the presence of hydrophilic GO. The same findings were observed for flat sheet FO membranes produced from PSf/GO mix via the NIPS method (Morales-Torres et al. 2016).

In another study, GO was first obtained via graphite oxide sonication, and subsequently reduced by cyanamide polycondensation with carbon nitride (C_3N_4). The cyanamide-GO nanosheets were then dispersed in a PES solution, which was then cast into flat sheet, prior to IP. The cyanamide-GO-incorporated PES FO TFN membranes showed improvement in water flux, due to lower structural parameter and reduction of ICP (Wang et al. 2015).

2.6.1.5. Carbon nanotubes

CNTs were dispersed in PSf solution and casted simultaneously with plain PSf to form double-skinned TFN membranes (Song et al. 2015). The membranes demonstrated not only enhancement in water flux, but also remarkable antifouling capacity, due to the fouling resistant property of CNTs.

Multi-walled CNTs were functionalized with carboxyl groups prior to dispersion into a PEi solution prior to electrospinning and IP, to form a nanofiber-supported PRO membrane with ultrathin PA layer (Tian et al. 2015a). The resultant membrane had a thin fine nanofiber reinforced with the functionalized CNTs, which allowed it to endure a trans-membrane pressure of up to 24 bars and generate a power density of around 17 Wm^{-2}.

Pristine and nitrate-functionalized multi-walled CNTs (by reaction with nitric acid) were blended in PSf, which was casted via NIPS into flat sheet, before IP (Morales-Torres et al. 2016). Those containing the functionalized CNTs were found to be more hydrophilic, thus they have higher water permeation than those with pristine CNTs.

Multi-walled CNTs were suspended in concentrated sulfuric acid and nitric acid (3:1 v/v) to oxidize the CNTs and produce carboxylated CNTs. The carboxylated CNTs were then dispersed in PES solution, which was used for flat sheet membrane fabrication via phase inversion (Wang et al. 2013c). Addition of the carboxylated multi-walled CNTs resulted in the formation of a finger-like porous structure, better tensile strength and water permeability.

2.6.1.6. Others

PAN flat sheet support layer formed via phase inversion was modified with the use of PBI and polyhedral oligomeric silsequioxane (POSS) as its selective layer (Fu et al. 2014). POSS was first dispersed in a PBI solution prior to casting to form a dual layer flat sheet PRO membrane. POSS provided the PBI substrate with a higher permeate flux and mechanical strength, while avoiding delamination which was earlier observed with polyvinylpyrrolidone (PVP) treatment. The membranes with a PBI and POSS active layer were found to have increase in both water flux and *RSF*, albeit very minimally for the latter. This method was then applied to the production of hollow fiber membranes with PAN substrate and PBI/POSS outer selective layer.

2.6.2. Chemical modification

Chemical modification of membranes is done to specifically improve the water permeation and salt rejection performance of membranes. Aside from incorporation of nanomaterials, chemical modification can also be performed with coating of the membrane supports in another chemical agent.

2.6.2.1. Coating materials

Coating with another chemical agent is the easiest way to modify the membrane support layer. Countless agents and combinations may be used for this purpose. For example, two previous studies coated commercial membranes with polydopamine (Arena et al. 2014, Lay et al. 2012), to increase the water flux almost twice as much.

Most membrane support layers are formed from hydrophobic polymeric materials, and one way to induce hydrophilicity on the membrane support layer is by coating it with hydrophilic materials. PAN nanofibers produced by electrospinning was coated with PVA and crosslinked with glutaraldehyde to increase the hydrophilicity and improve water flux during PRO operation in a particular study (Song et al. 2013).

Hollow fiber membranes can also be modified with chemical agents. A previous study coated a polyamide-imide (PAI) hollow fiber with an ionic substance, polyethyleneimine (PEI), to make the surface charge positive. The positive surface of the membranes was able to reduce RSF by supplying electric repulsions through the membranes (Setiawan et al. 2011). This study was further expanded to deposition of an ionic bilayer on the PAI hollow fiber, wherein it was first coated with cationic PEI, followed by anionic polystyrene sulfonate sodium (PSS) (Setiawan et al. 2012). This method further developed by the same research group, wherein hollow fiber membranes with double-skin layers were produced. One skin layer is the PA layer from MPD and TMC, and the other is the PEI layer, providing the outer layer of the hollow fiber with a positive charge. This resulted in a mechanically-stable membrane which minimizes ICP effect and mitigates scaling (Fang et al. 2012).

PEi hollow fiber membranes were first fabricated by dry-jet wet spinning and the hollow fibers underwent IP with MPD and TMC to form a hollow fiber TFC for PRO. The hollow fiber TFC was then immersed in a solution containing 3-aminopropyltrimethoxysilane (APTMS) to form APTMS-grafted TFC PEI hollow fiber membranes. Aminosilanes such as APTMS can modify both the support layer and the selective layer of the PRO membranes by providing remarkable hydrophilicity and minimization of pore-blockage, without sacrificing structure parameter and mechanical strength (Zhang et al. 2016a).

PBI hollow fiber membranes were initially fabricated using the phase inversion method and were observed to demonstrate high water flux and salt rejection, as well as high stability and mechanical strength (Wang et al. 2007). The same research group modified the PBI hollow fiber membranes by crosslinking with p-xylylene dichloride, resulting in a membrane with enhanced water flux and salt rejection (Wang et al. 2009).

Another study involved the fabrication of the PES flat sheet membrane, which was treated with 1,3-dioxolane and polyvinylpyrrolidone (PVP). The resultant membrane showed high performance for FO, due to increased porosity with a finger-like structure and nano-sized pores. Also, *RSF* was minimized by maintaining thinness of the membrane (Yu et al. 2011).

PES hollow fibers were grafted with the following zwitterionic polymers: [2-(methacryloyloxy)ethyl]dimethyl-(3-sulfopropyl)ammonium hydroxide (DMAPS), 2-methacryloyloxyethyl phosphorylcholine (MPC), & 2-metacryloyloxyethyl lipoate (MEL), to form hollow fiber membranes for PRO (Cai et al. 2016). The antifouling capacity of the membranes was dramatically improved, and osmotic power generation and water permeation was also enhanced.

2.6.2.2. Functionalization

PSf was sulfonated prior to use in fabrication of a TFC FO membrane which showed better performance when compared to the membrane prepared from non-functionalized PSf (Ren et al. 2016, Wang et al. 2012a).Sulfonated polyphenylenesulfone was used as the polymer, which involved the use of non-solvent induced phase separation (NIPS) prior to PA formation via IP (Han et al. 2016). This membrane has outstanding hydrophilicity and thickness, thus the membrane's structural parameter is low, resulting in excellent water permeability and salt selectivity.

A sulfonated co-polymer of PES and polyphenylsulfone (PPSU) is extremely hydrophilic and is known to precipitate very slowly, thus it was mixed with plain PES to prepare the substrates for FO TFC membranes (Widjojo et al. 2011a). The presence of the sulfonated co-polymer resulted in a sponge-like pore structure, while the membrane without the sulfonated co-polymer was found to exhibit finger-like structures. The sulfonated polymer then is integral to the formation of a macrovoid-free structure, enhanced hydrophilicity, and good water permeability. Also, the membranes showed good long-term membrane stability due to the anti-fouling properties of the sulfonated co-polymer. This study was further improved by the same research group, wherein another sulfonation reaction was performed, with the use of a 3,3'-di-sodiumdisulfate-4,4'-dichlorophenyl sulfone (sDCDPS) polymer. The new functionalization method resulted in an even more hydrophilic sulfonated co-polymer. Membrane support layer from the mixture of this co-polymer with PES resulted in excellent water permeability, improving water flux to 54 $Lm^{-2}h^{-1}$, from 33 $Lm^{-2}h^{-1}$ of their previous study (Widjojo et al. 2013).

Sulfonated poly(ether ketone) (SPEK) was synthesized in another study and mixed with PSf prior to flat sheet casting via phase inversion and the subsequent IP (Han et al. 2012b). The results of this study was that the SPEK helped achieve a fully sponge-like structure on the membrane support layer while enhancing both membrane hydrophilicity and structure parameter. The hydrophilicity and thinness of the membrane resulted in high water flux in FO and reduction of ICP.

Poly(phenylene oxide) (PPO) was sulfonated with chlorosulfonic acid and mixed with PSf to make membrane substrates for a TFC FO membrane (Zhou et al. 2014). The sulfonated PPO contained immobilized Na^+ ions, which served as counter ions, improving water transport across the membrane.

Hydrophilic materials may be used to prepare the membrane support; however, the hydrophilic materials should be crosslinked to make sure it will be able to withstand exposure to water without dissolution. Polyvinyl alcohol (PVA) nanofibers were used as the substrate in TFC membranes, and crosslinking with glutaraldehyde was performed prior to IP (Puguan et al. 2014).

2.6.2.3. Metal-organic framework

Metal-organic frameworks (MOF) are compounds that consist of metal ions coordinated to organic ligands to form multi-dimensional structures. These polymeric materials have high porosity, thus they can be used in the fabrication of engineered osmosis membranes. MOF-based mixed matrix membranes have been developed with the dispersion of MOF particles in an organic solvent and mixed with polymer, followed by casting the solution via phase inversion (Zornoza et al. 2013).

In a recent study, PAN dope solution mixed with the following MOF, aluminium terephthalate, copper benzene-1,3,5-tricarboxylate, and iron benzene-1,3,5-tricarboxylate, as membrane substrates was first introduced for FO application (Lee et al. 2015a). In this study, membrane substrate with high porosity with significantly enhanced water permeability was observed due to its enhanced tortuosity with the presence of MOF in

membrane support (Figure 2-10). ICP was also controlled and mitigated with the use of MOF in the membrane substrate. Later, a different type of MOF called UiO-66 was introduced to prepare nanocomposite membrane substrate for FO application (Ma et al. 2017). Various loadings of UiO-66 were applied to investigate the effect of nanomaterial in changes to membrane characteristics. This study observed that polymer dope solution mixed with UiO-66 changed the thermodynamic properties and kinetic condition, thus inducing a faster solvent-nonsolvent exchange rate that resulted in changing the top surface morphologies. These changes consequently provided the favourable conditions of a high permeable PA selective layer and improved FO water flux.

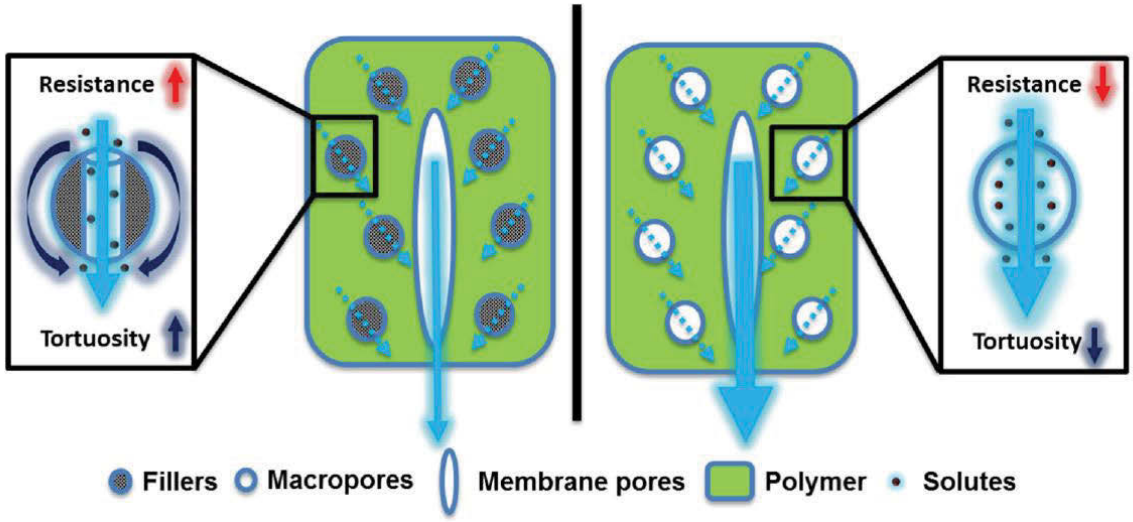

Figure 2 - 11. Schematic diagram of the importance of water transport through the macropores inside the MOF-based membrane substrate, which provide additional pathways for water molecules to pass through the support layer with lower resistance and shorter tortuosity (Lee et al. 2015b).

2.6.2.4. Other membrane supports with chemical modification methods

A flat sheet silica-PSf mixed matrix substrate membrane was fabricated by dispersing silica onto a PSf solution prior to casting and IP (Liu et al. 2015a). The membranes produced were found to have a layered configuration which helped mitigate ICP, and were observed to demonstrate improved water flux and salt rejection, compared to plain PSf membranes.

FO membranes with unprecedented water flux of 94 L m^{-2} h^{-1} were fabricated via bidirectional freezing of PVDF and DMSO, such that vertically-oriented porous substrates were produced (Liang et al. 2017). These membranes with vertically-oriented porous substrates have low structure parameter, thus reduction of ICP was observed.

A sacrificial layer approach was employed in a previous study (Xiao et al. 2015). PEI was co-casted beneath a PSf support layer, and after peeling off the PEI layer, the membrane support obtained an open-bottom structure, prior to IP. This method produced a membrane with lower structural parameter than the normal double-layer casting of PSf/PEI membrane.

2.7. Modification of selective layer for TFC membranes

Most membranes used for engineered osmosis are asymmetric membranes, whose thin selective layer is on top of the highly porous hydrophilic membrane support. This is mostly the case for TFC membranes, which have shown remarkable solute rejection and superior water flux (Wang et al. 2010a). Modification of the selective layer of TFC membranes not only improves both water flux and solute rejection, leading to better osmotic performance, but may also enhance mechanical strength, stability, and fouling capacity (Amini et al. 2013b).

2.7.1. Hydrophilic nanomaterials as a filler

Aside from the incorporation of hydrophilic nanomaterials in the support layer, nanomaterials can also be incorporated into the PA active layer to fabricate novel membranes for engineered osmosis. The nanomaterials are incorporated to enhance the permeability, selectivity, mechanical strength, and anti-fouling capacity of the TFN membranes.

In one study, multi-wall CNTs were functionalized with amino groups and were dispersed in the MPD solution via sonication and stirring prior to IP (Amini et al. 2013b). Not only was the surface hydrophilicity drastically improved, the TFN membranes exhibited high water permeability and satisfactory salt rejection, even only with 0.01 wt% of amine-functionalized multi-wall CNTs.

2.7.2. Modified techniques for IP reaction

One technique performed to modify IP is the use of a layer-by-layer configuration for TFC membranes (Choi et al. 2017). This approach results in membranes with high salt rejection, high water flux, good mechanical strength, and reduced incidence of fouling. Double-blade cast membranes were prepared to keep the membrane active layer intact for salt rejection in a previous study to address RSF and ICP issues (Liu et al. 2014b). PAN nanofibers were coated first with PEI, prior to IP to form nanofiber-supported TFC

membranes for PRO which could withstand applied hydraulic pressure up to 11.5 bars (Bui et al. 2014).

Synthesis of organic-inorganic TFC membranes was performed by involving PEi hollow fiber membranes (Zuo et al. 2013). Organic-inorganic hybrid amine monomers were synthesized from hyperbranched PEI and 3-glycidyloxypropyltrimethoxysilane (GOTMS). IP was proceeded with the use of plain hyperbranched PEI or the PEI-GOTMS hybrid amine monomer as the amine and TMC as the acid halide.

PVDF nanofibers were produced via electrospinning, and it was used for IP twice, once for surface modification, and the other for PA selective layer formation, to form a nanofiber-supported TFC membrane for PRO (Huang et al. 2016). Both IP methods made use of two different sets of amine and acid halide pairs. The PVDF nanofibers were modified via IP with 1,6-hexamethylene diamine and adipoyl chloride to form nylon 6,6 on the nanofiber mat surface. The modified nanofiber mat was then used as the substrate for IP with MPD and TMC. The membranes exhibited excellent flux and one of the lowest structural parameters in literature.

2.8. Membrane support fabrication for engineered osmosis membrane via electrospinning

Electrospinning is the process of application of a polymer solution driven by electrical potential, causing the polymeric solution to form nano-sized fibers (nanofibers) which are collected on a collector of lower electrical potential (Ramakrishna et al. 2005). The nonwoven nanofiber mat produced after electrospinning should display high porosity. Nanofiber-supported membranes exhibit higher porosity and lower tortuosity, making them suitable when applied in the FO process. Due to these reasons, electrospinning technique has become an attractive approach for engineered osmosis membranes fabrication. These characteristics of nanofiber-supported FO membranes can potentially lead to three to five times greater water flux due to the low ICP in nanofiber support layer, compared to conventional commercially-available phase inversion membranes (Bui et al. 2011, Song et al. 2011b).

Electrospinning, as a method, has the capacity to control fiber size, shape, morphology, and porosity of the nanofibrous membranes it produces (Tijing et al. 2014). The porosity of nanofibrous membranes provides direct routes for water and salt diffusion, thus it can be a good substrate or support for FO TFC membranes (Song et al. 2011b). A representation of nanofiber-supported FO TFC membrane is shown in Figure 2-11. Electrospun nanofibers can be further modified to improve hydrophilicity and selectivity.

Nanofibers in membrane fabrication literature are mostly used as the substrate for TFC membranes. A variety of polymeric materials can be used to form nanofibers, such as PAN (Pan et al. 2017), PSf (Bui et al. 2011), PES (Bui et al. 2011), CA (Bui et al. 2013a), PVDF (Huang et al. 2016, Tian et al. 2013), PVA (Puguan et al. 2014, Tian et al. 2014a), nylon 6,6 (Huang et al. 2014), and polyethylene terephthalate (PET) (Hoover et al. 2013, Tian et al. 2014a). FO and PRO membranes prepared via electrospinning are listed in Table 2-6.

Table 2 - 6. Electrospun nanofiber substrates for FO and PRO membrane fabrications.

Application	Materials	Performance	Reference
FO	PES nanofiber on PET nonwoven, post-treated at 220 ˚C & PA layer	J_w is 37.8 LMH (0.5 M NaCl as DS and DI water as FS) under AL-FS mode, high porosity (83%) resulted low S value of 80 μm.	(Song et al. 2011a)
FO	PAN/CA blend nanofiber on PET fabric & PA active layer	J_w (27.6 LMH) and J_s/J_w (0.14 g/L) under AL-FS mode (0.5 M NaCl as DS and DI water as FS), hydrophilicity increased with increase of PAN ratio, S value = 290.7 μm	(Bui et al. 2013a)
FO	Nylon 6,6 on PET fabric & PA layer via co-solvent assisted IP (CAIP)	J_w (21.0 LMH) and J_s/J_w (0.24 g/L) under AL-FS mode (1.0 M NaCl as DS and DI water as FS), S value = 315 μm, CAIP approach improved water permeability	(Huang et al. 2014)
FO	PVDF & PA active layer	J_w (28.0 LMH) and J_s/J_w (0.46 g/L) under AL-FS mode (1.0 M NaCl as DS and DI water as FS), S value = 315 μm	(Tian et al. 2013)
FO	PVA & PA active layer	J_w (27.24 LMH) and under AL-FS mode (0.5 M NaCl as DS and DI water as FS), S value = 66 μm, PVA nanofiber produced high porosity and hydrophilic substrate	(Puguan et al. 2014)
FO	Different ratios of PET/PVA & PA layer	J_w (47.2 LMH) and J_s (9.5 gMH) under AL-DS mode (0.5 M NaCl as DS and DI water as FS) when the ratio of PET/PVA is 1/4, increased PVA ratio improved hydrophilicity	(Tian et al. 2014a)
FO	Pei incorporated with f-CNTs & PA layer	J_w (33 LMH) and J_s/J_w (0.46 g/L) under AL-FS mode (0.5 M NaCl as DS and DI water as FS), S value = 310 μm, use of f-CNTs as a filler of PEi nanofiber improved porosity, mechanical property and reduced ICP effect	(Tian et al. 2015b)
FO	PAN nanofiber incorporated with SiO_2 & PA layer	J_w (≈ 48 LMH) and J_s/J_w (≈0.15 g/L) under AL-FS mode (1.0 M NaCl as DS and DI water as FS), S value = 65 μm, SiO_2 incorporation improved water channel and porosity.	(Bui et al. 2016)
FO	Surface modified PVDF nanofiber via nylon 6,6 coating	J_w (22 LMH) and J_s/J_w (0.17 g/L) under AL-FS mode (1.0 M NaCl as DS and DI water as FS), S value = 193 μm, modified membrane showed improved hydrophilicity and mechanical property, and prevented membrane swelling	(Huang et al. 2016)
FO	PEi nanofiber incorporated with SiO_2 & PA layer	J_w (42 LMH) and J_s/J_w (≈0.12 g/L) under AL-FS mode (1.0 M NaCl as DS and DI water as FS), S value = 174 μm, SiO_2 (1.6%) incorporation improved water channel and porosity (88%).	(Tian et al. 2017)

Application	Materials	Performance	Reference
PRO	PAN on PET fabric, PEI, & PA active layer	Best power density of 8.0 W m^{-1} at 150 psi (DS: 0.5 M NaCl, FS: DI water), high salt selectivity should be considered for further PRO performance improvement, S value = 273 μm	(Bui et al. 2014)
PRO	PAN/ SiO_2 via tetraethylorthosilicate (TEOS) addition, then PVA coating, & PA active layer	Highest power density of 15.2 W m^{-1} achieved at 15.2 bar (DS: 1.06 M NaCl, FS: 0.9 M NaCl), S value = 140 μm, improved mechanical strength and A value after PAN incorporated with SO_2 and PVA coating	(Song et al. 2013)
PRO	PEi incorporated with carboxyl-functionalized CNT, & PA layer	Optimized membrane revealed the power density of 17.3 W m^{-1} at 16.9 bar (DS: 1.0 M NaCl, FS: DI water), S value = 474 μm, designed dual-layered nanofiber support to control surface pore structure to endure high hydraulic pressure	(Tian et al. 2015a)

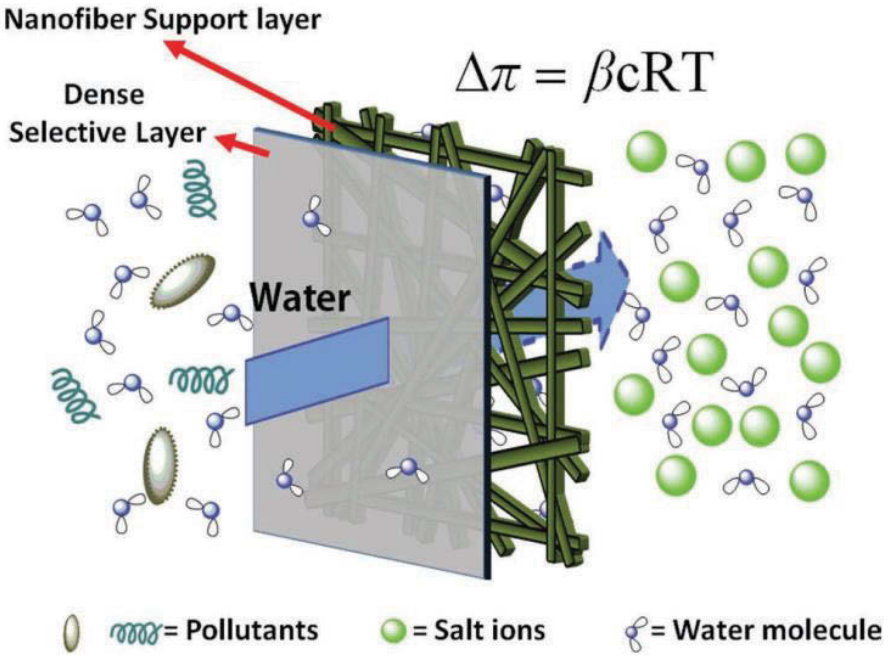

Figure 2 - 12. A schematic representation of a nanofiber-supported TFC-FO membrane (Song et al. 2011b).

An issue in the formation of nanofiber-supported membranes is the mechanical strength of the nanofiber mat. Most studies involving electrospinning utilized hydrophilic fabric, which may be woven or nonwoven, and mostly made of PET, as an additional support for the membrane nanofiber support (Bui et al. 2011, Bui et al. 2013a).

CHAPTER 3

MATERIALS AND METHODS

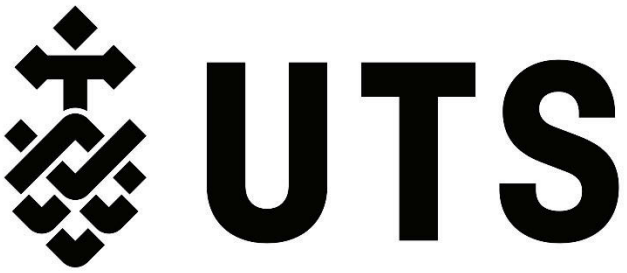

3.1. Introduction

Thin film composite (TFC) membranes were fabricated with novel approaches using various membrane preparation methods. Different types of membrane support layers such as flat-sheet, nanofiber and hollow fiber supports were prepared and modified to enhance the membrane performance. Membrane support layers for TFC forward osmosis (FO) membranes were fabricated via phase inversion and electrospinning methods to prepare flat-sheet and nanofiber membrane supports, respectively. TFC pressure retarded osmosis (PRO) membranes were prepared by hollow fiber membrane supports using hollow fiber spinning equipment.

All fabricated membranes including TFC membranes and membrane substrates were characterized. Intrinsic properties of TFC membranes such as pure water permeability (A), salt permeability coefficient (B) and structural parameter (S) were evaluated by RO performance experiments. Meanwhile, FO performance was assessed at different draw solution (DS) concentrations. In addition, FO and PRO performances such as water and salt fluxes were determined using respective membrane systems.

This chapter describes in detail the general experimental methods for lab-scale experiments in terms of fabrications and evaluations. More specific materials used in the studies and experimental details can be found in their respective chapters.

3.2. Preparation of TFC membranes

3.2.1. Flat-sheet TFC-FO membrane fabrication

3.2.1.1. Preparation of membrane supports

Flat-sheet membrane supports for TFC-FO membranes were prepared via a conventional phase inversion technique. Known polymer concentration was dissolved in an organic solvent with constant magnetic stirring. Then, all polymer solutions were de-gassed before membrane casting. Prepared polymer solutions were first poured on glass plates and then casted by a casting blade (Figure 3-1(A)) with the height of 150 μm using a casting machine (Figure 3-1(B)). The nascent films were immediately immersed in a water coagulation bath (30^{o}C) and then soaked in deionized water (DI) water for one day

to completely remove the residual solvents, followed by storage in the refrigerator at 4ºC before conduction of the interfacial polymerization (IP) process.

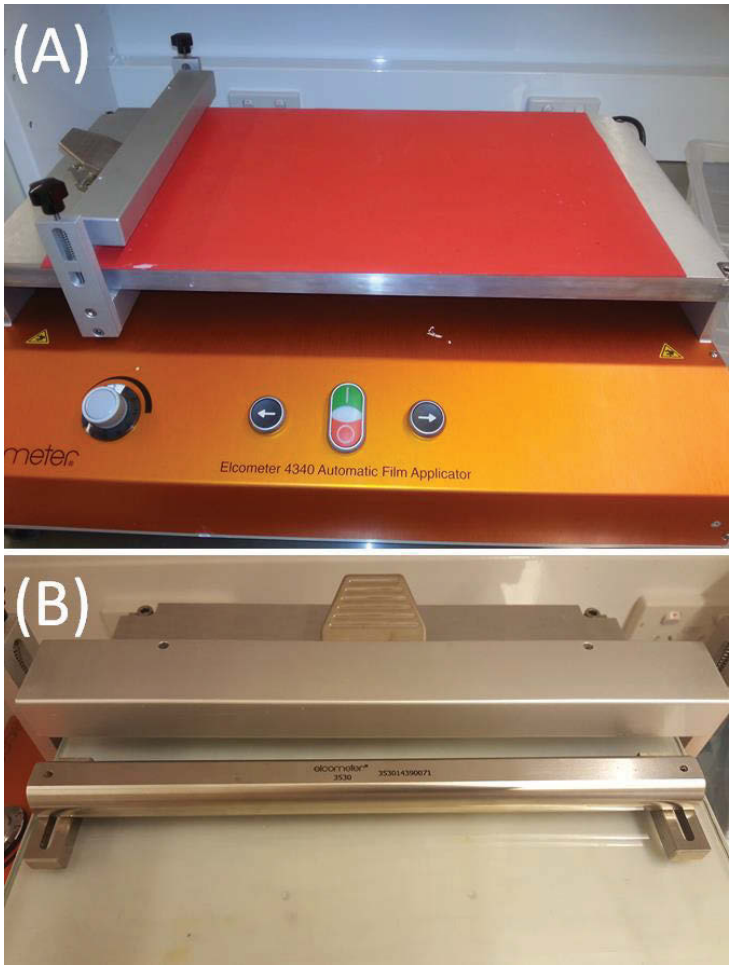

Figure 3 - 1. (A) Automatic film applicator (Elcometer 4340, Elcometer Aisa Pte Led) and (B) casting blade for flat-sheet membrane support fabrication

3.2.1.2. Thin film polyamide (PA) layer formation by IP process

The dense selective layer of PA was deposited on the flat-sheet membrane support layers by the IP process using 1,3-phenylenediamine (MPD) and trimesoyl chloride (TMC) monomers. Membrane substrates were first fixed in an acrylic frame, as shown in Figure 3-2, to allow the introduction of the monomer solutions only to one side of the membranes. An MPD aqueous solution of 50 mL was introduced on the membrane substrates for 2 min followed by the removal of excess MPD by an air knife. Then, TMC/n-hexane (50

mL) was reacted for 1 min. After the excess TMC solution was removed, the membranes were air-dried for 2 min and then cured at 100°C for 3 min.

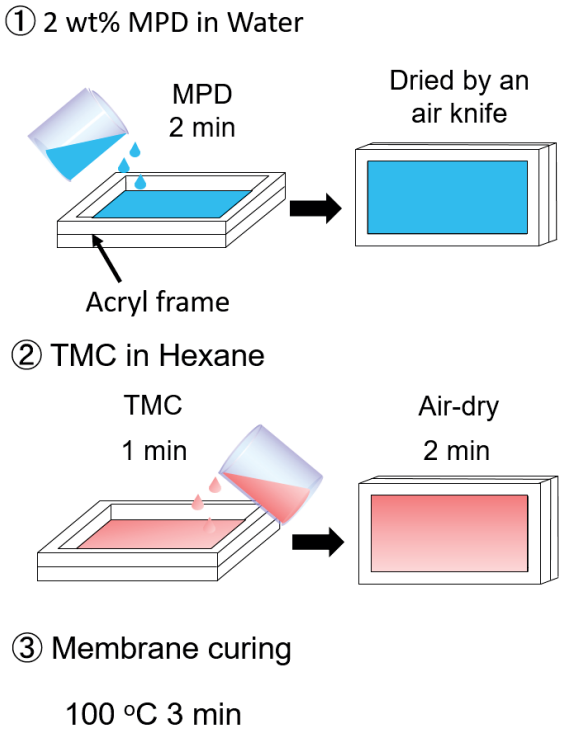

Figure 3 - 2. IP process for PA active layer deposition on the membrane supports.

3.2.2. TFC-FO membranes with electrospun nanofiber supports

3.2.2.1. Preparation of electrospun nanofiber supports

Electrospinning is a practical and inexpensive method for manufacturing nanofibers with high porosity, small diameter, high strength to weight ratio, and high surface to volume ratio. In addition, nanofibers fabricated via an electrospinning technique are known to exhibit low tortuosity as a function of the interconnected void spaces. Therefore, electrospun nanofiber supports were electrospun for TFC-FO membranes. Figure 3-3 represents the image of the electrospinning device used for nanofiber support fabrications. The electrospinning device is basically composed of syringe, needle, syringe pump, high voltage supplier (Max. 30 kV), and drum type collector as shown in Figure 3-3. First, various dope solutions were prepared by dissolving polymers in the mixtures of organic

solvents at known concentrations. The dope solution was transferred into a syringe, and delivered via a syringe pump at a constant volumetric flow rate throughout the nozzle. While producing the polymer solution to the nozzle, high voltage was applied to facilitate electrostatic repulsion of the dope solution and create nano-sized fibers, which were directly sputtered on a rotating drum roll-type collector with 50 rpm covered with aluminium foil. The distance between the needle and collector was fixed at 180 mm. The as-spun nanofiber membranes were peeled off from the aluminium foil and then dried in a drying oven at 50°C for 24 h to remove the residual solvents from the fibers. Prepared membranes were post-treated for each experimental purpose. More details are described in Chapters 6 and 7.

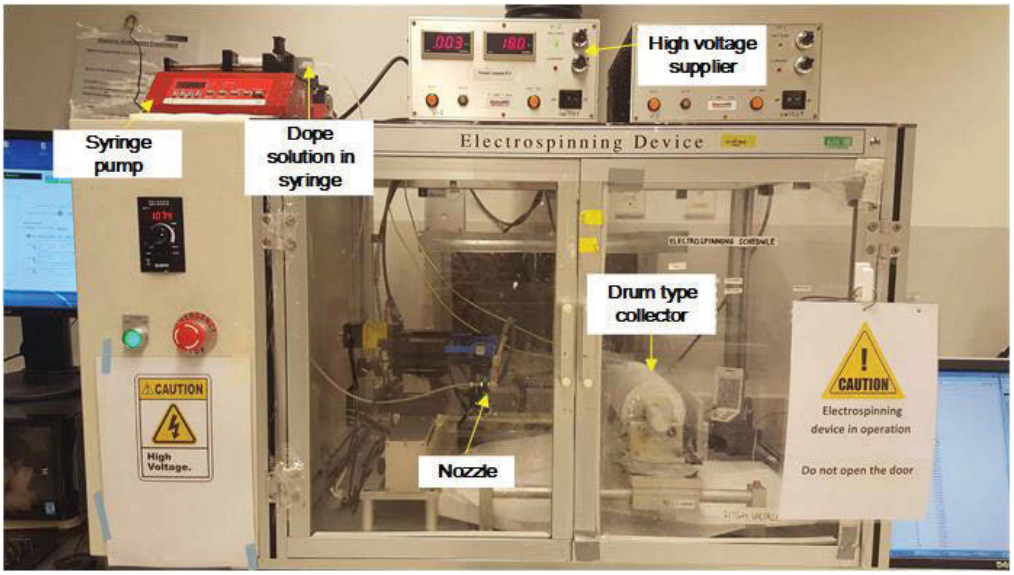

Figure 3 - 3. Electrospinning device for preparing nanofiber supports

3.2.2.2. IP process for TFC PA layer

Figure 3-4 describes the IP process on the electrospun nanofiber supports. The overall IP process for nanofiber supports is similar to that of the IP performed on flat-sheet membranes (in Section 3.2.1.2). However, electrospun nanofiber supports, due to its hydrophobicity and dried condition, were pre-wetted with isopropyl alcohol prior to the IP process. As described in Figure 3-4, MPD was first introduced only on one side of the substrates for a certain period and then the excess solution was removed by a rubber roller instead of using an air knife. This is because of the highly open structure of the nanofiber

surface which is very fragile when removing the MPD from the membrane surface; therefore using a rubber roller is deemed more suitable. Afterward, TMC in n-heptane was introduced to form a PA layer on the nanofiber supports for 1 min followed by air-dry for 2 min. Finally, the membranes were treated with an oven curing at 70°C for 10min.

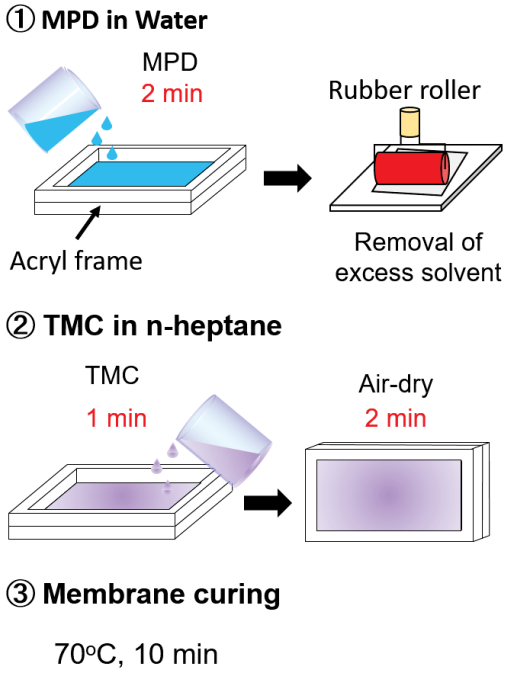

Figure 3 - 4. IP process for PA active layer deposition on the nanofiber supports.

3.2.3. Preparation of TFC-PRO membranes with hollow fiber membrane supports

3.2.3.1. Fabrication of hollow fiber support membranes

Polymer dope solutions for hollow fiber spinning were prepared in a glass reactor in Figure 3-5. The dope solution comprised of polymer, additives, and solvent, was prepared in a two-neck glass reactor stirred by a digital stirring machine equipped with a Teflon impeller. The temperature was at 70°C for 12 h and then cooled down with continuous stirring for another 12 h. Consequently, the prepared dope solutions were transferred into the syringe pump and then left for 24 h for degassing at room temperature prior to hollow fiber spinning.

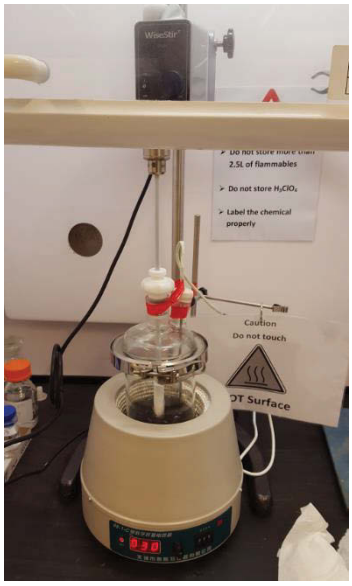

Figure 3 - 5. Preparation of polymer dope solutions for hollow fiber spinning

The hollow fiber support membranes for the TFC-PRO membranes were fabricated via a dry-jet wet phase inversion spinning process. Figure 3-6 represents the hollow fiber spinning machine used in this study. Generally, the dope solution and bore solution were simultaneously transferred to a nozzle by pumps and then quenched in a non-solvent coagulation bath to solidify the polymer solution via a non-solvent induced phase separation followed by the retrieval of the hollow fiber membranes. For desirable PRO membrane structure formation, a tri-orifice nozzle was adopted in this study as described in detail in Figure 3-7. The bore, dope and external solutions are simultaneously extruded through core, middle and outer channels of the spinneret, respectively, to obtain an hollow fiber membrane with a highly porous structure compared to the outer surface. In the spinneret, a quantitative volume of dope solution was delivered by a teledyne isco syringe pump (Teledyne Technologies Company, USA), and both bore and external solutions were delivered by gear pumps for low viscous solutions. Tap water was used as a coagulant and the as-spun hollow fiber membrane was collected to the winder without any tension. All spinning was performed at room temperature conditions such as bore, polymer and external solvent solutions including the coagulation bath. As-spun hollow fiber membranes were immersed in tap water for 2 days to remove residual solvents and then directly post-treated via soaking the membranes in 50 wt% glycerol aqueous solution for another 2 days. Subsequently, the membranes were dried in the air at room temperature conditions prior to modulation.

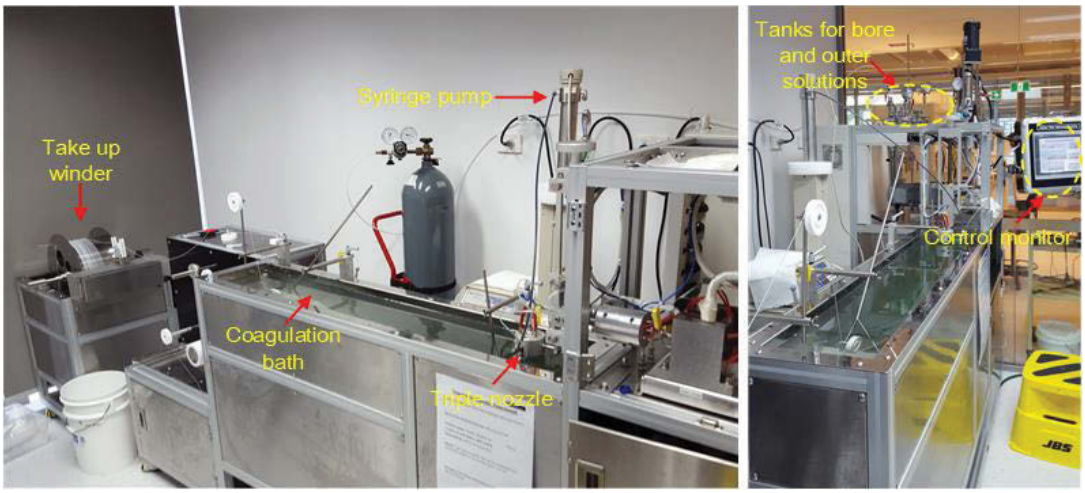

Figure 3 - 6. Spinning machine for hollow fiber support membranes fabrication.

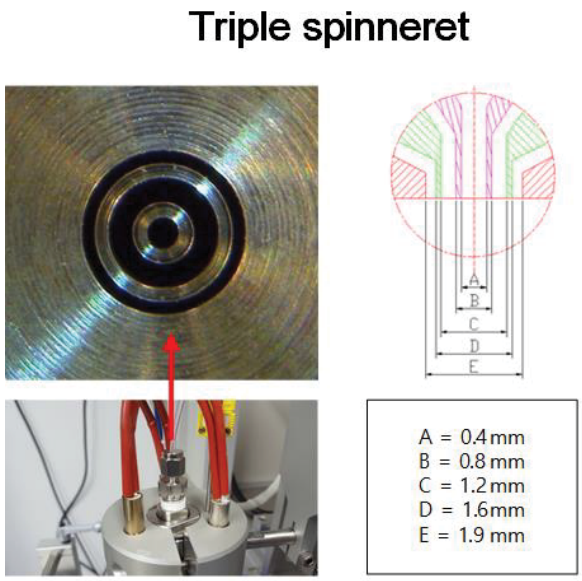

Figure 3 - 7. Specification of triple spinneret used for hollow fiber membranes fabrication

3.2.3.2. Formation of TFC PA layer via IP process

The post-treated hollow fiber membranes were modulated prior to the IP process. Five hollow fiber membranes were assembled into a mini-module as presented in Figure 3-8 (A) and then both ends were sealed with epoxy resin. Figures 3-8(B) and 3-8(C) show the setup for IP process and the schematic of IP process, respectively. The IP process for hollow fiber modules was conducted without pre-wetting of hollow fiber membranes. First, the module was held in a vertical position (Figure 3-8(B)) and the MPD aqueous

solution was introduced to the lumen side of hollow fibers from a bottom to top direction using a peristaltic pump with a flow rate of 4.1 mL/min for 3 min. Then excess MPD was removed by purging N_2 gas for 5 min at constant pressure of 0.1 bar. Afterwards, TMC solution was fed into the hollow fiber lumen side saturated with MPD at a flow rate of 2.3 mL/min for 5 min. Subsequently, residual TMC was purged by N_2 gas for 30 s then PA layer deposited hollow fiber membrane modules were submerged in DI water and stored in a refrigerator at 4°C prior to performance tests.

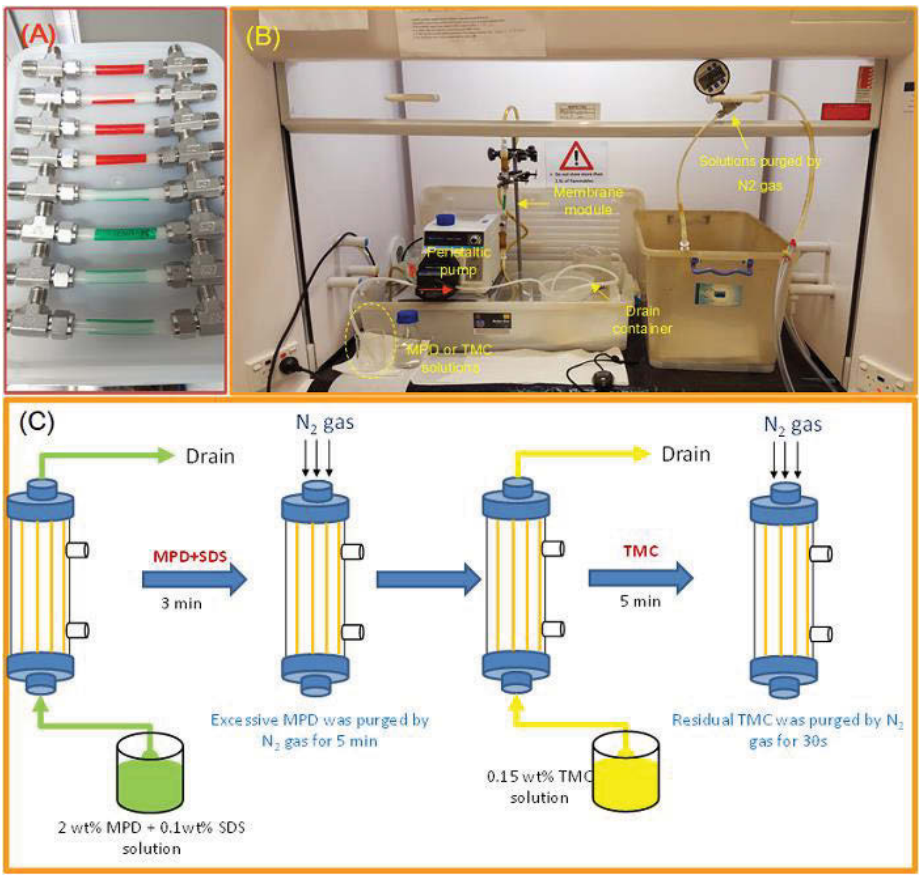

Figure 3 - 8. PA active layer formation on the lumen surface of hollow fiber membranes via IP process: (A) hollow fiber membrane modules, (B) IP setup for hollow fiber membrane modules, (C) IP process

3.3. Membrane characterizations

To characterize the membrane support and PA selective layers, various characterization tools were adopt in this study and those were summarized in Table 3-1. More detailed information for membrane characterizations can be found in the following Sections.

Table 3 - 1. Summary of membrane characterizations.

Targeted Parameter	Instrument
Membrane morphology observation	Field emission scanning electron microscope (FE-SEM), Scanning Transmission Electron Microscope (STEM, Talos F200X)
Chemical properties	Attenuated total reflectance-Fourier transform infrared spectroscopy (ATR-FTIR)
Mechanical properties measurement	Advanced Testing System (LS1, Lloyd instruments Ltd, UK)
Contact angle measurement	Optical tensiometer (Attension Theta Lite 100)
Membrane surface roughness	Atomic force microscopy (AFM, Dimension 310 Scanning Probe Microscope)
Pore size measurement	Capillary flow porometry (Porolux 100), Solute transport experiment
Chemical composition	X-ray photoelectron spectroscopy (XPS) (JPS-9010MS, JEOL, Japan)

3.3.1. Field emission scanning electron microscope (FE-SEM)

The morphologies of membrane support layers and PA active layers were observed in FE-SEM operated at 5-10 kV (Zeiss Supra 55VP, Carl Zeiss AG). For membrane cross-section observation, samples were fractured in liquid nitrogen (N_2). All samples were sputter-coated with Au/Pd of 5-10 nm thickness using a sputtering coater (EM ACE600, Leica) prior to the SEM analysis. Figure 3-9 shows the optical image of the FE-SEM equipment.

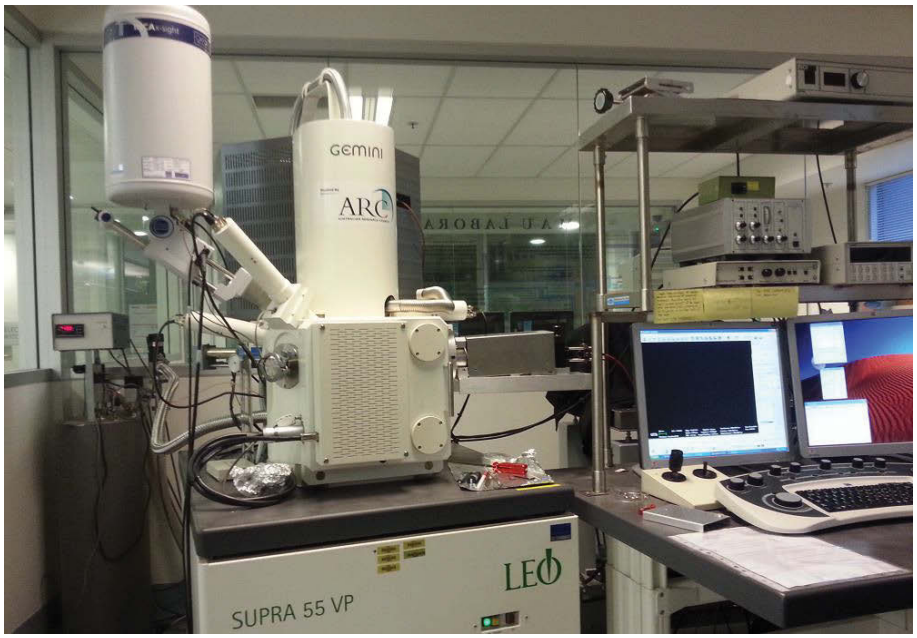

Figure 3 - 9. Field emission scanning electron microscope (FE-SEM) (Zeiss Supra 55VP, Carl Zeiss AG)

3.3.2. Attenuated total reflectance-Fourier transform infrared spectroscopy (ATR-FTIR)

Chemical properties of modified and un-modified membranes were characterized using an Attenuated total reflectance-Fourier transform infrared spectroscopy (ATR-FTIR) (IRAffinity-1, Shimadzu, Japan) equipped with a single reflection ATR accessory (MIRacle 10, ZnSe crystal) as shown in Figure 3-10. Prior to the ATR analysis, all samples were dried in a dry-oven to remove moistures in the samples. Multiple measurements were performed in the wavelength range of 600-4000 cm^{-1} with a signal resolution of 4 cm^{-1} and a minimum of 32 scans.

Figure 3 - 10. Attenuated total reflectance-Fourier transform infrared spectroscopy (ATR-FTIR) equipped with a single reflection ATR accessory.

3.3.3. Mechanical properties measurement

Mechanical properties of prepared membranes were evaluated using an Advanced Testing System (LS1, Lloyd instruments Ltd, UK) equipped with a 1 kN load cell as presented in Figure 3-11. Thin film vice action grip (Max. 500 N) was equipped to the load cell and used for flat type samples evaluation while a pair of wire grip with bollard and vice clamp (Max. 2 kN) was selected for testing hollow fiber membranes. The flat type membranes were cut with dimensions of 50 mm x 10 mm and the membrane thickness was determined by a digital micrometer (Model 293-330 Mitutoyo, Japan) for calculating the membrane cross sectional area. The samples were pre-loaded with 0.05 N and were analysed at a cross-head speed of 10 mm/min. For hollow fiber membrane, gauge length, pre-load and cross-head speed were set as 80 mm, 0.05 N and 30 mm/min, respectively. Cross sectional area (mm^2) of hollow fiber membranes was calculated with determining lumen and outer diameters by a digital microscope (Magnification ratio: ×500). All samples were measured at least five times and then the obtained values were averaged.

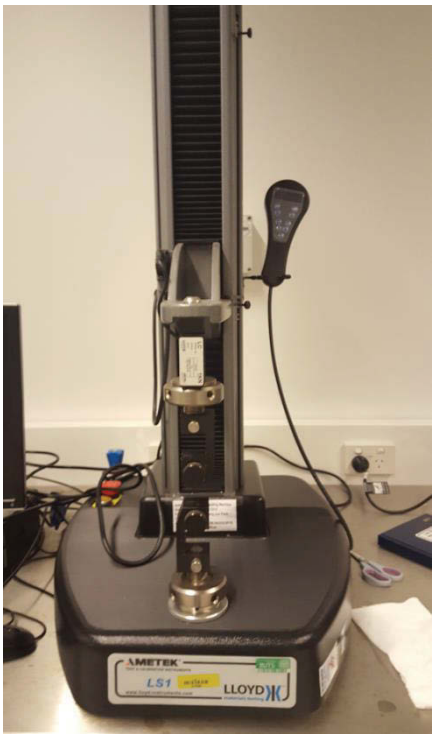

Figure 3 - 11. Advanced Testing System (LS1, Lloyd instruments Ltd, UK) for evaluating mechanical properties of membranes.

3.3.4. Contact angle measurement

Hydrophilicity of membranes was evaluated by contact angle measurement using an optical tensiometer (Attension Theta Lite 100) equipped with image processing software as described in Figure 3-12. Membrane samples were attached on the glass plate using a two-sided tape and then 5–7 µL of deionised (DI) water was dropped carefully on the membrane surface, wherein the drop is captured by a camera, and the imaging software estimates the contact angle directly. The contact angle results are average values of at least five measurements.

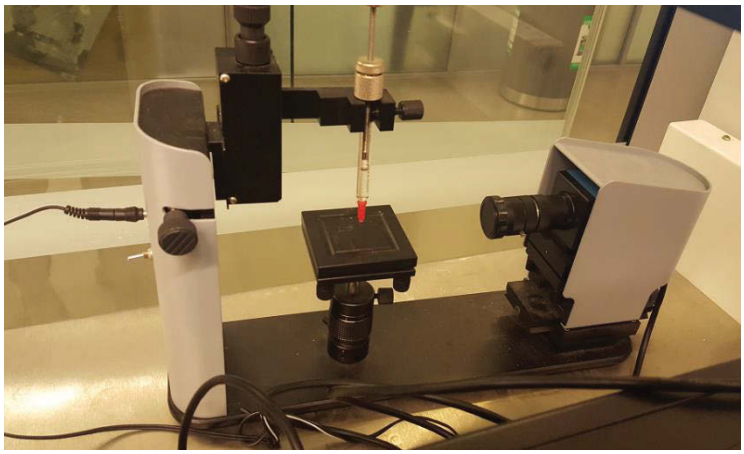

Figure 3 - 12. Optical tensiometer (Attension Theta Lite 100) for measuring contact angle of membranes.

3.3.5. Other characterizations

Atomic force microscopy (AFM) images of membrane samples were obtained from a Dimension 3100 Scanning Probe Microscope (Bruker) under tapping mode (scanning area of 5 μm × 5 μm). Capillary flow porometry (Porolux 100) was used for the pore size determination and for the N_2 gas permeability experiments. The pore size of prepared samples was determined by analyzing dried samples under dry-up/wet-up mode using a wetting agent (Porefil surface tension: 16 dynes cm^{-1}). For the gas permeability ($Lmin^{-1}$) experiment, N_2 was supplied as a feed gas ranged from 0 to 28 bar in dry membrane samples at the same effective membrane area (0.79 cm^2). A Scanning Transmission Electron Microscope (STEM, Talos F200X) equipped with Super-X energy dispersive x-ray spectroscopy (EDS) system (Bruker) was used to map the F and O elements and observe the boundaries of coating and core nanofiber layers for CA and PVDF composite nanofibers.

To characterize chemical composition of both membrane supports and TFC membranes, an X-ray photoelectron spectroscopy (XPS) (JPS-9010MS, JEOL, Japan) was used to analyze the membrane surface by a monochromatized spectrometer with an Al Kα radiation probe (1486 eV). For each measurement, survey scans were performed by sweeping over 0–1000 eV of electron binding energy with an energy step size of 1 eV. High-resolution scans were carried out by averaging 100 scans of the C 1s peak from 276 to 292 eV with a resolution of 0.1 eV. For all scans, sample charging was minimized with an electron flood gun operated at 3 eV.

3.3.6. Membrane porosity measurement

Membrane porosity (ε) of flat-sheet type and single layered electrospun nanofiber samples was determined via gravimetric analysis using Eq. (3-1) given the density of water (ρ_w = 1.00 g cm^{-3}) and each polymers (ρ_p). Dried samples were initially weighed (m_2, g) then were soaked in water for 24 h at 30^{o}C. Residual water was removed and then the wet samples were re-weighed (m_1, g). Reported results are average values of at least five measurements.

$$\varepsilon = \frac{(m_1 - m_2)/\rho_w}{(m_1 - m_2)/\rho_w + m_2/\rho_p} \tag{3-1}$$

However, membranes composed of two different polymers such as the blend and composite nanofiber supports used both Cellulose acetate (CA) and Polyvinylidene fluoride (PVDF), the densities and concentration ratio of both polymers were considered in calculation of membrane porosity as dipiced in Eq. (3-2). Polymer density of nanofiber membranes was calculated based on the ratio of PVDF (*a*) and CA (*b*), wherein *a* + *b* = 1. The density of water, PVDF, and CA applied for the calculation are ρ_w = 1.00 g cm^{-3}, ρ_p = 1.78 g cm^{-3} and ρ_c = 1.28 g cm^{-3}, respectively.

$$\varepsilon = \frac{(m_{wet} - m_{dry})/\rho_w}{\frac{m_{wet} - m_{dry}}{\rho_w} + m_{dry}/\left(\frac{a \times \rho_p + b \times \rho_c}{2}\right)} \tag{3-2}$$

In case of hollow fiber membrane due to their particular structure of hollow shape, the ε was calculated using Eq. (3-3) (Zhang et al. 2014). Wet samples of 5 cm in length (*l*, cm) were cut and then dried in a dry oven at 100^{o}C for 12 h, and placed in a desiccator for another 12 h to completely remove any remaining water from the samples. The dried membranes were weighed (*m*, g) with 5 fibers for each measurement.

$$\varepsilon = \frac{\frac{1}{4}\pi l \rho_p \left(OD^2 - ID^2\right) - m}{\frac{1}{4}\pi l \rho_p \left(OD^2 - ID^2\right)} \times 100\% \tag{3-3}$$

where OD and ID are the inner fiber diameter (m), and outer fiber diameter (m), respectively.

Water uptake ability, presented in Eq. 3-4, of the pristine and modified PVDF nanofiber mats was also measured via gravimetric analysis. To compare the water uptake abilities of the samples, they were pre-wetted via soaking in IPA for 1 min instead of directly soaking in water, followed by immersing in water to obtain the maximum water uptake ability, until samples are oversaturated with water.

$$\text{Water uptake (\%)} = \frac{m_{wet} - m_{dry}}{m_{dry}} \times 100\% \quad (3\text{-}4)$$

3.3.7. Membrane performance evaluation

3.3.7.1. RO performance test

Pure water flux (J_w), pure water permeability (A) and salt rejection (R) were calculated using Eqns. 3-5, 3-6 and 3-7, respectively, and determined by RO tests. The salt permeability coefficient (B) in Eqn. 3-8 was calculated based on the solution-diffusion theory (Jin et al. 2011, Tang et al. 2010).

$$J_w = \frac{\Delta V}{A_m \cdot \Delta t} \quad (3\text{-}5)$$

$$A = \frac{J_w}{\Delta P} \quad (3\text{-}6)$$

Where ΔV is the permeate volume, Δt is the sampling time, A_m is the effective membrane area in Eq. 3-5, and ΔP in Eq. 3-6 is the applied pressure while C_f and C_p in Eq. 3-7 are the salt concentrations at the feed and permeate solutions, respectively.

$$R = \left(1 - \frac{C_p}{C_f}\right) \times 100\% \quad (3\text{-}7)$$

$$B = J_w \frac{1-R}{R} \exp\left(-\frac{J_w}{k}\right) \quad (3\text{-}8)$$

The mass transfer coefficient (k) in Eq. 3-8 is a function of the Sherwood number (Sh), solute diffusion coefficient (D), and hydraulic diameter (d_h) of cross-flow cell as determined using Eq. 3-9. The Sherwood number is calculated based on the hydrodynamic conditions of the FO system using Eqs. 3-10 and 3-11 where Re is the Reynolds number, Sc is the Schmidt number and L is the length of the channel (Tan et al. 2008, 2013).

$$k = \frac{Sh \cdot D}{d_h} \tag{3-9}$$

$$Sh = 1.85\left(\mathrm{Re} \cdot Sc \frac{d_h}{L} \right)^{0.33} \quad (\mathrm{Re} < 2000) \tag{3-10}$$

$$Sh = 0.04\left(\mathrm{Re}^{0.75} \cdot Sc^{0.33}\right) \quad (\mathrm{Re} > 2000) \tag{3-11}$$

3.3.7.2. FO performance test

The performance of the FO membrane samples was evaluated using a lab-scale crossflow FO unit (Figure 3-13). Two variable speed gear pumps were used to circulate FS and DS concurrently. During the test, temperatures for both FS and DS were maintained in the range of 23 ~ 25 ˚C by a temperature control unit. FO membranes were tested under both FO (active layer facing FS, AL-FS) and PRO (active layer facing DS, AL-DS) modes. Changes in weight and conductivity of the FS were measured using a digital scale and a portable conductivity meter (D-74G, Horiba scientific, Kyoto, Japan), respectively. Both parameters were recoded every 1 min using a data auto-logging system. Subsequently, this obtained data were used for FO water flux and salt permeability calculations. The FO flux (J_v=J_w , L m^{-2} h^{-1}) was calculated using Eq. 3-12 where S_m is the effective membrane surface area.

$$J_v = \frac{\Delta m}{S_m \cdot \Delta t \cdot \rho_w} \tag{3-12}$$

Salt leakage from the draw solution or reverse salt diffusion J_s (g m^{-2} h^{-1}) was calculated using Eq. 3-13 where C_t is the salt concentration and V_t is the feed volume at time t. Thus, the total amount of leaked salt to the feed solution is quantified as the change in C_tV_t or $\Delta(C_tV_t)$ at time interval Δt.

$$J_s = \frac{\Delta(C_tV_t)}{S_m \cdot \Delta t} \tag{3-13}$$

3.3.7.3. Determination of membrane structural parameter (S)

Solute resistivity K was calculated using Eq. 3-14 where $\pi_{D,b}$ and $\pi_{F,m}$ are the osmotic pressures of the bulk draw solution and feed solution near the membrane surface, respectively (Cath et al. 2013). The $\pi_{F,m}$ was determined using Eq. 3-15 where $\pi_{F,b}$ is the osmotic pressure of the bulk feed.

$$K = \frac{1}{J_v} \ln \frac{B + \pi_{D,b}}{B + J_{v+\pi_{F,m}}} \tag{3-14}$$

$$\frac{\pi_{F,m}}{\pi_{F,b}} = \exp\left(\frac{J_v}{K}\right) \tag{3-15}$$

Membrane structural parameter S was calculated from the product of K and solute diffusivity (D), which is equivalent to the product of membrane tortuosity τ and membrane thickness t_s, divided by the membrane porosity ε as expressed in Eq. 3-16 (Cath et al. 2013).

$$S = KD = \frac{t_s \tau}{\varepsilon} \tag{3-16}$$

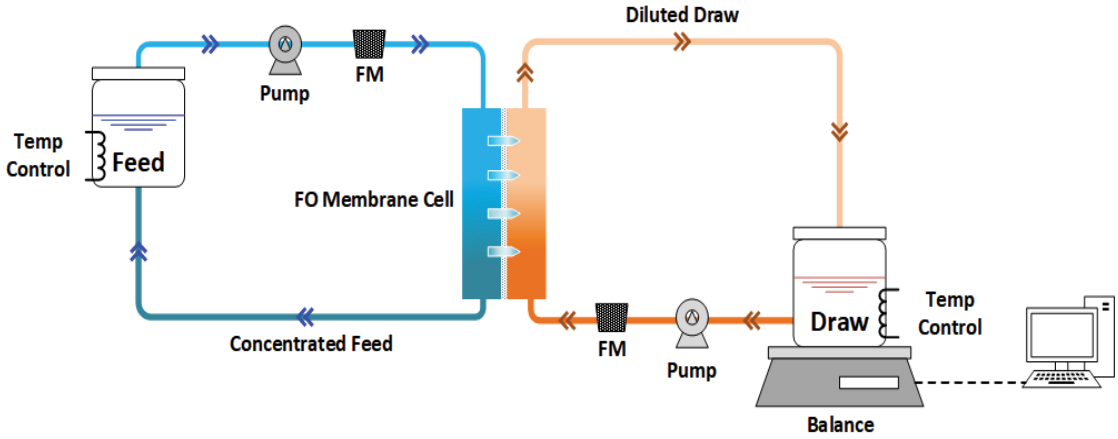

Figure 3 - 13. Schematic of the lab-scale crossflow FO unit for performance testing

3.3.7.4. PRO performance test

All the performance tests for the PRO hollow fiber membranes were conducted using a bench-scale PRO test unit. Figure 3-14 shows the schematic diagram of the bench scale PRO system (Figure 3-14(a)) and optical image of the PRO unit (Figure 3-14(b)) used in this study. The PRO test unit can be used for evaluating both flat sheet and hollow fiber membranes. Basically, a bench-scale PRO unit consists of two reservoirs for FS and DS, a high-pressure pump to pressurize and circulate the draw solution, a variable speed gear pump (Cole-Parmer, Vernon Hills, IL) to circulate the FS, a digital scale to measure the weight change of the FS, two digital-type pressure sensors at the membrane module outlet, two analogue-type pressure sensors at the membrane module inlet, two flow meters, a portable conductivity meter (D-74G, Horiba scientific, Kyoto, Japan) to measure conductivity changes in the FS, and a temperature control system. Throughout the data auto-logging system, values for conductivity of the FS, pressures for both FS and DS, and weight change of the FS were continuously monitored and recorded every 1 min for the entire experimental runs. It is worthwhile to note that the hydraulic pressure applied at the draw side was automatically controlled via a proportional integral derivative control, and thus kept identical during the operation. In the PRO operation, the DS was circulated at the lumen side of hollow fiber membranes while the FS was circulated at the membrane shell side because the PA active layer was produced to the lumen side of hollow fiber membrane. The constant flow rates for both DS and FS were set at 150 mL/min during

the performance tests. The temperature of all solutions was maintained at 23 ± 1°C during the tests.

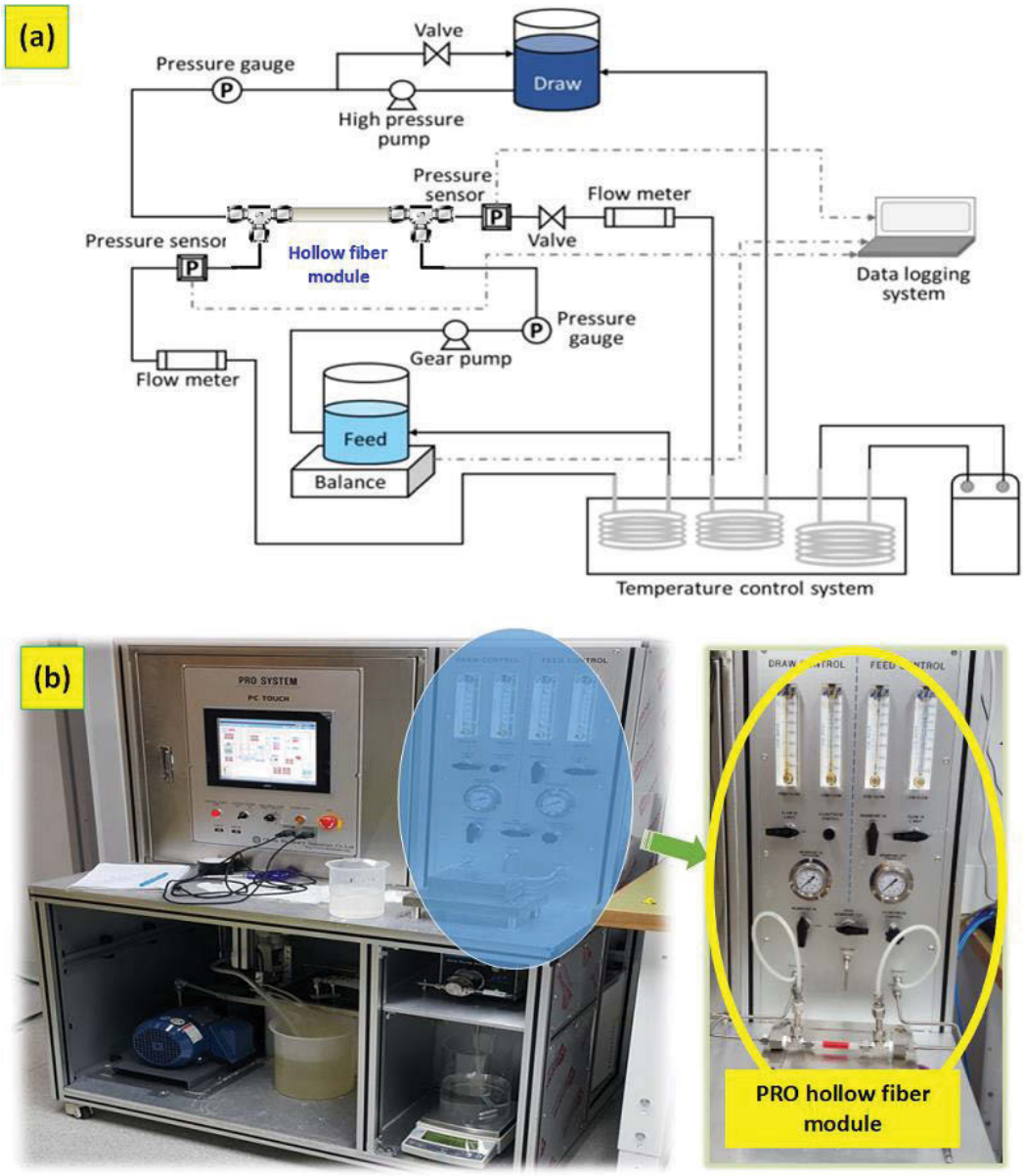

Figure 3 - 14. Bench scale PRO membrane process experimental setup. (a) Schematic diagram of the PRO setup and (b) PRO performance test unit

CHAPTER 4

GRAPHENE OXIDE INCORPORATED POLYSULFONE SHBSTRATE FOR THE FABRICATION OF HIGH PERFORMANCE FLAT-SHEET THIN-FILM COMPOSITE FORWARD OSMOSIS MEMBRANES

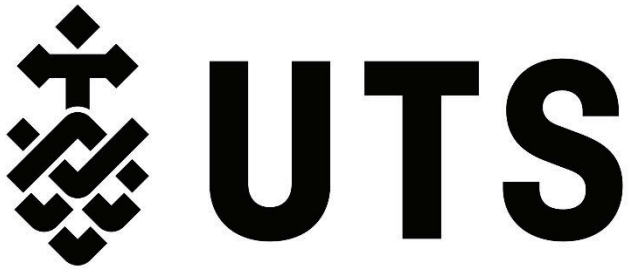

4.1. Introduction

GO is an attractive material choice to modify the support layer of TFC-FO membranes as it abundantly contains oxygenous functional groups such as carboxyl, epoxy and hydroxyl groups (Hu et al. 2013). A two-dimensional (2D) single-layer GO nanosheet is typically one atomic thick (thickness = 1~2 nm) (Hu et al. 2013, Stankovich et al. 2006). Compared to other types of fillers, the extremely high aspect- and surface area-to-volume ratios of GO nanosheets would promote better interaction with the polymer matrix (Stankovich et al. 2006). These unique dimensional and surface properties of GO nanosheets offer great potential for making composite materials with unique structural properties, high chemical stability, strong hydrophilicity, and excellent antifouling properties (Hu et al. 2013, Lee et al. 2013, Mi 2014, Perreault et al. 2014, Stankovich et al. 2006).

In this chapter, GO nanosheets prepared via a modified Hummer's method (Dimiev 2014, Hummers 1958) were used as fillers to modify the PSf support of TFC-FO membranes for the first time. Particularly, the physical and structural modification by GO on the support layer resulted in increased hydrophilicity and/or porosity, which remarkably improved the water flux of the TFC-FO membranes and at the same time lowered the effect of ICP phenomenon in the FO membrane. A series of characterizations were conducted to understand the influence of GO on the structural property and surface hydrophilicity of the PSf support. PSf supports with varied GO loadings were prepared and tested to determine the most suitable support material composition for FO operation. Finally, FO experiments were performed to assess the performance of the most suitable TFC-FO membrane under two modes of membrane orientations with the active layer facing either the feed or the draw solution during operation. This chapter is an extension of the research article published by the author in Journal of Membrane Science.

4.2. Experimental

4.2.1. Materials

Graphite powder was purchased from Acros, Korea. Sulfuric acid (H_2SO_4) and potassium permanganate ($KMnO_4$) were supplied from Junsei, whereas sodium nitrate ($NaNO_3$) and hydrogen peroxide (H_2O_2) were supplied by Shinyo and Showa, respectively.

Polysulfone (PSf, Udel P-3500) from Solvay Solexis, 1,2-phenylenediamine (MPD, 99%) and trimesoyl chloride (TMC, 98%) from Sigma-Aldrich were used for membrane fabrications. N,N-dimethylacetamide (DMAc, analytical grade), sodium chloride (NaCl) and n-hexane were purchased from Sinopharm Chemical Reagent Co., Ltd.

4.2.2 Preparation of GO nanosheets

The GO nanosheets were prepared according to a modified Hummer's method (Dimiev 2014, Hummers 1958). Approximately 3 g graphite was dispersed in a 70 mL chilled (ice bath: <20 ^{o}C) H_2SO_4, which was vigorously stirred until homogenous dispersion was achieved. About 1.5 g of $NaNO_3$ was subsequently added and stirred for 10 min, followed by addition of 9 g $KMnO_4$ (slow addition due to highly exothermic reaction). The reaction was kept at 40^{o}C for 30 min before adding 150 mL DI water and heating the reactor at 95^{o}C. After 15 min, 1 L DI was poured followed by dropwise addition of 15 mL H_2O_2. While still warm, the reacted dispersion was vacuum filtered to avoid precipitation of mellitic acid. The filtered cake was rinsed with 10 wt% HCl solution to remove unreacted residues. The cake was re-dispersed and sonicated for 1 h in 400 mL 10 wt% HCl solution and then centrifuged (5000 rpm, 30 min) to collect the expanded graphite. This step was performed twice and then was repeated using 400 mL DI water at longer sonication period (18 h). After several times of dispersion and sonication in DI, the dispersion was transferred in dialysis bags (Spectra/Por 2, Spectrum Laboratories, Inc. CA, USA) then immersed in 5 L DI water to remove residual acids. The DI water was replaced every two hours and the dialysis was conducted for at least one week. The dialyzed samples were transferred in a flask and then sonicated for 1 h. The dispersion was centrifuged (3000 rpm, 40 min) and the upper 75% of the supernatant was retrieved as the final GO dispersion. Dried GO sheets were obtained through vacuum evaporation of the dispersion.

4.2.3. Preparation of PSf/GO support layer

All PSf/GO substrates were fabricated by conventional phase inversion technique. Known amounts of dried GO sheets were first homogenously dispersed in DMAc via ultra-sonication. Next, the PSf pellets were added under vigorous stirring at 65^{o}C to obtain 18 wt% PSf with varied GO loading (0, 0.1, 0.25, 0.5 and 1.0 wt%) with respect to PSf

amount. Polymer viscosities (average of three measurements) were determined at 30ºC by a rotational viscometer (Brookfield DV-II+ Pro Viscometer) at different shear rates (0 to 17 s^{-1}) and rotation speeds (2.5 to 50 rpm). Before fabrication, all PSf/GO solutions were de-gassed at 30ºC. The bubble-free solutions were then poured on glass plates and then spread into films using a casting machine as more details described in Section 3.2.1.1. The nascent films were immersed in a water coagulation bath (30ºC) and then soaked in DI water for one day to completely remove the residual solvents.

4.2.4. Preparation of TFC-FO membranes by IP process

The dense active layer of polyamide was formed on one side of the PSf or PSf/GO surface through an IP method (Chen et al. 2015, Xiao et al. 2015). The IP process was conducted to form a selective PA layer and the procedure described in Section 3.2.1.2. The prepared TFC membranes were subsequently preserved in DI water until it was tested. The prepared TFC-FO composite membranes were denoted as GOT-0, GOT-0.1, GOT-0.25, GOT-0.5 and GOT-1.0, corresponding to the membrane supports GO-0, GO-0.1, GO-0.25, GO-0.5 and GO-1.0, which contain 0, 0.1, 0.25, 0.5 and 1.0 wt% GO loading (weight ratio to the PSf), respectively.

4.2.5. GO Characterization

Oxygenous groups on prepared GO nanosheets were examined by attenuated total reflectance-Fourier transform infrared spectroscopy (ATR-FTIR, Varian 2000). Hydrophilic COOH and OH groups were quantified via modified Boehm titration as detailed elsewhere (Goertzen et al. 2010, Oickle et al. 2010). The structure of GO nanosheets was examined under a transmission electron microscope (TEM, JEOL ARM 200F, Japan) at 100 kV.

4.2.6. RO experiment for pure water permeability and salt rejection determination

Pure water permeability and salt rejection performance of PSf/GO and PSf/GOT membranes were measured using a cross-flow RO filtration system (Sterlitech Corporation) with an effective membrane area of 42 cm^2. Pure water flux (PWF, J_w) of PSf/GO membranes was measured at different transmembrane pressure (TMP) from 1 to 5 bar. Prior to flux measurements, the membranes were pressurized with DI water at 5 bar for 1 h to eliminate the effect of membrane compaction and to obtain stable TMP. The PSf/GOT membranes were tested in cross-flow membrane permeation experiments operated at 10 bar with 1.5 L min^{-1} (0.25 m s^{-1}) cross-flow rate. Sampling was performed after the system stabilized at 25°C and P=10 bar for 1 h. For the rejection experiment, 1000 mg L^{-1} NaCl solution was used as feed solution. The salt concentrations at the feed and permeate solutions were measured using a conductivity meter.

4.2.7. Forward osmosis tests

The FO membrane cell with 0.4 cm flow channel depth has an effective membrane area of 30 cm^2. Two variable speed gear pumps were used to circulate the feed and draw solutions concurrently. Flow rates of the feed and draw solutions were monitored with rotameters and kept constant at 1.8 L min^{-1} (cross flow velocity = 0.25 m s^{-1}). The temperatures of the feed and draw solutions were kept at 25°C. The membranes were tested under the FO mode (i.e., active layer facing feed solution or AL-FS) and pressure retarded osmosis (PRO) mode (i.e., active layer facing draw solution or AL-DS).

To evaluate the FO performance of the PSf/GOT membranes, 0.5 M NaCl was used as draw solution and DI water as feed. The change in salt concentration at the draw solution was marginal as the ratio of permeated water volume to that of the draw solution was less than 2% during FO operation. With DI as feed, salt leakage was calculated by measuring the conductivity change in the feed solution and re-calculated back to the salt concentration of the draw solution. An electronic balance (CP2002, Ohaus Instrument Co., Ltd.) connected to a computer was used to record the mass of permeated water (m) into the draw solution. FO test was performed for at least 1 h to obtain stable measurements. The reported values were averages from calculated data taken in the last 30 min of operation.

4.3. Results and discussion

4.3.1. Characterization of GO

The presence of oxygenous groups in GO was confirmed via FTIR (Figure 4-1a). Compared to graphite which has a featureless spectrum, GO reveals several characteristic peaks attributable to COOH, OH and epoxide groups (Bose et al. 2012, Guo et al. 2009). Peaks at 3425 cm^{-1} and 1404 cm^{-1} are due to the O-H stretching and O-H deformation, respectively (Bose et al. 2012). The FTIR signal at 1720 cm^{-1} indicates the C=O stretching of the carboxyl group (COOH) whereas those at 1224 cm^{-1} and 1065 cm^{-1} are due to the C-O stretching of epoxy and alkoxy groups, respectively (Bose et al. 2012). The peak at 1620 cm^{-1} for C=C stretching suggests skeletal vibrations of unoxidized graphitic domains or the vibrations of the adsorbed water molecules on the sample (Guo et al. 2009). Furthermore, the presence of oxygenous groups was quantified via Boehm titrations which reveal 8.87 ± 0.29 mmol g^{-1} of acidic groups; from which 4.46 ± 0.59 mmol g^{-1} are COOH while 1.72 ± 0.22 mmol g^{-1} are OH groups. This indicates that the prepared GO was highly hydrophilic, which is a great pre-requisite for an additive of the PSf support for subsequent studies. TEM image (Figure 4-1a) reveals the appearance of an ultra-thin GO nanosheet which indicates the successful chemical exfoliation of graphite via the modified Hummer's method (Marcano et al. 2010).

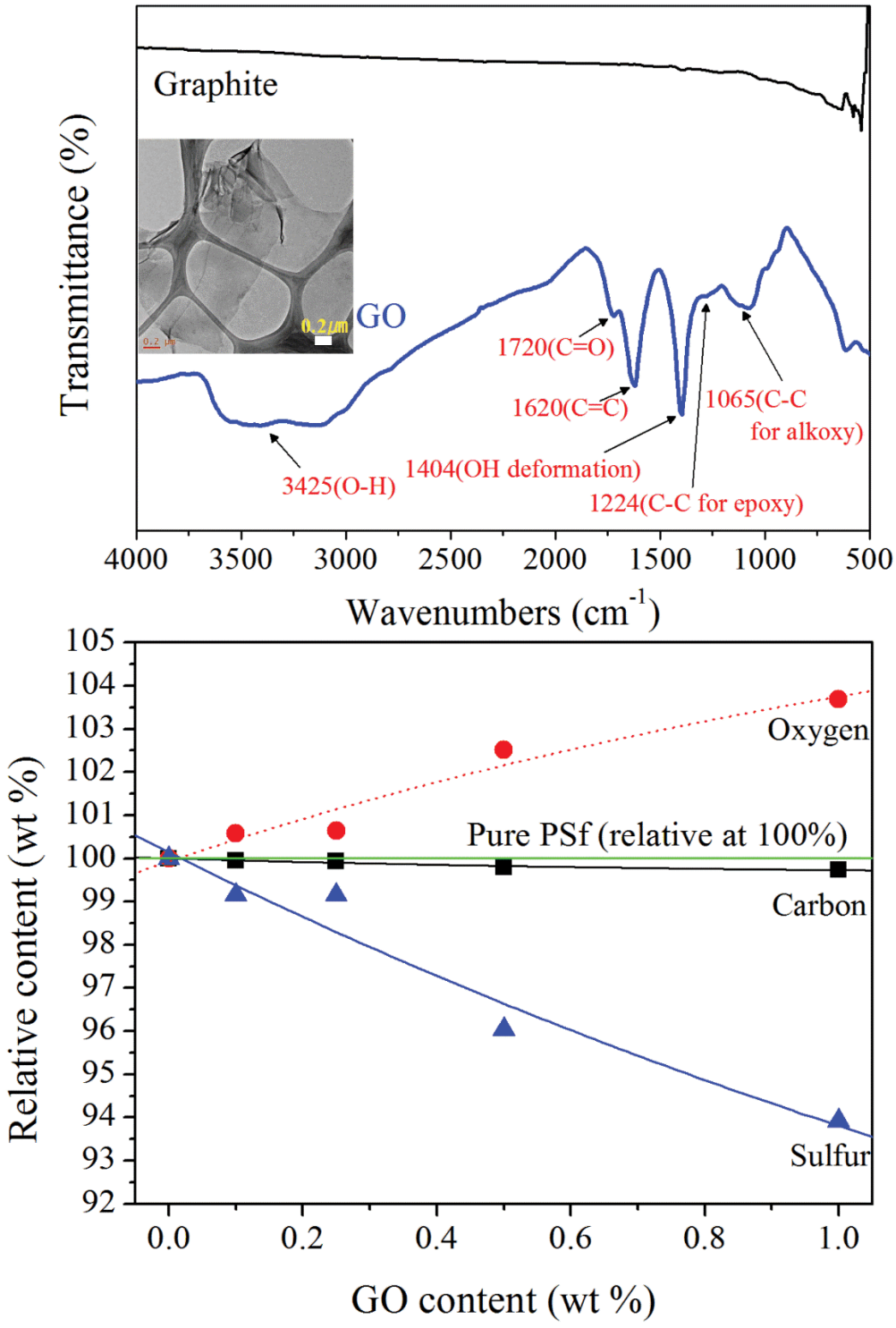

Figure 4 - 1. FTIR spectrum for (a) graphite and GO and (b) elemental proportions for membrane substrate surface conducted by EDS mapping.

4.3.2. GO presence in PSf substrates

Visible evidence directly reveals the presence of golden brown GO nanosheets in the PSf substrates as shown in Figure 4-2. The off-white pure PSf was gradually transformed into brownish color as GO content was increased in PSf/GO membranes. Elemental mapping of the membranes via EDS also indicates the presence of GO nanosheets in the PSf/GO (Figure 4-1b). Relative to pure PSf, decrease in sulfur content was observed concomitant with the increase in oxygen level as more GO nanosheets were added in the membranes. The relatively higher oxygen content in PSf/GO originated from the oxygenous groups of the nanosheets. But as GO also contained carbon, carbon content was almost the same for all PSf/GO. This trend is consistent with the EDS results from an earlier work on GO containing membrane prepared with antifouling properties (Lee et al. 2013). All of these results demonstrate the successful incorporation of GO in the PSf support.

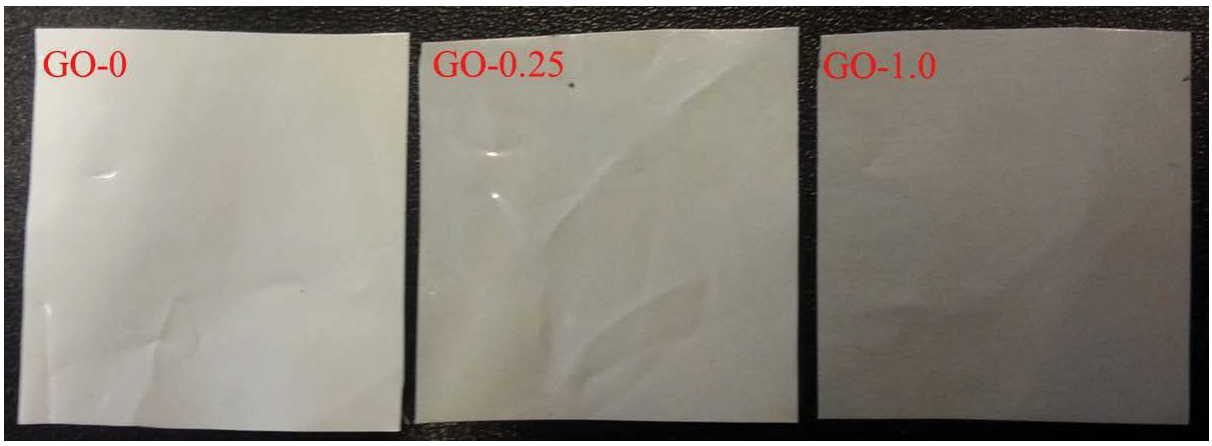

Figure 4 - 2. Optical images of membrane substrates (GO-0 wt%, GO-0.25 wt% and GO-1.0 wt%)

4.3.3. Effect of GO loading on PSf/GO supports

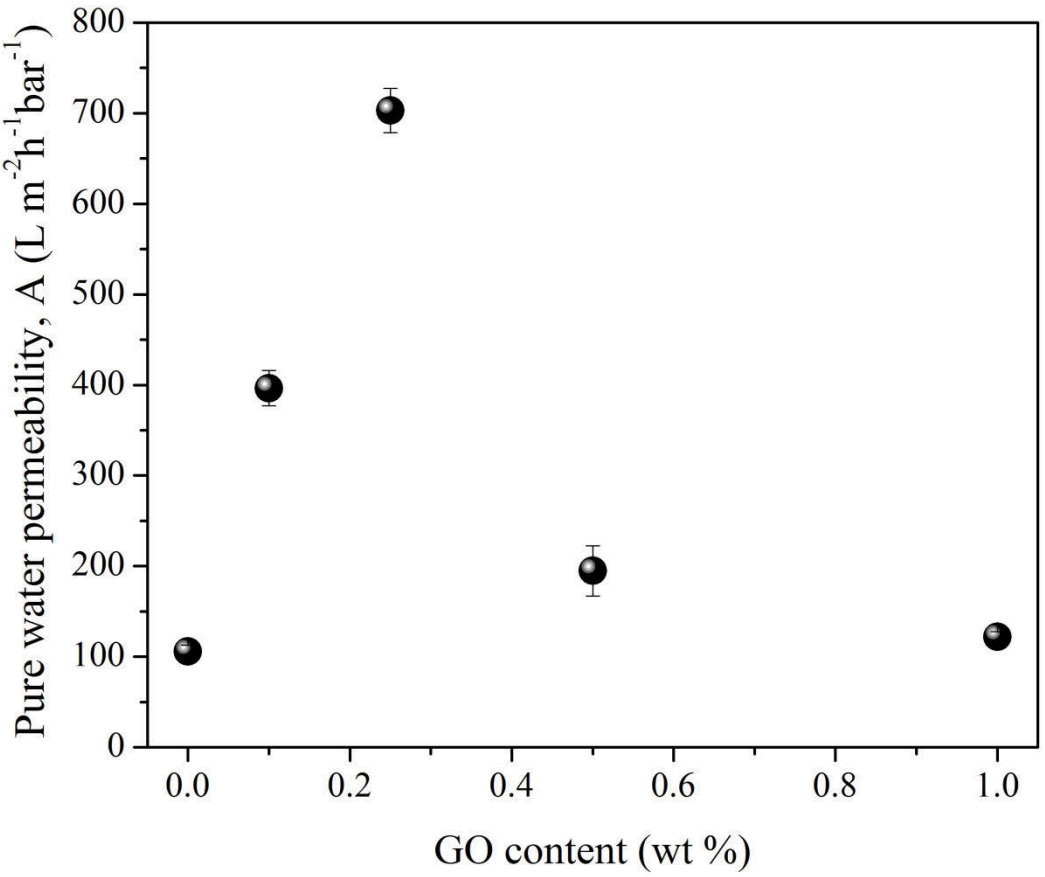

Figure 4 - 3. Pure water permeability with different pressure applications of membrane substrates which incorporated different GO contents.

Addition of GO at 0.1 and 0.25% loading significantly increased the pure water permeability to 400 and 720 L m^{-2} h^{-1} bar^{-1}, respectively, in comparison to that of pure PSf (100 L m^{-2} h^{-1} bar^{-1}) as shown in Figure 4-3. However, further increase in GO loading to 0.5 and 1.0 wt% in fact reduced the water flux. It is known that enhancement of surface hydrophilicity due to GO addition could facilitate easier permeation of water through the support (Hu et al. 2013, Lee et al. 2013). Likewise, attainment of appropriate morphological and structural properties such as porosity, pore structure, tortuosity, and membrane thickness could reduce hydraulic resistance and favor higher convective motion of water through the membrane. Thus, to decouple the effects of surface energy and structural property changes induced by GO on the obtained pure water permeability

trend of PSf/GO supports, several characterization and complementary experiments were performed.

4.3.4. Effect of GO loading on the surface hydrophilicity of PSf/GO supports

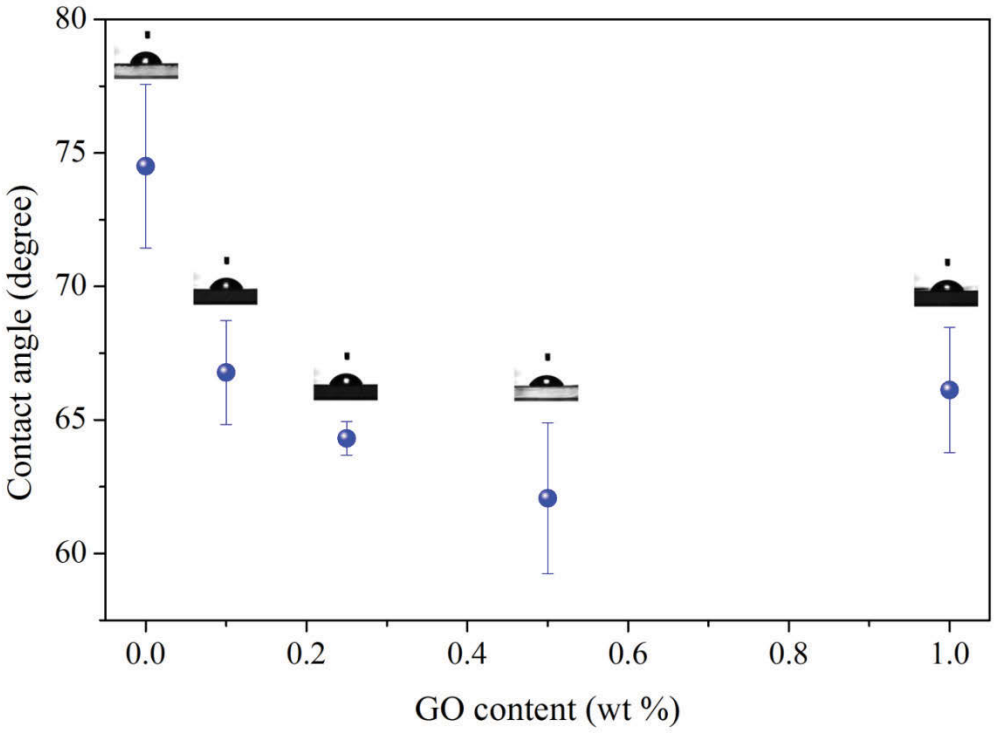

Figure 4 - 4. Contact angle results at various GO loading contents with respect to the PSf amount.

The water contact angle of pure PSf substrate was about 75° (Figure 4-4) but was reduced to as low as 62° as the GO loading was increased up to 0.5 wt%. This result is consistent with those from previous studies wherein composite membranes exhibited lower contact angles upon incorporation of hydrophilic nanomaterials as fillers (Emadzadeh et al. 2014a, Emadzadeh et al. 2014c, Lee et al. 2013, Wang et al. 2013d, Xu et al. 2014, Zinadini et al. 2014). Thus, the abundant presence of oxygenous functional groups such as hydroxyl, carboxyl and epoxy groups in GO might have improved the membrane hydrophilicity which resulted in higher water permeability for the composite membrane. However, membrane hydrophilisation by GO was effective only to some extent as further increase in GO loading to 1.0 wt% slightly increased the contact angle to 70°. Moreover, as the

pure water permeability trend is not fully consistent with that of contact angle results, the structural properties of the supports were further inspected to fully elucidate the effect of GO.

4.3.5. Effect of GO loading on the structure of PSf/GO supports

Figure 4-5 reveals FE-SEM images of top and bottom surfaces as well as cross-section of membrane supports with different GO loadings. All membranes have typical asymmetric structures; the dense top surface of all samples had no open pores. Meanwhile, cross-section images reveal long finger-like macro-voids near the top whereas pores as large as 1 μm are evident at the bottom section of the membranes. The morphology of pure PSf is characterized by the presence of few macrovoids which co-existed with sponge-like structure at the bottom section of the membrane. Meanwhile, GO loadings at 0.1 and 0.25 wt% resulted in membranes with larger finger-like pores and predominant presence of macrovoids at the bottom section with very minor presence of sponge-like structure. The increase in porosity and pore size as well as reduction in membrane thickness (Figure 4-8) at this GO loading range is consistent with the FE-SEM observation. Thus, the higher pure water permeability strongly suggests that the resultant morphological characteristics imparted by the addition of low amount of GO (≤ 0.25 wt%) promoted a less hindered transport of water through the membrane support. Due to its hydrophilicity, GO could increase the thermodynamic incompatibility between polymer and the solvent which often results in faster onset of phase inversion (Wang et al. 2015). Moreover, addition of small amount of hydrophilic GO might have accelerated the entrance of water (non-solvent) into the membrane which ensured quicker exchange between the solvent and non-solvent. This occurrence suppressed the formation of sponge-like structures and favored the formation of larger finger-like voids, which resulted in membranes with higher porosity and larger pore sizes (Lee et al. 2013, Wang et al. 2015).

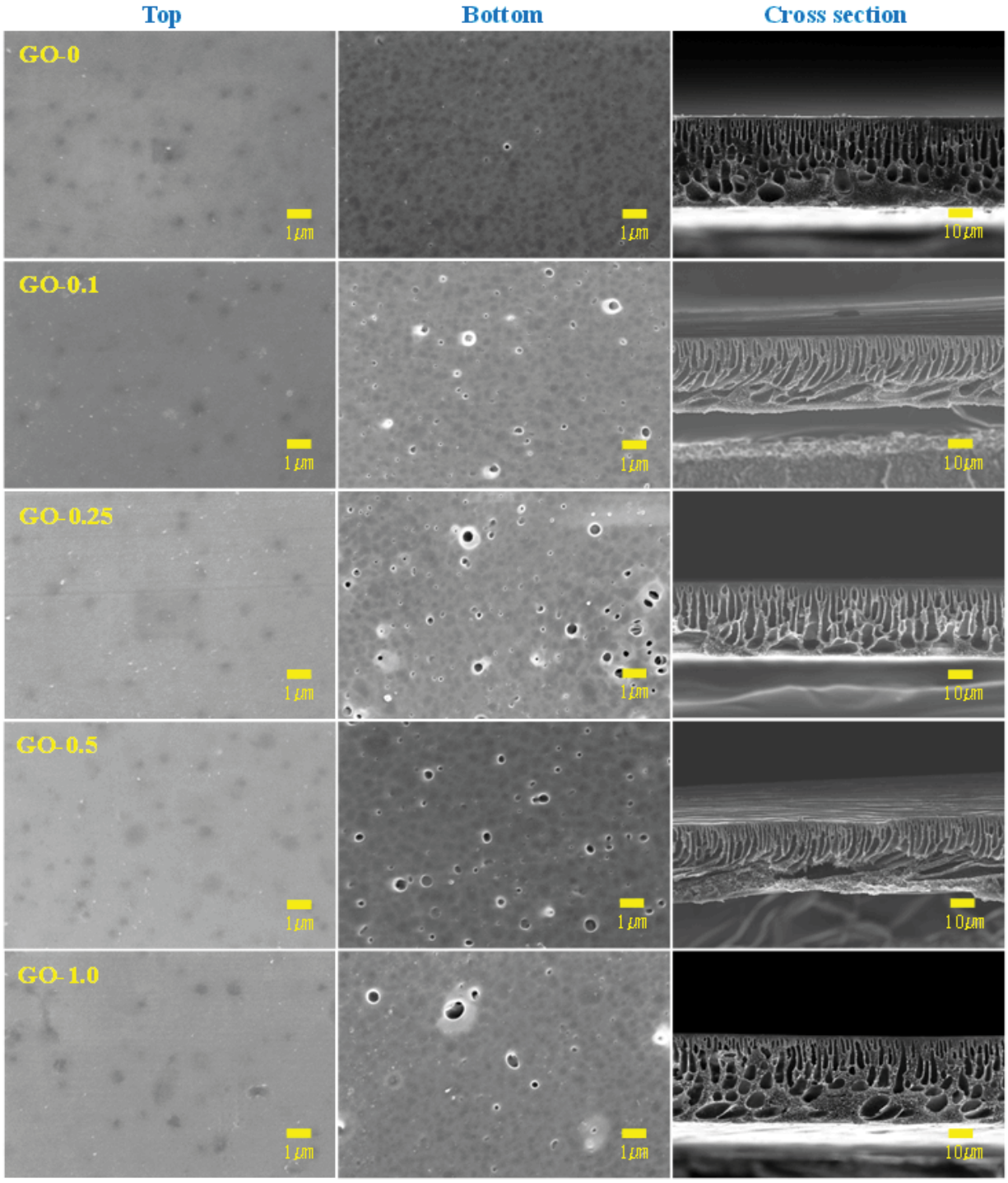

Figure 4 - 5. FE-SEM images of top and bottom surface and cross section area for membrane substrates.

But as GO loading was further increased up to 1.0 wt%, the sponge-like structures re-appeared which could be due to two reasons. First, Figure 4-6 illustrates no drastic change in polymer solution viscosity until 0.25 wt% GO loading. The more evident viscosity

increase at GO loading ≥ 0.5 wt% might have retarded the demixing process between the solvent and non-solvent which decreased the phase-separation rate (Lee et al. 2013, Yeow et al. 2004). Relative to GO-0.25 wt%, the kinetic hindrance in phase separation of membranes with higher GO loading might have promoted the formation of sponge-like structures over the finger-pores, which consequently resulted in less improvement of pure water permeability. This was also reflected by the lower porosity and pore diameter at GO ≥ 0.5 wt% than those at lower loading (Figure 4-8). Second, evidence of GO aggregation was observed at high GO loading as shown in Figure 4-7. At 1.0 wt% GO loading, lateral pore structures were evident at the cross-section of the membrane. This occurrence was also documented by earlier studies when higher amount of GO were embedded in the membranes (Yeow et al. 2004, Zinadini et al. 2014). It is probable that the remarkable increase in viscosity of polymer solution at GO loading ≥0.5 wt% has made it more difficult to disperse the nanosheets. Consequently, membranes with GO loading higher than 0.25 wt% showed less pronounced effect on the structural properties (Figure 4-5 and Figure 4-8) of the support which explains the pure water permeability trend in Figure 4-3.

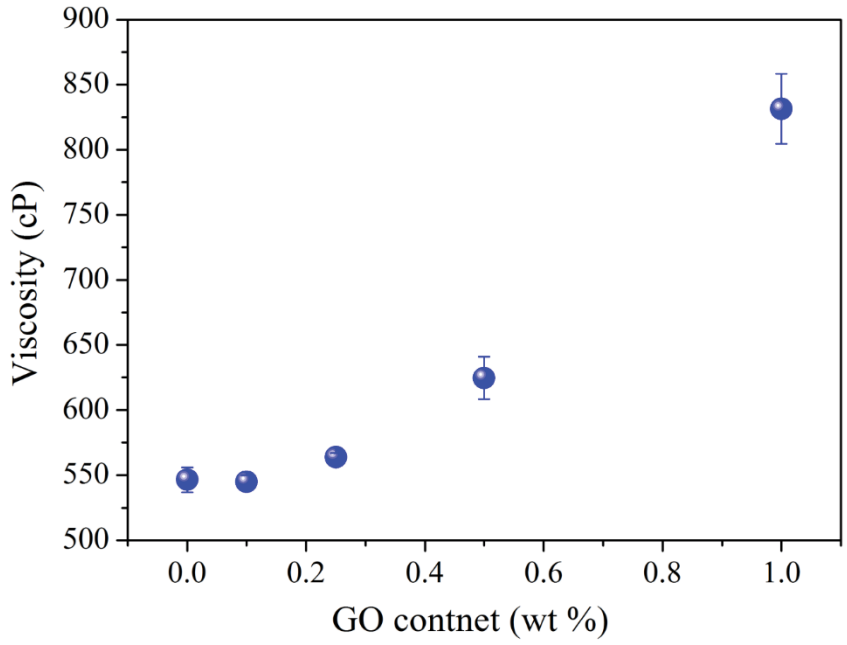

Figure 4 - 6. Polymer solution viscosities at various GO loadings respect to the PSf amount.

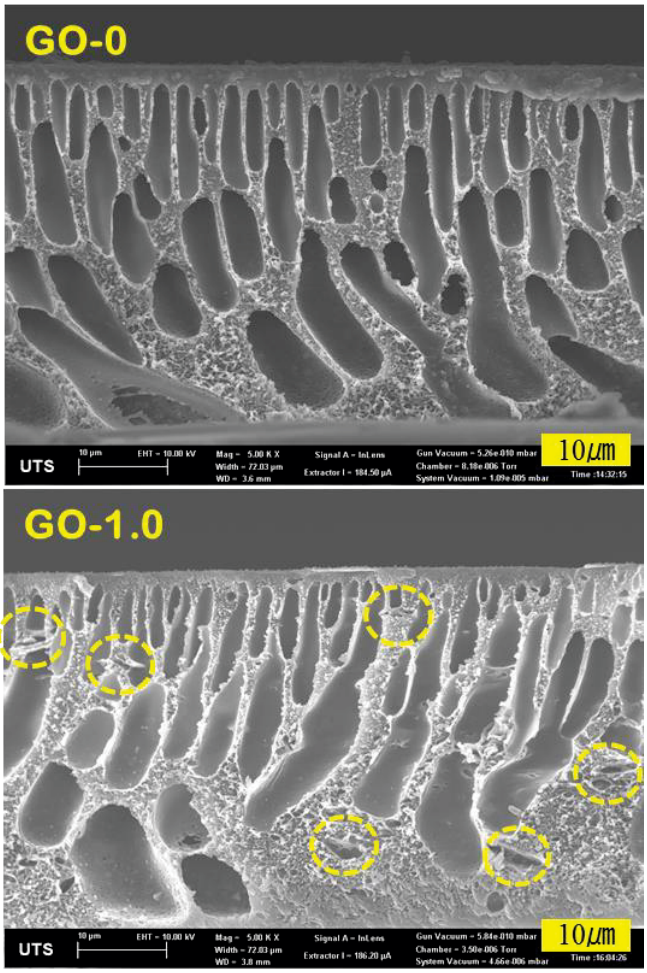

Figure 4 - 7. FE-SEM images of PSf membrane substrate and GO-1.0 membrane substrate.

To further ascertain this finding, gas permeation (N_2) was also conducted to eliminate the surface property effect (i.e. hydrophilicity effect on water transport) of GO on pure water permeability. Figure 4-9(a) showed striking similarity of N_2 gas volumetric flow rate with that of pure water flux trend (Figure 4-9(b)) which can be arranged in the sequence: GO-0.25 > GO-0.1 > GO-0.5 > GO-1.0 > pure PSf. This suggests that structural change imparted by hydrophilic GO has more influence on the water permeability properties of the membrane than that of the improved wettability.

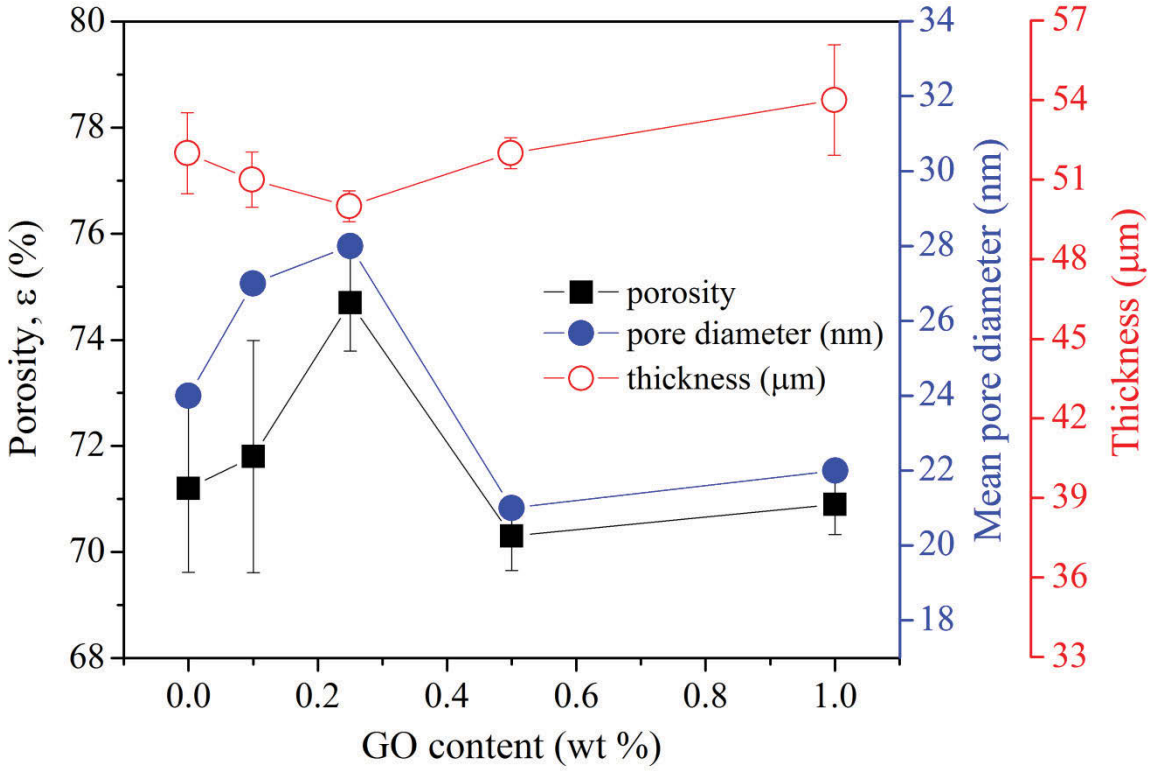

Figure 4 - 8. Effect of GO contents in membrane substrate on membrane porosity, pore diameter and thickness.

These findings eventually offer that the amount of GO that can be added in the PSf support must be optimized to maximize the enhancement in membrane performance. Specifically, the results herein highlight that more than the enhanced surface hydrophilicity effect of hydrophilic additives like GO, their influence on membrane formation can be exploited to manipulate the structural properties of the FO support which predominantly influenced the water permeability of the membrane.

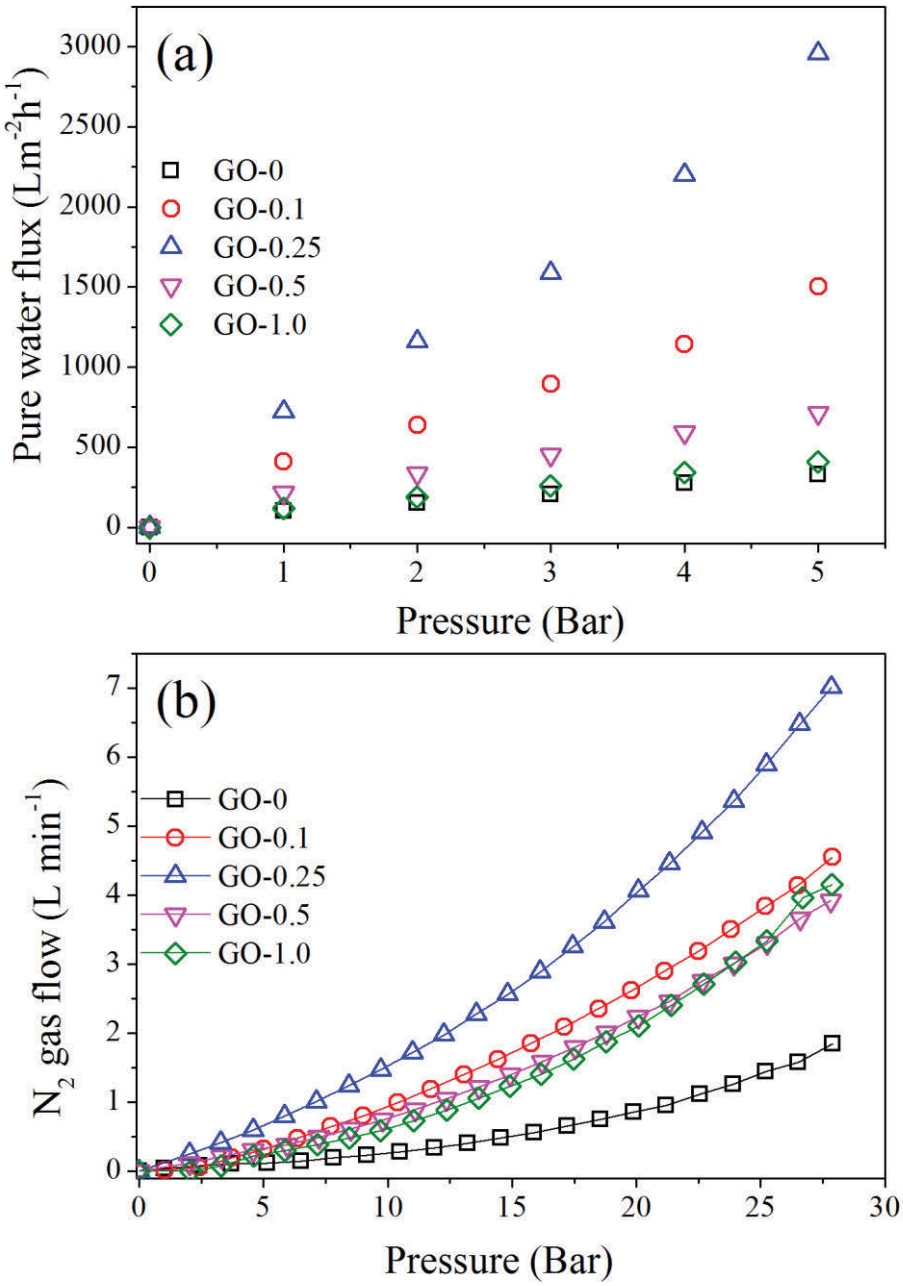

Figure 4 - 9. (a) Pure water flux and (b) N_2 gas permeability of membrane substrates at different pressure applications.

4.3.6. Mechanical properties

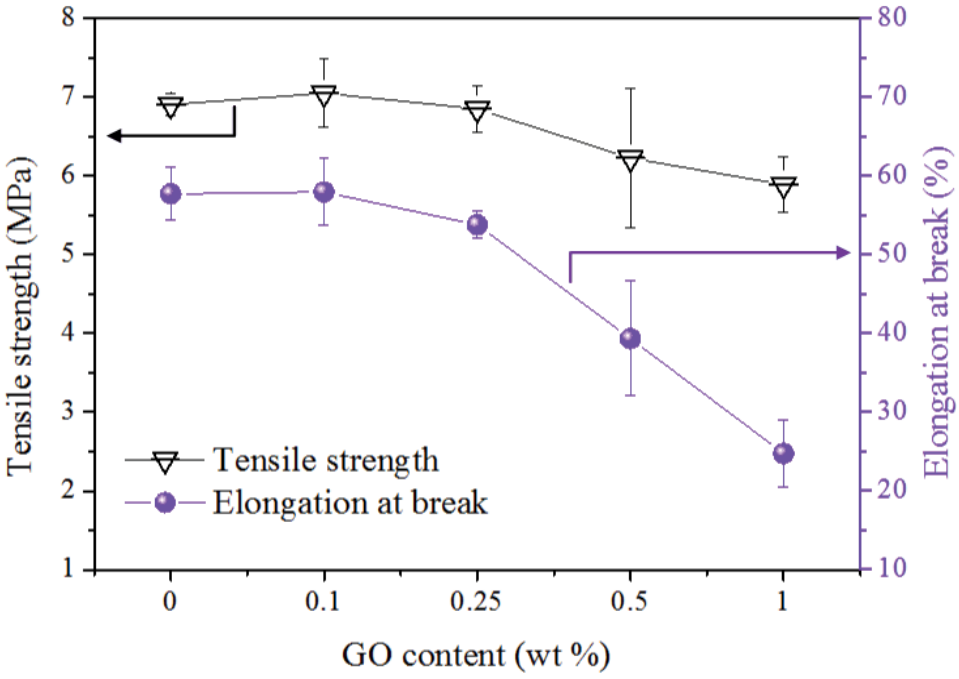

Figure 4 - 10. Mechanical properties (tensile strength and elongation at break) for membrane substrates.

Figure 4-10 shows the mechanical properties of PSf/GO membrane substrates at different GO loadings. The tensile strength and elongation at break of pure PSf was maintained up to 0.25 wt% GO loading. The stable measurements indicate that low GO loading has no significant effect on the bulk mechanical property of PSf. However, further increase in GO loading from 0.5 to 1.0 wt% resulted in slightly lower tensile strength and more remarkable decrease in elongation at break. These results remain consistent with the dispersion of GO in PSf at various loadings. The comparable mechanical properties at low loading (≤ 0.25 wt%) with that of pure PSf suggest well dispersion of GO nanosheets into the polymer matrix. However, excessive presence of GO (≥0.5 wt%) resulted in its aggregation that introduced some micro-defects, which ultimately resulted to mechanically weaker membranes (Lee et al. 2013, Wang et al. 2012b, Yu et al. 2013).

4.3.7. Effect of GO incorporation for TFC-FO membranes

4.3.7.1. Characteristic and RO performance of TFC-FO membranes

FE-SEM images in Figure 4-11 show the ridge-and-valley structures on the surface and near the top cross-section of the prepared TFC-FO membranes, which indicate the presence of polyamide (PA) layer formed via interfacial polymerization (Ma et al. 2012). Compared to the TFC membrane with pure PSf support, all TFCs prepared from PSf/GO with varied GO loadings have thinner top cross-section.

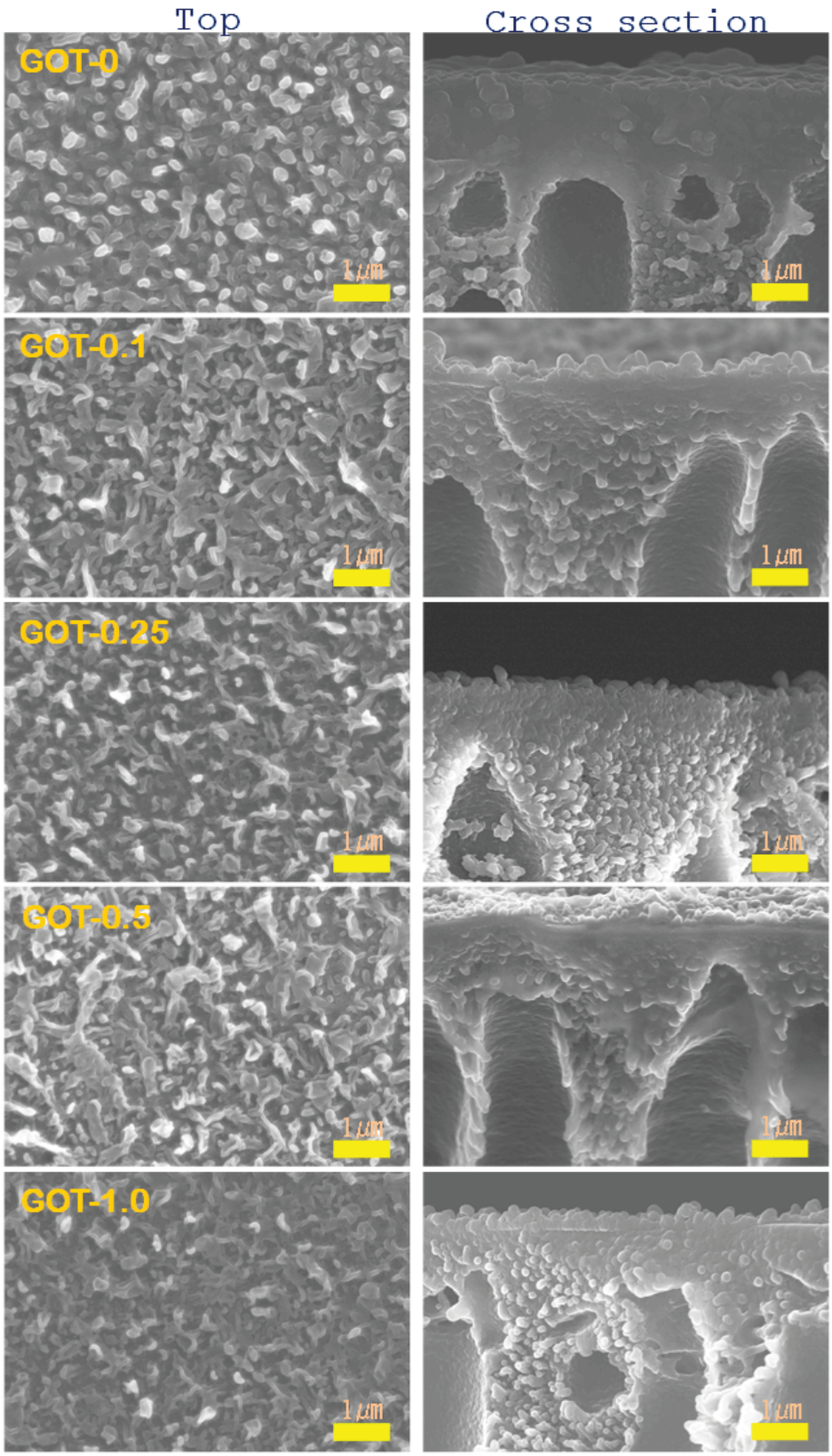

Figure 4 - 11. FE-SEM images of PA selective layer and cross section for TFC-FO membranes (GOT-0. 0.1, 0.25, 0.5, and 1.0).

Table 4 - 1. Effect of GO loading on the membrane performance for TFC-FO membranes.

TFC-FO membranes	*A* (L m^{-2} h^{-1} bar^{-1})	*B* (L m^{-2} h^{-1})	*B/A* (bar)	R (%)	*S* (μm)	τ
GOT-0	0.91	0.24	0.26	97.04	1060	14.51
GOT-0.1	1.23	0.39	0.32	96.56	697	9.81
GOT-0.25	1.76	0.19	0.11	98.71	191	2.85
GOT-0.5	0.99	0.62	0.63	93.09	765	10.34
GOT-1.0	0.91	0.91	0.99	90.09	1630	21.40

From cross-flow RO operation results listed in Table 4-1, GOT-0 had pure water permeability of A=0.91 L m^{-2} h^{-1} bar^{-1}. Except GOT-1.0, all GOT membranes with GO nanosheets had higher A values than that of GOT-0. In fact, the trend of A values is consistent with that of pure water permeability of PSf/GO substrate wherein the highest A=1.76 L m^{-2} h^{-1} bar^{-1} was obtained from GOT-0.25. Likewise, highest salt rejection of R=98.7% was obtained from GOT-0.25 which explains the lowest salt permeability (B=0.11 bar) from this TFC-FO membrane. Among the FO membranes prepared, GOT-0.25 had the highest separation efficiency as it exhibited the lowest B/A value. A low B/A is favorable as it directly suggests low reverse solute diffusion from draw solution to the feed and therefore, low propensity to fouling caused by solute accumulation in FO systems (Wei et al. 2011). The lower salt rejections in other TFC membranes maybe due to the ineffective PA layer formation, especially at higher GO loading ≥ 0.5 wt%.

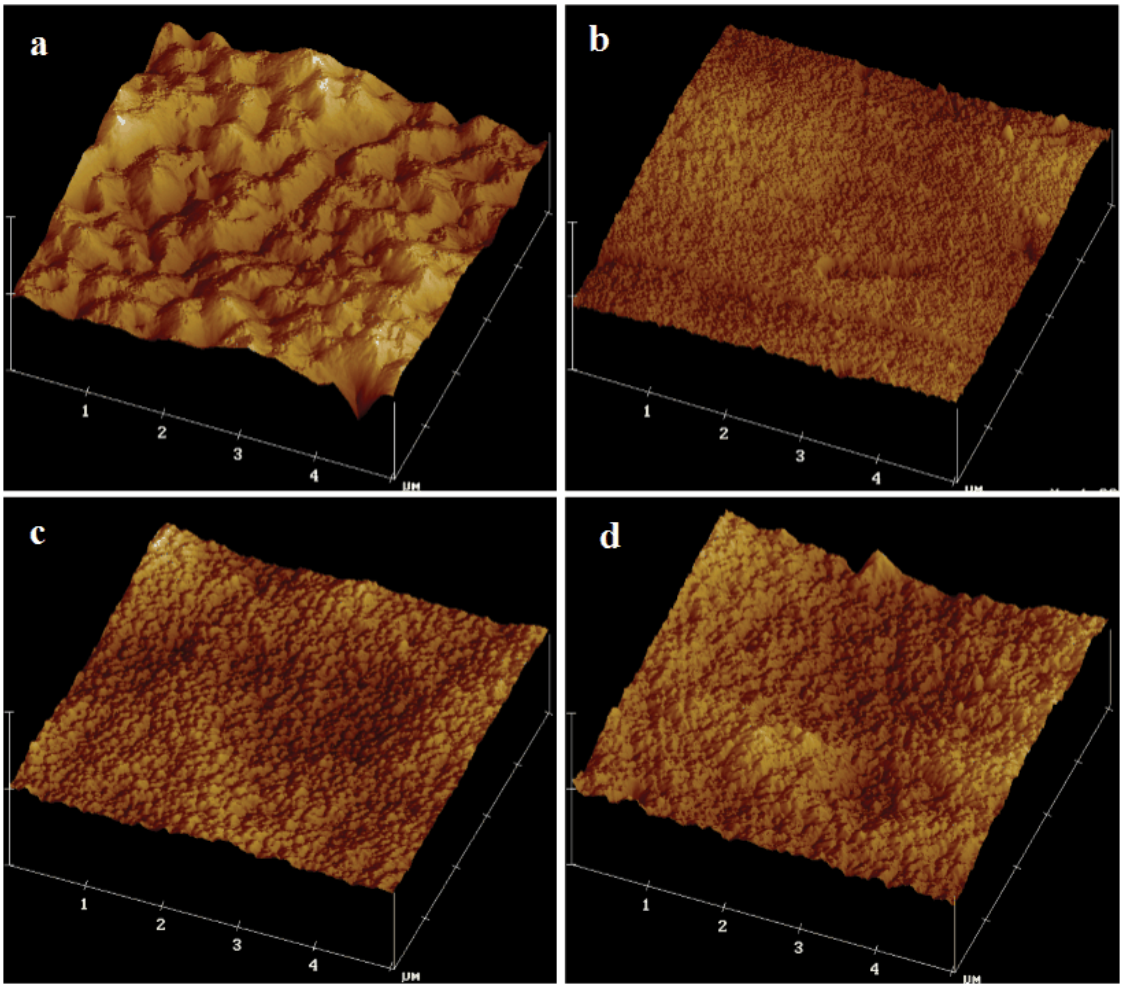

Figure 4 - 12. AFM images for membrane substrates, (a) GO-0, (b) GO-0.1, (c) GO-0.25, (d) GO-1.0.

Table 4 - 2. Surface roughness of membrane substrates via AFM analysis.

Membrane substrates	R_a (nm)	R_{ms} (nm)	R_{max} (nm)
GO-0	14.09	17.56	30.45
GO-0.1	6.75	8.56	15.27
GO-0.25	6.48	8.26	12.97
GO-0.5	8.03	9.76	17.25
GO-1.0	7.97	9.48	17.06

*Note: R_a= mean roughness, R_{ms}= root mean square of z values, R_{max}= maximum vertical distance between the highest data points

The observed trends on salt rejection and salt permeability from RO operation were elucidated in terms of the surface roughness of the membrane supports via AFM (Figure 4-12). The results reveal the broad asperities on pure PSf surface, with mean roughness R_a = 14 nm, root mean square ridge elevations R_{ms} = 17.56 nm, and maximum ridge

elevation R_{max} = 30.45 nm (Table 4-2). Meanwhile, addition of GO resulted in sharper and denser asperities on PSf/GO supports than that of pure PSf (Zhao et al. 2013b, Zinadini et al. 2014). Nonetheless, based on R_a, R_{ms} and R_{max} values, the roughness properties of PSf/GO declined as GO loading were increased to 0.25 wt% and then increased again at ≥ 0.5 wt% loadings. This indicates that well-dispersed GO could smoothen the surface of PSf/GO, which was most remarkable in GO-0.25 (Qiu et al. 2009). This characteristic could be most favorable for the formation of PA layer via interfacial polymerization, which positively influenced the salt rejection performance of GOT-0.25 (Wang et al. 2015). On the other hand, GO aggregation at higher loading might have contributed on the surface roughness of the support which reduced the interfacial polymerization efficiency and thereby negatively affected the salt rejection ability of GOT-0.5 and GOT-1.0 membranes (Emadzadeh et al. 2014a, Emadzadeh et al. 2014c). Meanwhile, the higher salt rejection of GOT-0 than that of GOT-0.1 could be explained as follows. While GOT-0 had rougher surface than GOT-0.1 based on R values, the asperities were broad (Figure 4-12) which might not have significantly reduced the contact area of reaction for interfacial polymerization. This indicates that PA layer formation efficiency via interfacial polymerization could not be solely related to R values but also on the density and morphology of the asperities.

4.3.7.2. Effect of GO loading on FO performance

The TFC-FO membranes with different GO loadings were operated under AL-FS and AL-DS modes using 0.5 M NaCl draw solution and DI water as feed (Figure 4-13). In AL-DS mode, concentrative ICP is considered negligible since DI water was used as feed. On the other hand, AL-FS mode experienced dilutive ICP which reduces the osmotic pressure gradient within the support layer. This explains the lower flux values of all membranes operated under AL-FS mode (at all GO loadings) than those operated under AL-DS (Figure 4-13a) (Xiao et al. 2015). Meanwhile, the higher J_s values obtained under AL-DS mode might be due to higher concentration differences across the membrane as indicated by the higher J_v values (Figure 4-13b) than those under AL-FS mode (Cath et al. 2013).

Regardless of the mode of operation, the J_v trend with respect to GO loading was similar with that of pure water permeability (RO mode Figure 4-3). Under both modes of operational-FS, J_v significantly improved at 0.1 and 0.25 wt% GO additions relative to GOT-0, despite the low osmotic pressure gradient (0.5 M NaCl). Relative to GOT-0, the highest improvement in J_v was measured at GOT-0.25 for AL-FS (from 6.08 to 19.77 L $m^{-2} h^{-1}$) and AL-DS modes (from 15.73 to 40.50 L $m^{-2} h^{-1}$). Thus, the favorable structural changes in the support induced upon addition of 0.25 wt% GO (as explained in Section 4.3.3.2) also positively affected the FO performance of TFC-FO membranes (Emadzadeh et al. 2014a, Lay et al. 2012, Tiraferri et al. 2011a).

These findings were further confirmed by the S values (Table 4-1) calculated from the RO and FO performance data. Results indicate that an optimal amount of GO addition (0.25 wt%,) led to the lowest S value of 191 μm among all tested membranes. Similarly, it exhibited the lowest tortuosity (τ) value (Table 4-1), which suggests that addition at 0.25 wt% GO has led to the formation of PSf/GO support with the shortest diffusive path length resulting in the most convenient transport of water through the membrane.

Meanwhile, J_s values also increased with GO contents in the membrane substrates. While J_v is expected to be directly related with J_s, the results at GOT-0.25 deviated from this relation. Albeit GOT-0.25 exhibited the highest J_v, moderate J_s was obtained relative to other membranes. However, the reverse flux selectivity (J_v/J_s) (Figure 4-13c), defined as the volume of water produced per the moles (or mass) of draw solute lost was observed highest at GOT-0.25 indicating that at this GO loading the modified PSf support layer is most favorable for the formation of PA active layer since J_v/J_s value is independent of DS properties and structural parameter (Phillip 2010, Xiao et al. 2015). This result is consistent with the ability of the active PA layer to reject salts wherein as discussed in Section 4.3.4.1, the highest rejection was achieved by PSf/GO with 0.25 wt% loading. Meanwhile, the ineffective formation of PA layer at GO loadings (≥0.5 wt%) could explain the low selectivity or J_v/J_s values of the corresponding TFC-FO membranes.

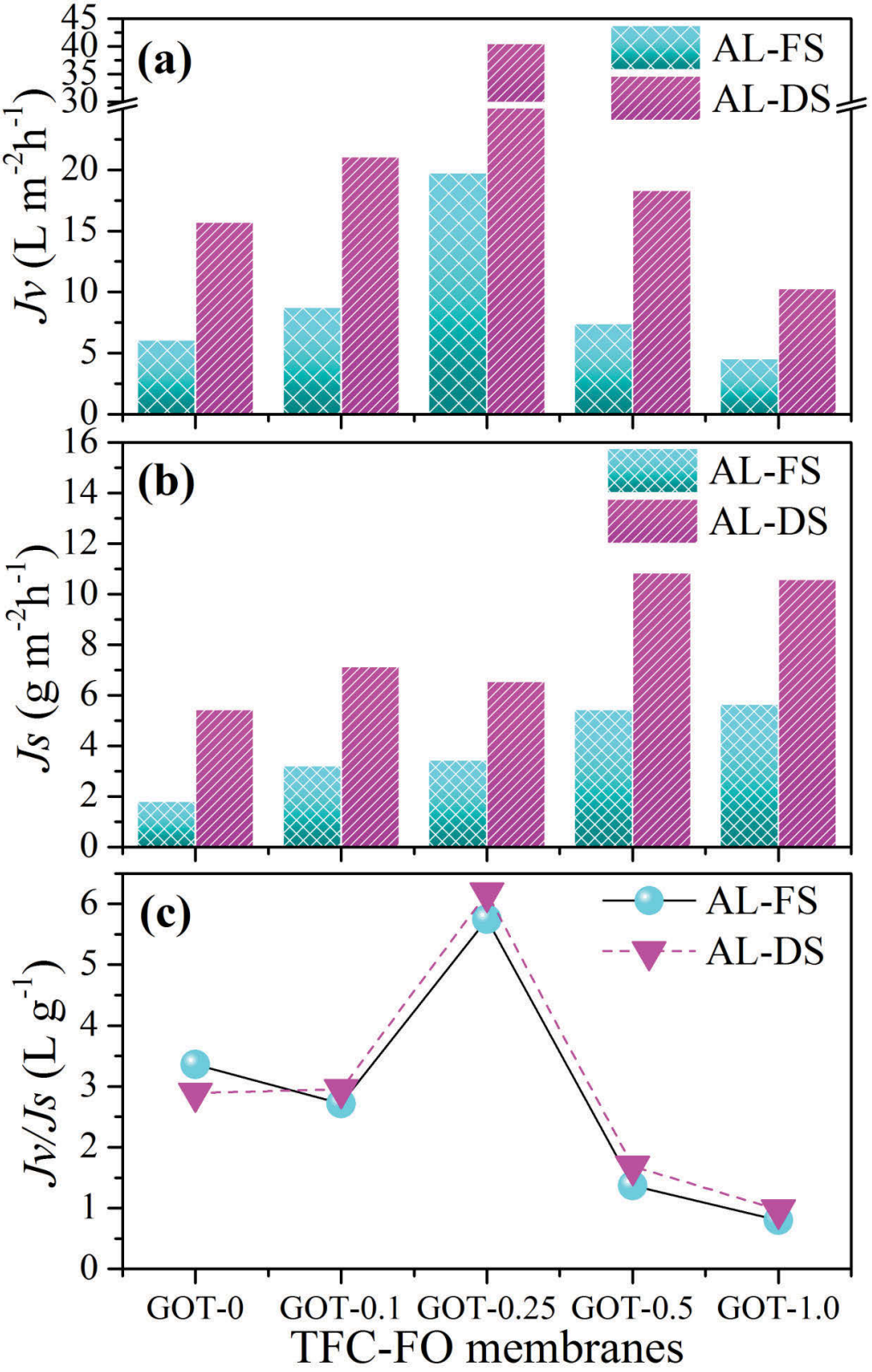

Figure 4 - 13. Effect of GO contents in membrane substrates for TFC-FO membrane performance (DI water as feed solution and 0.5 M NaCl as draw solution), (a) water flux (L $m^{-2}h^{-1}$, J_v), (b) reverse salt flux (g $m^{-2}h^{-1}$, J_s), (c) reverse flux selectivity (L g^{-1}, J_v/J_s).

4.3.8. Effect of NaCl draw solution concentrations with DI water and seawater as feed solutions

The performance of GOT-0.25 TFC-FO membrane was conducted under AL-FS mode to study the effect of draw solution concentration (0.5 - 4.0 M NaCl). With DI water as feed, results in Figure 4-14a reveal the steady increase in water flux from 19.77 to 43.68 L m^{-2} h^{-1} as the osmotic driving force increased with draw solution salt concentration. Meanwhile, increase in J_s values can be ascribed to the similar increase in salt concentration gradient across the active layer of GOT-0.25 FO membrane (Wang et al. 2015). However, the J_v/J_s value remains fairly constant and this is expected given that its value is independent of DS concentrations as described in the previous section 4.3.4.2 (Phillip 2010, Xiao et al. 2015).

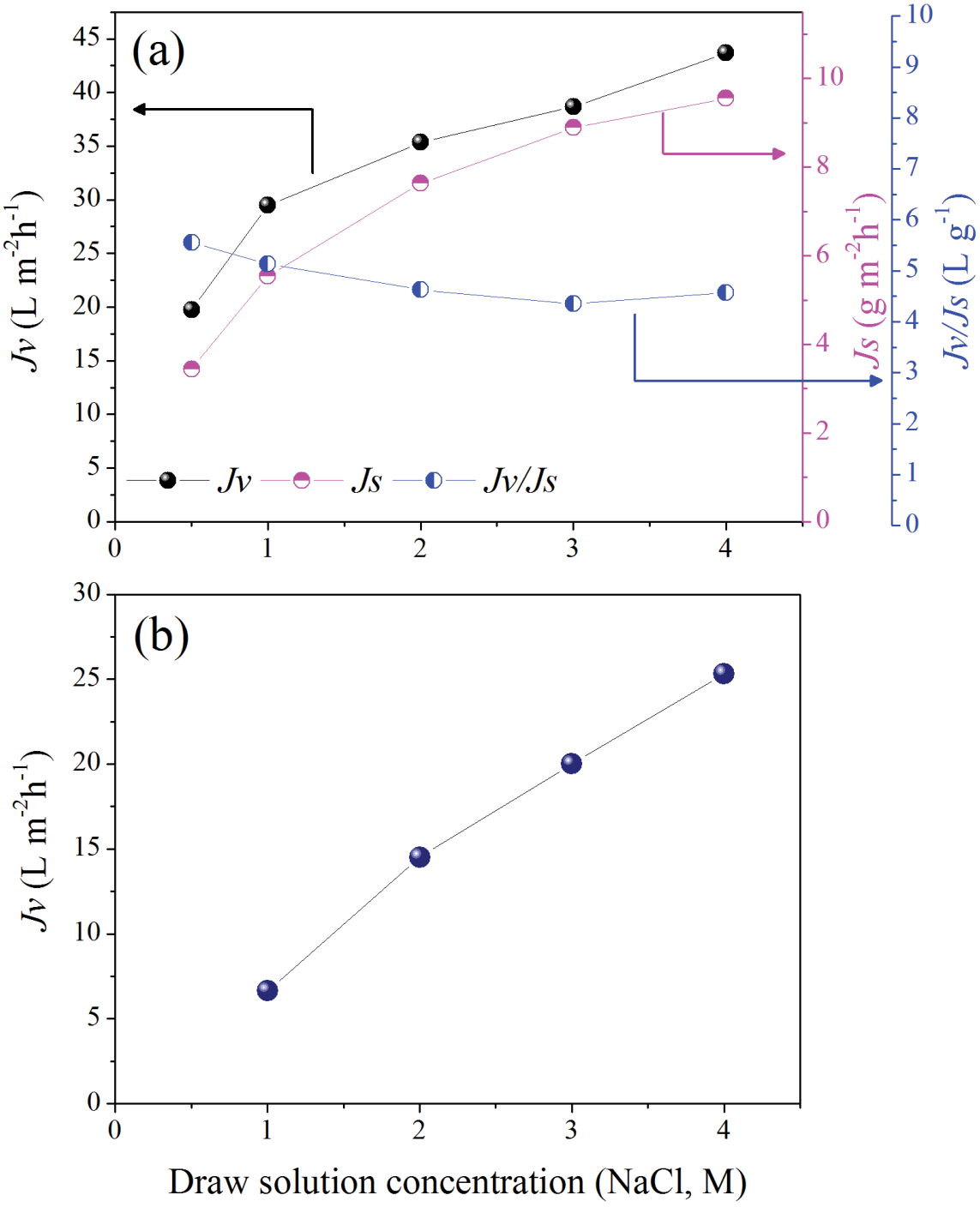

Figure 4 - 14. FO performance under AL-FS mode for GOT-0.25 at different concentration of NaCl (0.5, 1.0, 2.0, 3.0, 4.0 M NaCl) as draw solutions and, (a) DI water and (b) 3.5 wt% NaCl (model seawater, 0.6 M) as feed solutions.

Using 3.5 wt% (0.6 M) of NaCl as simulated seawater feed solution, the GOT-0.25 FO membrane exhibited J_v = 6.65 L m^{-2} h^{-1} at 1 M NaCl draw solution (Figure 4-14b) which significantly increased to 25.31 L m^{-2} h^{-1} at 4 M NaCl draw solution.

Overall FO performance of GOT-0.25 is quite comparable with previous studies which also incorporated hydrophilic nanomaterials in membrane substrates such as TiO_2 (Emadzadeh et al. 2014a), zeolite (Ma et al. 2013) and carbon nanotube (Wang et al. 2013d). But the facile and efficient preparation steps for GO-modified supports could be a viable option to produce TFC-FO membranes with enhanced water flux and selectivity performances.

4.4. Conclusions

In this chapter, incorporation of GO nanosheets in the PSf support successfully enhanced the FO performance of the TFC-FO membrane. Results reveal that a small but optimal amount of added GO (0.25 wt%) resulted in improved structural properties within the support layer, significantly enhancing the water permeability of the PSf/GO supported TFC-FO membrane. Regardless of the modes of membrane orientations, this PSf/GO supported TFC FO membrane at optimum GO loading exhibited the highest membrane selectivity. On the other hand, further increase in GO loadings beyond 0.5 wt% on PSf substrate resulted in less favorable structural properties of the support which directly affect water permeability and PA rejection layer formation due to ineffective or non-homogenous dispersion of GO in the PSf which resulted in the formation of membrane with sponge-like support structures with less porosity and smaller pore size. Non-homogeneous distribution of GO at higher loading also resulted in inefficient formation of PA selective layer via interfacial polymerization adversely affecting the salt rejection property of PSf/GO supported TFC-FO membranes. Nonetheless, the overall results in this study demonstrate that, the GO-modified PSf support layer could be a promising technique to produce TFC-FO membranes with enhanced water flux and flux selectivity.

CHAPTER 5

THIN-FILM COMPOSITE HOLLOW FIBER MEMBRANE INCORPORATED WITH GRAPHENE OXIDE IN POLYETHERSULFONE SUPPORT LAYER FOR ENHANCED OSMOTIC POWER DENSITY

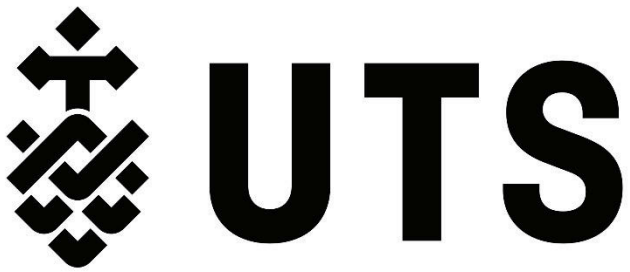

5.1. Introduction

TFC-PRO hollow fiber membrane itself should have high mechanical properties to be able to withstand against high hydraulic pressures in order to achieve high power density. Therefore, recent studies on developing TFC-PRO hollow fiber membrane have been focused on designing robust membranes via various fiber spinning techniques, different polymers and spinning conditions (Chou et al. 2013, Fu et al. 2013, Han et al. 2014, Li et al. 2014, Sun et al. 2013, Zhang et al. 2014).

In the previous chapter (Chapter 4) on the development of FO membranes, we used graphene oxide (GO) as filler for the membrane substrates in the fabrication of flat-sheet TFC-FO membranes, and found that the FO performance was significantly improved by lowering the *S* value at a suitable GO loading rate without significantly compromising its mechanical properties.

Despite significant improvement in the performance of TFC-FO membranes observed with nanomaterial incorporation, the fabrication of mixed matrix hollow fiber support for TFC-PRO membranes has yet to be fully explored. Thus, in this study, we investigated the fabrication of high performance TFC-PRO membrane by incorporating hydrophilic GO nanosheets in the polyethersulfone (PES) hollow fiber support layer. Three different TFC-PRO membranes were prepared and their PRO performances were compared in terms of osmotic power density. The effects of GO incorporation on the mechanical stability against hydraulic pressure were systematically investigated by determining membrane burst pressure for both hollow fiber supports and TFC membranes. In addition, the effect of pre-stabilization of PA selective layer and transport properties of TFC hollow fiber membranes were also explored. The membrane properties such as pore size, porosity, hydrophilicity, permeability, selectivity and mechanical properties were comparatively evaluated.

5.2. Experimental

5.2.1. Materials

Polyethersulfone (PES, Veradel® 3000P, Mw = 62,000 ~ 64,000 g/mol), purchased from Solvay Specialty Polymers, Republic of Korea, was used as the polymer material. N-methyl-2-pyrrolidone (NMP, Merck) and polyethylene glycol 400 (PEG, Mw = 400 g/mol, Merck) were used as a solvent and an additive, respectively, for hollow fiber support membrane preparation. Glycerol (99.5%) from Chem-Supply Pty. Ltd. (Australia) was used for post-treatment of as-spun hollow fiber membrane supports. For a selective layer formation, 1,3-phenylenediamine (MPD, 99%), trimesoyl chloride (TMC, 98%) and sodium dodecyl sulfate (SDS, ≥99.0%) were purchased from Sigma-Aldrich. Hexane (99.9%) from Merck was used as an organic solvent for dissolving TMC and sodium chloride (NaCl, Chem-Supply, Australia) was used to evaluate membrane performance. Different molecular weights of polyethylene glycol (PEG, MW = 12,000-35,000) and polyethylene oxide (PEO, MW = 100,000-600,000) purchased from Sigma-Aldrich were used for measuring pore size distributions.

5.2.2. Fabrication of hollow fiber supports

Dope solution compositions and spinning parameters for the fabrication of hollow fiber membrane substrates are presented in Table 5-1. Three different membrane supports were prepared in this study. A digital stirring machine, with constant speed of 800 rpm at 80^{o}C for 12 h, was used to mix a certain amount of PES with NMP as a solvent, and PEG and GO as additives, in a two-neck glass reactor. The dope solutions were then cooled down in room temperature with continuous stirring for another 12 h, transferred into a syringe pump and then degassed for 24 h at room temperature prior to hollow fiber spinning. To evaluate the effects of GO addition in the membrane supports, a control substrate without GO addition was prepared and denoted as HF-0. For the preparation of GO-incorporated dope solutions, various amounts of GO nanosheets were first homogeneously dispersed in NMP via sonication prior to addition of PES and PEG. According to the GO loadings with respect to PES amounts, hollow fiber supports were denoted as HF-GO-0.1 and HF-GO-0.2 which contain 0.1 and 0.2 wt% GO loading (weight ratio to the PES), respectively.

Table 5 - 1. Hollow fiber support membranes spinning parameter.

Spinning parameter	Hollow fiber supports		
Sample code	HF-0	HF-GO-0.1	HF-GO-0.2
Dope solution composition (wt%)	PES/PEG/NMP (20/40/40)	PES/PEG/NMP (20/40/40)	PES/PEG/NMP (21/39.5/39.5)
GO loadings in polymer (wt%)	0	0.1	0.2
Bore solution	DI water		
Outer solution	Pure NMP		
Dope flow rate (ml/min)	1.8		
Bore flow rate (ml/min)	1.2		
Outer flow rate (ml/min)	0.2		
Air gap distance (cm)	1.0		
Take up speed (m/min)	2.2		
External coagulant	Tap water		

In this study, a wet-wet spinning process was applied to prepare the hollow fiber membranes with highly porous structure to the outer surface by using a triple nozzle and hollow fiber spinning machine. As demonstrated in Figure 5-1, DI water, polymer dope, and pure NMP were separately supplied into the bore, inner, and outer channels, respectively, of the triple spinneret spinning machine design. The solutions were simultaneously extruded and immediately immersed in coagulation water bath with an air gap distance of 1 cm to solidify the polymer. The as-spun samples were collected by a drum type winder with a take up speed of 2.2 m/min, at an almost free fall condition. All parameters were set at the same conditions except the dope solution compositions as shown in Table 5-1. As-spun hollow fiber membranes were then kept in tap water for 2 days to remove residual solvents and then were post-treated by soaking in water/glycerol (50/50 wt%) aqueous solution for another 2 days to prevent membrane shrinkage upon drying. Subsequently, the post-treated hollow fiber samples were dried in air for membrane modulation. For membrane performance tests, hollow fibers were modulated by assembling 5 fibers with an effective length of around 13 - 14 cm, as shown in Figure 3-8 (A). The module ends were afterwards sealed with epoxy resin. The prepared samples were used for evaluating membrane performances.

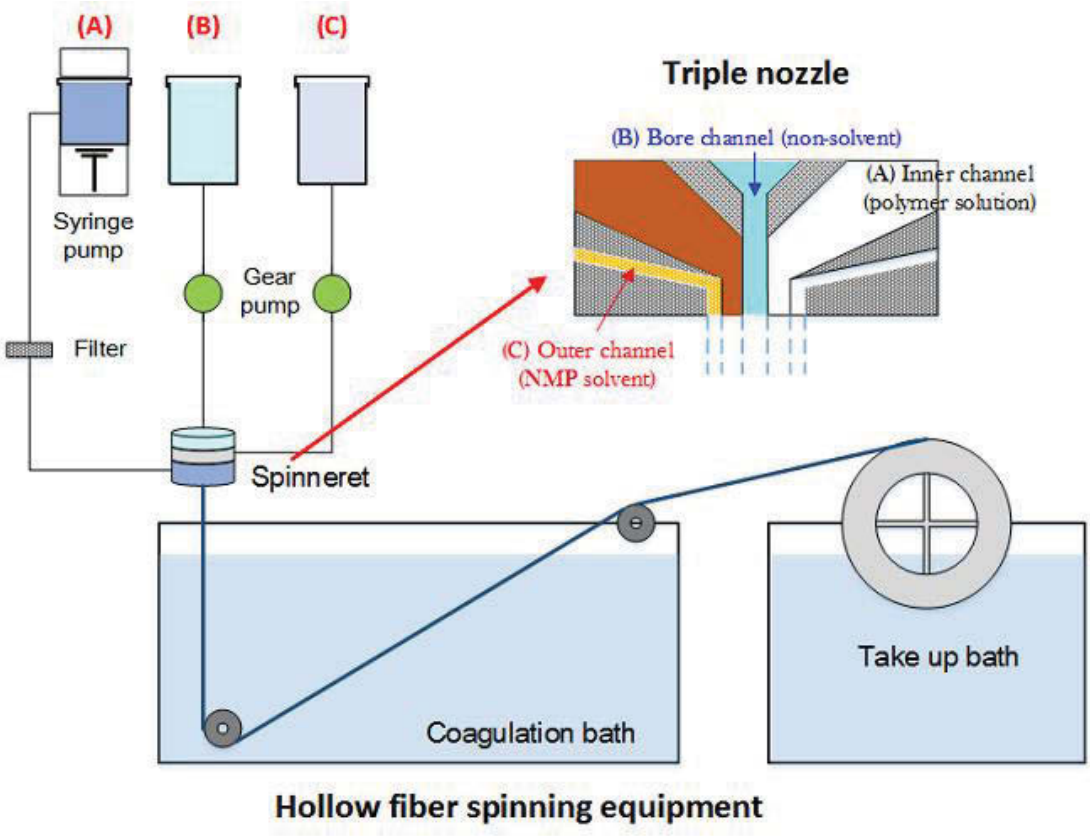

Figure 5 - 1. Schematic diagram of hollow fiber spinning set-up. (A) polymer dope solution, (B) bore solution, (C) pure NMP

5.2.3. IP onto the lumen side of membrane supports

Figure 3-8 illustrates the IP process of hollow fiber membranes, during which a polyamide (PA) active layer was deposited on the lumen side of hollow fibers. First, the inlet side (lumen side) of vertically-held membrane module was connected to the peristaltic pump with silicone tube to introduce an aqueous solution (2 wt% MPD + 0.1 wt% SDS solution) with a flow rate of 4.1 mL/min for 3 min. Excess solution was removed by purging N_2 gas at a pressure of 100 kPa for 5 min. To complete the IP reaction, 0.15 wt% TMC in hexane was introduced with a flow rate of 2.3 mL/min for 5 min to provide enough time to react with residual MPD in the lumen side of hollow fiber membranes. Finally, the unreacted TMC was removed by purging N_2 gas (100 kPa) for 30s. All membrane modules were then soaked in DI water without further treatment, and

kept in cool condition prior to performance experiments and membrane characterizations. According to the sample codes of hollow fiber supports, PA layer deposited samples were denoted from the HF-0, HF-GO-0.1 and HF-GO-0.2 to the THF-0, THF-GO-0.1 and THF-GO-0.2, respectively.

5.2.4. Pore size measurement of hollow fiber supports

Mean pore size and pore size distribution of hollow fiber supports were characterized by solute transport experiments employing different molecular weights of PEG and PEO as feed solutions and the procedure is described elsewhere (Lim et al. 2017, Liu et al. 2014a, Ong et al. 2015, Sukitpaneenit et al. 2012b). The feed solutions of 200 mg L^{-1} with different molecular weights of PEG or PEO were filtered by hollow fiber membranes under a trans-membrane hydraulic pressure of 1 bar at a cross-flow mode. The concentrations of feed and permeate solutions were measured by a total organic carbon analyzer (multi N/C® 3100, Germany). The relationship between Stokes radius, r_s (nm) and molecular weight (g mol^{-1}) of PEG and PEO can be expressed by Eq. 5-1 and Eq. 5-2, respectively.

$$r_s = 16.73 \times 10^{-3} \times MW^{0.557} \quad (5\text{-}1)$$

$$r_s = 10.44 \times 10^{-3} \times MW^{0.587} \quad (5\text{-}2)$$

When the solute rejection (R_s) is plotted against the solute diameter (d_p) on a log-normal scale, a linear correlation can be obtained. The mean effective pore size (μ_p) was determined as the d_p at R_s=50%, and the geometric standard deviation (σ_p) was found as ratio of the d_p at R_s=84% and R_s=50%. The pore size distributions of hollow fiber supports were derived by the probability density function presented in Eq. 5-3 (Ong et al. 2015, Sukitpaneenit et al. 2012b).

$$\frac{dR(d_p)}{d(d_p)} = \frac{1}{dp \ln \sigma_p \sqrt{2\pi}} \exp\left[\frac{(\ln d_p - \ln \mu_p)^2}{2(\ln \sigma_p)^2}\right] \quad (5\text{-}3)$$

5.2.5. RO performance and burst pressure evaluation for hollow fiber supports and TFC hollow fiber membranes

5.2.5.1. Determination of pure water permeability and burst pressure of hollow fiber supports

Pure water permeability (*PWP*, L m^{-2} h^{-1} bar^{-1}) and burst pressure (bar) of hollow fiber supports were determined using a lab scale membrane test unit. DI water as feed was circulated for both the lumen and the shell sides of hollow fiber module at a constant flow rate of 150 mL min^{-1}. Prior to the measurement of weight changes to the permeate side, the tested samples were stabilized at the applied trans-membrane pressure (from lumen to shell side) of 1 bar for 1h. The *PWP* was calculated using the Eqns. 3-5 and 3-6.

Afterwards, the pressure in the lumen side was gradually increased in increments of 2 to 3 bar until the membranes exhibited complete failure. The *PWP* at each pressures was measured by averaging the data collected for 20 min.

5.2.5.2. Evaluation of burst pressure and intrinsic properties of the TFC-PRO membranes

To determine the burst pressure (or critical pressure) and RO performances for TFC-PRO membranes, an experiment similar to that was performed for hollow fiber supports (section 5.2.5.1) was also conducted using the PRO unit. Evaluation of burst pressures for TFC-PRO membranes was performed without any membrane compaction. Initial pressure of 5 bar was applied with the DI water to the lumen side at flow rate of 150 mL min^{-1}, stabilized for 20 min, and the average *PWP* was determined. Then, the pressure was increased in 2 bar increments until the pressure reached 13 bar while being stabilized for 20 min at each pressure and then it was increased by 1 bar per increment until the membrane breakage occurred within 20 min and the membrane breakage pressure was

defined as 'burst pressure'. In addition, the 'critical point' at certain pressures for TFC-PRO membranes was also determined where the membranes started to show considerable deformation and damage determined by sudden increase of water permeability.

Intrinsic properties of TFC-PRO membranes such as pure water permeability (*A* or *PWP*, L m^{-2} h^{-1} bar^{-1}) and salt rejection (*R*, %) were evaluated at two different operation conditions. First, prepared TFC-PRO membranes were pre-stabilized at 8 bar for 1 h, and then the *A* value was determined via collecting permeated pure water and *R* value was obtained from the rejection rate of 2000 ppm NaCl when the feed water operated at 8 bar. Conductivity and volume changes of the permeated water as well as applied pressures were monitored and recorded by a conductivity meter and data auto-logging system. The salt rejection and salt permeability (*B*) was calculated using Eq. 3-7 and Eq. 5-4, respectively (Xiong et al. 2016).

$$B = \frac{1-R}{R}(\Delta P - \Delta\pi)A \tag{5-4}$$

where $\Delta\pi$ in Eq. 5-4 is the osmotic pressure difference across the membrane.

Alternatively, the TFC-PRO samples for THF-0, THF-GO-0.1 and THF-GO-0.2 were pre-stabilized for 1 h below their critical points which were found to be at 13.5 bar, 13.5 bar and 16.5 bar, respectively, prior to performance evaluation. This was followed by determination of *A* and *R* values of samples at different pressures. The critical point for each membrane was decided from the results of RO mode operations at varied applied pressures. The temperature of all solutions was maintained at 23 ± 1°C during the tests.

5.2.6. PRO performance evaluation for TFC-PRO membranes

To evaluate the PRO performance of the TFC-PRO membranes, 1.0 M NaCl (5 L) was used as draw solution circulating to the lumen side (facing active layer) of hollow fiber membrane and DI water (2 L) as feed to the shell side using the PRO unit. The flow rate was set for both streams at 150 mL min^{-1}. Before conducting PRO evaluations, the TFC-PRO membranes of THF-0, THF-GO-0.1 and THF-GO-0.2 were stabilized for 1 h at 13.5

bar, 13.5 bar and 16.5 bar, respectively, of which pressures are below the critical points of each membranes. After the membrane stabilization, each sample was tested from 0 bar stepwise up to the stabilized pressures and this test was denoted as 1st-run. In order to confirm the stability and reproducibility of each tested samples, second (2nd-run) operation was conducted right after 1st-run at the same ranges of applied pressures.

The power density (W, W m^{-2}) can be obtained from Eq. 5-5 where ΔP is the pressure difference across the TFC-PRO membrane.

$$W = J_w \Delta P \tag{5-5}$$

5.2.7. Determination of membrane structural parameter

The J_w in the presence of ICP in the PRO process can be expressed as follows (Achilli et al. 2009, Chou et al. 2012a):

$$\frac{J_w}{k} = ln\left[\frac{(A\,\pi_D - A\,\Delta P - J_w) + B\left[\left(\frac{A\Delta P}{J_w}\right)+1\right]}{A\pi_F + B\left[\left(\frac{A\Delta P}{J_w}\right)+1\right]}\right] \tag{5-6}$$

where π_F and π_D are the bulk osmotic pressures. A and B are determined under RO conditions and their units are converted to m s^{-1} bar^{-1} and m s^{-1}, respectively.

5.3. Results and discussion

5.3.1. Effect of GO loading on the characteristics of hollow fiber supports

The effect of GO loadings on the morphological changes of PES hollow fiber membrane supports was characterized by FE-SEM analysis as shown in Figure 5-2 which reveals the inner and outer surfaces as well as the cross-section of all prepared membranes for HF-0, HF-GO-0.1 and HF-GO-0.2. A typical asymmetric structure with finger-like and sponge-like structures appeared in the cross-section of all membranes. In case of outer

surface, all membranes revealed a sponge-like structure with highly porous and rough surface without skin-layers formation. This is because the co-extrusion of pure NMP (solvent) in the outer fluid channel during spinning likely induced a delayed demixing (Han et al. 2013b, Li et al. 2014, Sukitpaneenit et al. 2012b, Zhang et al. 2014). In contrast, due to the fast phase inversion induced by strong non-solvent (water) as a bore fluid, relatively dense skin-layer with small pores were formed on the inner surface of all the prepared hollow fiber membrane supports. The simultaneous extrusion of three different solutions via triple spinneret as described in Figure 5-1 also subsequently induced the formation of dual-layered structure in the cross-section: 1) the finger-like structures are dominantly formed near the lumen side of hollow fiber membranes due to the faster demixing by the water as bore fluid and 2) the less finger-like but more sponge-like structures are appeared as close to the outer surface because the NMP solvent as the outer channel strongly influenced to a slower phase inversion from out to inward (Han et al. 2013b).

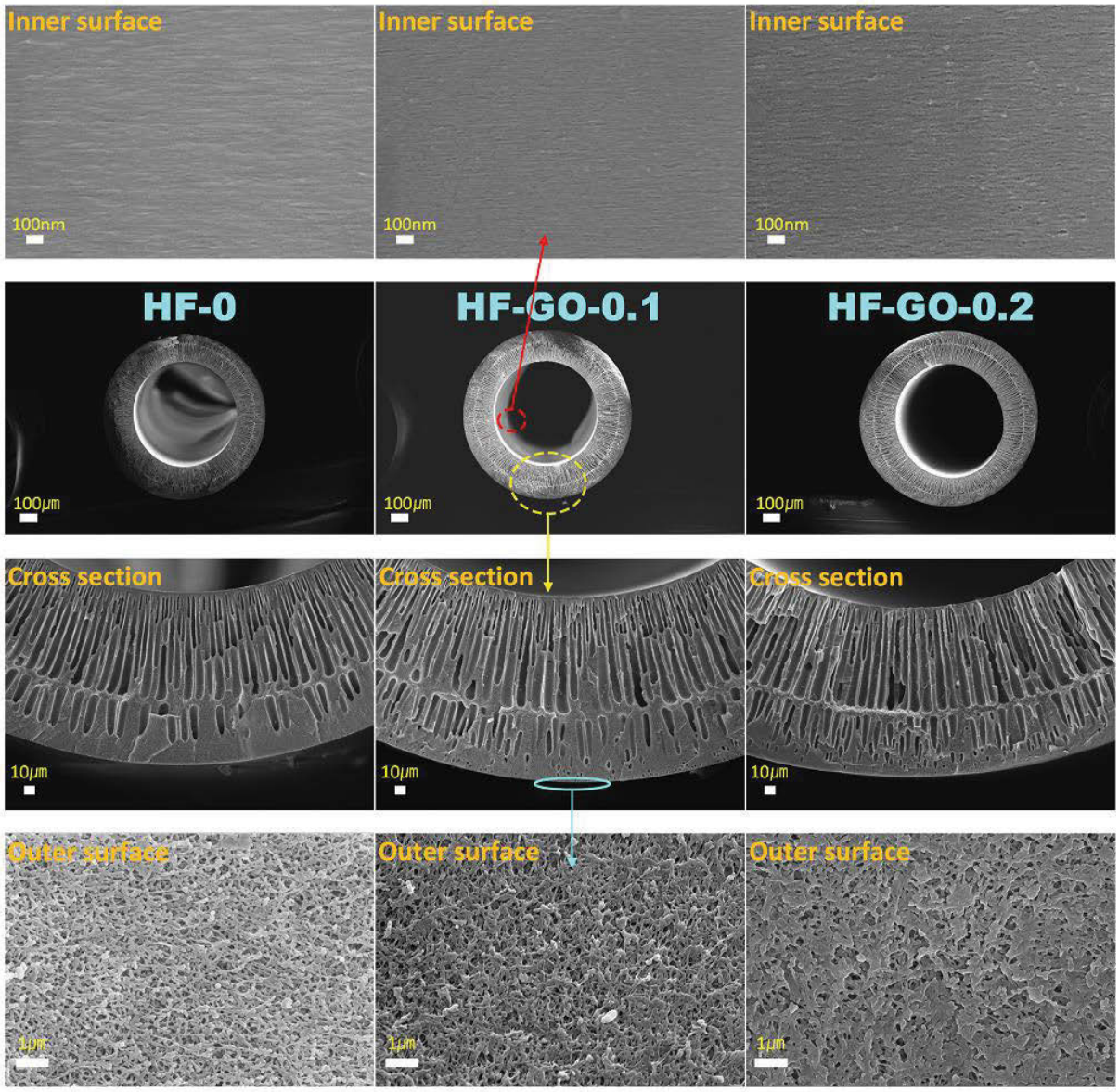

Figure 5 - 2. FE-SEM images of inner surface, outer surface and cross-section areas of hollow fiber supports (HF-0, HF-GO-0.1 and HF-GO-0.2).

Interestingly, it can be clearly distinguished from the cross-section SEM images that the number of macrovoid structures increased with an increase in GO loadings. As the GO loadings increased from 0 to 0.2 wt%, the density and length of finger-like pores increased at the internal zone of the hollow fibers near the membrane lumen. Furthermore, the number of outward-pointed macrovoids increased instead of sponge-like structure at the outer region. This trend was also observed in our previous studies (Lim et al. 2017) and other studies (Shukla et al. 2017, Zinadini et al. 2014) in which GO was incorporated in

the polymeric membrane substrates. Low loading rates of GO with uniform dispersion in the polymer dope solution increase the thermodynamic incompatibility between polymer and solvent due to the hydrophilicity of the nanomaterial. Thus, the hydrophilic GO enhanced the exchange rate between the solvent and non-solvent during the phase separation which resulted in hindrance of sponge-like structure formation (Wang et al. 2015). It can be noted that more finger-like morphologies were obtained for HF-GO-0.2 against HF-GO-0.1. The polymer concentration increase from 20 to 21 wt% and the GO concentration increase for HF-GO-0.2 may both increase the dope solution viscosity, but only 0.1 wt% increase of GO loading seemed to predominantly affect the phase separation kinetics than the polymer solution viscosity(Han et al. 2014).

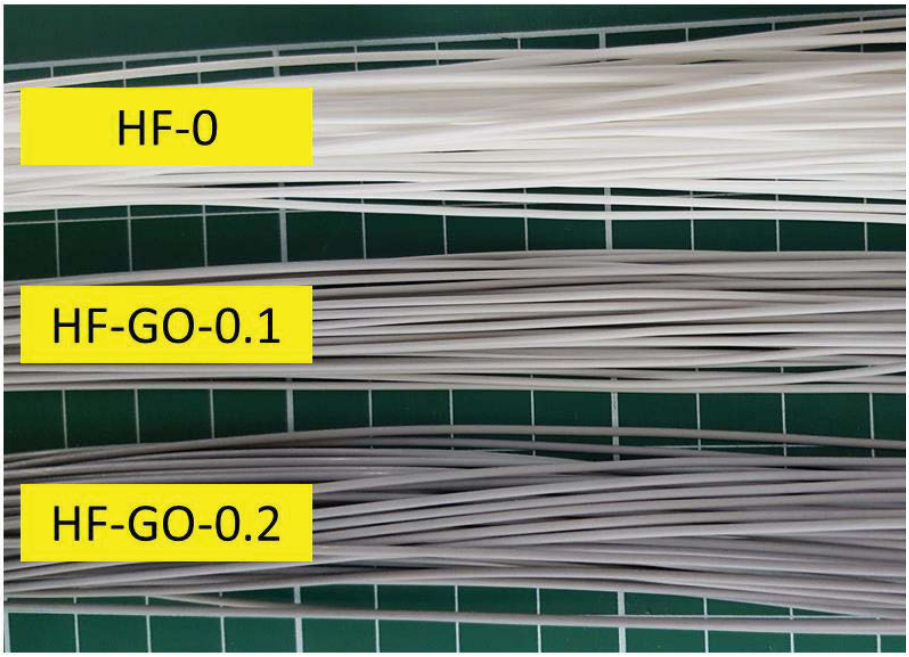

Figure 5 - 3. Photo images of hollow fiber membrane substrates for HF-0, HF-GO-0.1, HF-GO-0.2.

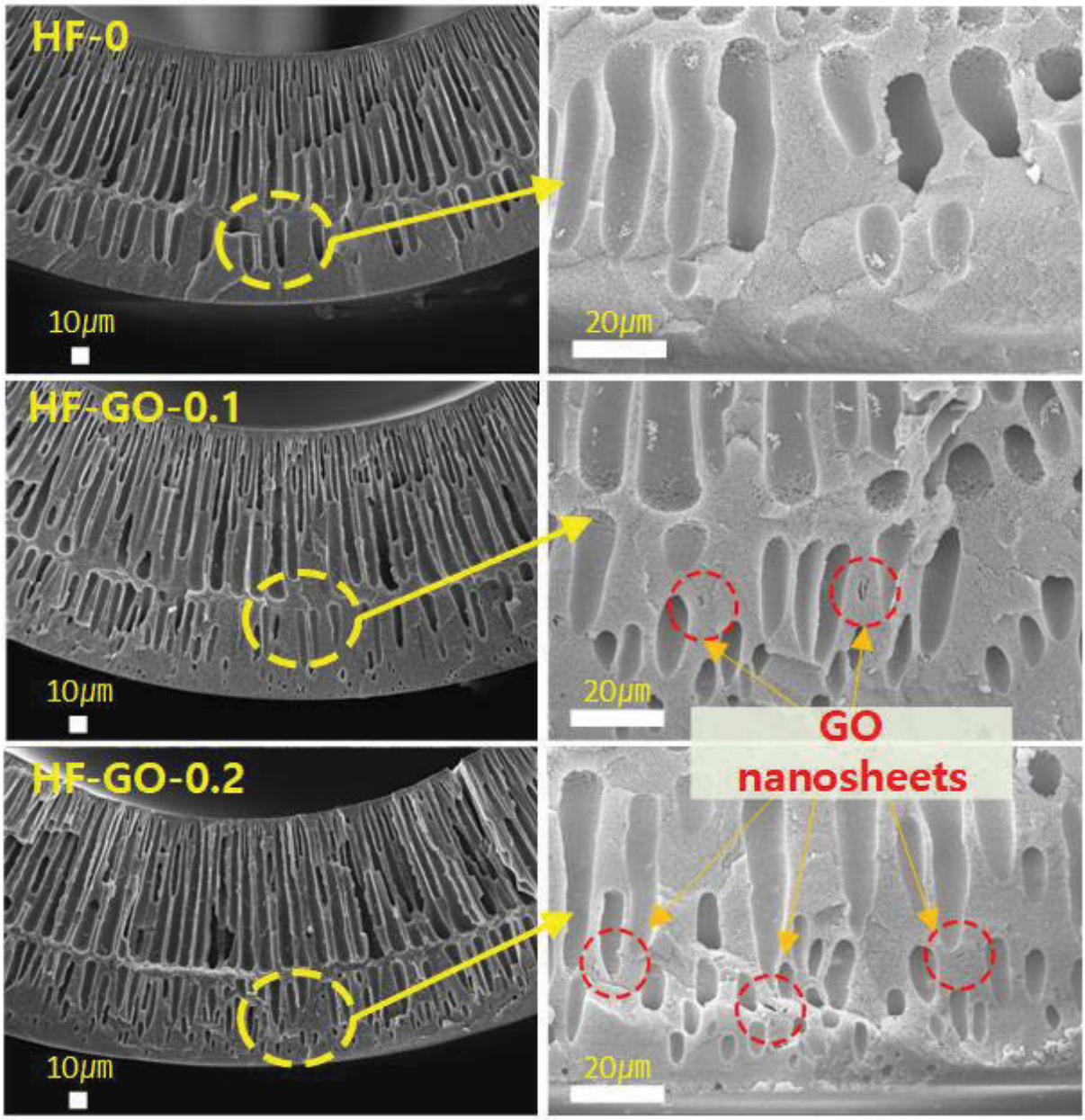

Figure 5 - 4. SEM images of hollow fiber membrane supports for cross-section area (HF-0, HF-GO-0.1, HF-GO-0.2)

The presence and incorporation of GO in the hollow fiber substrates were confirmed by photographs and SEM images from Figures 5-3 and 5-4, respectively. After incorporation of GO in PES substrates, the color of hollow fiber surfaces has become darker from off-white to brownish gray as GO loadings increased as shown in Figure 5-3. The presence of GO in the PES substrates also observed in the cross-section of SEM images (Figure 5-4) as red circles for HF-GO-0.1 and HF-GO-0.2 indicate some GO aggregation. Although

assumed not significant, some GO nanoparticles might likely aggregated even though the GO loadings were small (≤ 0.2 wt%), which is due to the high dope solution viscosity increased by high polymer concentration of 20-21 wt% and the high content of PEG as an additive (Wang et al. 2015). However, this minor GO aggregation in the membrane substrates did not cause deterioration of mechanical properties. Table 5-2 summarized the physical properties of fabricated hollow fiber supports including mechanical properties. The tensile strength and the elongation at break for HF-0 were 5.18 MPa and 47.37%, respectively, and incorporation of 0.1 wt% GO (HF-GO-0.1) did not alter these values significantly. Thus, it can be concluded that the mechanical properties of the PES support was not affected by a small amount of GO incorporation. In fact, the tensile strength of HF-GO-0.2 slightly increased to 5.56 MPa although this might not be due to increased GO loading (0.2 wt%) only but also likely due to the increase of polymer concentration.

Table 5 - 2. Hollow fiber sizes, mechanical properties, pure water permeability and pore size distribution of prepared hollow fiber supports.

Membrane properties	**Hollow fiber supports**		
	HF-0	HF-GO-0.1	HF-GO-0.2
ID/OD (μm)	663/1050	664/1044	685/1070
Thickness (μm)	196	190	193
Tensile strength (MPa)	5.18 ± 0.14	5.20 ± 0.21	5.56 ± 0.20
Elongation at break (%)	47.37 ± 4.52	46.96 ± 4.16	46.36 ± 3.16
Toughness[1)] (N m^{-2})	2.50 ± 0.12	2.53 ± 0.15	3.08 ± 0.09
PWP (L m^{-2} h^{-1} bar^{-1})	322	361	387
Mean pore diameter, μ_p (nm)	8.28	8.85	9.03
Geometric standard deviation, σ_p	1.86	1.90	1.94

[1)] Toughness was calculated by obtaining the intergral underneath the stress-strain curve.

The mean pore diameter and *PWP* of hollow fiber supports are presented in Table 5-2. Without GO incorporation, the HF-0 showed the mean pore diameter of 8.28 nm, however it continuously increased as GO loadings increased to HF-GO-0.1 and HF-GO-0.2 with the mean pore diameter of 8.85 nm and 9.03 nm, respectively. This trend is a result of hydrophilic GO effect that accelerated the rate of the phase inversion inducing the increase of macro pores as visible in the cross-section images (Figure 5-2) especially an

increase of lumen surface pores, and the reduction of membrane thickness (Table 5-2). The *PWP* results also revealed a consistent trend with the pore size of the hollow fiber supports. GO embedded in PES supports at 0.1 and 0.2 wt% loading significantly improved the *PWP* to 361 and 387 L m^{-2} h^{-1} bar^{-1}, respectively, as compared to that of pure PES support (322 L m^{-2} h^{-1} bar^{-1}). The enhanced *PWP* could be not only due to enhanced membrane porosity but also due to improved surface hydrophilicity by GO addition (Hu et al. 2013, Lee et al. 2013). This enhanced hydrophilicity is evident from Figure 5-5 where the contact angle decreased correspondingly with an increase of GO content. The contact angle of HF-0 was 81.56° which decreased to 77.13° at 0.1 wt% GO loading and further decreased to 73.41° at 0.2 wt% GO loading. GO is known to contain abundant functional groups such as hydroxyl, carboxyl and epoxy groups which may improve hydrophilicity by decreasing surface energy of the membrane surface. Similar results were reported from previous studies where GO was used as a filler of composite membranes (Lee et al. 2013, Qin et al. 2015, Shukla et al. 2017, Zhao et al. 2013b, Zinadini et al. 2014).

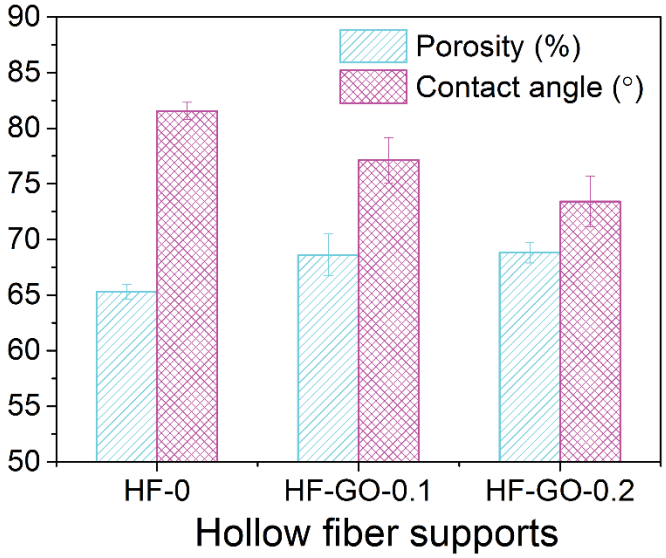

Figure 5 - 5. Effect of GO loadings in hollow fiber membrane support on membrane porosity and contact angle.

Figure 5-5 show that the overall porosity of membranes increased from 65.3% to 68.6% with 0.1 wt% GO loading while this increase to 68.8% was very marginal at 0.2 wt% GO loading. This is probably due to the effect of higher polymer concentration of dope solution that produced denser matrix of overall membrane structure although the membrane morphology of HF-GO-0.2 in the cross-section of SEM image seemed more porous than that of HF-GO-0.1.

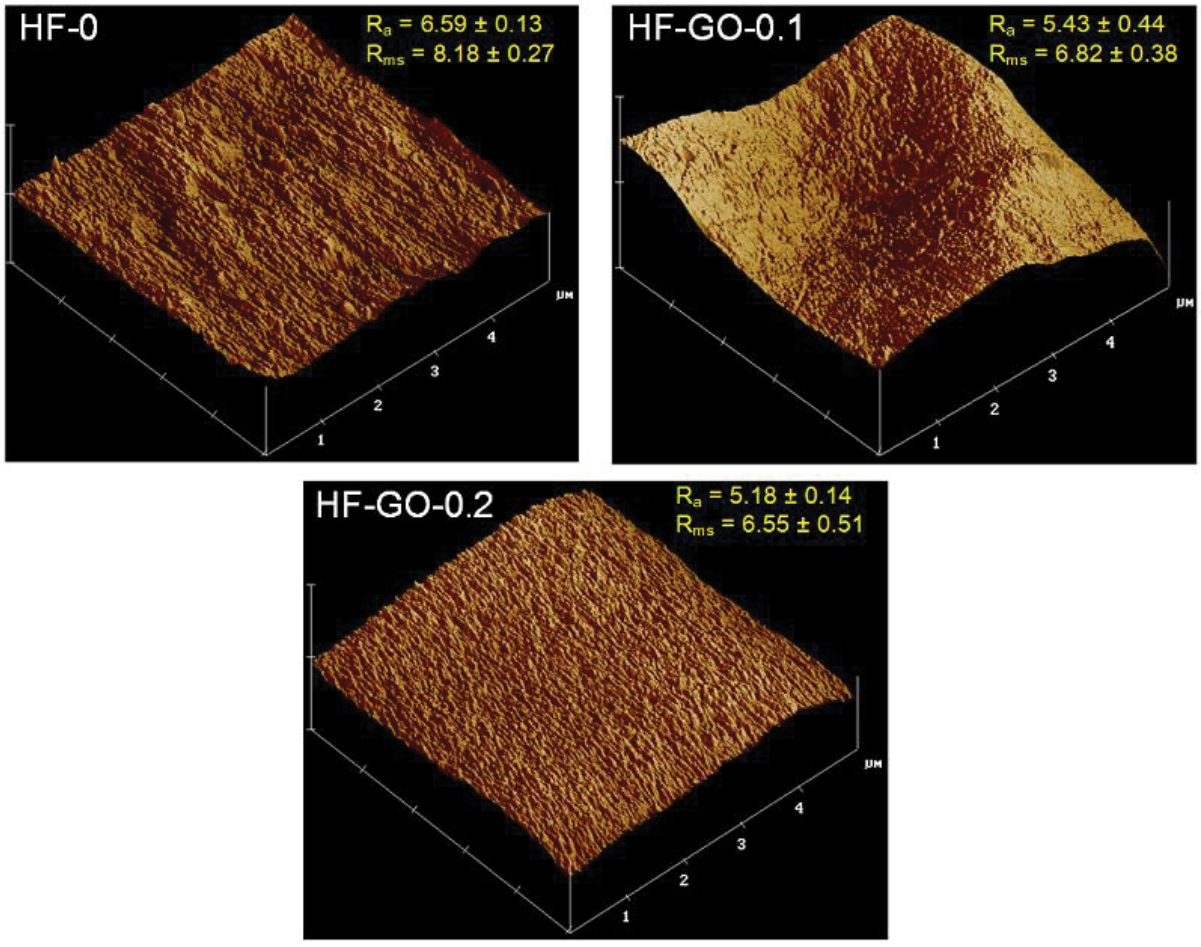

Figure 5 - 6. AFM images of inner surface of hollow fiber supports for HF-0, HF-GO-0.1 and HF-GO-02 (R_a= mean roughness (nm), R_{ms}= root mean square of z values (nm)).

The surface morphology or roughness of the lumen side of the prepared hollow fiber membranes was characterized using AFM analysis. Figure 5-6 shows the three-dimensional (3D) AFM images of the membrane lumen surfaces for HF-0, HF-GO-0.1

and HF-GO-0.2. Additionally, the mean roughness (R_a, nm) and root mean square ridge elevation (R_{ms}, nm) are determined from the scanning area of 5 μm × 5 μm and averaged values are presented in the images. The R_a and the R_{ms} of HF-0 were 6.59 nm and 8.18 nm, respectively. However, the R_a and the R_{ms} values for HF-GO-0.1 and HF-GO-0.2 membrane samples were relatively lower due to GO incorporation. The AFM images also shows the uniform and smoother surface morphologies for HF-GO-0.1 and HF-GO-0.2 membrane samples, which is likely a result of well-dispersed GO in the PES substrate (Shukla et al. 2017, Zhao et al. 2013a, Zinadini et al. 2014).

5.3.2. Morphology and membrane stability evaluation of TFC-PRO membranes

The successful depositions of PA selective layer on the inner surface of hollow fiber membranes were confirmed by FE-SEM observation as depicted in Figure 5-7. The top surface of PA layer for hollow fiber samples were shown on the left-side images of Figure 5-7 (a, b and c) and the images on the right (d, e and f) show the cross-section at near the inner surface of hollow fiber. The typical ridge-and-valley structures were seen on the membrane surfaces for all prepared TFC membranes from the SEM images, which affirms the presence of well-formed thin film of PA layer via interfacial IP process (Chou et al. 2013, Han et al. 2014, Han et al. 2013b). From the cross-sectional SEM images of TFC-PRO membranes, interestingly, the average thickness (averaged from the ten randomly measured) of PA layers have significantly decreased in the order of 269 nm, 181 nm and 163 nm for THF-0, THF-GO-0.1 and THF-GO-0.2, respectively.

Similar trend was observed in previous studies which reported that the relatively smaller pore size (Table 5-2) for pure PES support may have caused the MPD monomer to stay at the mouth of the membrane pores, and rapidly diffuse into the organic phase and then react with TMC during the IP (Yan et al. 2016, Zhang et al. 2014). Moreover, rougher surface morphology (Figure 5-6) may cause the MPD with non-uniformly filled-up on the membrane surface. Therefore, this characteristic of the membrane surface in the IP reaction is a result of creation of a relatively thick, rough and ineffective formation of PA

layer (Ren et al. 2017, Yan et al. 2015b, Zhang et al. 2014). The membrane surface with larger pore size and smoother surface, but with hydrophilic property formed by GO incorporation may prove to be the more favourable conditions for the regular deposition of thin MPD layer prior to the IP reaction. Consequently, this induces the formation of homogeneous PA selective layer with thinner and defect-free PA deposition. It is an evident that THF-GO-0.2 had the thinnest PA layer among the three prepared samples, which has the characteristics of the biggest surface pore but lowest roughness and strong hydrophilicity. Similar trend was also observed in the literature (Lay et al. 2012).

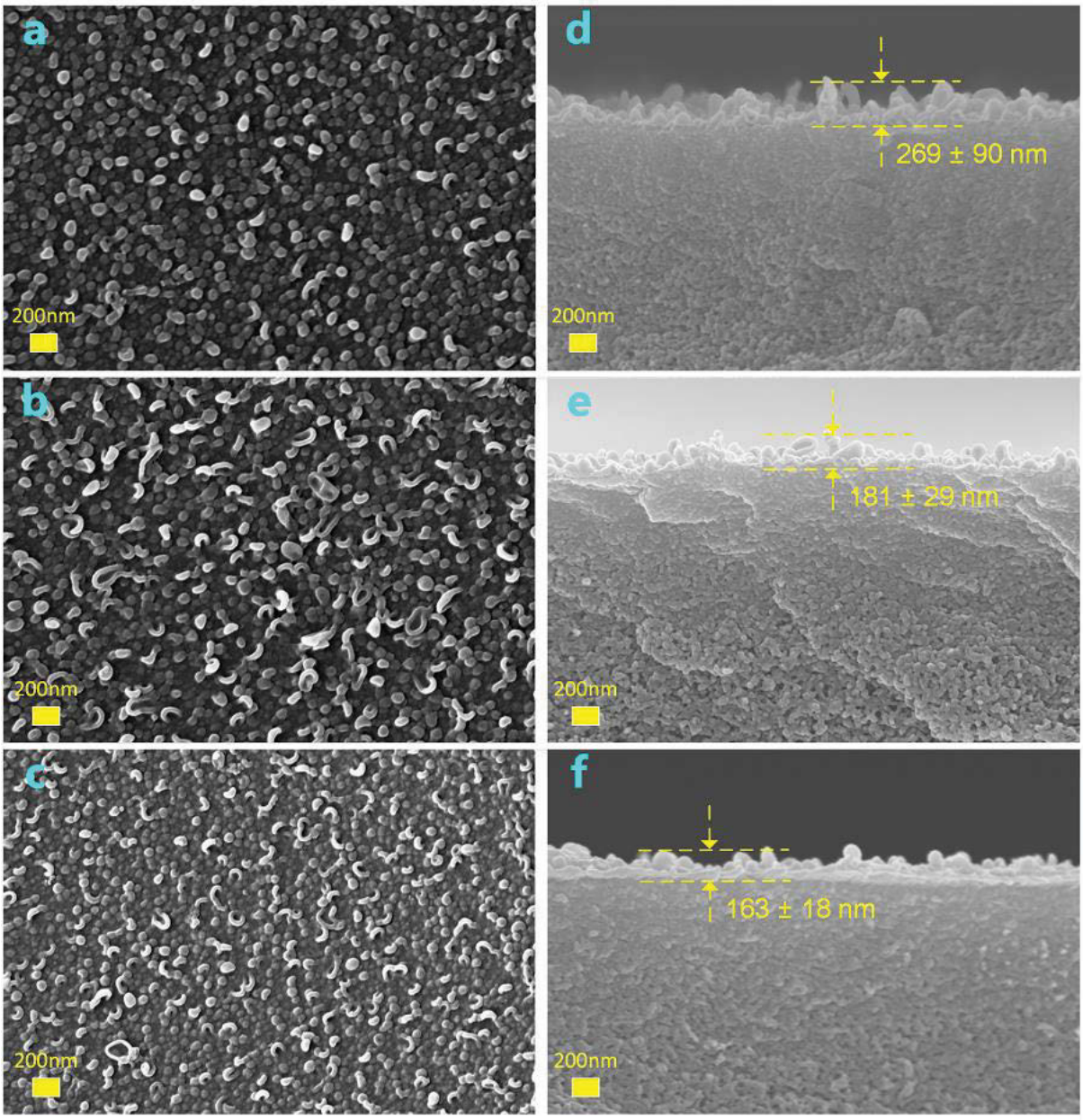

Figure 5 - 7. FE-SEM images of PA active layer top view and cross-section images near to the PA layer of THF-0 (a and d), THF-GO-0.1 (b and e) and THF-GO-0.2 (c and f).

Evaluation of membrane stability and determination of their maximum ability against high hydraulic pressure are very important parameters especially for TFC-PRO hollow fiber membranes, in which the active layer (PA layer) is deposited on the inner surface of the hollow fiber. This is because the application of the high hydraulic pressures from inside to outside will induce physical stress resulting in an expansion of membrane inner (lumen) diameter, and considerably affect the integrity of PA layer due to deformation. Therefore, the TFC-PRO hollow fiber membranes should possess strong mechanical properties to withstand against hydraulic pressure on the lumen side, otherwise the hollo fiber membrane may burst especially when the pressure exceed its critical pressure. Polymeric membranes in general without any support materials have limitations with its mechanical properties (Chen et al. 2016). For the long-term performance stability of the membrane with minimum membrane damage, the robustness of the fabricated membranes should be evaluated and this was done by determining the burst pressure and the critical point of each hollow fiber membrane samples (Chen et al. 2016, Han et al. 2014, Han et al. 2013b, Li et al. 2014).

The burst pressure of the hollow fiber supports and TFC-PRO membranes were tested based on their pure water permeability at increasing hydraulic pressure as shown in Figure 5-8. The normalized *PWP* (Figure 5-8(a)) for all hollow fiber supports indicated a rapid reduction in the *PWP* values with the increase of applied pressures up to somewhat mainly due to membrane compaction (Han et al. 2014). There was about 30% decrease of the *PWP* for HF-0 at 13.9 bar and then suddenly increased when the membrane deformation starts, until the membrane is completely burst at 16.3 bar. Similar pattern was also observed with HF-GO-0.1 membrane sample with a burst pressure of 16.2 bar. Meanwhile, the highest burst pressure of 18.6 bar was observed for HF-GO-0.2 membrane however, this same membrane sample also showed the most severe reduction rate in normalized *PWP* which was then followed by HF-GO-0.1 and HF-0. This may be related with the pore sizes of the hollow fiber supports (Table 5-2) which follows the order of HF-GO-0.2 > HF-GO-0.1 > HF-0. The larger pores and higher surface porosities of the membranes likely results in more compaction of the membrane.

In contrast to the normalized *PWP* trend, all TFC-PRO membranes showed a gradual increase in *PWP* with the increase in applied pressures (Fig. 5-8(b)). This phenomenon may be the result of the two effects: (1) the increase of membrane effective area attributed by the stretching and thinning of the PA selective layer, and (2) the reduced water transport resistance due to the decreased membrane thickness, when the hydraulic pressure is applied to the membrane lumen side (Gai et al. 2016, Han et al. 2014, Han et al. 2013b). The steady increase of *A* values for TFC-PRO membranes was observed up to the pint of critical pressures of around 14 bar for HF-0 and HF-GO-0.1, and 17.3 bar for HF-GO-0.2. At pressures above the critical pressures, a sudden increase of *A* values was observed until the membranes reached complete failure (burst) at around 16.0 bar for both THF-0 and THF-GO-0.1, and 18.8 bar for THF-GO-0.1. These findings indicate that the damage of PA layer by irreversible changes or minor defects, will be experienced before reaching the burst pressure of hollow fiber support layer, where the support layer deformation begins with significant increase of *PWP* from Figure 5-8(a) and Figure 5-8(b) (Han et al. 2013b).

The evaluation of mechanical stability of the hollow fiber membranes showed that addition of 0.1 wt% GO into PES hollow fiber support layer did not undermine the overall mechanical stabilities compared to pure PES support. On the other hand, the hollow fiber membrane whose PES concentration was increased by 1 wt% polymer with 0.2 wt% GO incorporation, showed significant improvement in mechanical stability, even though this membrane was observed to have more macrovoids and higher porosity (Figure 5-2) compared to the other membranes. Membrane toughness, which was determined by integrating the stress-strain curve as listed in Table 5-2, further confirms the robustness of these fabricated membranes. The highest membrane toughness of 3.08 N m^{-2} was obtained for HF-GO-0.2 while the HF-0 (2.50 N m^{-2}) and HF-GO-0.1 (2.53 N m^{-2}) showed similar toughness. This trend was consistent with the results from the robustness tests (Figure 5-8) and the mechanical strength (Table 5-2). Overall, the HF-GO-0.2 membrane sample showed desirable characteristic of the membrane support for TFC-PRO membrane with improved hydrophilicity and porosity, and best mechanical properties, while exhibiting the lowest surface roughness amongst all the samples prepared in this study.

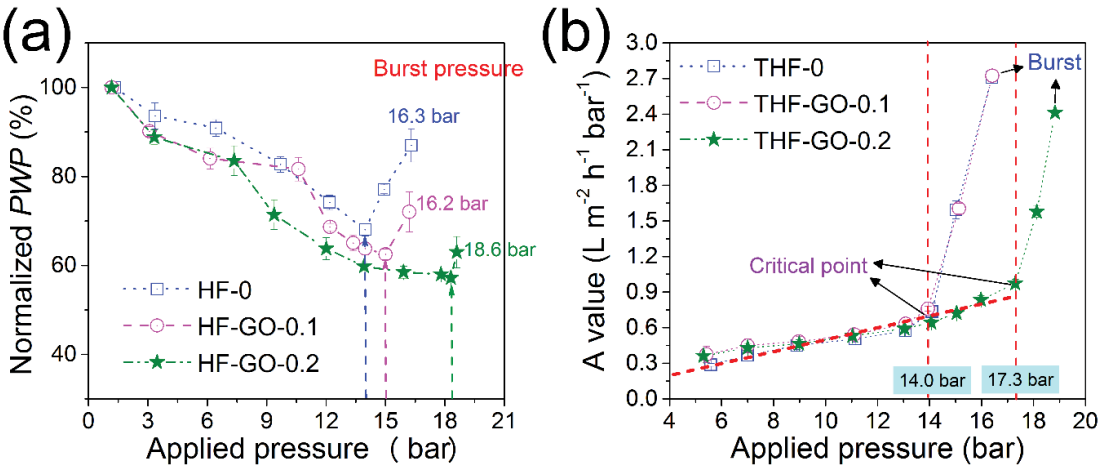

Figure 5 - 8. (a) Normalized Pure water permeability (*PWP*, %) of hollow fiber supports (HF-0, HF-GO-0.1 and HF-GO-0.2) and (b) pure water permeability (*A*) of TFC hollow fiber membranes (THF-0, THF-GO-0.1 and THF-GO-0.2) as a function of applied hydraulic pressure (ΔP) to the membrane lumen side to evaluate the membrane stability tested until the membrane to be burst (DI water used as feed solution).

5.3.3. Effect of pre-stabilization on PA selective layer and transport properties of TFC-PRO membranes

In order to minimize the effect of membrane deformation during PRO performance testing, of the as-spun TFC membranes were operated at maximum operating pressures (below critical pressure point) set at 13.5 bar, 13.5 bar and 16.5 bar for THF-0, HHF-GO-0.1 and THF-GO-0.2, respectively. Figure 5-9 exhibits the variations of the *A* of the three TFC-PRO membranes with operating time when operated under the RO mode during membrane pre-stabilization period at its maximum operating pressure. It can be seen that the *A* values for all membranes show a steep increase at initial stage mainly due to the stretching and thinning of the PA layer that increases the effective membrane area, and then remained stable with minor increase after about 60 min. Similar trend was also observed and has been discussed in previous studies (Chen et al. 2016, Chou et al. 2013, Gai et al. 2016). Recently, Gai et al. reported that membrane pre-stabilization at a high applied pressure but slightly below their burst pressure for a certain duration is an effective approach to enhance the membranes' PRO performance without damaging the TFC-PRO membranes (Gai et al. 2016). Based on the results shown in Figure 5-9, we

fixed the membrane pre-stabilization period to be 1 h at the maximum operation pressure for each membranes prior to PRO tests that were conducted to obtain the desirable PRO performance.

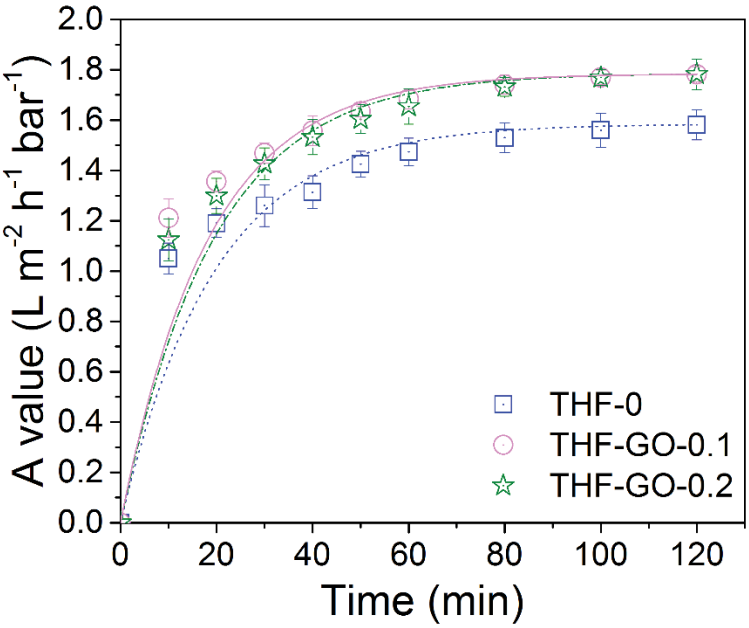

Figure 5 - 9. Pure water permeability (*A*) trends of the TFC-PRO membranes at different applied pressures of 13.5 bar, 13.5 bar and 16.5 bar for THF-0, THF-GO-0.1 and THF-GO-0.2, respectively, as a function of time (min). The water permeability value of each points was determined with the averaged values of permeated water volume for 10 min.

Table 5-3 shows the mass transport properties of the as-spun TFC-PRO hollow fiber membranes. The membranes were tested after pre-stabilization at their specified maximum operation pressures. The prepared TFC-PRO membranes had generally similar *A* values ranging from 1.22 to 1.36 L m^{-2} h^{-1} bar^{-1}. However, slightly improved *A* values were obtained from the THF-GO-0.1 and THF-GO-0.2. As seen from the SEM images of PA selective layer (Figure 5-7), relatively thinner PA layer is formed on the GO-incorporated hollow fiber samples compared to THF-0 which might have reduced the mass transport resistance across the PA layer. Meanwhile, significant improvement in *R* is observed for THF-GO-0.1 (96.1%) and THF-GO-0.2 (97.7%) compared to THF-0 with 93.4%, a trend consistent with the GO loading rate. A similar observation was made in

our previous studies which showed that a suitable GO loading in the membrane substrate can result in the most favorable condition for subsequent PA layer formation by IP process (Lim et al. 2017). The hollow fiber supports with lower surface roughness, larger pore size, and hydrophilic membrane surface induced via GO incorporation might have enhanced the thin film PA formation for higher permeability with higher salt selectivity.

Table 5 - 3. Intrinsic membrane properties and *S* values of TFC-PRO membranes.

TFC-PRO membranes	*A* (L m^{-2} h^{-1} bar^{-1})	*B* (L m^{-2} h^{-1})	*B/A* (bar)	R (%)	*S* (μm)
THF-0	1.22 ± 0.12	0.55	0.45	93.40 ± 2.55	769
THF-GO-0.1	1.36 ± 0.05	0.35	0.26	96.14 ± 1.27	577
THF-GO-0.2	1.27 ± 0.06	0.19	0.15	97.67 ± 1.19	522

*Test conditions: Tested PRO membranes for THF-0, THF-GO-0.1 and THF-GO-0.2 were conducted pre-stabilization at the pressure of 13.5 bar, 13.5 bar and 16.5 bar, respectively, for 1 h prior to the RO tests. Pure water permeability (*A*) value was determined at the applied pressure of 8 bar with the DI water as feed solution. The *R* and *B* values were obtained at the applied pressure of 8 bar with the 2000 mg L^{-1} NaCl as feed solution.

An additional RO experiment for TFC membranes was conducted as presented in Table 5-4. In order to compare the their intrinsic membrane properties under similar conditions, all TFC membranes were pre-stabilized at 8 bar for 1 h before determining the intrinsic properties of the membrane. These values were than compared with the intrinsic membrane properties obtained after pre-stabilizing at their maximum pressure (slightly lower than the burst pressure). Figure 5-10 shows the comparison of *A* value and salt rejection properties of the TFC membranes pre-stabilized at different pressures. Both A value and salt rejection performances for TFC membranes stabilized at 8 bar revealed similar trends to those stabilized at higher pressures in the range of 13.5-16.5 bar. One of the most noticeable finding from these results is that, both *A* values and salt rejection for all TFC membranes were significantly enhanced when they were pre-stabilized at higher applied pressures of 13.5-16.5 bar. When the TFC hollow fiber membranes is pre-stabilized at higher hydraulic pressures, the hollow fiber lumen may expand mostly likely with irreversible structural change. This may result in slightly increased membrane effective area after pre-stabilization, which then results in increased water permeability values as same membrane area is considered for calculation of *A* values. In addition, elongated elliptical voids in the PA layer induced by further increased pressure may have caused higher water passage while maintaining the salt selectivity (Gai et al. 2016).

Table 5 - 4. Intrinsic membrane properties of PRO membranes tested after membrane stabilized at 8 bar for 1 h.

TFC-PRO membranes	*A* (L m^{-2} h^{-1} bar^{-1})	*B* (L$m^{-2}h^{-1}$)	*B/A* (bar)	R (%)
THF-0	0.53 ± 0.06	0.42	0.79	89.08 ± 1.51
THF-GO-0.1	0.63 ± 0.03	0.20	0.32	95.26 ± 1.13
THF-GO-0.2	0.59 ± 0.06	0.15	0.26	96.17 ± 1.02

*Test conditions: Pure water permeability (*A*) value was determined at the applied pressure of 8 bar with the DI water as feed solution. The *R* and *B* values were obtained at the applied pressure of 8 bar with the 2000 mg L^{-1} NaCl as feed solution.

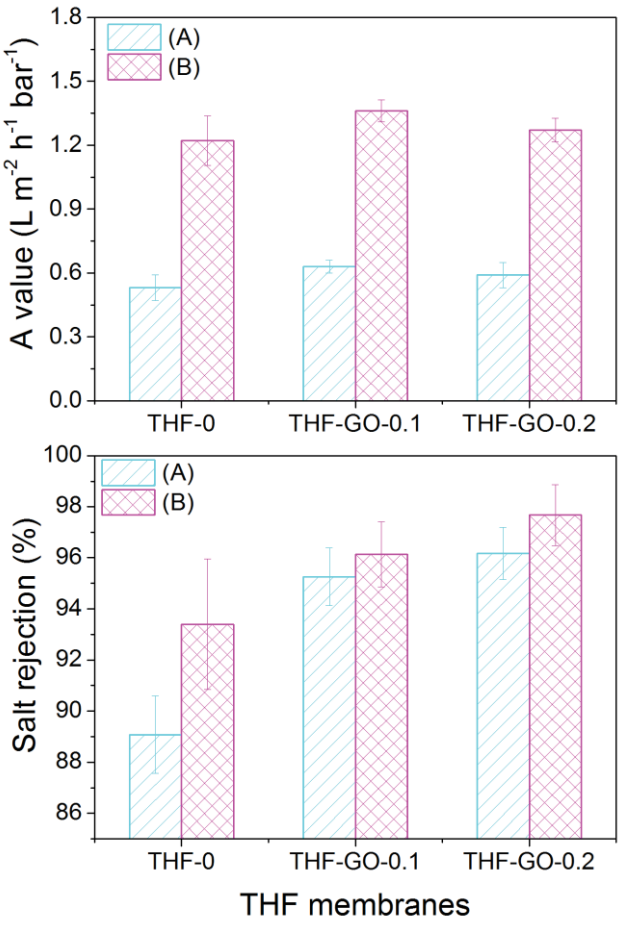

Figure 5 - 10. Pure water permeability (*A value*) and salt rejection performances determined at ΔP = 8 bar after pre-stabilization of TFC-PRO membranes: (A) all samples were pre-stabilized at 8 bar for 1 h, (B) the samples THF-0, THF-GO-0.1 and THF-GO-0.2 were pre-stabilized for 1 h at the pressure of 13.5 bar, 13.5 bar and 16.5 bar, respectively. (DI water used as feed for *A* values determination and 2000 mg L^{-1} NaCl used as feed for salt rejection evaluation)

5.3.4. Effect of GO on TFC-PRO hollow fiber membrane performances

The PRO performance of the TFC hollow fiber membranes in terms of J_w, J_s/J_w, and power density, using 1 M NaCl as DS and DI water as FS, is presented in Figure 5-11. The highest J_w at ΔP=0 bar was observed for THF-GO-0.2 (43.74 L m^{-2} h^{-1}) followed by THF-GO-0.1 (42.51 L m^{-2} h^{-1}) and THF-0 (38.62 L m^{-2} h^{-1}). On the other hand, J_s/J_w of TFC-PRO membranes at ΔP=0 bar follows the order of THF-0 (0.10 g L^{-1}) > THF-GO-0.1 (0.07 g L^{-1}) > THF-GO-0.2 (0.04 g L^{-1}). These trends are mostly consistent with the intrinsic properties (A and B values) of those TFC membranes presented in Table 5-3. In particular, the initial J_w of the THF-GO-0.1 is lower compared to the THF-GO-0.2 membrane although its A value is higher. This is likely because of the improved hydrophilicity of the hollow fiber support at higher GO loading which significantly helped reduce the ICP effect in the membrane support layer. In addition, the structural parameter values presented in Table 5-3 also corresponded well with the PRO performances of the TFC membranes. The lowest S value of 522 μm was observed for THF-GO-0.2 membrane, marking the most significant improvement as compared to control membrane (THF-0, 769 μm). Several studies have observed the positive effect of hydrophilic membrane support layer in reducing the ICP effects which depends on the S values (Arena et al. 2011, Ingole et al. 2014, Lim et al. 2017, Sahebi et al. 2016). Similar trends of J_w reductions were observed for all TFC membranes as hydraulic pressure increased.

Meanwhile, the J_s/J_w values gradually increased in the first operation (1st-run) due to the expansion of the hollow fiber membrane and thinning of the PA layers. The samples THF-GO-0.1 and THF-GO-0.2 showed a very stable J_s/J_w (< 0.60 g L^{-1}) at their maximum applied pressures of 13.5 bar and 16.5 bar, respectively. However, as hydraulic pressure was increased, relatively higher rate of J_s/J_w increment was noticed with THF-0, whose value reached 1.18 g L^{-1} at 13.5 bar as shown in Figure 5-11. As presented in Table 5-3, the lowest salt rejection and the highest B/A value (0.45 bar) for THF-0 indicate the lowest separation efficiency among the fabricated TFC membranes. This is a likely result of the less complete formation of PA layer further accelerated the PA deformation due to stress

from the hydraulic pressure. Apparently, a considerable increase in J_s/J_w with pressure was observed in the second stage (2^{nd}-run) for the THF-0 membrane compared to the 1^{st}-run which is likely due to PA layer deformation under repeated operation while the other membrane samples showed relatively stable or low J_s/J_w values. It is interesting to note for THF-0 membrane that more J_w decrease occurred in the 2^{nd}-run than during the 1^{st}-run and this is probably affected by the increased reverse salt flux that consequently caused more severe ICP in the membrane support layer which reduces the osmotic driving force across the PA selective layer (Han et al. 2014). However for HF-GO-0.1 membrane, relatively higher J_w in the 2^{nd}-run compared to the 1^{st}-run was observed which might have been caused by continued membrane expansion (increased effective membrane surface) with an increase in operation time as well as reduced PA layer thickness with elongated free volume, but without significant defects in the PA layer (Gai et al. 2016). As comparison between THF-0 and THF-0.1 in terms of mechanical stability when the same hydraulic pressure applied, therefore, it can be concluded that THF-0.1 has more stable performance compared to THF-0 as it continuously retained J_s/J_w as low values although more membrane expansion occurred, while significant PA layer deformation appeared for THF-0. Overall, the TFC-PRO hollow fiber membrane incorporated with 0.2 wt% GO exhibited the most stable PRO performance compared to other membranes. Although HF-GO-0.2 was tested at a higher applied pressure of 16.5 bar however almost no changes in J_w and J_s/J_w was observed in the 2^{nd}-run indicating the high stability of this PRO membrane.

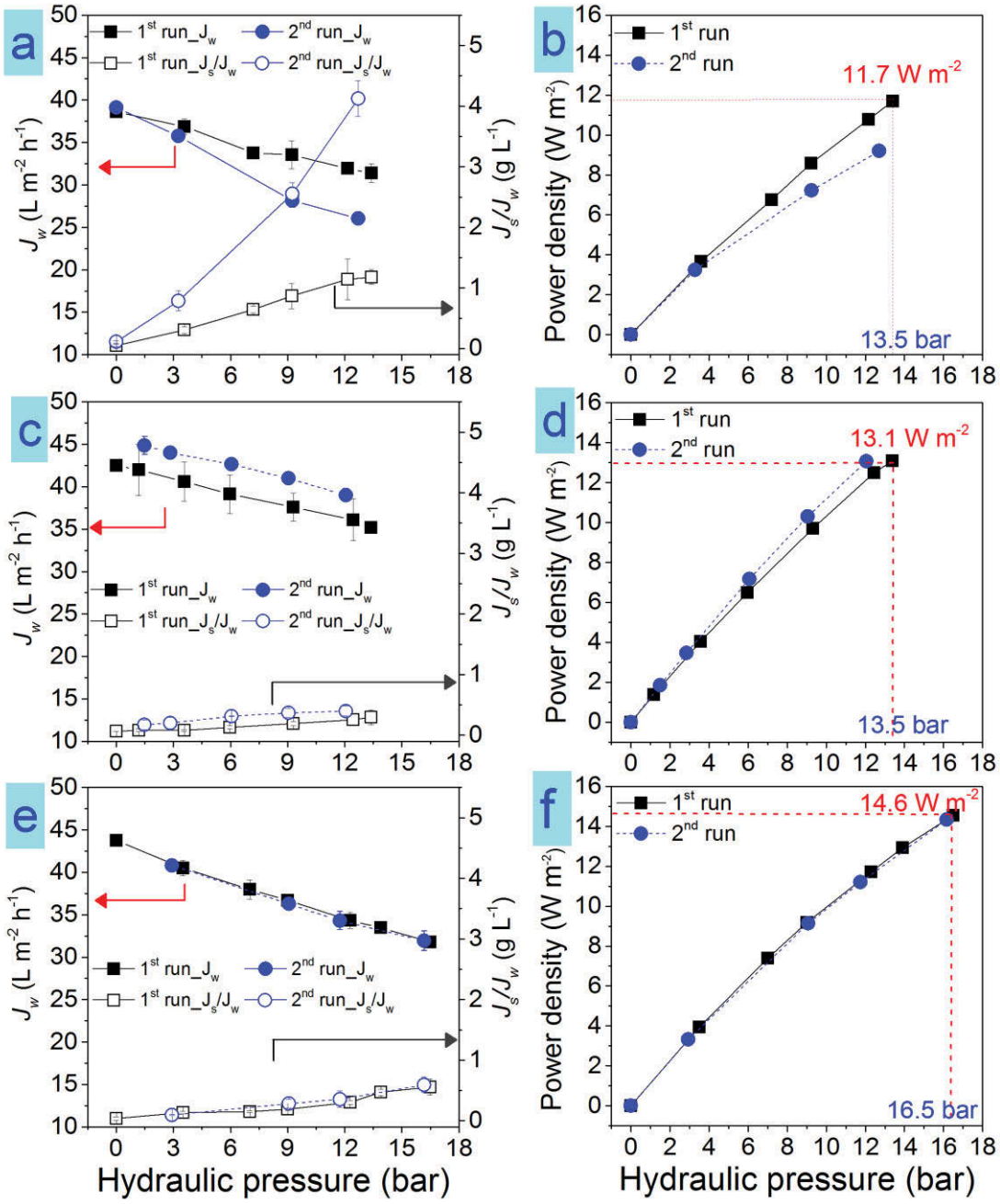

Figure 5 - 11. PRO water flux (J_w), specific reverse salt flux (J_s/J_w) and power density for THF-0 (a, b), THF-GO-0.1 (c, d), and THF-GO-0.2 (e, f) with 1 M NaCl as DS and DI water as FS (The samples THF-0, THF-GO-0.1 and THF-GO-0.2 were pre-stabilized for 1 h at the pressure of 13.5 bar, 13.5 bar and 16.5 bar, respectively).

In the PRO process, a straightforward evaluation of membrane performance can be obtained by calculating the power density (W m^{-2}) of the membrane. From Figure 5-11, the maximum power density of 11.7 W m^{-2} (1^{st}-run) at the pressure of 13.5 bar was

achieved for THF-0 membrane which improved to 13.1 W m^{-2} (1^{st}-run) at same the test conditions on incorporating 0.1 wt% GO in the PES hollow fiber support. The highest power density of 14.6 W m^{-2} (1^{st}-run) at 16.5 bar applied pressure was achieved with 0.2 wt% GO loading and 1 wt% increase of polymer concentration as a result of enhanced mechanical properties and water permeability, reduction of ICP effect, and achieved low *S* value. Nevertheless, the membrane THF-GO-0.2 showed the most stable PRO performance during the reproducibility tests (2^{nd}-run test) among all prepared TFC membranes.

5.4. Conclusions

In this chapter, high performance TFC hollow fiber membranes were developed via incorporation of hydrophilic GO nanosheets in the PES support layer for PRO applications. The study indicated that addition of GO (≤ 0.2 wt%) in the PES hollow fiber support layer resulted in significantly improved structural morphologies as well as surface chemistry within the support layer. These results in increased overall membrane porosity with larger pore size on the surface of membrane lumen side and enhanced hydrophilicity which significantly improved water permeability without undermining the mechanical properties of the support layer. The GO incorporated hollow fiber support layer provided the most favorable lumen surface structure for the effective IP reaction producing the PA layer with higher water permeability and higher salt selectivity. The TFC-PRO hollow fiber membrane with 0.2 wt% GO incorporation in the PES support layer presented the highest PRO flux of 43.6 L m^{-2} h^{-1} and the lowest specific reverse salt flux of 0.04 g L^{-1} and significantly lower structural parameter and ICP effects compared to the control membrane. The highest power density of 14.6 W m^{-2} was achieved at 16.5 bar using 1 M NaCl as DS and DI water as FS. In this study, optimization of GO loadings in PES supports was not fully addressed, however, the effect of GO on the PRO performance indicated sufficiently from experiment results. Therefore, incorporation of controlled amount of nanomaterials such as GO nanosheets or other hydrophilic nanomaterials in hollow fiber supports could be one of the promising approaches in fabricating TFC-PRO hollow fiber membranes with enhanced PRO performance.

CHAPTER 6

NOVEL CA/PVDF NANOFIBER SUPPORTS STRATEGICALLY DESIGNED VIA COAXIAL ELECTROSPINNING FOR HIGH PERFORMANCE THIN-FILM COMPOSITE FORWARD OSMOSIS MEMBRANES FOR DESALINATION

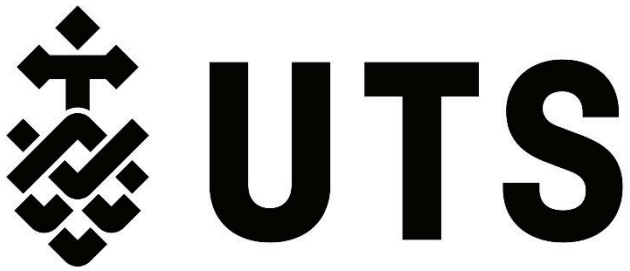

6.1. Introduction

In this study, we report the design of a new type of TFC FO membrane composed of electrospun nanofiber support layer fabricated via coaxial electrospinning technique that simultaneously produces a dual-layer PVDF core/CA sheath composite nanofiber support. This new concept of FO membrane support preparation aims to produce highly porous, mechanically strong, and hydrophilic nanofiber-supported TFC-FO membrane. PVDF polymer is well known and widely used for membrane fabrication due to its excellent properties, such as high mechanical properties, thermal stability, and chemical stability (Huang et al. 2016). However, pure PVDF membrane has poor wettability because of its hydrophobic property, making it unsuitable as a material for FO support. On the other hand, CA is a hydrophilic material with low mechanical strength and high susceptibility to swelling. Combining these two polymers to develop a membrane support could potentially have a synergistic effect, where the strength of one polymer is able to overcome the weakness of the other. PVDF was used as a material for the core of composite nanofiber to maintain high mechanical properties, while CA was used on the sheath side (as a cover) to provide a hydrophilic surface to the PVDF nanofibers essential for enhanced solute and solvent diffusion that can significantly help mitigate ICP in the membrane support layer. The performances of the composite nanofiber TFC FO membrane was also compared with TFC FO membranes prepared using single CA, single PVDF and blended CA-PVDF (CA/PVDF = 75/25 wt% ratio) nanofiber membrane supports through various characterization methods, and performance experiments. Recently, a few studies have proposed electrospun nanofiber membranes prepared via coaxial electrospinning as antimicrobial mats for water filtration (Kao et al. 2015) and as membrane distillation membranes (Lee et al. 2017) incorporated with nanomaterials or with different polymers. To the best of our knowledge, this is the first study to report on the design and performance of nanofiber supported TFC FO membrane fabricated via coaxial electrospinning technique to obtain hydrophilic-sheath/hydrophobic-core composite nanofiber support.

6.2. Experimental

6.2.1. Materials and chemicals

Polyvinylidene fluoride (PVDF, Kynar® 761, MW=441,000 g/mol) and cellulose acetate (CA, MW=100,000 g/mol) were provided by Arkema Inc., Australia and Acros Organics, respectively, and used as the polymers for electrospinning. *N,N*-Dimethylacetamide (DMAc, ReagentPlus®, 99%) and acetone (analytical reagent, 99%) were used as organic solvents for the polymers and purchased from Sigma-Aldrich and Chem-Supply Pty. Ltd., respectively. For polyamide (PA) selective layer formation, 1,3-phenylenediamine (MPD, 99%) and trimesoyl chloride (TMC, 98%) as monomers and heptane (anhydrous, 99%) as an organic solvent were used and these all chemicals were supplied from Sigma-Aldrich. 2-propanol (isopropanol, IPA, Merck) and sodium chloride (NaCl, Chem Supply) were used as membrane wetting agent and draw solution, respectively. Deionized (DI) water was supplied by a Milli-Q ultra-pure water system (Millipore) and used as a feed solution for FO tests.

6.2.2. Fabrication of nanofiber supports

Three different types of electrospinning techniques as shown in Figure 6-1 were adapted to prepare single, blend, and composite (dual-layer) nanofiber supports. For single nanofiber substrates, as demonstrated in Figure 6-1(a), PVDF (15 w/v%) or CA (18 w/v%) solutions dissolved in mixture of DMAc/acetone (5:5 v/v ratio) were prepared and applied to an electrospinning device equipped with a single nozzle to produce nanofiber supports for pure PVDF and pure CA, respectively. A blend nanofiber support (Blended) was prepared using a single nozzle for electrospinning a mixture of CA/PVDF (75/25 wt% ratio) solution. In order to fabricate dual-layer composite nanofiber supports (Composite-1 and Composite-2), two different dope solutions of PVDF and CA were prepared for core and sheath sides, respectively, and simultaneously extruded out of a coaxial nozzle as described in Figure 6-1(c). The detailed dope solutions, electrospinning conditions and parameters are presented in Table 6-1. The prepared dope solutions were put into a plastic syringe and were then supplied through the nozzles via a syringe pump by applying high voltage of 21~24 kV. All the electrospun nanofiber membrane support samples were

collected on an aluminum foil- covered drum type collector over a period of 3 h. The distance between the collector and the nozzle was 18 cm and temperature and humidity conditions during the electrospinning were maintained at 22 ~ 25°C and 40 ~ 60%, respectively. The as-spun nanofiber supports were carefully peeled off for the aluminum foil and then dried in an oven at 50 °C for overnight to remove the residual solvents from fibers.

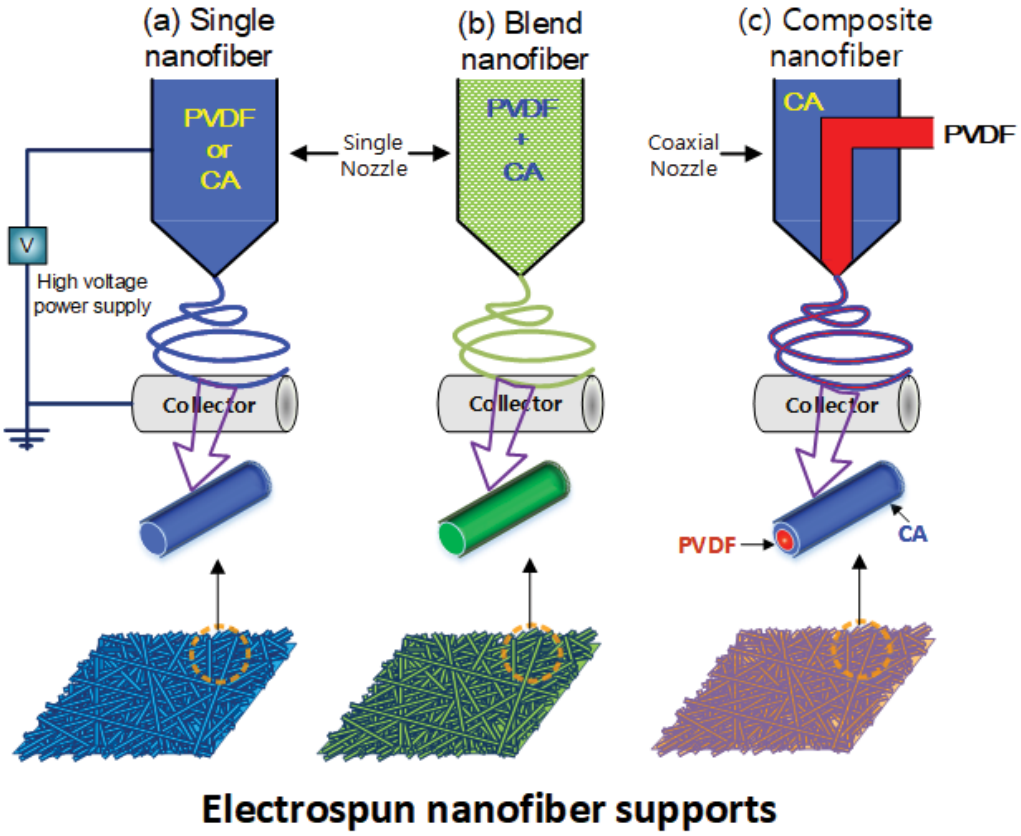

Figure 6 - 1. Schematic diagram of electrospinning techniques for fabricating nanofiber supports.

Table 6 - 1. Electrospinning conditions for nanofiber supports preparation.

FO membrane/ Support layer	Membrane support fabrication					
	Spinning technique		Dope solution	Electrospinning condition		
				Flow rate (mL/min)	Voltage (kV)	Distance (cm)
PVDF	Single (PVDF)		15 w/v% PVDF in DMAc/acetone (5:5 v/v ratio)	2		
CA	Single (CA)		18 w/v% CA in DMAc/acetone (5:5 v/v ratio)	2		
Blended	Blend (CA/PVDF)		15 w/v% CA/PVDF (25/75 wt% ratio) in DMAc/acetone (5:5 v/v ratio)	2		
Composite-1	Composite (CA/PVDF)	Core-PVDF	15 w/v% PVDF in DMAc/acetone (5:5 v/v ratio)	0.7	21-24	18
		Sheath-CA	17 w/v% CA in DMAc/acetone (5:5 v/v ratio)	1.3		
Composite-2	Composite (CA/PVDF)	Core-PVDF	15 w/v% PVDF in DMAc/acetone (5:5 v/v ratio)	0.5		
		Sheath-CA	17 w/v% CA in DMAc/acetone (5:5 v/v ratio)	1.5		

6.2.3. Preparation of TFC-FO membranes

Thin film PA selective layer was formed on nanofiber substrates via IP of MPD and TMC monomers. Due to the hydrophobicity of the as-spun nanofiber mats, all samples were pre-wetted in IPA for 30 s. The nanofiber supports were then rinsed with DI water for several times to remove the residual IPA in the fibers and stored in DI water prior to IP process. The excess water from the membrane surface was removed using a rubber roller then equipped in an acrylic frame to expose only one side of the nanofiber mats to MPD and TMC monomers. The membrane surface was immersed in 2 wt% MPD solution for 2 min then the excess solution was removed by a rubber roller. After which, 0.15 w/v % of TMC in heptane was poured onto the surface for exactly 1 min to allow the IP reaction to take place and form a thin PA selective layer. The TFC membranes were then air-dried for 2 min and heat-treated in the oven at 70°C for 10 min to complete the IP reaction. The TFC membranes were then stored in DI water at 4°C prior to performance tests and membrane characterizations. The TFC FO membranes produced using PVDF, CA, Blended, Composite-1 and Composite-2 electrospun support layers were designated as PVDF-TFC, CA-TFC, Blended-TFC, Composite-TFC-1 and Composite-TFC-2, respectively.

6.2.4. FO performance evaluation of the TFC membranes

The FO performance of TFC membranes was evaluated using a lab-scale membrane test unit. The effective membrane area of the FO cell was 14 cm^2 (2 cm width, 7 cm length and 0.3 cm channel height). The operation was conducted under co-current crossflow direction at a fixed flow rate of 400 ml/min (cross-flow velocity of 13.88 cm/s) using a gear pump. The initial volume for both FS and DS was 2 L and the solutions were recirculated to their respective FS/DS tanks. Different concentrations of NaCl (0.5, 1.0, 1.5 and 2.0 M) as DS with DI water as FS were used in this study for evaluating the FO performance. The temperature of both solutions was maintained at 23 °C ± 1 and the conductivity of the FS was measured by a portable conductivity meter (D-74G, Horiba

scientific, Kyoto, Japan) to evaluate reverse salt flux of the membrane. Prior to FO test, all TFC membranes were fully pre-wetted by soaking in 50% IPA/water for 1 min then washed with DI water several times to remove the residual IPA from the membrane. All FO tests were conducted under active layer facing FS (AL-FS) mode in this study.

The intrinsic membrane properties, pure water permeability (A), solute permeability coefficient (B), and structure parameter (S), of the tested FO membranes were determined based on FO experimental data using the 4-stage prediction model designed by Tiraferri et al. (Tiraferri et al. 2013). The water flux and reverse salt flux values of the FO membranes were determined at the four different concentrations of draw solutions (0.5, 1.0, 1.5, and 2.0 M). All experimental conditions were kept the same as those of the performance tests in the osmotically driven process.

6.3. Results and discussion

6.3.1. Characterization of the electrospun nanofiber supports

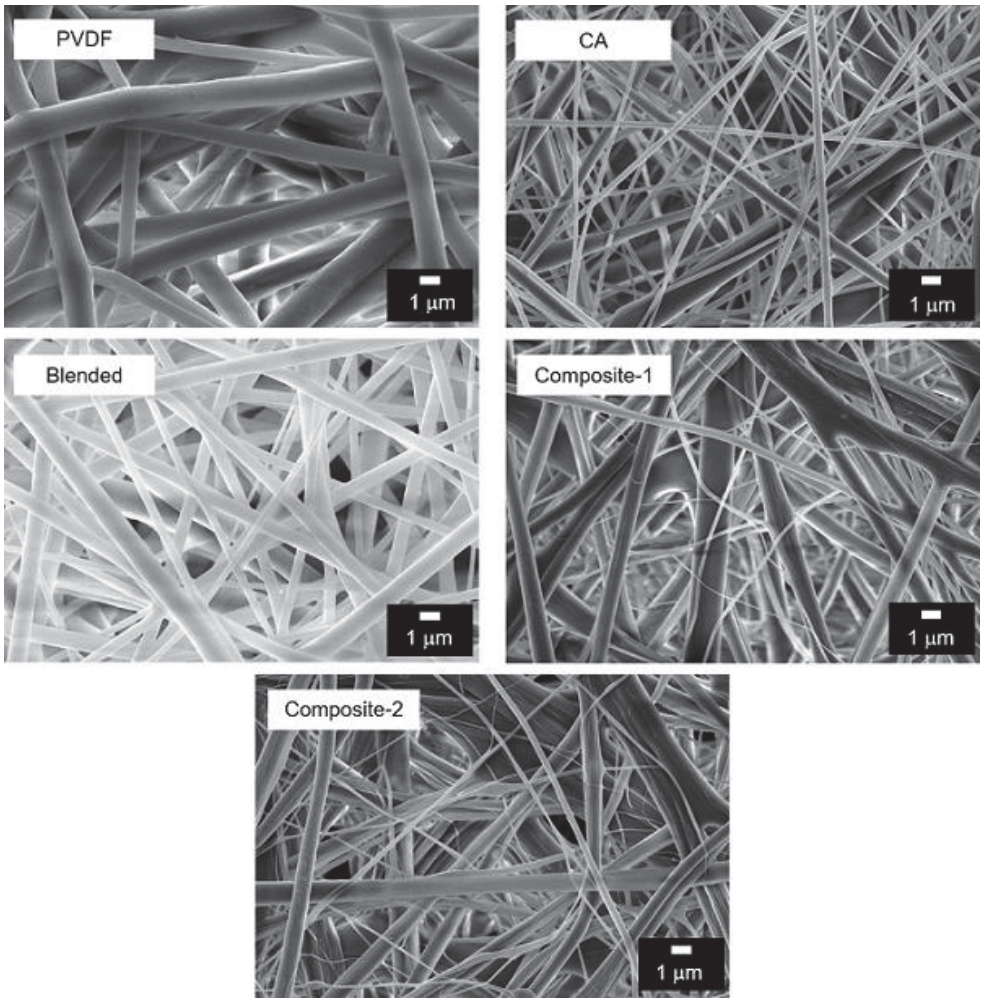

Figure 6 - 2. SEM images of electrospun nanofiber support membranes for PVDF, CA, Blended (CA 75 wt%, PVDF 25 wt%), Composite-1 (Composite: Core-0.7 mL/min for PVDF, Sheath-1.3 mL/min for CA) and Composite-2 (Composite: Core-0.5 mL/min for PVDF, Sheath-1.5 mL/min for CA)

Figure 6-2 presents the FE-SEM images for five different electrospun nanofiber supports prepared with single, blend, and composite polymers (designated as PVDF, CA, Blended, Composite-1 and Composite-2). Overall, the electrospun nanofibers exhibited fine fiber size and a bead-free structure, which indicate a three-dimensional and highly porous open structure for all the membranes. The images also reveal CA produced finer nanofibers compared to PVDF under the same electrospinning conditions. The finer average fiber size of CA can be attributed to the lower viscosity of CA dope solution and its considerably lower molecular weight (100,000 g/mol) as compared to PVDF (440,000 g/mol), despite CA having a higher polymer concentration (18 wt%) than PVDF (15 wt%) (Bui et al. 2013b, Guo et al. 2017). Therefore, a blended nanofiber support, fabricated by blending CA/PVDF polymers in 75/25% ratio, also showed relatively smaller fiber sizes compared to the PVDF nanofiber, but not bigger than that of the CA nanofiber. The polymer

solution with high percent ratio of CA (75%) against PVDF (25%) could have resulted in decrease of solution viscosity, thus forming smaller nanofibers. Particularly, a broader nanofiber size distribution was observed for both Composite-1 and Composite-2 electrospun nanofibers with the presence of both fine and relatively large nanofibers, as shown in Figure 6-2. However, these two nanofiber membranes had even smaller average fiber size compared to the blended nanofiber support. The average fiber sizes for Composite-1 and Composite-2 supports were consequently reduced using coaxial nozzle that simultaneously electrospun the two polymers of hydrophilic CA to the sheath side and hydrophobic PVDF to the core side.

Figure 6-3 reveals the cross-sectional images of as-spun nanofiber membranes for PVDF, Blended, Composite-1 and Composite-2. All nanofiber samples exhibit the random arrangement of fibers characteristic to the electrospinning method. As shown, PVDF nanofibers have more uniform and more defined fibers than those of Blended, Composite-1 and Composite-2 samples. This is also reflected in the average fiber diameter results listed in Table 6-2. The less consistent fiber morphology of Blended, Composite-1 and Composite-2 samples is likely caused by the different behaviors of the polymer components in the dope solutions to the applied voltage during electrospinning. Nonetheless, these factors had minimal effect on the overall structural properties of the substrates in terms of % porosity, membrane thickness and pore sizes (Table 6-2) as discussed in the subsequent sections.

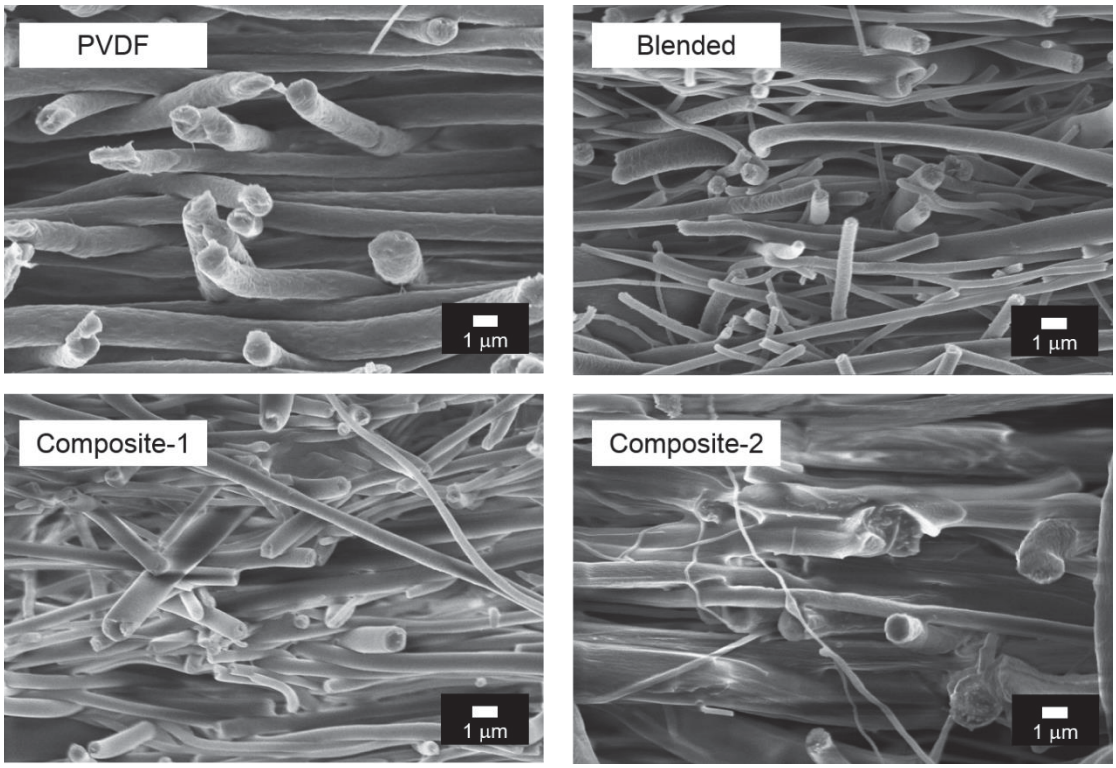

Figure 6 - 3. Cross-sectional SEM images of electrospun nanofiber support membranes for PVDF, Blended (CA 75 wt%, PVDF 25 wt%), Composite-1 (Composite: Core-0.7 mL/min for PVDF, Sheath-1.3 mL/min for CA) and Composite-2 (Composite: Core-0.5 mL/min for PVDF, Sheath-1.5 mL/min for CA)

Meanwhile, dual-layered PVDF core/CA sheath composite membranes were not distinct via SEM images (Figure 6-2), and Composite-2 membrane was thus further characterized by STEM and EDS analysis as shown in Figure 6-4. In the STEM image, the inner portion of the fiber appears darker than its outer (sheath) side but no clear boundary between the two layers (i.e. core PVDF and CA sheath) were observed. To further visualize the formation of PVDF core/CA sheath, EDS mapping of F and O elements were carried out which clearly distinguished the PVDF and CA regions. The distribution of F from PVDF is localized only within the core region whereas the O-rich phase of CA can be seen evenly dispersed to the entire fiber. This suggests that CA completely and evenly was covered with the core PVDF fiber. Overlaid O, F EDS maps clearly showed that PVDF was the core of the fiber while CA was located at the outer portion of the fiber surface. These results from STEM-EDS indicate the successful formation of dual-layered PVDF core/CA sheath composite membrane.

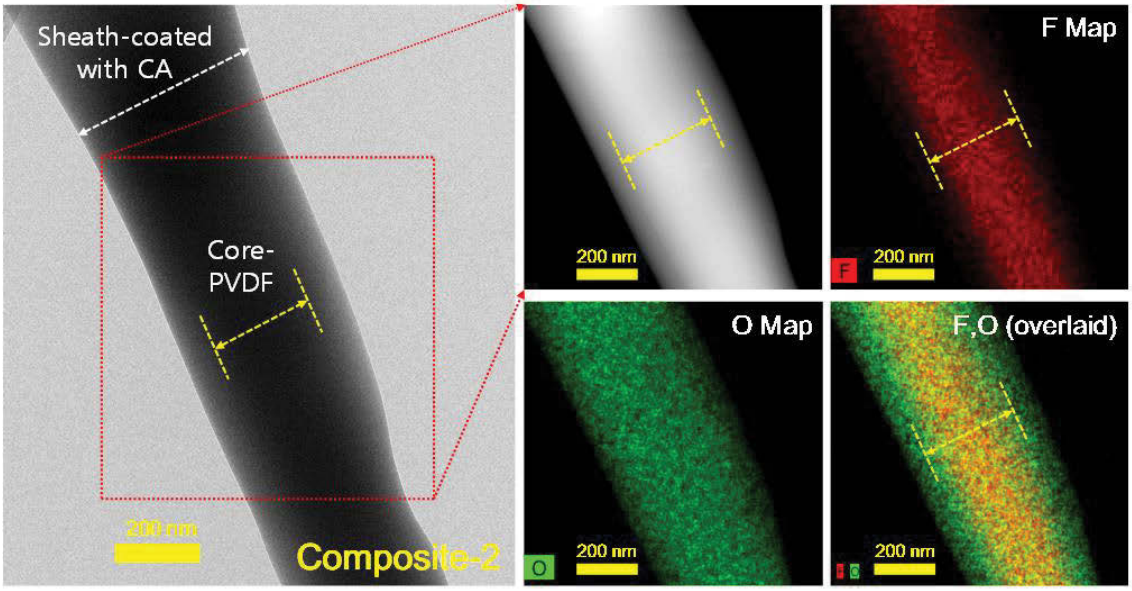

Figure 6 - 4. STEM microscopy and EDS mapping images (F and O components) for Composite-2 membrane

The characteristics of the nanofiber support membranes are summarized in Table 6-2. The PVDF nanofiber showed the largest average fiber diameter of 1260.6 nm, followed by Blended nanofiber (788.6 nm), Composite-1 (696.2 nm), Composite-2 (452.2 nm), and pure CA which had the smallest average fiber diameter of 259.2 nm. Among the blend and composite membranes, the fiber diameter of Composite-2 membrane was close to that of the pure CA nanofiber, due to higher CA concentration as opposed to PVDF and the increased flow rate for CA directed to the sheath side. When the flow rate of sheath side for CA was increased from 1.3 mL/min to 1.5 mL/min, average nanofiber diameter decreased about 35%.

Furthermore, hydrophilicity of fabricated nanofiber supports was evaluated via contact angle measurement and water content as shown in Table 6-2. As expected, the PVDF showed the highest contact angle (147.2 ^{o}) due to its hydrophobic character with low surface energy (Pan et al. 2014). This is followed by the blended support despite the presence of CA component. It is likely that random entanglement of higher molecular weight PVDF (MW 441,000 g/mol) with CA (MW 100,000 g/mol) resulted in higher PVDF exposure on the nanofiber surface resulting in its higher contact angle. Moreover, increased surface roughness of nanofibers might have also contributed to the high contact angles in all substrate samples (Kaur et al. 2012, Liu et al. 2016a, Moradi et al. 2015).

This was clearly observed with the supports made of pure CA and PVDF. In general, the contact angle of hydrophilic CA membranes fabricated by phase inversion is < 70° (Choi et al. 2015, Liu et al. 2016a, Shibuya et al. 2015, Zhang et al. 2010) whereas that of PVDF is around 80~90° (Hudaib et al. 2018). However, higher contact angles were measured from pure CA and PVDF nanofiber supports (Table 6-2). In case of the coaxial electrospun composite nanofiber supports, the contact angle of Composite-2 (136.7^{o}) was lower than Composite-1 (141.6^{o}) due to the increase of the flow rate for the CA solution on the sheath side during coaxial electrospinning, resulting in higher CA content on the nanofiber surface. In fact, the contact angle for Composite-2 was mostly similar to the pure CA support among the fabricated nanofiber membranes, indicating that these two membranes have similar hydrophilicity.

The water content of the fabricated membranes also showed similar trend with the result from the contact angle measurement, but these results indicate the differences between hydrophilicity and water absorption ability more clearly. The pure PVDF nanofiber support has only 5.4% of the water content and water content significantly improved to 33.8% after blending with CA. Also, the hydrophilicity was further improved through CA coating onto the sheath side of PVDF via coaxial electrospinning, as shown by the water content for both Composite-1 (42.1%) and Composite-2 (43.7%) nanofiber supports, which were found to be very similar to that of pure CA support (46.1%). In conclusion, coaxial electrospun composite support membranes can achieve similar hydrophilic property to that of pure CA nanofiber membrane, based on the results of contact angle and water content. Meanwhile, the mean pore size of electrospun nanofiber membrane was high for PVDF while those of the other three substrates had similarly lower values. However, the mean pore size displayed a no correlation with the membrane porosities. As presented in Table 6-2, the porosity of membrane samples was found to be in the range of 85.9% ~ 89.1% which is significantly higher compared to typical membranes prepared by phase inversion method (Choi et al. 2015). Based on these results, it can be noted that membrane porosity was not significantly altered by the spinning techniques and the polymer compositions in this study.

Table 6 - 2. Characterization of nanofiber support membranes.

Membrane properties	PVDF	CA	Blended	Composite-1	Composite-2
Average fiber diameter [nm]	1260.6 ± 308.9	259.2 ± 114.6	788.6 ± 326.3	696.2 ± 342.5	452.2 ± 326.8
Water content [%]	5.4 ± 0.4	46.1 ± 1.5	33.8 ± 1.6	42.1 ± 1.9	43.7 ± 1.5
Porosity [%]	86.5 ± 1.4	85.9 ± 1.2	88.2 ± 0.9	88.4 ± 1.8	89.1 ± 2.0
Contact angle [°]	147.2 ± 0.3	130.3 ± 3.2	145.1 ± 3.1	141.6 ± 1.8	136.7 ± 2.9
Membrane thickness [μm]	40.8 ± 2.1	33.6 ± 1.3	37.2 ± 1.0	39.3 ± 1.6	38.4 ± 1.1
Mean pore size [μm]	3.7	2.0	2.2	2.6	2.4
Max. pore size [μm]	4.0	2.6	2.9	3.6	3.2

Figure 6-5 and Table 6-3 show the XPS spectrum and chemical compositions of the nanofiber support membranes, respectively. As shown in Figure 5, there are three main peaks for F, O, and C elements which appeared the binding energy at around 700 eV, 530 eV, and 280 eV, respectively. In general, the O-atom peak should not be observed in the PVDF nanofiber spectrum because PVDF is only composed of C, H and F atoms; however, a small amount of oxygen (1.83% as presented in Table 3) was found, which could be impurities from the fabrication process (Wang et al. 2017). The CA nanofiber membrane support presents a typical spectrum of CA showing two main peaks of oxygen and carbon. It is interesting to note that the O1s peak significantly increased from 1.83% to 24.4% and the F1s peak decreased from 45.7% to 13.6% when PVDF was blended with CA. This increase of oxygen percentage confirms the presence of CA on the surface of PVDF-CA blended nanofibers (Mu et al. 2010). In the case of composite nanofiber membranes, both Composite-1 and Composite-2 showed higher oxygen percentage as compared to pure PVDF support. On the other hand, Composite-2 (14.2%) was revealed to have a slightly higher oxygen content than Composite-1 (12.3%). Higher CA flow rate was used for the sheath side during the coaxial electrospinning for Composite-2 and this might have resulted in higher CA content on the shell side (surface) of nanofibers. Thus, Composite-2 nanofiber support is likewise expected to have a more hydrophilic property

on the membrane surface, as supported by the results of water content and contact angle measurement summarized in Table 6-2.

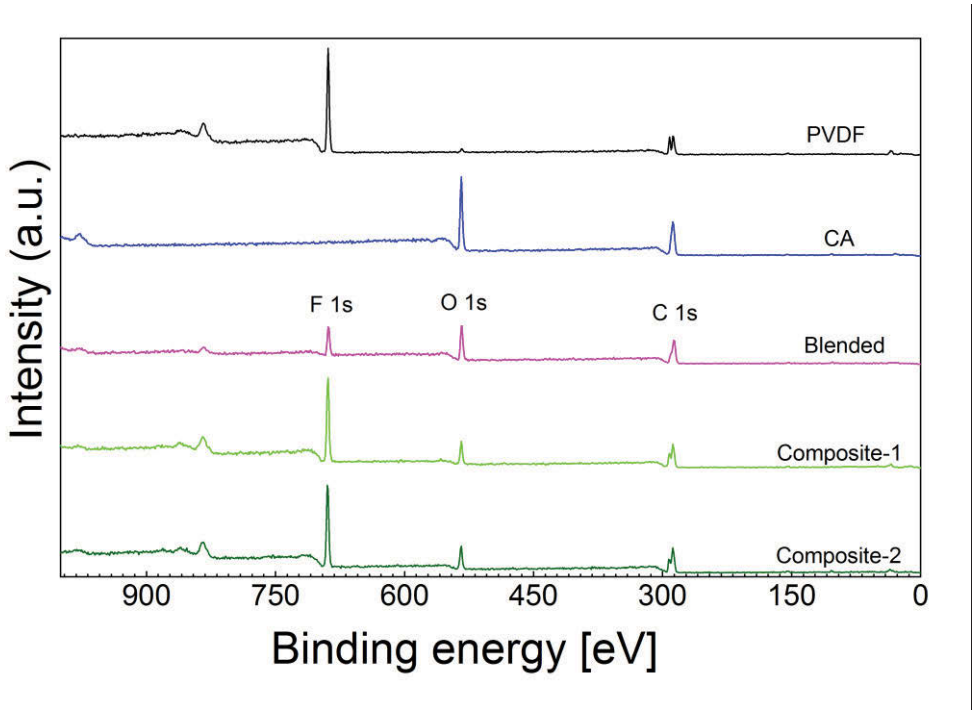

Figure 6 - 5. XPS spectrum of nanofiber support membranes for PVDF, CA, Blended (CA 75 wt%, PVDF 25 wt%), Composite-1 (Core-0.7 mL/min for PVDF, Sheath-1.3 mL/min for CA) and Composite-2 (Core-0.5 mL/min for PVDF, Sheath-1.5 mL/min for CA)

Table 6 - 3. Chemical composition of nanofiber support membranes calculated from XPS measurement.

Samples	C [%]	O [%]	F [%]
PVDF	52.4	1.8	45.7
CA	61.4	38.7	—
Blended	62.1	24.4	13.6
Composite-1	54.8	12.3	32.9
Composite-2	52.2	14.2	33.6

6.3.2. Mechanical properties of nanofiber support membranes

PVDF nanofiber support was preferred for TFC FO membranes because it is mechanically strong and resistant to membrane swelling (Huang et al. 2016, Huang et al. 2014). In this study, therefore, PVDF modified with CA was utilized to enhance hydrophilicity, without compromising mechanical properties. The mechanical properties of the membrane supports were evaluated in terms of their mechanical strength and the elongation at break. As seen from Figure 6-6, the PVDF support revealed the highest values for both mechanical strength and elongation at break with 3.61 MPa and 34.5%, respectively, among the fabricated membrane supports. The nanofiber support prepared using single hydrophilic CA exhibited the lowest mechanical strength of 0.59 MPa and this is expected since CA polymer is generally observed to have low mechanical properties (Guo et al. 2017). On the other hand, the mechanical strength of the Blended nanofiber support improved by about three-fold compared to the pure CA nanofiber support by blending with 25% PVDF, although its elongation at break was similar (6.9%) with the pure CA support. This indicates that although blending the CA with PVDF enhances its mechanical strength but the CA-PVDF blended support is still weaker than the pure PVDF support. This is due to the brittleness and mechanically weak property of CA polymer which was present in a high polymer ratio (75%) in the CA-PVDF blended membrane (Bui et al. 2013b). The mechanical strength of Composite-1 and Composite-2 supports with 3.27 MPa and 3.16 MPa, respectively, were however almost similar to the pure PVDF nanofiber support. This is probably due to the structural design of the composite nanofiber supports consisting of dual-layers with PVDF core with CA on the sheath side separately, thus retaining the intrinsic mechanical strength of the PVDF layer. The mechanical strength and elongation at break for Composites 1 and 2 were not significantly different. However, the elongation at break for Composite-1 (11.1%) and Composite-2 (10.7%) nanofiber supports was significantly lower than the pure PVDF support although higher than the pure CA or blend membrane supports. This is probably due to the dominant effect of brittleness of CA on overall modulus of elasticity of composite membranes (Bui et al. 2013b, Guo et al. 2017).

Considering the comparable mechanical strength of the pure PVDF, with the composite substrates, these supports are sufficiently robust for the application in TFC-FO membranes with the low pressure requirement of the process.

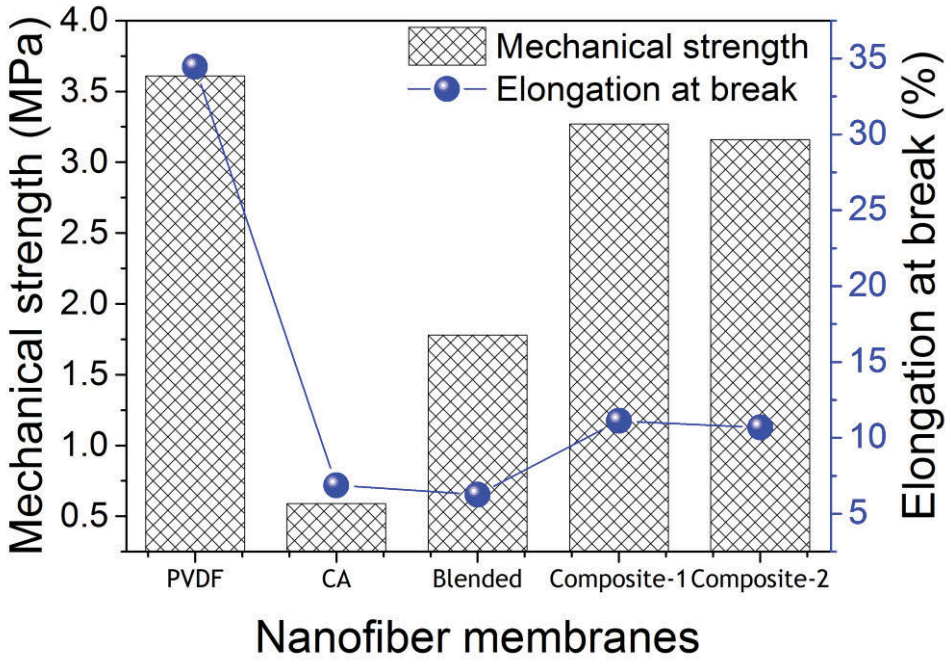

Figure 6 - 6. Mechanical properties of electrospun nanofiber support membranes for PVDF, CA, Blended (CA 75 wt%, PVDF 25 wt%), Composite-1 (Core-0.7 mL/min for PVDF, Sheath-1.3 mL/min for CA) and Composite-2 (Core-0.5 mL/min for PVDF, Sheath-1.5 mL/min for CA)

6.3.3. Characterization of TFC-FO membranes

The TFC FO membranes prepared using nanofiber support layers were characterized by FE-SEM, as presented in Figure 6-7. It can be seen from the SEM images that the PA layer on the nanofiber supports was well formed without noticeable defects for all samples. In addition, the ridge-and-valley structures, which are typically observed to indicate presence of well-formed PA, were also clearly visible. The images of all the TFC membranes in Figure 6-7 clearly show the imprinted patterns of nanofibers on the TFC membrane surface which is not as usually seen with the TFC flat-sheet membranes prepared by phase inversion. The high open porosity and randomly deposited three-dimensional structure of nanofiber induced the formation of this type of PA film on the amorphous pore structures and similar PA morphology was also observed in previous studies (Bui et al. 2013b, Huang et al. 2016, Obaid et al. 2016a, Puguan et al. 2014, Tian

et al. 2014b). In the case of CA-TFC, however, the imprinted pattern of nanofibers was less significant compared to other TFC membranes. CA nanofiber support has the smallest average fiber diameter (corresponding to a smaller pore size) among the prepared membrane supports and highest intrinsic hydrophilic property, resulting in the formation of smoother PA layer surface.

The chemical composition of PA active layers for TFC-FO membranes was characterized via XPS analysis to confirm the cross-linking degree of fabricated TFC membranes, as shown in Table 6-4. Theoretically, the ideally cross-linked aromatic PA synthesized by MPD and TMC monomers should contain an O/N ratio of 1.0 (Do et al. 2012, Tang et al. 2007). The O atom from TMC and the N atom from MPD are mainly related with the formation of amide group and full cross-linkage with a 1:1 O/N ratio. Therefore, it can be said that a smaller O/N ratio of PA active layer may be a result of tightened (smaller) membrane pore size. The smaller pore sizes then result in a higher density PA layer with a higher membrane selectivity (Tang et al. 2007). The O/N ratio of TFC membranes summarized in Table 6-4 shows in the order of CA-TFC > PVDF-TFC = Composite-TFC-1 > Blended TFC > Composite-TFC-2. Based on these results, Composite-TFC-2 is expected to have the highest selectivity of PA layer, while CA-TFC is anticipated to have the lowest selectivity.

Table 6 - 4. Chemical composition of TFC membranes calculated from XPS measurement.

TFC membranes	C [%]	O [%]	N [%]	O/N ratio [-]
PVDF-TFC	73.5	16.9	9.6	1.8
CA-TFC	77.7	15.2	7.2	2.1
Blended-TFC	79.9	11.1	9.0	1.2
Composite-TFC-1	77.1	14.6	8.3	1.8
Composite-TFC-2	79.3	11.3	9.4	1.2

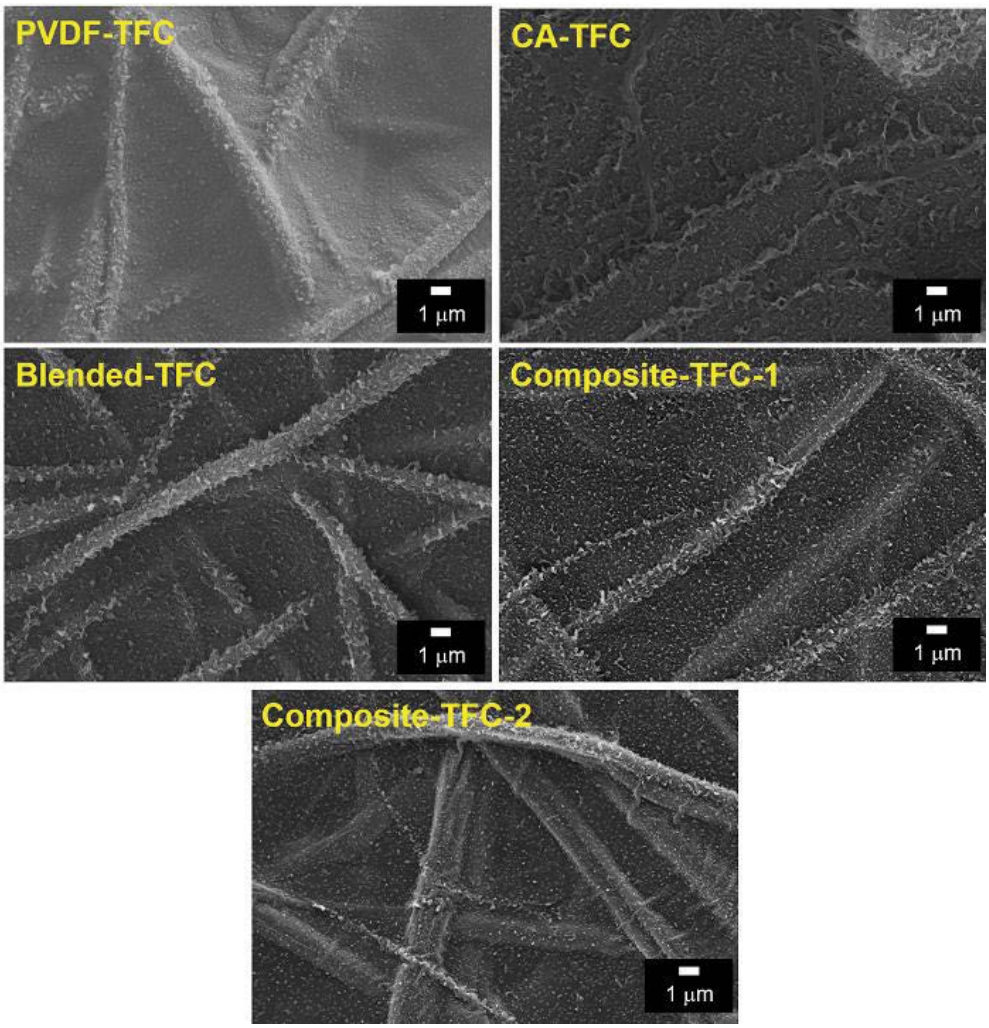

Figure 6 - 7. FE-SEM images of the PA selective layer deposited on the electrospun nanofiber support membranes.

6.3.4. FO performance of the TFC-FO membranes with various nanofiber supports

In this study, nanofiber supports for TFC-FO membranes were strategically designed via coaxial electrospinning to produce a PVDF core/CA sheath dual layer structure. To evaluate the efficiency of this strategy to produce electrospun nanofiber support for TFC FO membranes, FO performances were conducted and compared with single (CA or PVDF) and Blended (PVDF-CA) nanofiber supports. Figure 6-8 displays the FO performance of TFC-FO membranes fabricated with various nanofiber supports tested under AL-FS membrane orientation. The CA-TFC FO membrane with pure hydrophilic CA support layer showed the highest water flux of 42.45 L m^{-2} h^{-1} compared to all other

nanofiber supported TFC FO membranes in the study. As presented in Table 6-2, the pure CA nanofiber support has the highest water content and the lowest contact angle due to the hydrophilic property, thus explaining why it exhibited the highest FO water flux.

The hydrophilicity of the originally-hydrophobic membranes improves the transport of water or solute molecules in the support layer of TFC membranes, which consequently reduces the concentration polarization phenomenon in the FO process (Han et al. 2016, Lim et al. 2017, Liu et al. 2016b, Tian et al. 2014b, Zhang et al. 2017b). Although the membrane support layer porosity of CA-TFC (86.5%) is comparable to PVDF-TFC (87.8%) and even lower than other membrane samples, the lowest membrane thickness of CA-TFC (32 μm) could also have probably contributed to the high FO water flux by reducing the structural parameter which is directly influenced by the membrane porosity, tortuosity, and support layer thickness (Klaysom et al. 2013a). However, the specific reverse solute flux or J_s/J_w value, which indicates the salt selectivity of PA active layer (lower J_s/J_w presents high selectivity), for the CA-TFC membrane with 0.18 g L^{-1} was higher than any other membrane samples and this trend matches well with the result from XPS data depicted in Table 6-4. The CA-TFC membrane had a higher O/N ratio of 2.1 while 1.8 for PVDF-TFC which means that lower cross-linkage of PA for CA-TFC formed loose pore structures causing more salt to pass through during FO process.

Meanwhile, only a slight improvement in both FO water flux and J_s/J_w was observed from 18.55 L m^{-2} h^{-1} and 0.14 g L^{-1} for pure PVDF-TFC membrane to 20.3 L m^{-2} h^{-1} and 0.10 g L^{-1} for CA-PVDF (75/25 %) blended TFC membrane, respectively, due to enhanced hydrophilicity of the blended support, based on the water content result (Table 6-2). However, a further improvement in FO performance was observed for the two composite TFC membranes prepared on the coaxial electrospun support layer. The water flux of the Composite-TFC-2 (31.2 L m^{-2} h^{-1}) membrane was higher than the Composite-TFC-1 (26.5 L m^{-2} h^{-1}) membrane. This is likely due to the higher CA content used on the sheath side ensuring better coverage of the PVDF nanofiber by CA layer, which is also evident from the slightly higher hydrophilicity of Composite-TFC-2. It is interesting to note that even J_s/J_w was also significantly reduced from 0.05 g L^{-1} for Composite-TFC-1 membrane to 0.03 g L^{-1} for Composite-TFC-2 membrane. In fact, this was the lowest specific reverse salt flux value obtained in this study. Therefore, instead of blending CA with the PVDF to prepare electrospun support layer, coaxial electrospinning to prepare the TFC FO

nanofiber supports is a better approach to improve the performance of the TFC FO membranes in terms of water flux and specific reverse solute flux. The enhancement of hydrophilicity in the support layer (Table 6-2) reduces the ICP effect during the FO process, resulting in improved solution diffusivity and enhanced water flux (Liu et al. 2016b, Tian et al. 2014b). In addition, the particular characteristics of membrane support for Composite-TFC-2 membrane composed of PVDF-core/CA-sheath composite nanofibers would be preferable to form a highly cross-linked PA layer, as confirmed from XPS analysis (Table 6-4). There was some disparity on the J_s/J_w trend of TFC membranes as compared with cross-linkage illustrated by O/N ratio from XPS result (Table 6-4) but similar tendency was observed.

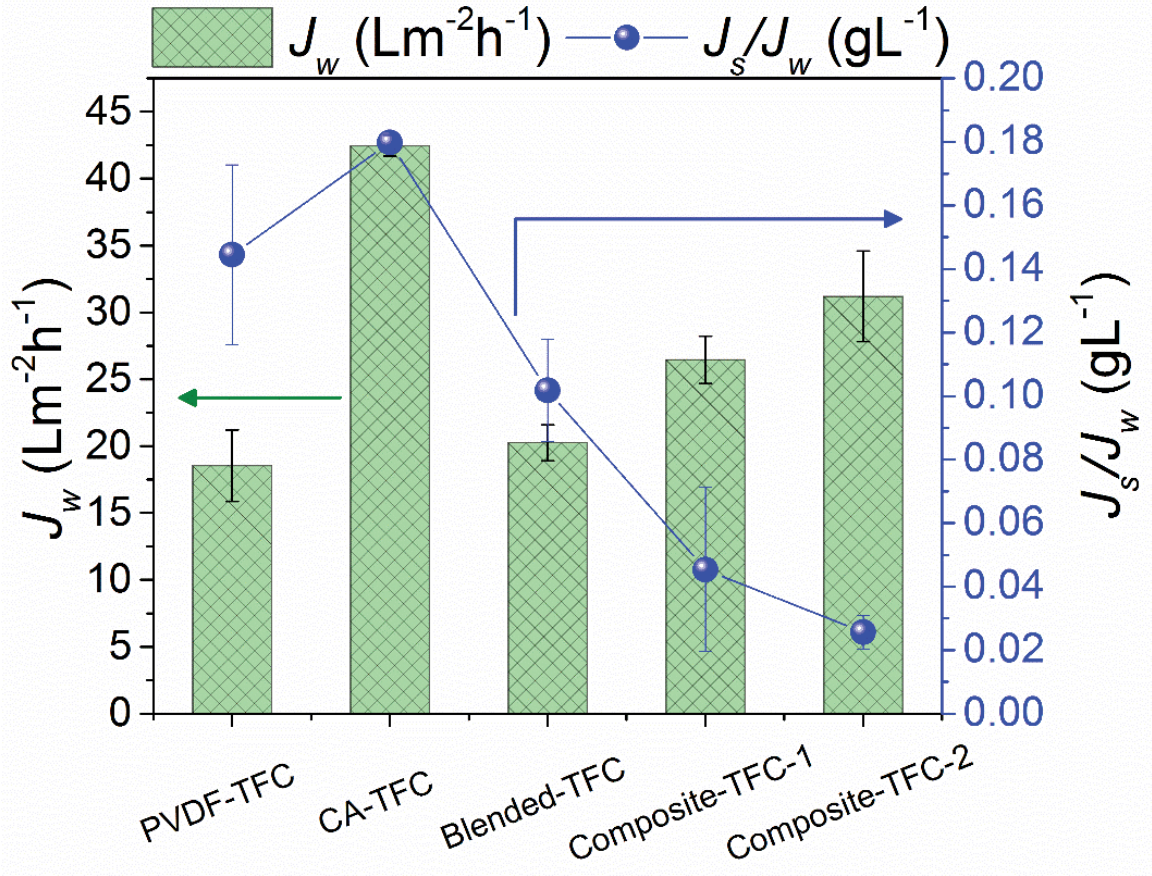

Figure 6 - 8. Performance (J_w: water flux and J_s/J_w :specific reverse salt flux) under AL-FS with 0.5 M NaCl as DS and DI water as FS for PVDF, CA, Blended (CA 75 wt%, PVDF 25 wt%), Composite-TFC-1 (Core-0.7 mL/min for PVDF, Sheath-1.3 mL/min for CA) and Composite-TFC-2 (Core-0.5 mL/min for PVDF, Sheath-1.5 mL/min for CA)

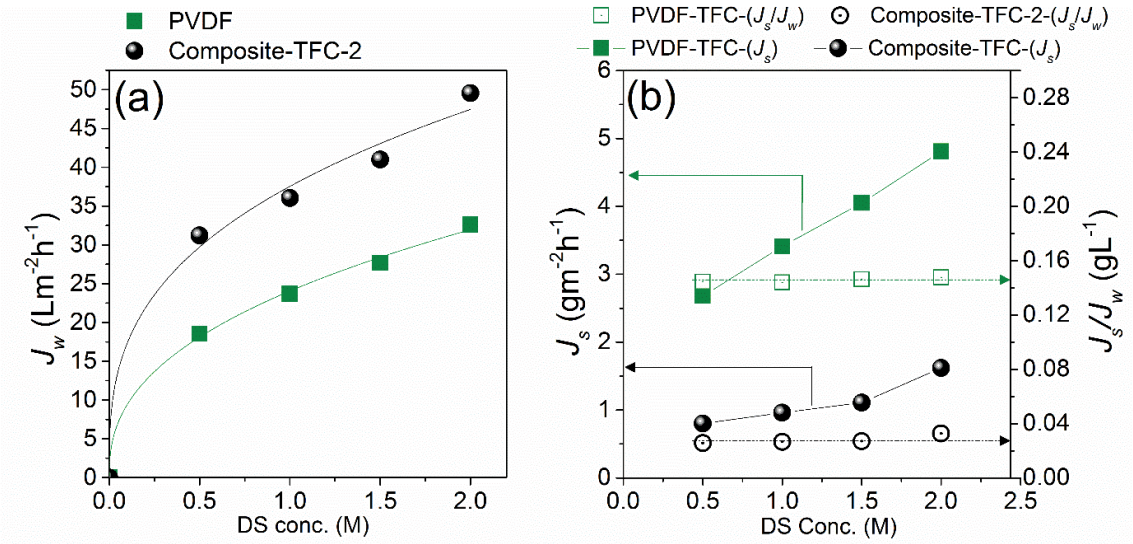

Figure 6 - 9. FO flux (J_w), reverse salt flux (J_s) and specific reverse salt flux (J_s/J_w) of the prepared TFC-FO membranes for PVDF and Composite-TFC-2 under AL-FS orientation at different DS concentrations at 0.5, 1.0, 1.5 and 2.0 M NaCl and DI water as FS.

Considering the performances of the TFC FO membranes in terms of the water flux and specific reverse solute flux along with their mechanical strength, it can be concluded that the Composite-TFC-2 is the best membrane for FO process applications as it shows the combined positive properties of CA (hydrophilicity) and PVDF (mechanical strength). We then conducted further FO performance tests at different DS concentrations and also determined the intrinsic membrane properties of Composite-TFC-2 membrane and compared with the PVDF-TFC membrane (used here as a control) and their results are presented in Figure 6-9 and Table 6-5.

Figure 6-9 shows that J_w and J_s increased for both PVDF-TFC and Composite-TFC-2 at higher DS concentrations as expected due to the higher osmotic driving force leading to higher water and salt fluxes (Han et al. 2016, Tian et al. 2017). The Composite-TFC-2 membrane however shows remarkably higher J_w and lower J_s values compared to PVDF-TFC membrane. This resulted in much lower J_s/J_w values (< 0.04 g L^{-1}) for Composite-TFC-2 membrane while PVDF-TFC shows J_s/J_w values of around 0.15 g L^{-1} at different

DS concentrations. This can be also explained with the intrinsic membrane properties of *A*, *B* and *S* values obtained from FO performances tests at different DS concentrations (Figure 6-9), as presented in Table 6-5 (Tiraferri et al. 2013). As expected, the *B* value of Composite-TFC-2 (0.07 L m^{-2} h^{-1}) membrane was remarkably lower than that of PVDF-TFC (0.25 L m^{-2} h^{-1}) membrane whereas the *A* value with 2.79 L m^{-2} h^{-1} bar^{-1} was higher for Composite-TFC-2 membrane than for PVDF-TFC membrane with 1.99 L m^{-2} h^{-1} bar^{-1}. From these results, the formation of PA active layer was significantly affected by the modification of membrane support properties. In addition, the *S* value was significantly reduced from 305 μm for PVDF-TFC to 190 μm for the strategically designed coaxial electrospun CA/PVDF nanofiber composite membrane.

Table 6 - 5. Intrinsic membrane parameters obtained by FO performances at different DS concentrations using a model fitting (Tiraferri et al. 2013).

Sample membranes	Water permeability coefficient, *A* [L m^{-2} h^{-1} bar^{-1}]	Salt permeability coefficient, *B* [L m^{-2} h^{-1}]	Structural parameter, *S* [μm]
PVDF-TFC	1.99	0.25	305
Composite-TFC-2	2.79	0.07	190

Table 6-6 shows the comparative FO performances of TFC membranes recently reported in the literature (Bui et al. 2013b, Huang et al. 2016, Huang et al. 2014, Lim et al. 2017, Liu et al. 2016b, Obaid et al. 2016a, Obaid et al. 2016b, Tian et al. 2014b, Tian et al. 2013, Widjojo et al. 2013, Yasukawa et al. 2015a). Our coaxial electrospun fabricated TFC-FO membrane with CA/PVDF composite nanofiber support (Composite-TFC-2) showed one of the highest FO performances among the TFC-FO membranes reported in the literature, regardless the use of nanofiber or phase inversion membrane support. The most significant contribution of this study is that, the specific reverse solute flux or the J_s/J_w value of 0.03 g L^{-1} for the Composite-TFC-2 FO membrane is the lowest values obtained so far compared to the values reported in the literature (Bui et al. 2013b, Huang et al. 2016, Huang et al. 2014, Lim et al. 2017, Liu et al. 2016b, Obaid et al. 2016a, Obaid et al. 2016b, Tian et al. 2014b, Tian et al. 2013, Widjojo et al. 2013, Yasukawa et al. 2015a). Reverse solute flux is one of the significant impediments of the commercial application of the FO process, as it not only results in economic loss of the draw solutes but also

contaminates the feed brine with the draw solutes which may complicate brine management, hence increasing costs. For example, reverse diffusion for a fertilizer drawn FO process is a big challenge since the brine contaminated with fertilizer nutrients cannot be discharged to the environment if it does not meet the effluent standard for nutrients (Phuntsho et al. 2016). Reverse solute flux is also a big challenge for FO application in the food industries because it can contaminate food during the concentration of food products, such as juice (Garcia-Castello et al. 2011). The very low specific reverse solute flux value is therefore a very promising aspect of this study, as it is highly significant for any FO applications. These results therefore show that the electrospun nanofiber membrane supports fabricated via coaxial electrospinning can be one of the efficient approaches of designing a dual-layered nanofiber structure of different polymers with different mechanical and hydrophilic properties to complement the strength and weakness of each polymer.

Table 6 - 6. Comparison of the FO performances with previous studies in the literature (All data were obtained under AL-FS orientation; FS: DI water).

Support type	DS (NaCl) [M]	J_w [L m^{-2} h^{-1}]	J_s [g m^{-2} h^{-1}]	J_s/J_w [g L^{-1}]	Ref.
Nanofiber membrane support					
PVDF-TFC	0.5	18.5	2.7	0.14	This work
CA-TFC	0.5	42.5	7.6	0.18	This work
Blended-TFC	0.5	20.2	2.1	0.10	This work
Composite-TFC-2	0.5	31.3	0.8	0.03	This work
CA/PAN-PET	1.5	27.6	3.85	0.14	(Bui et al. 2013b)
Nylon 6,6	1.0	21	5.2	0.24	(Huang et al. 2014)
PET/PVA (1/4)	0.5	47.2	9.5	0.20	(Tian et al. 2014b)
Modified-PVDF	0.5	16	2.7	0.17	(Huang et al. 2016)
PVDF-0.5SiO_2	1.0	52	34.8	0.67	(Obaid et al. 2016a)
TFC-PVDF-TEA	2.0	68	2	0.03	(Obaid et al. 2016b)
TFC-2#	1.0	28.0	12.9	0.46	(Tian et al. 2013)
Phase-inversion membrane support					
TFC-PSf_dGO	1.0	33.8	6.4	0.19	(Lim et al. 2017)
Polyketone	0.6	29.3	3.8	0.13	(Yasukawa et al. 2015a)
sPPSU-5	2.0	62.8	14.9	0.24	(Widjojo et al. 2013)
PES/PAA5/$CaCO_3$	2.0	52	16.8	0.32	(Liu et al. 2016b)

6.4. Conclusions

A novel TFC-FO membrane with dual-layered nanofiber support was successfully designed and fabricated using a coaxial electrospinning technique. This approach used a coaxial nozzle and two different polymers: mechanically-strong PVDF and weak but hydrophilic CA for the core and sheath sides, respectively. The performances of the polyamide based TFC FO membrane prepared via coaxial electrospun CA/PVDF nanofiber support layer were then compared with those membranes prepared using pure PVDF, pure CA and PVDF and CA blended electrospun nanofiber support layer. The following conclusions have been drawn from this study:

- The coaxial electrospun PVDF-CA nanofiber support layer exhibited a mechanical strength comparable to pure PVDF electrospun support layer. Although the hydrophilicity was lower than that of the pure CA nanofiber support, hydrophilicity of the composite membrane had significant improvement compared to pure PVDF or blended membrane support layer.

- Although the FO water flux (31.2 L m^{-2} h^{-1} using 0.5 M NaCl DS and DI FS) of the coaxial electrospun TFC membrane (Composite-TFC-2) is lower than the TFC membrane on pure CA support layer (42.5 L m^{-2} h^{-1}), the flux was much higher than the TFC membranes formed with pure PVDF-TFC (18.5 L m^{-2} h^{-1}) or blended (20.3 L m^{-2} h^{-1}) electrospun nanofiber membrane support. Coating hydrophobic PVDF nanofiber with hydrophilic CA by coaxial electrospinning technique can significantly improve the hydrophilic property of the electrospun support layer, thereby reduction structural parameter (*S*) value and ICP effects.

- The specific reverse solute flux of 0.03 g L^{-1} for the coaxial electrospun CA/PVDF TFC FO membrane is by far the lowest value so far reported in the literature. This value is highly significant for the commercial application of the FO technology, as reverse solute flux is one of the biggest challenges of the FO process.

- These results therefore show that the electrospun nanofiber membrane supports fabricated via coaxial electrospinning can be one of the efficient and practical approaches of designing a dual-layered nanofiber structure of different polymers

with different mechanical and hydrophilic properties to complement the strength and weakness of each polymer.

CHAPTER 7

HYDROPHILIC POLYVINYL ALCOHOL COATING ON HYDROPHOBIC ELECTROSPUN NANOFIBER MEMBRANE FOR HIGH PERFORMANCE THIN FILM COMPOSITE FORWARD OSMOSIS MEMBRANE

7.1. Introduction

Recently, electrospun nanofiber supports were applied as a membrane substrate for TFC-FO membrane. Several studies introduced fabrication of the TFC-FO membrane support layer using hydrophilic polymers (Bui et al. 2013b, Puguan et al. 2014, Song et al. 2011a, Tian et al. 2014b) and these hydrophilic FO membranes showed high performance. However, one major issue pointed out was the low mechanical stability of hydrophilic nanofiber support layers due to membrane swelling when it is exposed to liquids (Huang et al. 2016, Huang et al. 2014). To address this problem, in this chapter, a hydrophobic PVDF was used to prepare the nanofiber substrate for TFC-FO membrane. PVDF is a well-known membrane material that is characterized by its high mechanical and chemical stabilities. Nevertheless, the hydrophobicity of PVDF may not be suitable for FO membrane because the presence of the hydrophobic support layer of the FO membrane induces the solvent transport and membrane wettability (Chen et al. 2017, Liu et al. 2016b). In addition, membrane dehydration easily occurs especially when high salinity water is used as DS, which reduces the effective diffusion area thus increasing ICP and reducing FO flux (Zhang et al. 2016b). Therefore, the hydrophilic property of PVA was exploited to improve the wettability and mechanical properties of the TFC FO membrane that was prepared using PVDF nanofiber support. The PVDF nanofiber support mat prepared via electrospinning, was modified with PVA via dip coating and crosslinking methods prior to formation of polyamide active layer on it via interfacial polymerization. The influence of PVA coating on the PVDF nanofibers was assessed through a number of characterization methods. FO bench-scale experiments were also performed to assess the performance of the TFC membrane with PVA-coated support layer as a suitable semi-permeable layer for FO process. This chapter is an extension of the research article published by the author in Desalination.

7.2. Experimental

7.2.1. Materials

Polyvinylidene fluoride (PVDF, Kynar® 761, MW=441,000 g/mol) provided by Arkema Inc., Australia, was used as the electrospinning polymer. Polyvinylalcohol (PVA, 96% hydrolyzed, Mw 85,000~124,000) and glutaraldehyde (GA, 25% aqueous solution) from Sigma-Aldrich and hydrochloric acid (HCl, 32%) from RCI Labscan Limited, Thailand were used for nanofiber membrane coating. *N,N*-Dimethylacetamide (DMAc, ReagentPlus®, 99%) and acetone (analytical reagent, 99%) were purchased from Sigma-Aldrich and Chem-Supply Pty. Ltd., respectively, and used as organic solvents. 1,3-phenylenediamine (MPD, 99%), trimesoyl chloride (TMC, 98%) and heptane (anhydrous, 99%) from Sigma-Aldrich were used for polyamide layer formation. 2-propanol (isopropanol, IPA, Merck) and sodium chloride (NaCl, Chem Supply) were used as membrane wetting agent and draw solution, respectively.

7.2.2. Preparation PVDF nanofiber support

PVDF nanofiber supports were prepared via electrospinning technique with high voltage supply of 21~23 kV. PVDF (15 w/v %) was first dissolved in DMAc/acetone (5:5 v/v ratio) at constant stirring speed of 300 rpm and temperature of 60°C for 12 h, then the solution was cooled down prior to electrospinning. The polymer solution was transferred into a plastic syringe, and then delivered at (2 mL h^{-1}) by a syringe pump (G21, ID 0.51mm). The nanofibers were produced over a period of 3 h and during this period, they were being collected aluminum foil cover on a drum which was 180 mm apart from the needle. Temperature and humidity conditions inside the electrospinning chamber were 22 ~ 25°C and 35 ~ 55%, respectively. The as-spun nanofiber mats were peeled off from the aluminum foil and then dried in a dry oven at 50°C for 24 h to remove the residual solvents from the fibers. Afterwards, the PVDF nanofiber mats were heat-treated using a heat-press machine (Digital Combo, Geo Knight & Co Inc., USA) for 10 s at 160°C for further improvement of mechanical properties and stabilization of nanofiber mats (Park et al. 2016, Woo et al. 2017).

7.2.3. Modification of PVDF nanofiber mat via PVA dip coating

The PVDF nanofiber supports were modified to increase its hydrophilicity via PVA dip coating and crosslinking methods. 1 wt% of PVA dipping solution was prepared in water at 95°C with constant stirring for 6 h, and the solution was kept in a dry oven at 60°C. Prior to PVA dip coating, the nanofiber mats were pre-wetted by soaking in IPA for 1 min, then rinsed with DI water several times to remove the residual IPA. To remove the residual water on the nanofibers, the PVDF nanofibers were sandwiched in paper towels. The nanofibers were then soaked in PVA solution at 60°C for 1 h. A rubber roller was used to remove the excess PVA solution. Then, the samples were dried in the oven at 100°C for 10 min. The PVA coated on the PVDF nanofibers was subsequently crosslinked by soaking the membranes in a solution containing 50 mM GA and 20 mM HCl in acetone/DI water (5:5 volume ratio) for 1 h at room temperature. After the cross-linking reaction, the samples were cured at 100°C for 10 min to enhance the crosslinking reaction. The modified nanofiber mats were then stored in DI water prior to use.

7.2.4. Deposition of PA selective layer on nanofiber supports

Thin film PA selective layer was deposited on the electrospun nanofiber mats via IP process, with MPD and TMC as the monomers. The nanofiber supports were pre-wetted by soaking in IPA for 30 s followed by rinsing several times with DI water. The nanofibers were preserved in DI water for 24 h (Huang et al. 2016, Tian et al. 2013). The excess solvents for both PVDF and PVA-coated PVDF were removed by a rubber roller. The membranes were then equipped in an acrylic frame to allow introduction of the monomer solutions only to one side of the membranes. 2 wt% MPD aqueous solution was poured onto the membranes for 2 min each and then the excess solution was carefully removed using a rubber roller. 0.15 w/v% TMC in heptane was then introduced for 1 min to form a thin film PA layer, after which the TMC solution was immediately drained from the samples to control the reaction. The membranes were air-dried for 2 min and then placed in the oven at 70°C for 10 min to facilitate curing. All prepared TFC membranes were kept in DI water and stored at 4-6°C until use. The TFC membranes produced using

PVDF and PVA-coated PVDF nanofiber support layers are designated as TFC-PVDF and TFC-PVDF-PVA, respectively, in this study.

7.2.5. Evaluation of membrane performance

The water permeability and salt rejection performance of FO membranes were conducted with a lab-scale membrane test unit. An FO membrane test cell with 0.3 mm channel height and an effective area of 14 cm^2 (2 cm width and 7 cm length) was used. The unit was operated with co-current flow mode at a cross-flow velocity of 13.88 cm/s (0.5 L/min) using a variable speed gear pump for both feed and draw solution sides. Varied concentrations of aqueous NaCl (0.5, 1.0, 1.5 and 2.0 M) solutions were used as draw solutions whereas DI water was used as the feed. Both membrane orientations, FO mode (i.e., active layer facing feed solution or AL-FS) and PRO mode (i.e., active layer facing draw solution or AL-DS) were conducted in the FO tests. Temperature of both feed and draw solutions were maintained at 23°C ± 1 to minimize the effect of temperatures on FO performance. Due to the dehydration of samples after the membrane curing at high temperature (70°C) in the IP process, the TFC-PVDF membrane was pre-wetted via soaking in 50% IPA/water for 1 min then washed with DI water for several times to remove the residual IPA from the membrane prior to FO performance test. A non-pre-wetted TFC-PVDF membrane was also used for FO performance test as control. To provide a comparison with a commercially-available membrane, a membrane supplied by Hydration Technology Innovation (HTI, Albany, USA), CTA-HTI membranes was tested at the same conditions as the prepared TFC FO membranes.

The intrinsic membrane properties, pure water permeability (*A, A-FO*), solute permeability coefficient (*B*), and structure parameter (*S*) of the tested FO membranes were determined based on FO experimental data using the 4-stage prediction model designed by Tiraferri et al. (Tiraferri et al. 2013). All experimental conditions were kept the same as those of the performance tests in the osmotically driven process. In order to confirm the reliability of the results from model prediction, the pure water permeability (*A, A-RO*) of FO membranes was also evaluated by conducting reverse osmosis (RO) test with applying hydraulic pressure of 5 bar and with an effective membrane area of 19.5 cm^2.

The device used for these tests was described in detail in another previous study (Kim et al. 2016). All membranes were pre-compacted at a pressure of 5 bar for 30 min prior to the RO tests.

7.3. Results and discussion

7.3.1. Effect of PVA coating on PVDF nanofiber supports

The fibrous TFC support was fabricated via electrospinning using PVDF, which has the melting point of 165~172°C. The PVDF nanofiber was heat-treated at a temperature near its melting temperature (160°C) to enhance the mechanical properties of the fibers. Figure 7-1a shows a typical nanofibrous bead-free matrix with smooth surface of PVDF nanofibers. The conjugation of PVDF nanofibers after heat treatment was more apparent at higher magnification, as shown in Figure 7-1c. On the other hand, modified PVDF coated with PVA (PVDF-PVA) and cross-linked by GA presented in Figures 7-1b and 7-1d showed relatively rough fiber surface. In addition, some nano-sized branches were observed around the junctions of the fibers caused by PVA coating. Figures. 7-1e and 7-1f reveal the cross-sectional images of PVDF and PVDF-PVA, respectively, and both images show cylindrical-shaped non-woven fibers deposited randomly.

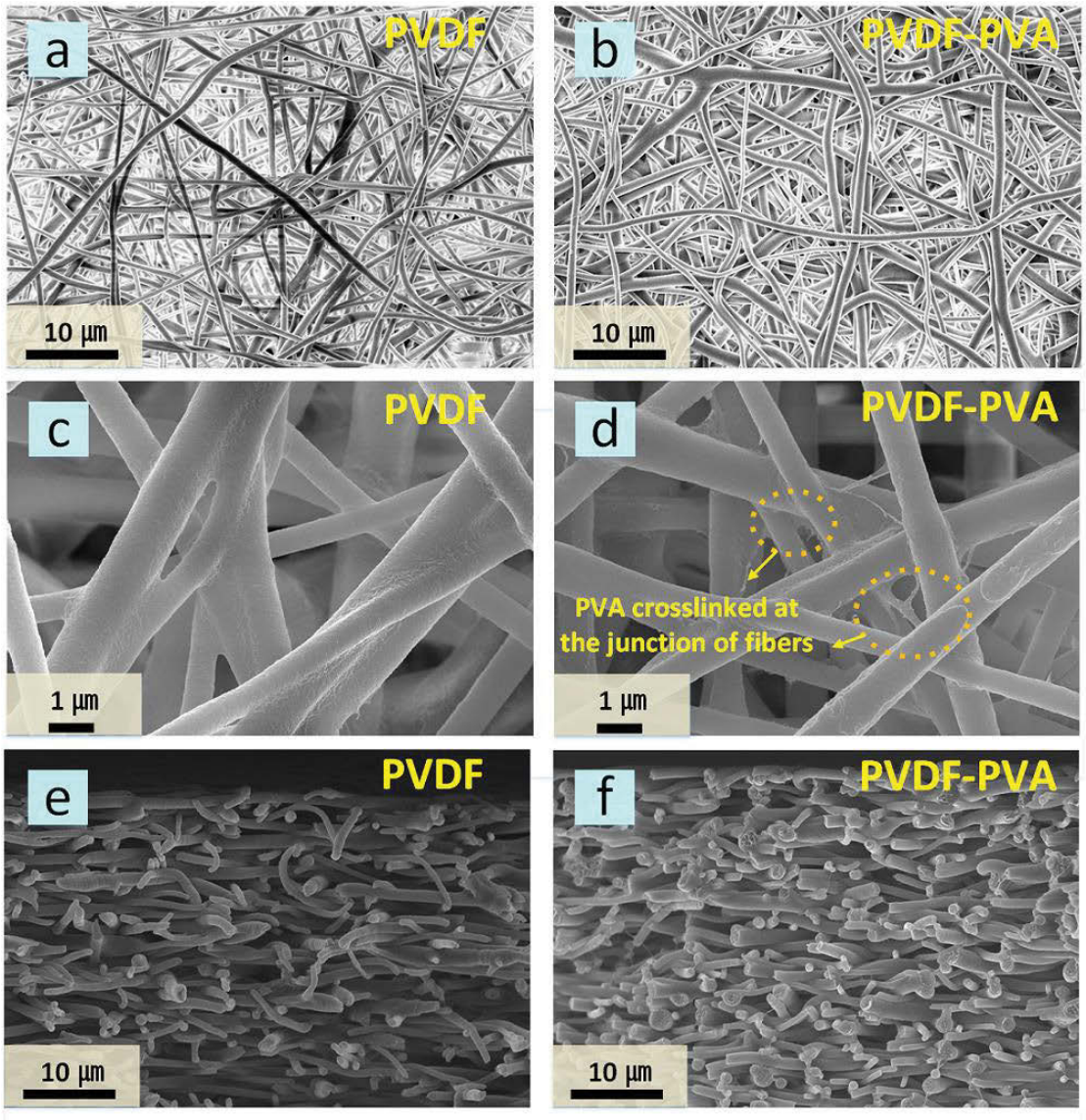

Figure 7 - 1. FESEM images of pure PVDF and PVDF-PVA nanofiber supports for top surface (a and b), top surface at higher magnification (c and d), and cross-section near the top surface (e and f).

A summary of the properties of PVDF and PVDF-PVA is listed in Table 7-1. Membrane thickness and average fiber diameter were mostly similar for both the membranes. Only a slight increase in average fiber diameter was observed from 910 nm to 926 nm after PVA coating, indicating that the PVA was coated thinly on PVDF. Even though almost no difference in surface morphology was observed after PVA dip coating, the hydrophilicity of the membrane surface significantly improved, as confirmed by the decrease in contact angle from 138.15° to 66.15°. While the abundant presence of –OH groups (96% hydrolyzed) in PVA resulted in a more hydrophilic nanofiber surface, it is

a water-soluble material. But the use of GA as cross-linker via acid-catalyzed acetalization made the coating highly stable in water (Nisola et al. 2015). Thus, the residual uncrosslinked fraction of hydroxyl groups of PVA provided the hydrophilic properties for the modified PVDF (Nisola et al. 2015).

Meanwhile, the results in Table 7-1 show that the mechanical properties of the PVDF membranes were enhanced after PVA coating. The PVA modification also significantly improved the tensile strength (by about 30% from 6.92 MPa to 9.04 MPa), the percentage elongation and Young's modulus. As can also be seen from the FE-SEM images (Figures 7-1d and 7-1f), the mechanical properties were reinforced by the fusion of PVDF fibers at the fiber junctions and with some cross-linked PVA branches and lumps of PVA between fibers.

Table 7 - 1. Comparison of membrane properties between PVDF nanofiber supports before (PVDF) and after (PVDF-PVA) modification.

Samples	PVDF	PVDF-PVA
Average fiber diameter (nm)	910 ± 271	926 ± 267
Membrane thickness (μm)	41.08 ± 5.53	41.88 ± 6.21
Contact angle (degree)	138.15 ± 2.48	66.15 ± 4.71
Tensile strength (MPa)	6.92 ± 0.59	9.04 ± 0.45
Elongation (%)	143.04 ± 23.59	190.79 ± 13.06
Young's modulus (MPa)	31.94 ± 9.17	75.17 ± 3.42

7.3.2. FTIR-ATR analysis

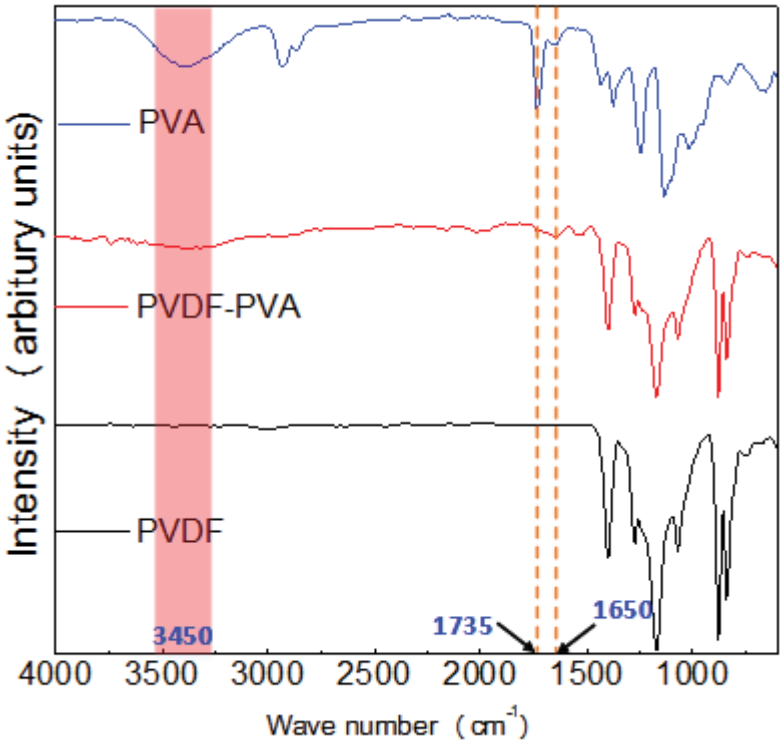

Figure 7 - 2. FTIR spectra of unmodified (PVDF) and modified (PVDF-PVA) nanofiber substrates, and PVA nanofiber.

The chemical composition of PVDF and PVDF-PVA membranes was characterized by ATR-FTIR spectrum as shown in Figure 7-2. Electrospun PVA nanofiber mat cross-linked with GA was also prepared to compare the spectrum with a PVDF-PVA. A full spectrum of pristine PVDF nanofiber support shows a typical trend of peaks for PVDF polymer. The strong peak at around 1404 cm^{-1} represents the C-H stretching vibration, whereas the peaks at 1172 cm^{-1} and 1273 cm^{-1} correspond to the vibration of C-F bonds that are found in PVDF (Obaid et al. 2016a, Zeng et al. 2016). The weak broad bands at 3200-3600 cm^{-1} and 1650 cm^{-1} associated with O-H can be found in the PVDF-PVA spectrum, indicating the presence of unreacted O-H groups of PVA after cross-linking with GA. Another peak at 1735 cm^{-1} can be attributed to the –C=O groups present in the PVDF-PVA nanofiber membrane due to the presence of unreacted residual aldehyde groups of GA after acetalization cross-linking reaction (Nisola et al. 2015). These all confirm the successful coating and crosslinking of PVA on the PVDF nanofibers via HCl-catalyzed acetalization with GA.

7.3.3. Surface properties of nanofiber support mat

As shown in Table 7-1, the initial contact angle of a modified PVDF (66.15°) was much lower than that of pristine PVDF (138.15°). The contact angle difference can be seen more clearly in the time profile measurement shown in Figure 7-3. The contact angle for PVDF steadily remained at around 140° for more than 10 s. The high contact angle for the pristine PVDF membrane is due to the hydrophobic character and low surface energy of PVDF (Pan et al. 2014). The contact angle of TFC FO membrane supports prepared via phase inversion using PVDF is less than 100°, which is significantly lower than that of pure PVDF nanofiber mats due to its smoother and less porous membrane surface (Moradi et al. 2015). Thus, it can be said that the non-uniform and rough surface of a nanofibrous structure would also result to a high hydrophobicity of the PVDF nanofiber support. It is also notable that pristine PVDF nanofiber was able to maintain its contact angle measurement for an extended period of more than 10 s. On the other hand, a PVA modified PVDF membrane has started with contact angle of 65.95°. However, the contact angle gradually decreased with time and the water droplet almost disappeared after 10 s with a contact angle of 17.80°, as seen in Figure 7-3. The decrease of contact angle with time is a result of excellent wettability of PVDF-PVA with hydrophilic surface property.

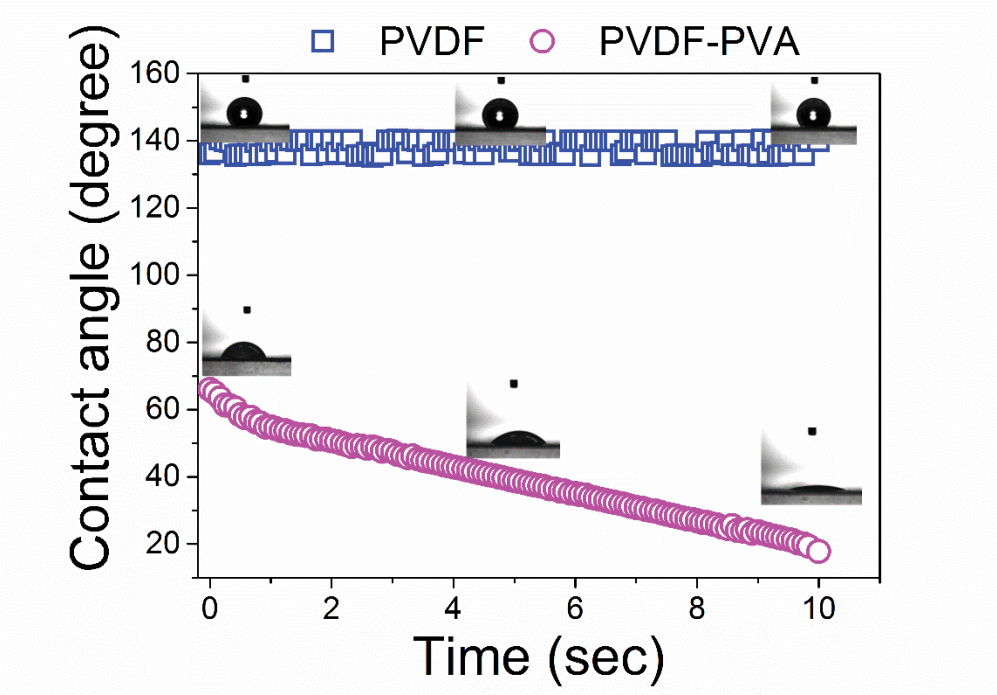

Figure 7 - 3. Contact angle trends in terms of time profile for PVDF and PVDF-PVA.

Membrane porosity and wetting abilities are summarized in Table 7-2. The porosity of PVDF was revealed to be about 76%. Porosity slightly decreased to 75% after PVA coating, however this change is almost negligible. FE-SEM images shown in Figure 7-1 also support that there are no apparent changes in membrane morphology via PVA coating. Therefore, PVA coating on PVDF nanofiber did not significantly affect the membrane porosity. Meanwhile, as expected, water was marginally absorbed at around 2.5% by pristine PVDF, while the water-saturated condition of PVDF has a water uptake of 176%. PVDF-PVA exhibited a water uptake of 159%, which is close to the maximum water uptake of 175%. The presence of cross-linked PVA coating on the PVDF fibers definitely improved the membrane's hydrophilic property and hence its water absorption capacity. The pure PVA nanofiber mat had water uptake and maximum water uptake values of 459% and 496%, respectively, due to its higher porosity and excellent swelling capacity (Nisola et al. 2015).

Table 7 - 2. Membrane porosity, water uptake and maximum water uptake for PVDF, PVDF-PVA and PVA.

Samples	Porosity (%)[1]	Water uptake (%)	Max. water uptake (%)[2]
PVDF	76.15 ± 0.92	2.48 ± 0.27	176.36 ± 2.48
PVDF-PVA	75.00 ± 1.28[1]	159.03 ± 7.87	175.19 ± 1.81
PVA	85.49 ± 3.27	459.42 ± 10.37	495.71 ± 13.25

[1]Density of only PVDF was used in the calculation.
[2]Samples were fully wetted by IPA, then immersed in water

7.3.4. Mechanical properties

One advantage of using hydrophobic nanofiber substrates as support for TFC FO membranes is to prevent membrane swelling which may weaken the membrane once it is exposed to liquids (Huang et al. 2016, Huang et al. 2014) and this is one reason for exploring PVDF support layer. In this study, electrospun PVDF nanofibers were first heat-pressed to improve the interconnectivity between fibers in order to enhance overall mechanical properties. Then, the heat-treated PVDF support was dip coated PVA to enhance its hydrophilic property as well as to prevent support membrane swelling. The PVA coating on the heat-treated PVDF nanofiber support is also expected to further improve its mechanical properties. The mechanical properties of non-heat treated PVDF support, PVDF (heat-treated) and PVDF-PVA supports at dry and wet conditions are shown in Figure 7-4. The as-spun PVDF without heat treatment shows mechanical strength at break and elongation at break of 3.84 MPa and 47.20%, respectively under dry condition and both these properties did not significantly decease even under wet condition. Similarly, PVDF and PVDF-PVA samples also did not show a significant decrease in their mechanical properties under dry and wet conditions. The differences of mechanical properties between dry and wet samples for all membranes were in fact less than 10%, which is not very significant. This shows noteworthy advantage of using electrospun hydrophobic PVDF nanofiber mat with hydrophilic PVA coating rather than a fully hydrophilic electrospun support mat that swells and loses mechanical properties on wetting in water since the hydrophobic nature of electrospun PVDF prevents membrane swelling (Huang et al. 2016).

The other noteworthy observation is the significant improvement in the mechanical properties of the electrospun PVDF support upon heat treatment and then PVA coating without swelling issues. As depicted in Figure 7-4, the mechanical strength of the electrospun PVDF support improved by about 80% (6.92 MPa) after heat-treatment and 135% (9.04 MPa) after PVA dip coating of heat-treated PVDF support, as compared to the non-heat treated PVDF support (3.84 MPa). Likewise, the elongation property was also enhanced from 47% of the dry samples to 143% for PVDF and to 191% for PVDF-PVA compared to non-heat treated PVDF support.

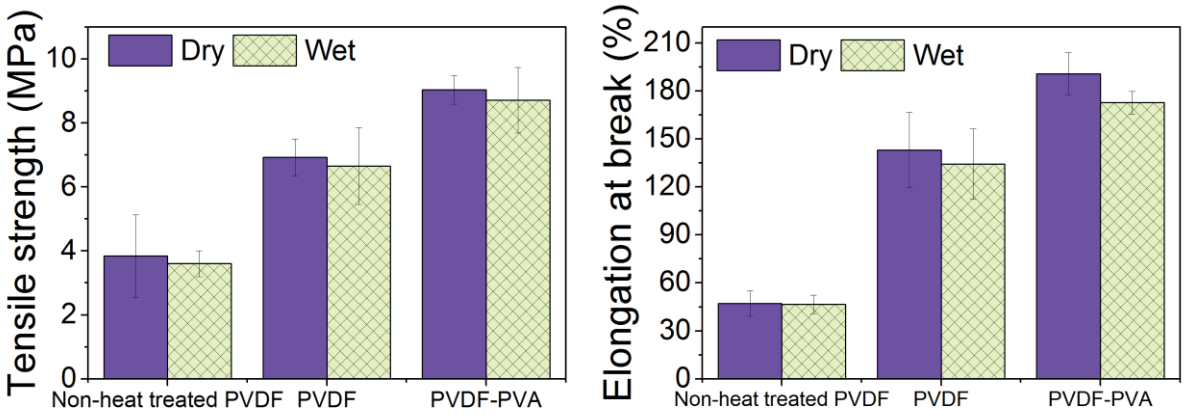

Figure 7 - 4. Tensile strength and elongation at break of non-heat treated PVDF, PVDF (heat treated) and PVDF-PVA (IPA was used for membranes wetting).

7.3.5. Thin film composite membrane deposition and its active layer morphologies

The thin film PA selective layers were deposited only on the heat-treated PVDF and PVDF-PVA nanofiber supports via IP process and were characterized by FE-SEM as shown in Figure 7-5. Typical rigid-and-valley structures for both TFC-PVDF (Figure 7-5a) and TFC-PVDF-PVA (Figure 7-5b) were observed on the membrane surfaces, which indicate the successful formation of PA selective layers. However, it is interesting to notice that the shapes and patterns of electrospun nanofibers were clearly imprinted under the polyamide layers, typically not seen in the TFC membranes prepared via phase inversion (Lim et al. 2017). Similar pattered PA layer has been observed previously when

the PA layer is formed on electrospun nanofiber supports (Bui et al. 2013b, Huang et al. 2016, Obaid et al. 2016a, Puguan et al. 2014, Tian et al. 2014b). The nanofiber supports have higher surface roughness, higher porosity, and bigger interstitial pore structures which likely induced the formation of this particular type of PA layers. The cross sectional images shown in Figure 7-5c (TFC-PVDF) and Figure 7-5d (TFC-PVDF-PVA) indicate the presence of a thin film of PA layer formed on the surface of the highly porous electrospun fiber support layer.

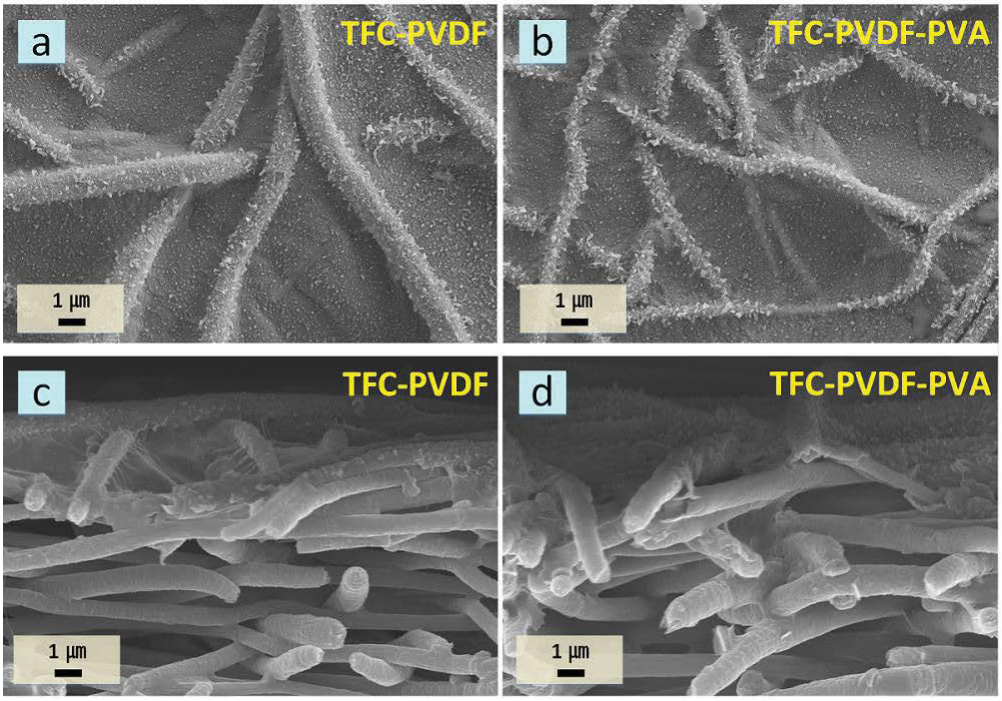

Figure 7 - 5. FE-SEM images of top surfaces and cross section area near to the PA selective layers for TFC-PVDF (a, c) and TFC-PVDF-PVA (b, d).

7.3.6. Evaluation of membranes performance for the osmotic process

The performance of each of the TFC-PVDF and TFC-PVDF-PVA membranes was tested and compared with the commercial HTI-CTA membrane. Since PVDF is a hydrophobic material, the TFC-PVDF membrane was also pre-wetted with IPA/water solution to temporarily improve its hydrophilicity. Figure 7-6 displays the performance of the

membranes under the FO and PRO modes of membrane orientations. All tests were conducted using 0.5 M NaCl as the draw solution and DI water as the feed solution.

As shown in Figure 7-6, the pre-wetted TFC-PVDF and TFC-PVDF-PVA membranes exhibited significantly higher water fluxes compared to TFC-PVDF membrane without pre-wetting and the commercial CTA membranes under both the membrane orientations. The TFC-PVDF membrane without pre-wetting showed even lower J_w in FO mode compared to commercial CTA FO membrane. Without pre-wetting of the TFC-PVDF membrane, the hydrophobic nature of the PVDF support layer prevents membrane pores from complete wetting with the draw solution (FO mode) thereby increasing the mass transfer resistance and resulting in very poor water flux (Huang et al. 2016). Hydrophobic support layer with low surface energy could offer high resistance to the solution diffusivity reaching the PA active layer through the membrane support layer and thus results in inefficient osmotic process. This phenomenon is evident from the dynamic contact angle measurement carried out on the support layer surface with time as presented earlier in Figure 7-3. However, the J_w for the TFC-PVDF membrane was higher than that of the commercial CTA membrane under the PRO mode of operation. This is because the DS located on the active layer side of the TFC membrane remains unaffected by the hydrophobic support layer which is located on the other side of the TFC membrane in contact with the DI water FS. The significantly higher J_w under the PRO mode (19.2 LMH) than that under FO mode (5.1 LMH) for the un-wetted hydrophobic TFC-PVDF membrane therefore indicates that using a hydrophobic support layer would significantly lose the osmotic driving force during the FO process.

It is important to note that the water flux for TFC-PVDF membrane improved significantly from 5.1 to 16.0 LMH (FO mode) and from 19.2 to 29.1 LMH (PRO mode) after pre-wetting with the IPA/water. This shows the advantage of pre-wetting the PVDF support layer that temporarily enhances its hydrophilicity and thereby reducing the ICP effects under both the modes of membrane orientations. Further improvement in FO performance was observed for TFC-PVDF-PVA membrane with J_w values of 24.8 LMH under FO mode and 32.6 LMH under PRO mode, the highest water flux among all membranes tested in this study. Despite slight decrease in the porosity of PVDF support layer, the enhanced water flux of the TFC-PVDF-PVA membrane is attributed to the highly improved hydrophilic property of the PVDF support layer due to PVA coating.

Improved hydrophilicity of the support layer reduces the ICP effect on it during the osmotic process thereby resulting in improved solution diffusivity and enhanced water flux (Liu et al. 2016b). This study reaffirms the significance of the hydrophilicity of the membrane support layer in reducing the ICP effect that largely controls the water flux and overall membrane performance in the osmotic process.

All membranes presented in Figure 7-6 exhibit higher FO fluxes (J_w) when operated in PRO mode as compared to FO mode. This is due to the occurrence of severe dilutive internal concentration polarization which, reduces the osmotic pressure gradient within the membrane support. Although FO operation at PRO mode allowed more water to pass across the selective layer, it also permitted more salts to counter diffuse through the membrane. This resulted in higher reverse salt flux (J_s) at PRO mode than that at FO mode. However, the specific reverse salt flux (J_s/J_w) remained similar for both orientations in all FO membranes. J_s/J_w values indicate the selectivity of the active layer of the membrane, such that lower J_s/J_w values are observed for more selective membranes. It is interesting to note that J_s/J_w values for all fabricated samples in both FO and PRO orientations depicted similar values in the range of 0.11~0.14 g/L. This can be attributed to the careful control of the IP process, which ensured the proper formation of the PA layer on each membrane. In fact, these J_s/J_w values were significantly lower than that of a commercial membrane, achieving a significant improvement in the selectivity of the TFC FO membranes.

Table 7 - 3. Intrinsic properties and structural parameters of FO membranes.

Samples	*A-RO*[1]	*A-FO*[2]	*B*[2]	*S*[2]	R^2,J_w	R^2,J_s
HTI-CTA	0.63 ± 0.05	0.62	0.31	690	0.99	0.99
TFC-PVDF	1.81 ± 0.12	0.73	0.08	1380	0.96	0.90
TFC-PVDF-Pre-wet	1.86 ± 0.18	2.26	0.26	431	0.99	0.98
TFC-PVDF-PVA	2.10 ± 0.09	1.94	0.22	154	0.99	0.98

[1]Pure water permeability (A-RO, LMH/bar) was conducted in RO mode with the applied pressure of 5 bar
[2]Pure water permeability (A-FO, LMH/bar), B (LMH) and S (μm) values were calculated and obtained from average values of FO performances at different draw solute concentrations using an excel-based algorithm designed by Alberto Tiraferri et al. (**Tiraferri et al. 2013**)

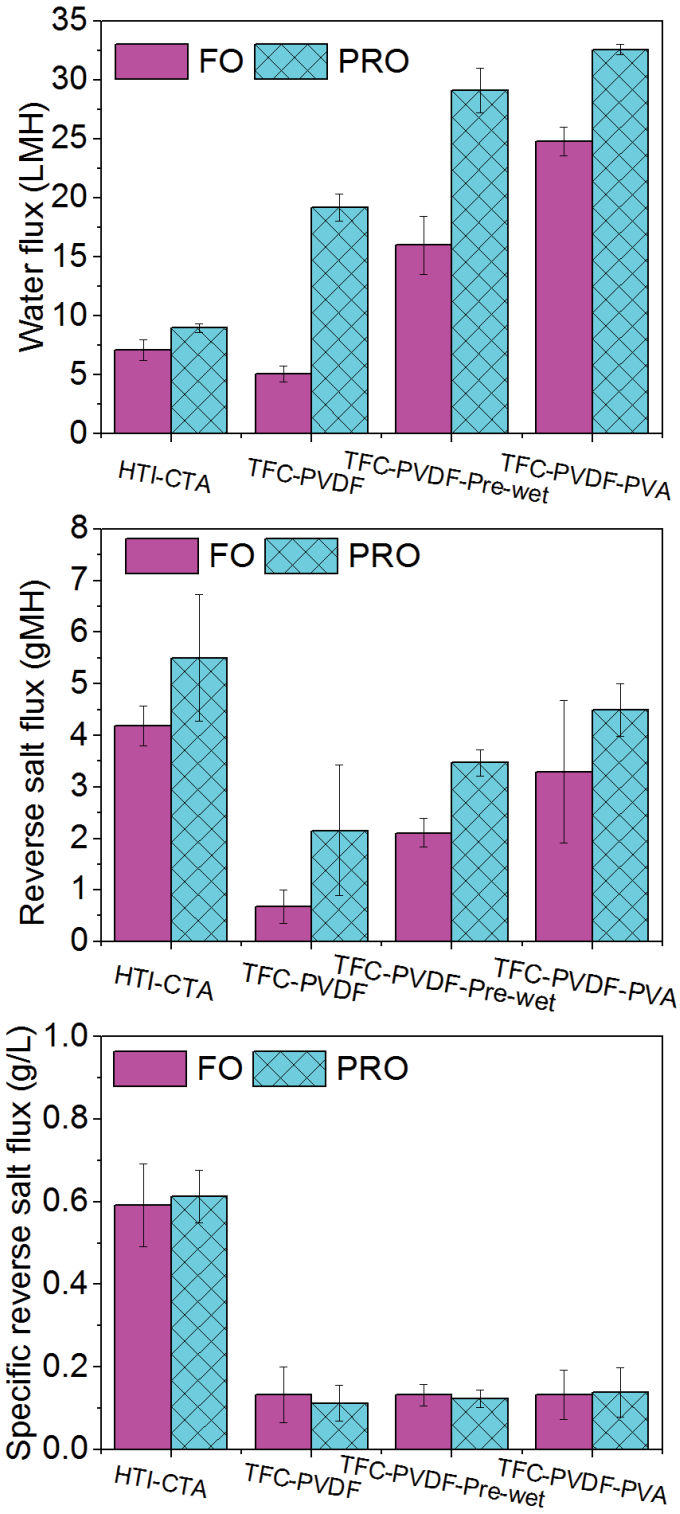

Figure 7 - 6. FO performance of commercial HTI-CTA and prepared TFC membranes under FO and PRO modes operation with 0.5 M NaCl as draw solution and DI water as feed solution (Test conditions: operation temperature = 23°C ± 1, cross-flow velocity = 13.88 cm/s, effective membrane area = 14 cm^2).

The intrinsic properties and *S* values of the fabricated FO membranes are summarized in Table 7-3. Pure water permeability of FO membranes was evaluated using two different approaches: 1) *A-RO* value was determined under the RO mode of membrane operation at hydraulic pressure of 5 bar and 2) *A–FO* value was calculated using an excel-based algorithm using data obtained FO test operations designed by Alberto Tiraferri et al. (Tiraferri et al. 2013). The values of both R^2-J_w and R^2-J_s were higher than 0.9, represent the precision of the data acquired from the FO tests (Tiraferri et al. 2013). The pure water permeability coefficients (*A*, LMH/bar) for all the membranes were relatively similar in values obtained under RO or FO mode as shown in Table 7-3. This confirms the match of coefficient values obtained from model calculations.

As shown in Table 7-3, the *A* values obtained for HTI-CTA were quite similar for both calculation approaches; *A-RO* of 0.63 LMH/bar and *A-FO* of 0.62 LMH/bar. The A values for HTI membrane were much lower than that for the TFC membranes fabricated in this study with the PVDF nanofiber supports. The pre-wetted TFC-PVDF membrane sample had a slightly higher *A* value of 2.26 LMH/bar obtained from FO mode compared to 1.86 LMH/bar obtained from RO mode. On the other hand, the TFC-PVDF-PVA membrane showed a slightly higher *A* value (2.10 LMH/bar) from the RO mode compared to the FO mode (1.94 LMH/bar). Although the TFC-PVDF membrane showed a comparable *A* value of 1.84 LMH/bar to the pre-wetted TFC-PVDF membrane (1.86 LMH/bar) under the RO mode however, its *A* value obtained from FO mode (0.73 LMH/bar) is much lower. The *B* value for all the TFC membranes were lower than that of the commercial HTI membrane with TFC-PVDF membrane showing the lowest *B* value of 0.08 LMH.

The comparable *A* values observed (obtained from RO mode) for all of the PVDF TFC membranes indicate that there is no significant effect on the formation of the PA selective layer after membrane support modification via PVA dip coating. However, smaller *A* and *B* values for the TFC-PVDF membrane (based on FO mode calculation) compared to the other two TFC membranes are because of the hydrophobic nature of the PVDF nanofiber support layer that resulted in significantly lower FO water fluxes compared to the pre-wetted TFC-PVDF and TFC-PVDF-PVA presented in Figure 7-7 at different draw solution concentrations. Support layer properties including hydrophobicity do not influence the *A* or *B* values determined under the RO mode as the hydraulic driving force is on the feed side and ICP phenomenon is absent. In contrary, *A* and *B* values determined

under the FO mode can be significantly affected by the hydrophobicity of the support layer because hydrophobicity can significantly enhance ICP and hence the driving force thereby lowering the water flux and potentially solute flux as evident from the low *SRSF* of the TFC-PVDF membrane.

Figure 7-7 shows that in general, both water flux and reverse salt flux for all FO membranes increase when a higher draw solution concentrations are used due to a larger concentration difference (or the driving force) that leads to higher water and salt passages as expected and reported in the literature (Han et al. 2016, Tian et al. 2017). However, the J_w/J_s values for all tested samples were consistently similar irrespective of any draw solution concentrations used. Among the evaluated FO membranes, the highest FO flux was observed for the TFC-PVDF-PVA membrane followed by TFC-PVDF-Pre-wet, HTI-CTA and TFC-PVDF membranes. At higher DS draw solution concentrations, the differences in the water fluxes among the membranes were more strikingly higher due to their differences in the severity of the ICP effects. A membrane support with lower porosity and membrane wettability results in more severe ICP effects especially at higher osmotic pressures, consequently resulting in the effective osmotic driving force. This can also be supported by the *S* values, which indicate the membrane porosity and wettability of the membranes, that membranes with higher *S* values had shown greater ICP occurrence.

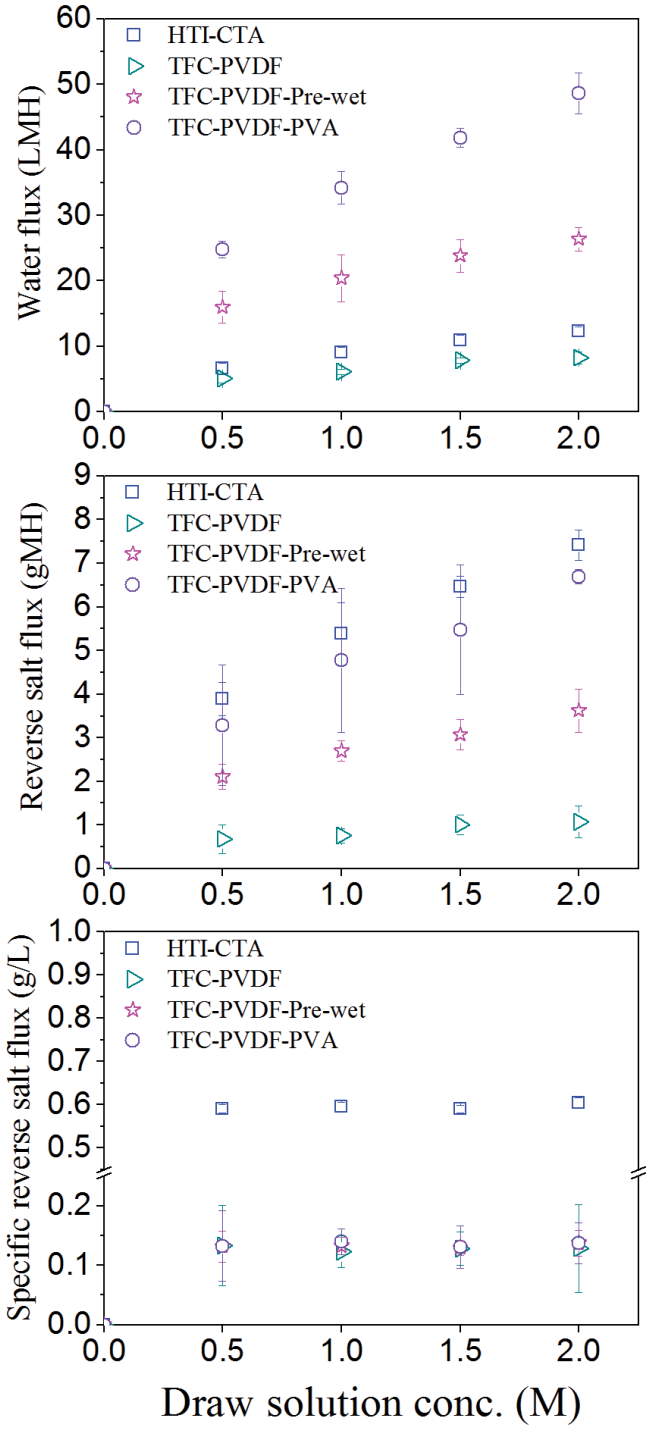

Figure 7 - 7. FO performance of commercial HTI-CTA and prepared TFC membranes under FO mode at different draw solution concentrations at 0.5, 1.0, 1.5 and 2.0 M NaCl and DI water as feed solution (Test conditions: operation temperature = 23°C ± 1, cross-flow velocity = 13.88 cm/s, effective membrane area = 14 cm^2).

As exhibited in Table 7-3, the *S* value decreased in this order: TFC-PVDF > HTI-CTA > TFC-PVDF-Pre-wet > TFC-PVDF-PVA consistent with their water flux performance at all draw solution concentrations tested. The highest *S* value (1380 μm) was observed for TFC-PVDF without pre-wetting due to the hydrophobic nature of the support layer that do not allow DS to flow through the support layer. The *S* value was however significantly reduced to 431 μm after pre-wetting the TFC-PVDF membrane with IPA/water prior to FO operation. A further significant reduction in the *S* value was observed for the TFC-PVDF-PVA membrane due to hydrophilization of the support layer. TFC-PVDF-PVA membrane showed the *S* value of 154 μm, which is significantly lower than the commercial HTI-CA and this value is only one third of the *S* value of the TFC-PVDF-Pre-wet membrane without pre-wetting. It is assumed that a hydrophilic membrane support layer enhances the water and solute molecule transport, as well as support layer wettability. Also, it increases the effective porosity, resulting to reduction of the ICP effect and improvement of the FO flux. The FO flux is inversely proportional to the *S* parameter when the solute resistivity is considered in relation to *S* parameter (Chen et al. 2017). Most previous studies on modified membrane support layer for enhanced the hydrophilic property obtained FO flux improvement, thus indicating lower *S* values (Chen et al. 2017, Han et al. 2012a, Lim et al. 2017, Liu et al. 2016b, Obaid et al. 2016b). Therefore, the modification of hydrophobic PVDF membrane support layer to increase its hydrophilicity resulted in reducing the *S* value without significantly altering its membrane intrinsic properties.

Table 7-4 presents a comparison of FO performances in this study with previous studies which introduce the effect of hydrophilic substrates on FO performance. The TFC-FO membrane (TFC-PVDF-PVA) with the PVDF electrospun nanofiber support coated with PVA showed competitive FO performances compared to other TFC membranes.

Table 7 - 4. Comparison of the FO performances with previous studies in the literature (All data were obtained under AL-FS orientation; FS: DI water).

Support type	DS (NaCl) [M]	J_w [LMH]	J_s [gMH]	J_s/J_w [g/L]	Ref.
TFC-PVDF-Pre-wet	0.5	16.0	2.1	0.13	This work
TFC-PVDF-PVA	0.5	24.8	3.3	0.13	This work
CA/PAN-PET	1.5	27.6	3.85	0.14	(Bui et al. 2013b)
Nylon 6,6	1.0	21	5.2	0.24	(Huang et al. 2014)
PET/PVA (1/4)	0.5	47.2	9.5	0.20	(Tian et al. 2014b)
Modified-PVDF	0.5	16	2.7	0.17	(Huang et al. 2016)
TFC-PVDF-TEA	2.0	68	2	0.03	(Obaid et al. 2016b)
SPSFco-TFC	0.5	22.4	≈ 3.2	≈ 0.14	(Chen et al. 2017)
TFC-2#	1.0	28.0	12.9	0.46	(Tian et al. 2013)
TFC-PSf_dGO	1.0	33.8	6.4	0.19	(Lim et al. 2017)
Polyketone	0.6	29.3	3.8	0.13	(Yasukawa et al. 2015a)
sPPSU-5	2.0	62.8	14.9	0.24	(Widjojo et al. 2013)
PES/PAA5/$CaCO_3$	2.0	52	16.8	0.32	(Liu et al. 2016b)

7.4. Conclusions

Electrospun hydrophobic PVDF nanofiber membrane support layer was successfully modified via PVA dip coating and acid-catalyzed crosslinking using GA to prepare a high performance TFC-FO membrane. The hydrophobic PVDF nanofiber first underwent heat-press treatment prior to PVA dip coating and crosslinking in order to reduce membrane swelling in water and also to improve its mechanical properties. The PVA dip coating of the nanofibers significantly enhanced the membrane hydrophilicity without compromising the membrane support porosity. This consequently resulted in significant reduction in the ICP effects and hence improvements in the FO performances in terms of water flux and J_s/J_w. The lowest structural parameter value of 154 μm was achieved for the PVA coated TFC-FO membrane and its performances were comparable with other

high-performance FO membranes reported in the literature. This study therefore indicated that dip coating of the nanofiber support with PVA is a useful approach for improving hydrophilic property of membrane supports layer and it can be a viable option in the fabrication of high performance TFC-FO membranes.

CHAPTER 8

CONCLUSIONS AND RECOMMENDATIONS

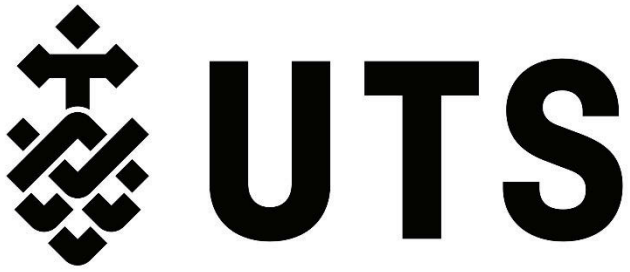

8.1. Conclusions

Osmotically driven process such as FO and PRO have been proposed as new alternative processes to provide sustainable solutions for the global needs of fresh water and clean energy. On the other hand, several challenges remain for this economically viable osmotically driven process such as the lack of suitable membranes for FO and PRO processes. Therefore, this research has focused on the development of high performance membrane materials for engineered osmosis including FO and PRO via various approaches to provide useful techniques for commercializaion. Different membrane preparation techniques using hollow fiber spinning, electrospinnig, and flat-sheet membrane casting were conducted to prepare the membrane supports for TFC membranes. Conclusions for each chapter are summarized below and recommendations are presented for further development of high performance engineered osmosis membranes.

8.1.1. Effect of GO incorporation in the membrane support layer for FO and PRO membrane performances

In this study, novel TFC-FO membranes with GO-modified support layers were fabricated, characterized and evaluated (Chapter 4). Different loadings of home-made GO (0.1- 1.0 wt%) were blended with a PSf solution to produce mixed matrix flat-sheet membrane supports by phase inversion method. Subsequently, the PA selective layer was deposited on the PSf/GO membranes via an IP reaction to finally produce the TFC-FO membranes. The TFC-FO membranes were comprehensively characterized in terms of its morphology, surface- and mechanical properties.

At an optimal GO loading (0.25 wt%) in PSf support, the TFC-FO membrane afforded the highest water flux and reverse flux selectivity, under AL-FS mode using 0.5 M NaCl as DS and DI water as FS. The PSf/GO (0.25 wt%) sublayer structure thus formed an ideal structural property of a support layer for the TFC-FO membrane. In addition, GO also improved the hydrophilic property of the support layer and allowed effective PA layer formation. All these improvements in the support PSf and active PA layer due to GO incorporation under optimal conditions subsequently resulted in improved FO performance by reducing the ICP effect in the support layer. The *S* value at 0.25 wt% GO loading was only S = 191 μm, which is remarkably lower than that of the TFC membrane

with pure PSf support (S =1060 μm). This result further supports the benefit of using GO as support filler for an improved FO performance of the TFC membrane.

However, the results also reveal that high GO loading (≥0.5 wt%) can negatively affect the membrane properties due to GO aggregation. Poor GO dispersion (at high loading) supressed the finger-like structure formation which resulted in low membrane porosity of the support layer. Consequently, FO performance was adversely affected due to the severe ICP in the support layer. Therefore, these findings suggest that FO performance of TFC-FO membranes can be significantly improved through membrane substrate modification under controlled incorporation of GO nanosheets.

As we observed the advantages of GO incorporation in the support layer for FO membrane, similar perspectives for PRO membrane fabrication can be considered. Because the ideal charateristics of a PRO membrane are in fact similar to that of FO membranes, which should also have a membrane property of high water permeability, low ICP and reverse salt flux, and high mechanical properties to achieve the high power density. However, high mechanical stability of the membrane support is one major important parameter for the PRO membrane. Therefore, we have investigated the effect of GO for TFC-PRO membrane fabricaiton in chapter 5. In this chapter, TFC-PRO membranes were fabricated using PES hollow fiber supports and GO was also used as a filler with controlled loadings (≤0.2 wt%) in the PES support layer to improve its performance.

Considering that GO loading must be controlled to obtain enhanced membrane performance, thus the maximum loading of GO was limited at 0.2 wt% to minimize the agglomerization of GO in the support layer, which could only provide the negative effects on membrane performance. At only 0.2 wt% GO loading, significant improvements in PES-supported TFC-PRO membrane structure and surface chemistry were observed. The water permeability of both PES hollow fiber supports and TFC-PRO hollow fiber membranes improved with increase in GO loadings from 0 to 0.2 wt%. The PRO flux for TFC membranes was also improved. These results indicate that incorporation of GO as a filler in hollow fiber membrane support for TFC-PRO membrane fabrication can improve the PRO flux without deteriorating the mechanical stability. Moreover, this study confirms that mixed matrix support has a high potential to enhance PRO performance, not only with GO for TFC hollow fiber membrane but also with other hydrophilic

nanomaterials. By controlling GO loading and PES concentration during dope solution preparation, strucutral morphologies, such as surface pore size and porosity, as well as the mechanical strength of hollow fiber membrane substrate were enhanced to achieve a higher power density. Although mixed matrix hollow fiber composite membrane (THF-GO-0.2) with GO improved the significant PRO performance, it may not be sufficient to extract maximum power density from high salinity DS solution. For example, when the RO retentate (1.2 M NaCl ≈ 57 bar) is used as DS, the hollow fiber membrane needed to sustain a hydraulic pressure of least 29 bar (half of osmotic pressure) to reach the maximum power density. However, the burst pressure of THF-GO-0.2 is only 17.3 bar, so this membrane may not be fully harvest the energy from the high salinity water. Due to this reason, future study on developing PRO hollow fiber membranes needs more focus on improving the PRO hollow fiber mechanical strength and high PRO flux for commercially available membrane development. To satisfy this requirement, hollow fiber membranes with a thicker membrane wall (> 200 μm) may be considered to increase burst pressure. Furthermore, smaller diameter to reduce the stressed area and increase polymer density of membrane matrix.

8.1.2. Novel CA/PVDF nanofiber supports prepared via coaxial electrospinning for TFC-FO membranes

This study (Chapter 6) introduces a novel approach to fabricate a dual-layered hydrophilic/hydrophobic nanofiber TFC-FO support membrane via coaxial electrospinning. The technique produces a dual layer core/sheath composite nanofiber composed of two different polymers: PVDF with high mechanical properties as core fiber and weak but hydrophilic CA polymer as the sheath side of nanofibers using a coaxial nozzle. The fabricated TFC-FO membrane had a comparable mechanical strength with pure PVDF support. Its hydrophilic CA/PVDF composite nanofiber support improved the FO performance by reducing the ICP. In addition, this electrospinning technique eliminates the necessity to further hydrophilize the membrane surface.

The performance of a novel composite nanofiber TFC FO membrane was evaluated and compared to other TFC membranes with supports prepared from pure CA, pure PVDF and, also with blended CA/PVDF (75/25 wt% ratio) nanofiber membrane support through various characterization methods and performance experiments. The FO membrane

prepared with Composite-TFC-2 showed significantly higher FO flux than those prepared with pure PVDF or blended nanofiber support. This Composite-TFC-2 prepared via coaxial electrospinning technique showed the FO flux of 31.3 LMH which is even much higher than that of TFC-GO-0.2 (19.77 LMH) under same operating condition. Basically high porosity and low tortuosity of electrospun nanofiber support as well as hydrophilic modification might contribute to a high FO performance as compared to TFC membrane prepared via phase inversion method.

Hydrophobic PVDF nanofiber coated with hydrophilic CA via coaxial electrospinning efficiently improved the hydrophilicity in the nanofiber support thereby reduced the ICP in the support layer. This study therefore suggests that fabrication of nanofiber support for TFC-FO membranes via a coaxial electrospinning is a practical approach to designing a dual-layered support structure with different characteristics of two polymers which, when combined, can result in enhanced membrane properties and performance.

8.1.3. FO performance improved by hydrophilic PVA coating on the PVDF nanofiber support

From the previous study (Chapter 6), it was confirmed that a dual-layered CA/PVDF electrospun nanofiber support via coaxial electrospinning for TFC-FO membrane is an efficient way to design a multi-functional FO membrane support that is hydrophilic with acceptable mechanical properties. However, the durability of the prepared CA/PVDF nanofiber support remains uncertain for long-term operation and commercialization. Although, CA-PVDF nanofiber support (Composite-2) exhibited a comparable tensile strength of 3.16 MPa with pure PVDF nanofiber support (3.61 MPa), this mechanical property may not be satisfactory for real applications. Thus, the present study (Chapter 7) introduces a novel TFC-FO nanofiber membrane with enhanced mechanical stability of the electrospun nanofiber support and at the same time has improved FO performance via a simple modification with hydrophilic PVA dip coating and heat-press treatment. Hydrophilic modification of the FO membrane support layer has been proposed from the previous studies and the results indicate that it is an effective approach to enhance the FO performance.

The PVDF nanofiber support via electrospinning was first prepared and then post-treated via heat-press at a temperature of 160°C near the melting point of PVDF (165~172°C) to

improve its overall mechanical property by enhancing the interconnectivity between fibers as well as to prevent support membrane swelling. The PVDF nanofiber support after heat-press exhibited the tensile strength of 6.92 MPa which is remarkably higher than without heat-press (3.61 MPa, presented in Chapter 6). The mechanically improved PVDF nanofiber support was additionally modified with PVA to enhance its surface hydrophilicity. This step also resulted in improvement of its mechanical properties. Dip coated PVA must be cross-linked with another material due to its high water solubility. Cross-linking with GA not only reduced PVA water solubility but also further improved the tensile strength. The effect of PVA coating and GA crosslinking on nanofiber support porosity further confirmed that it did not hinder the overall porosity of the support layer. Therefore, significantly improved FO flux was achieved after hydrophilic modification. This is because the enhanced membrane wettability reduced the ICP in the support layer and consequently obtained the lowest *S* value of 154 μm for the PVA coated TFC-FO membrane. Dip coating of the nanofiber support in PVA can be a one another useful modification approach for the improvement of PVDF support hydrophilicity to fabricate high performance TFC FO membranes.

8.2. Recommendations and future work

Osmotically driven processes or its hybrid systems combined with other technologies have been a growing interest in recent years due to their high potential in replacing the conventional technologies (Chekli et al. 2016). With these perspectives, developments of high performance TFC osmosis membranes for FO and PRO applications were introduced in this study using various membrane preparation techniques and modifications. Although various TFC membranes have been successfully fabricated and tested, there are still several issues arising that need to be considered for future membrane developments.

Both FO and PRO membranes first modified by hydrophilic GO incorporation in the membrane substrates prepared via a typical phase inversion technique showed the outstanding improvement in membrane performance at an small loadings of ≤ 0.25 wt%, therefore GO can be an excellent nanomaterial filler for the development of TFC membranes. Especially, the unique structure of hydrophilic GO with 2D one atomic thick single-layer, which has the extremely high aspect- and surface area-to-volume ratio

(owing to its nearly atom-thick sheets around 1-2 nm) as compared to other hydrophilic fillers like spherical (i.e. SiO_2, TiO_2, MOF and COF) and tubular (i.e. CNT and MWCNT) types. Thus, only small amount of GO was needed to obtain the desired properties of the composite membranes as proven in these studies for FO and PRO applications. From these perspectives, 2D atomic thick materials similar to GO have great potential for composite membrane development for various applications.

The previous studies have introduced that GO also provides the anti-fouling propensity, as the material itself or when it incorporated with other materials (i.e. polymer) for water treatment membranes. Although membrane fouling performance with GO incorporated substrates for FO and PRO applications, was not evaluated in this study, but it is highly expected that hydrophilic GO-polymer composite membranes can mitigate the membrane fouling when high salinity waters contained with organic or inorganic compounds use as draw solutes such as seawater and RO brine. Therefore, further studies can be investigated the effect of GO on the membrane fouling mitigation. On the other hand, application of GO at commercial scale TFC membrane manufacture may increase the overall production cost since GO remains an expensive nanomaterial. In the previous studies, various kinds of nanomaterials have been selected and demonstrated as fillers which effectively reduced the structural parameter of TFC membranes. However, none of the studies specifically explored and considered practical aspects of TFC membrane fabrication with fillers at the support layer. Therefore, an economic evaluation of using fillers such as GO must be conducted to determine its realistic potential for scale-up.

In this research, the TFC-FO membranes were developed with hydrophilic modification of electrospun nanofiber supports. These hydrophilic membrane supports provided better water transport thus reducing the ICP in the membrane support. To date, although electrospun nanofiber materials have high potential as support layers for FO or PRO TFC membranes, their weak mechanical properties and intensive membrane swelling still limit their full application. To counter this drawback, two novel approaches were conducted to improve their membrane properties.

First, the TFC-FO membrane with a dual-layered CA/PVDF nanofiber support prepared via a coaxial electrospinning exhibited highly improved FO performance with good hydrophilicity as well as comparable mechanical strength as compared with the pure PVDF membrane. As discussed earlier, the composite-TFC-2 showed the significantly

high FO flux than that of TFC-FO membrane incorporated with 0.25 wt% GO as presented in Chapter 4. Thus, this study indicates that a coaxial electrospinning technique, which simultaneously produces the dual component of nanofibers using two different characteristics of polymers, can be a practical approach to improve the FO membrane performance and mechanical stability. Thus far, this study used only two different polymers of hydrophilic CA and hydrophobic PVDF, but other types of polymers and their combinations can be explored to further improve the FO membrane properties especially for both hydrophilic and mechanical properties. Because it was found that CA does not provide the sufficient mechanical properties which somewhat deteriorated the overall mechanical properties of the composite membranes. Other hydrophilic polymers such as polyacrylonitrile (PAN) or nylon 6,6 can be a good candidate for the fabrication of composite nanofiber membranes via a coaxial electrospinning due to their relatively high mechanical strength and hydrophilicity as compared to CA. In addition, optimization of coaxial electrospinning conditions such as polymer concentrations, flow rate ratio of two different dope solutions, applied voltage, humidity, and the distance between collector and nozzle need to be additionally investigated to obtain the ideal membrane support characteristics for future studies.

Secondly, the present study prepared the heat-treated PVDF electrospun nanofiber support, which was coated with hydrophilic PVA for TFC-FO membrane. This surface modification has successfully improved the hydrophilicity and mechanical strength of PVDF nanofiber support without adversely affecting the support porosity; its overall effect enhanced the FO performance of the TFC membrane.

Overall, these two approaches, for developing FO membranes with the electrospun nanofiber supports, showed the high potentials in an improving FO performance with high mechanical properties. However, TFC-FO membranes with nanofiber supports should be considered for specific applications in the FO process due to their particular characteristics. For instance, the TFC-FO membranes composed of 3D matrix with highly porous nanofiber supports may be advantageous when the polymer type of osmotic agents use as DS in the FO process. Due to the larger molecular sizes as compared to monovalent or divalent salts, polymeric draw agents show an extraordinary low reverse diffusion but their relatively higher solute viscosity increase the ICP in the membrane support. To reduce the ICP effect, porous nanofiber support layer of TFC-FO membrane may be more

suitable than that of membrane support prepared via phase inversion method. On the other hand, TFC-FO nanofiber membranes are probably unfit when the high salinity waters (i.e. seawater) contained with membrane foulants use as a draw solute in FO processes, because the faster accumulation of foulants in the porous nanofiber support layer may reduce the overall porosity thus cause the severe ICP.

REFERENCE

Achilli, A., Cath, T.Y. and Childress, A.E. (2009) Power generation with pressure retarded osmosis: An experimental and theoretical investigation. Journal of Membrane Science 343(1), 42-52.

Achilli, A. and Childress, A.E. (2010) Pressure retarded osmosis: From the vision of Sidney Loeb to the first prototype installation — Review. Desalination 261(3), 205-211.

Akther, N., Sodiq, A., Giwa, A., Daer, S., Arafat, H.A. and Hasan, S.W. (2015) Recent advancements in forward osmosis desalination: A review. Chemical Engineering Journal 281, 502-522.

Alsvik, I. and Hägg, M.-B. (2013a) Pressure Retarded Osmosis and Forward Osmosis Membranes: Materials and Methods. Polymers 5(1), 303-327.

Alsvik, I.L. and Hägg, M.-B. (2013b) Pressure retarded osmosis and forward osmosis membranes: Materials and methods. Polymers 5, 303-327.

Alzahrani, S. and Mohammad, A.W. (2014) Challenges and trends in membrane technology implementation for produced water treatment: A review. Journal of Water Process Engineering 4, 107-133.

Amini, M., Jahanshahi, M. and Rahimpour, A. (2013a) Synthesis of novel thin film nanocomposite (TFN) forward osmosis membranes using functionalized multi-walled carbon nanotubes. Journal of Membrane Science 435, 233-241.

Amini, M., Jahanshani, M. and Rahimpour, A. (2013b) Synthesis of novel thin film nanocomposite (TFN) forward osmosis membranes using functionalized multi-walled carbon nanotubes. Journal of Membrane Science 435, 233-241.

Amy, G. (2008) Fundamental understanding of organic matter fouling of membranes. Desalination 231(1), 44-51.

Arena, J.T., Manickam, S.S., Reimund, K.K., Freeman, B.D. and McCutcheon, J.R. (2014) Solute and water transport in forward osmosis using polydopamine modified thin film composite membranes. Desalination 343, 8-16.

Arena, J.T., McCloskey, B., Freeman, B.D. and McCutcheon, J.R. (2011) Surface modification of thin film composite membrane support layers with polydopamine: Enabling use of reverse osmosis membranes in pressure retarded osmosis. Journal of Membrane Science 375(1-2), 55-62.

Banasiak, L.J., Kruttschnitt, T.W. and Schäfer, A.I. (2007) Desalination using electrodialysis as a function of voltage and salt concentration. Desalination 205(1), 38-46.

Bhalla, G. and Deen, W.M. (2009) Effects of charge on osmotic reflection coefficients of macromolecules in fibrous membranes. Biophysical Journal 97, 1595-1605.

Blandin, G., Verliefde, A.R.D. and Le-Clech, P. (2015) Pressure enhanced fouling and adapted anti-fouling strategy in pressure assisted osmosis (PAO). Journal of Membrane Science 493, 557-567.
Bose, S., Kuila, T., Mishra, A.K., Kim, N.H. and Lee, J.H. (2012) Dual role of glycine as a chemical functionalizer and a reducing agent in the preparation of graphene: an environmentally friendly method. Journal of Materials Chemistry 22(19), 9696.
Bui, N.-N., Lind, M.L., Hoek, E.M.V. and McCutcheon, J.R. (2011) Electrospun nanofiber supported thin film composite membranes for engineered osmosis. Journal of Membrane Science 385-386, 10-19.
Bui, N.-N. and McCutcheon, J.R. (2013a) Hydrophilic nanofibers as new supports for thin film composite membranes for engineered osmosis. Environ Sci Technol 47(3), 1761-1769.
Bui, N.-N. and McCutcheon, J.R. (2014) Nanofiber supported thin-film composite membrane for pressure-retarded osmosis. Environ Sci Technol 48, 4129-4136.
Bui, N.-N. and McCutcheon, J.R. (2016) Nanoparticle-embedded nanofibers in highly permselective thin-film nanocomposite membranes for forward osmosis. Journal of Membrane Science 518, 338-346.
Bui, N.N. and McCutcheon, J.R. (2013b) Hydrophilic nanofibers as new supports for thin film composite membranes for engineered osmosis. Environ Sci Technol 47(3), 1761-1769.
Cadotte, J.E., Petersen, R.J., Larson, R.E. and Erickson, E.E. (1980) A new thin-film composite seawater reverse osmosis membrane. Desalination 32, 25-31.
Cai, T., Li, X., Wan, C. and Chung, T.-S. (2016) Zwitterionic polymers grafted poly (ether sulfone) hollow fiber membranes and their antifouling behaviors for osmotic power generation. Journal of Membrane Science 497, 142-152.
Cath, T.Y., Adams, D. and Childress, A.E. (2005) Membrane contactor processes for wastewater reclamation in space. Journal of Membrane Science 257(1-2), 111-119.
Cath, T.Y., Childress, A.E. and Elimelech, M. (2006) Forward osmosis: Principles, applications, and recent developments. Journal of Membrane Science 281, 70-87.
Cath, T.Y., Elimelech, M., McCutcheon, J.R., McGinnis, R.L., Achilli, A., Anastasio, D., Brady, A.R., Childress, A.E., Farr, I.V., Hancock, N.T., Lampi, J., Nghiem, L.D., Xie, M. and Yip, N.Y. (2013) Standard Methodology for Evaluating Membrane Performance in Osmotically Driven Membrane Processes. Desalination 312, 31-38.
Chanukya, B.S., Patil, S. and Rastogi, N.K. (2013) Influence of concentration polarization on flux behavior in forward osmosis during desalination using ammonium bicarbonate. Desalination 312, 39-44.

Chekli, L., Phuntsho, S., Kim, J.E., Kim, J., Choi, J.Y., Choi, J.-S., Kim, S., Kim, J.H., Hong, S., Sohn, J. and Shon, H.K. (2016) A comprehensive review of hybrid forward osmosis systems: Performance, applications and future prospects. Journal of Membrane Science 497, 430-449.

Chekli, L., Phuntsho, S., Shon, H.K., Vigneswaran, S., Kandasamy, J. and Chanan, A. (2012) A review of draw solutes in forward osmosis process and their use in modern applications. Desalination and Water Treatment 43, 167-184.

Chen, G., Liu, R., Shon, H.K., Wang, Y., Song, J., Li, X.-M. and He, T. (2017) Open porous hydrophilic supported thin-film composite forward osmosis membrane via co-casting for treatment of high-salinity wastewater. Desalination 405, 76-84.

Chen, G., Wang, Z., Nghiem, L.D., Li, X.-M., Xie, M., Zhao, B., Zhang, M., Song, J. and He, T. (2015) Treatment of shale gas drilling flowback fluids (SGDFs) by forward osmosis: Membrane fouling and mitigation. Desalination.

Chen, Y., Setiawan, L., Chou, S., Hu, X. and Wang, R. (2016) Identification of safe and stable operation conditions for pressure retarded osmosis with high performance hollow fiber membrane. Journal of Membrane Science 503, 90-100.

Cheng, Z.L., Li, X., Liu, Y.D. and Chung, T.-S. (2016) Robust outer-selective thin-film composite polyethersulfone hollow fiber membranes with low reverse salt flux for renewable salinity-gradient energy generation. Journal of Membrane Science 506, 119-129.

Choi, H.G., Son, M., Yoon, S., Celik, E., Kang, S., Park, H., Park, C.H. and Choi, H. (2015) Alginate fouling reduction of functionalized carbon nanotube blended cellulose acetate membrane in forward osmosis. Chemosphere 136, 204-210.

Choi, W., Jeon, S., Kwon, S.J., Park, H., Park, Y.-I., Nam, S.-E., Lee, P.S., Lee, J.S., Choi, J., Hong, S., Chan, E.P. and Lee, J.-H. (2017) Thin film composite reverse osmosis membranes prepared via layered interfacial polymerization. Journal of Membrane Science 527, 121-128.

Chou, S., Shi, L., Wang, R., Tang, C.Y., Qiu, C. and Fane, A.G. (2010) Characteristics and potential applications of a novel forward osmosis hollow fiber membrane. Desalination 261(3), 365-372.

Chou, S., Wang, R. and Fane, A.G. (2013) Robust and High performance hollow fiber membranes for energy harvesting from salinity gradients by pressure retarded osmosis. Journal of Membrane Science 448, 44-54.

Chou, S., Wang, R., Shi, L., She, Q., Tang, C. and Fane, A.G. (2012a) Thin-film composite hollow fiber membranes for pressure retarded osmosis (PRO) process with high power density. Journal of Membrane Science 389(Supplement C), 25-33.

Chou, S., Wang, R., Shi, L., She, Q., Tang, C. and Fane, A.G. (2012b) Thin-film composite hollow fiber membranes for pressure retarded osmosis (PRO) process with high power density. Journal of Membrane Science 389, 25-33.

Chung, T.-S., Li, X., Ong, R.C., Ge, Q., Wang, H. and Han, G. (2012a) Emerging forward osmosis (FO) technologies and challenges ahead for clean water and clean energy applications. Current Opinion in Chemical Engineering 1(3), 246-257.
Chung, T.-S., Luo, L., Wan, C.F., Cui, Y. and Amy, G. (2015) What is next for forward osmosis (FO) and pressure retarded osmosis (PRO). Separation and Purification Technology 156, 856-860.
Chung, T.-S., Zhang, S., Wang, K.Y., Su, J. and Ling, M.M. (2012b) Forward osmosis processes: Yesterday, today and tomorrow. Desalination 287, 78-81.
Clausi, D.T. and Koros, W.J. (2000) Formation of defect-free polyimide hollow fiber membranes for gas separations. Journal of Membrane Science 167(1), 79-89.
Cui, Y., Liu, X.-Y. and Chung, T.-S. (2014) Enhanced osmotic energy generation from salinity gradients by modifying thin film composite membranes. Chemical Engineering Journal 242, 195-203.
Dimiev, A.M., J.M. Tour (2014) Mechanism of Graphene Oxide Formation. ACS NANO 8, 3060-3068.
Do, V.T., Tang, C.Y., Reinhard, M. and Leckie, J.O. (2012) Degradation of polyamide nanofiltration and reverse osmosis membranes by hypochlorite. Environ Sci Technol 46(2), 852-859.
Elimelech, M. and Phillip, W.A. (2011) The future of seawater desalination: Energy, technology, and the environment. Science 333(6043), 712.
Emadzadeh, D., Lau, W.J., Matsuura, T., Ismail, A.F. and Rahbari-Sisakht, M. (2014a) Synthesis and characterization of thin film nanocomposite forward osmosis membrane with hydrophilic nanocomposite support to reduce internal concentration polarization. Journal of Membrane Science 449, 74-85.
Emadzadeh, D., Lau, W.J., Matsuura, T., Rahbari-Sisakht, M. and Ismail, A.F. (2014b) A novel thin film composite forward osmosis membrane prepared from PSf-TiO2 nanocomposite substrate for water desalination. Chemical Engineering Journal 237, 70-80.
Emadzadeh, D., Lau, W.J., Matsuura, T., Rahbari-Sisakht, M. and Ismail, A.F. (2014c) A novel thin film composite forward osmosis membrane prepared from PSf–TiO2 nanocomposite substrate for water desalination. Chemical Engineering Journal 237, 70-80.
Fang, W., Wang, R., Chou, S., Setiawan, L. and Fane, A.G. (2012) Composite forward osmosis hollow fiber membranes: Integration of RO-and NF-like selective layers to enhance membrane properties of anti-scaling and anti-internal concentration polarization. Journal of Membrane Science 394, 140-150.

Fu, F.-J., Sun, S.-P., Zhang, S. and Chung, T.-S. (2014) Pressure retarded osmosis dual-layer hollow fiber membranes developed by co-casting method and ammonium persulfate (APS) treatment. Journal of Membrane Science 469, 488-498.
Fu, F.-J., Zhang, S., Sun, S.-P., Wang, K.-Y. and Chung, T.-S. (2013) POSS-containing delamination-free dual-layer hollow fiber membranes for forward osmosis and osmotic power generation. Journal of Membrane Science 443, 144-155.
Gai, W., Li, X., Xiong, J.Y., Wan, C.F. and Chung, T.-S. (2016) Evolution of micro-deformation in inner-selective thin film composite hollow fiber membranes and its implications for osmotic power generation. Journal of Membrane Science 516, 104-112.
Garcia-Castello, E.M. and McCutcheon, J.R. (2011) Dewatering press liquor derived from orange production by forward osmosis. Journal of Membrane Science 372(1-2), 97-101.
Geise, G.M., Lee, H.-S., Miller, D.J., Freeman, B.D., McGrath, J.E. and Paul, D.R. (2010a) Water purification by membranes: The role of polymer science. Journal of Polymer Science Part B: Polymer Physics 48, 1685-1718.
Geise, G.M., Lee, H.S., Miller, D.J., Freeman, B.D., McGrath, J.E. and Paul, D.R. (2010b) Water purification by membranes: the role of polymer science. Journal of Polymer Science Part B: Polymer Physics 48(15), 1685-1718.
Gerstandt, K., Peinemann, K.V., Skilhagen, S.E., Thorsen, T. and Holt, T. (2008) Membrane processes in energy supply for an osmotic power plant. Desalination 224(1), 64-70.
Ghanbari, M., Emadzadeh, D., Lau, W.J., Riazi, H., Almasi, D. and Ismail, A.F. (2016) Minimizing structural parameter of thin film composite forward osmosis membranes using polysulfone/halloysite nanotubes as membrane substrates. Desalination 377, 152-162.
Ghosh, A.K. and Hoek, E.M.V. (2009) Impacts of support membrane structure and chemistry on polyamide-polysulfone interfacial composite membranes. Journal of Membrane Science 336, 140-148.
Goertzen, S.L., Thériault, K.D., Oickle, A.M., Tarasuk, A.C. and Andreas, H.A. (2010) Standardization of the Boehm titration. Part I. CO2 expulsion and endpoint determination. Carbon 48(4), 1252-1261.
Goh, K., Setiawan, L., Wei, L., Jiang, W., Wang, R. and Chen, Y. (2013) Fabrication of novel functionalized multi-walled carbon nanotube immobilized hollow fiber membranes for enhanced performance in forward osmosis process. Journal of Membrane Science 446, 244-254.
Gray, G.T., McCutcheon, J.R. and Elimelech, M. (2006) Internal concentration polarization in forward osmosis: Role of membrane orientation. Desalination 197, 1-8.
Greenlee, L.F., Lawler, D.F., Freeman, B.D., Marrot, B. and Moulin, P. (2009) Reverse osmosis desalination: water sources, technology, and today's challenges. Water Res 43(9), 2317-2348.

Guo, H.-L., Wang, X.-F., Qian, Q.-Y., Wang, F.-B. and Xia, X.-H. (2009) A green approach to the synthesis of graphene nanosheets. ACS NANO 3, 2653-2659.
Guo, Z., Tang, G., Zhou, Y., Shuwu, L., Hou, H., Chen, Z., Chen, J., Hu, C., Wang, F., De Smedt, S.C., Xiong, R. and Huang, C. (2017) Fabrication of Sustained-release CA-PU Coaxial Electrospun Fiber Membranes for Plant Grafting Application. Carbohydr Polym 169, 198-205.
Han, G., Cheng, Z.L. and Chung, T.-S. (2017) Thin-film composite (TFC) hollow fiber membrane with double-polyamide active layers for internal concentration polarization and fouling mitigation in osmotic processes. Journal of Membrane Science 523, 497-504.
Han, G. and Chung, T.-S. (2014) Robust and high performance pressure retarded osmosis hollow fiber membranes for osmotic power generation. AIChE Journal 60(3), 1107-1119.
Han, G., Chung, T.-S., Toriida, M. and Tamai, S. (2012a) Thin-film composite forward osmosis membranes with novel hydrophilic supports for desalination. Journal of Membrane Science 423-424, 543-555.
Han, G., Chung, T.-S., Toriida, M. and Tamai, S. (2012b) Thin-film composite forward osmosis membranes with novel hydropholic suppports for desalination. Journal of Membrane Science 423-424, 543-555.
Han, G., Wang, P. and Chung, T.-S. (2013a) Highly robust thin-film composite pressure retarded osmosis (PRO) hollow fiber membranes with high power densities for renewable salinity-gradient energy generation. Environ Sci Technol 47(14), 8070-8077.
Han, G., Wang, P. and Chung, T.S. (2013b) Highly robust thin-film composite pressure retarded osmosis (PRO) hollow fiber membranes with high power densities for renewable salinity-gradient energy generation. Environ Sci Technol 47(14), 8070-8077.
Han, G., Zhang, S., Li, X. and Chung, T.-S. (2013c) High performance thin film composite pressure retarded osmosis (PRO) membranes for renewable salinity-gradient energy generation. Journal of Membrane Science 440, 108-121.
Han, G., Zhang, S., Li, X. and Chung, T.-S. (2015) Progress in pressure retarded osmosis (PRO) membranes for osmotic power generation. Progress in Polymer Science 51, 1-27.
Han, G., Zhang, S., Li, X., Widjojo, N. and Chung, T.-S. (2012c) Thin film composite forward osmosis membranes based on polydopamine modified polysulfone substrates with enhancements in both water flux and salt rejection. Chemical Engineering Science 80, 219-231.
Han, G., Zhao, B., Fu, F., Chung, T.-S., Weber, M., Staudt, C. and Maletzko, C. (2016) High performance thin-film composite membranes with mesh-reinforced hydrophilic sulfonated polyphenylenesulfone (sPPSU) substrates for osmotically driven processes. Journal of Membrane Science 502, 84-93.
Hancock, N.T. and Cath, T.Y. (2009) Solute coupled diffusion in osmotically driven membrane processes. Environ Sci Technol 43(17), 6769-6775.

Hancock, N.T., Phillip, W.A., Elimelech, M. and Cath, T.Y. (2011) Bidirectional permeation of electrolytes in osmotically driven membrane processes. Environ Sci Technol 45(24), 10642-10651.
Hoek, E.M.V. and Elimelech, M. (2003) Cake-enhanced concentration polarization: A new fouling mechanism for salt-rejecting membranes. Environ Sci Technol 37(24), 5581-5588.
Holloway, R.W., Childress, A.E., Dennett, K.E. and Cath, T.Y. (2007a) Forward osmosis for concentration of anaerobic digester centrate. Water Res 41(17), 4005-4014.
Holloway, R.W., Childress, A.E., Dennett, K.E. and Cath, T.Y. (2007b) Forward osmosis for concentration of anaerobic digester centrate. Water Research 41(17), 4005-4014.
Hoover, L.A., Schiffman, J.D. and Elimelech, M. (2013) Nanofibers in thin-film composite membrane support layers: Enabling expanded application of forward and pressure retarded osmosis. Desalination 308, 73-81.
Hu, M. and Mi, B. (2013) Enabling graphene oxide nanosheets as water separation membranes. Environ Sci Technol 47(8), 3715-3723.
Huang, L., Arena, J.T. and McCutcheon, J.R. (2016) Surface modified PVDF nanofiber supported thin film composite membranes for forward osmosis. Journal of Membrane Science 499, 352-360.
Huang, L., Bui, N.-N., Meyering, M.T., Hamlin, T.J. and McCutcheon, J.R. (2013) Novel hydrophilic nylon 6,6 microfiltration membrane supported thin film composite membranes for engineered osmosis. Journal of Membrane Science 437, 141-149.
Huang, L. and McCutcheon, J.R. (2014) Hydrophilic nylon 6,6 nanofibers supported thin film composite membranes for engineered osmosis. Journal of Membrane Science 457, 162-169.
Huang, L. and McCutcheon, J.R. (2015) Impact of support layer pore size on performance of thin film composite membranes for forward osmosis. Journal of Membrane Science 483, 25-33.
Hudaib, B., Gomes, V., Shi, J., Zhou, C. and Liu, Z. (2018) Poly (vinylidene fluoride)/polyaniline/MWCNT nanocomposite ultrafiltration membrane for natural organic matter removal. Separation and Purification Technology 190, 143-155.
Hummers, W.S., R.E. Offeman (1958) Preparation of Graphitic Oxide. National Lead Company.
Ingole, P.G., Choi, W., Kim, K.H., Park, C.H., Choi, W.K. and Lee, H.K. (2014) Synthesis, characterization and surface modification of PES hollow fiber membrane support with polydopamine and thin film composite for energy generation. Chemical Engineering Journal 243, 137-146.
Jang, W.G., Jeon, K.S. and Byun, H.S. (2013) The preparation of porous polyamide-imide nanofiber membrane by using electrospinning for MF application. Desalination and Water Treatment 51(25-27), 5283-5288.

Jin, L., Wang, Z., Zheng, S. and Mi, B. (2017) Polyamide-crosslinked Graphene Oxide Membrane for Forward Osmosis. Journal of Membrane Science.
Jin, X., Tang, C.Y., Gu, Y., She, Q. and Qi, S. (2011) Boric acid permeation in forward osmosis membrane processes: modeling, experiments, and implications. Environ Sci Technol 45(6), 2323-2330.
Johnson, P.M., Yoon, J., Kelly, J.Y., Howarter, J.A. and Stafford, C.M. (2012) Molecular layer-by-layer deposition of highly crosslinked polyamide films. Journal of Polymer Science Part B: Polymer Physics 50(3), 168-173.
Kao, T.-H., Cheng, C.-C., Huang, C.-F. and Chen, J.-K. (2015) Using coaxial electrospinning to fabricate core/shell-structured polyacrylonitrile–polybenzoxazine fibers as nonfouling membranes. RSC Adv. 5(72), 58760-58771.
Kaur, S., Rana, D., Matsuura, T., Sundarrajan, S. and Ramakrishna, S. (2012) Preparation and characterization of surface modified electrospun membranes for higher filtration flux. Journal of Membrane Science 390-391, 235-242.
Kim, J., Jeong, K., Park, M., Shon, H. and Kim, J. (2015) Recent Advances in Osmotic Energy Generation via Pressure-Retarded Osmosis (PRO): A Review. Energies 8(10), 11821-11845.
Kim, J., Park, M.J., Park, M., Shon, H.K., Kim, S.-H. and Kim, J.H. (2016) Influence of colloidal fouling on pressure retarded osmosis. Desalination 389, 207-214.
Kim, J.E., Phuntsho, S. and Shon, H.K. (2013a) Pilot-scale nanofiltration system as post-treatment for fertilizer-drawn forward osmosis desalination for direct fertigation. Desalination and Water Treatment 51(31-33), 6265-6273.
Kim, T.-W., Kim, Y., Yun, C., Jang, H., Kim, W. and Park, S. (2012) Systematic approach for draw solute selection and optimal system design for forward osmosis desalination. Desalination 284, 253-260.
Kim, Y.C. and Elimelech, M. (2013b) Potential of osmotic power generation by pressure retarded osmosis using seawater as feed solution: Analysis and experiments. Journal of Membrane Science 429, 330-337.
Klaysom, C., Cath, T.Y., Depuydt, T. and Vankelecom, I.F. (2013a) Forward and pressure retarded osmosis: potential solutions for global challenges in energy and water supply. Chem Soc Rev 42(16), 6959-6989.
Klaysom, C., Cath, T.Y., Depuydt, T. and Vankelecom, I.F.J. (2013b) Forward and pressure retarded osmosis: potential solutions for global challenges in energy and water supply. Chem Soc Rev 42(16), 6959-6989.
Klaysom, C., Hermans, S., Gahlaut, A., Van Craenenbroeck, S. and Vankelecom, I.F.J. (2013c) Polyamide/Polyacrylonitrile (PA/PAN) thin film composite osmosis membranes: Film

optimization, characterization and performance evaluation. Journal of Membrane Science 445, 25-33.
Kong, C., Kanezashi, M., Yamomoto, T., Shintani, T. and Tsuru, T. (2010) Controlled synthesis of high performance polyamide membrane with thin dense layer for water desalination. Journal of Membrane Science 362(1), 76-80.
Kong, F.-x., Yang, H.-w., Wang, X.-m. and Xie, Y.F. (2014) Rejection of nine haloacetic acids and coupled reverse draw solute permeation in forward osmosis. Desalination 341, 1-9.
kuang, W., Liu, Z., Yu, H., Kang, G., Jie, X., Jin, Y. and Cao, Y. (2016) Investigation of internal concentration polarization reduction in forward osmosis membrane using nano-CaCO 3 particles as sacrificial component. Journal of Membrane Science 497, 485-493.
Lau, W.J., Gray, S., Matsuura, T., Emadzadeh, D., Paul Chen, J. and Ismail, A.F. (2015) A review on polyamide thin film nanocomposite (TFN) membranes: History, applications, challenges and approaches. Water Res 80, 306-324.
Lay, W.C.L., Zhang, J., Tang, C., Wang, R., Liu, Y. and Fane, A.G. (2012) Factors affecting flux performance of forward osmosis systems. Journal of Membrane Science 394-395, 151-168.
Le, N.L., Bettahalli, N., Nunes, S.P. and Chung, T.-S. (2016) Outer-selective thin film composite (TFC) hollow fiber membranes for osmotic power generation. Journal of Membrane Science 505, 157-166.
Lee, E.-J., An, A.K., Hadi, P., Lee, S., Woo, Y.C. and Shon, H.K. (2017) Advanced multi-nozzle electrospun functionalized titanium dioxide/polyvinylidene fluoride-co-hexafluoropropylene (TiO 2 /PVDF-HFP) composite membranes for direct contact membrane distillation. Journal of Membrane Science 524, 712-720.
Lee, J.-Y., She, Q., Huo, F. and Tang, C.Y. (2015a) Metal-organic framework-based porous matrix membranes for improving mass transfer in forward osmosis membranes. Journal of Membrane Science 492, 392-399.
Lee, J.-Y., She, Q., Huo, F. and Tang, C.Y. (2015b) Metal–organic framework-based porous matrix membranes for improving mass transfer in forward osmosis membranes. Journal of Membrane Science 492, 392-399.
Lee, J., Chae, H.-R., Won, Y.J., Lee, K., Lee, C.-H., Lee, H.H., Kim, I.-C. and Lee, J.-m. (2013) Graphene oxide nanoplatelets composite membrane with hydrophilic and antifouling properties for wastewater treatment. Journal of Membrane Science 448, 223-230.
Lee, K.L., Baker, R.W. and Lonsdale, H.K. (1981) Membranes for power generation by pressure-retarded osmosis. Journal of Membrane Science 8(2), 141-171.
Lee, S., Boo, C., Elimelech, M. and Hong, S. (2010) Comparison of fouling behavior in forward osmosis (FO) and reverse osmosis (RO). Journal of Membrane Science 365(1-2), 34-39.

Li, G., Li, X.-M., He, T., Jiang, B. and Gao, C. (2013a) Cellulose triacetate forward osmosis membranes: Preparation and characterization. Desalination and Water Treatment 51, 2656-2665.
Li, X., Chou, S., Wang, R., Shi, L., Fang, W., Chaitra, G., Tang, C.Y., Torres, J., Hu, X. and Fane, A.G. (2015a) Nature gives the best solution for desalination: Aquaporin-based hollow fiber composite membrane with superior performance. Journal of Membrane Science 494, 68-77.
Li, X. and Chung, T.-S. (2013b) Effects of free volume in thin-film composite membranes on osmotic power generation. AIChE Journal 59(12), 4749-4761.
Li, X. and Chung, T.-S. (2014) Thin-film composite P84 co-polyimide hollow fiber membranes for osmotic power generation. Applied Energy 114, 600-610.
Li, X., Wang, K.Y., Helmer, B. and Chung, T.-S. (2012a) Thin-film composite membranes and formation mechanism of thin-film layers on hydrophilic cellulose acetate propionate substrates for forward osmosis processes. Industrial & Engineering Chemistry Research 51, 10039-10050.
Li, X., Wang, K.Y., Helmer, B. and Chung, T.-S. (2012b) Thin-Film Composite Membranes and Formation Mechanism of Thin-Film Layers on Hydrophilic Cellulose Acetate Propionate Substrates for Forward Osmosis Processes. Industrial & Engineering Chemistry Research 51(30), 10039-10050.
Li, X., Zhang, S., Fu, F. and Chung, T.-S. (2013c) Deformation and reinforcement of thin-film composite (TFC) polyamide-imide (PAI) membranes for osmotic power generation. Journal of Membrane Science 434, 204-217.
Li, Y., Wang, R., Qi, S. and Tang, C.Y. (2015b) Structural stability and mass transfer properties of pressure retarded osmosis (PRO) membrane under high operating pressures. Journal of Membrane Science 488, 142-153.
Liang, H.-Q., Hung, W.-S., Yu, H.-H., Hu, C.-C., Lee, K.-R., Lai, J.-Y. and Xu, Z.-K. (2017) Forward osmosis membranes with unprecedented water flux. Journal of Membrane Science 529, 47-54.
Lim, S., Park, M.J., Phuntsho, S., Tijing, L.D., Nisola, G.M., Shim, W.-G., Chung, W.-J. and Shon, H.K. (2017) Dual-layered nanocomposite substrate membrane based on polysulfone/graphene oxide for mitigating internal concentration polarization in forward osmosis. Polymer 110, 36-48.
Liu, C., Li, X., Liu, T., Liu, Z., Li, N., Zhang, Y., Xiao, C. and Feng, X. (2016a) Microporous CA/PVDF membranes based on electrospun nanofibers with controlled crosslinking induced by solvent vapor. Journal of Membrane Science 512, 1-12.

Liu, Q., Li, J., Zhou, Z., Xie, J. and Lee, J.Y. (2016b) Hydrophilic Mineral Coating of Membrane Substrate for Reducing Internal Concentration Polarization (ICP) in Forward Osmosis. Sci Rep 6, 19593.
Liu, X. and Ng, H.Y. (2014a) Double-blade casting technique for optimizing substrate membrane in thin-film composite forward osmosis membrane fabrication. Journal of Membrane Science 469, 12-126.
Liu, X. and Ng, H.Y. (2014b) Double-blade casting technique for optimizing substrate membrane in thin-film composite forward osmosis membrane fabrication. Journal of Membrane Science 469, 112-126.
Liu, X. and Ng, H.Y. (2015a) Fabrication of layered silica-polysulfone mixed matrix substrate membrane for enhancing performance of thin-film composite forward osmosis membrane. Journal of Membrane Science 481, 148-163.
Liu, X. and Ng, H.Y. (2015b) Fabrication of layered silica–polysulfone mixed matrix substrate membrane for enhancing performance of thin-film composite forward osmosis membrane. Journal of Membrane Science 481, 148-163.
Lu, P., Liang, S., Qiu, L., Gao, Y. and Wang, Q. (2016a) Thin film nanocomposite forward osmosis membranes based on layered double hydroxide nanoparticles blended substrates. Journal of Membrane Science 504, 196-205.
Lu, P., Liang, S., Zhou, T., Mei, X., Zhang, Y., Zhang, C., Umar, A. and Wang, Q. (2016b) Layered double hydroxide/graphene oxide hybrid incorporated polysulfone substrate for thin-film nanocomposite forward osmosis membranes. RSC Advances 6(61), 56599-56609.
Luo, L., Wang, P., Zhang, S., Han, G. and Chung, T.-S. (2014) Novel thin-film composite tri-bore hollow fiber membrane fabrication for forward osmosis. Journal of Membrane Science 461, 28-38.
Ma, D., Han, G., Peh, S.B. and Chen, S.B. (2017) Water-Stable Metal–Organic Framework UiO-66 for Performance Enhancement of Forward Osmosis Membranes. Industrial & Engineering Chemistry Research 56(44), 12773-12782.
Ma, N., Wei, J., Liao, R. and Tang, C.Y. (2012) Zeolite-polyamide thin film nanocomposite membranes: Towards enhanced performance for forward osmosis. Journal of Membrane Science 405-406, 149-157.
Ma, N., Wei, J., Qi, S., Zhao, Y., Gao, Y. and Tang, C.Y. (2013) Nanocomposite substrates for controlling internal concentration polarization in forward osmosis membranes. Journal of Membrane Science 441, 54-62.
Makaremi, M., De Silva, R.T. and Pasbakhsh, P. (2015) Electrospun Nanofibrous Membranes of Polyacrylonitrile/Halloysite with Superior Water Filtration Ability. The Journal of Physical Chemistry C 119(14), 7949-7958.

Marcano, D.C., Kosynkin, D.V., Berlin, J.M., Sinitskii, A., Sun, Z., Slesarev, A., Alemany, L.B., Lu, W. and Tour, J.M. (2010) Improved Synthesis of Graphene Oxide. ACS NANO 4, 4806-4814.
McCutcheon, J.R. and Elimelech, M. (2006) Influence of concentrative and dilutive internal concentration polarization on flux behavior in forward osmosis. Journal of Membrane Science 284, 237-247.
McCutcheon, J.R. and Elimelech, M. (2008) Influence of membrane support layer hydrophobicity on water flux in osmotically driven membrane processes. Journal of Membrane Science 318(1), 458-466.
Mehta, G.D. and Loeb, S. (1978) Internal polarization in the porous substructure of a semipermeable membrane under pressure-retarded osmosis. Journal of Membrane Science 4, 261-265.
Mi, B. (2014) Graphene Oxide Membranes for Ionic and Molecular Sieving. Science 343(6172), 740-742.
Mi, B. and Elimelech, M. (2010) Gypsum scaling and cleaning in forward osmosis: Measurements and mechanisms. Environ Sci Technol 44(6), 2022-2028.
Moradi, R., Karimi-Sabet, J., Shariaty-Niassar, M. and Koochaki, M. (2015) Preparation and Characterization of Polyvinylidene Fluoride/Graphene Superhydrophobic Fibrous Films. Polymers 7(8), 1444-1463.
Morales-Torres, S., Esteves, C.M.P., Figueiredo, J.L. and Silva, A.M.T. (2016) Thin-film composite forward osmosis membranes based on polysulfone supports blended with nanostructured carbon materials. Journal of Membrane Science 520, 326-336.
Mu, C., Su, Y., Sun, M., Chen, W. and Jiang, Z. (2010) Remarkable improvement of the performance of poly(vinylidene fluoride) microfiltration membranes by the additive of cellulose acetate. Journal of Membrane Science 350(1-2), 293-300.
Nguyen, A., Zou, L. and Priest, C. (2014) Evaluating the antifouling effects of silver nanoparticles regenerated by TiO2 on forward osmosis membrane. Journal of Membrane Science 454, 264-271.
Nguyen, T.P.N., Yun, E.-T., Kim, I.-C. and Kwon, Y.-N. (2013) Preparation of cellulose triacetate/cellulose acetate (CTA/CA)-based membranes for forward osmosis. Journal of Membrane Science 433, 49-59.
Nicolaisen, B. (2003) Developments in membrane technology for water treatment. Desalination 153(1), 355-360.
Nisola, G.M., Limjuco, L.A., Vivas, E.L., Lawagon, C.P., Park, M.J., Shon, H.K., Mittal, N., Nah, I.W., Kim, H. and Chung, W.-J. (2015) Macroporous flexible polyvinyl alcohol lithium

adsorbent foam composite prepared via surfactant blending and cryo-desiccation. Chemical Engineering Journal 280, 536-548.
Obaid, M., Ghouri, Z.K., Fadali, O.A., Khalil, K.A., Almajid, A.A. and Barakat, N.A. (2016a) Amorphous SiO2 NP-Incorporated Poly(vinylidene fluoride) Electrospun Nanofiber Membrane for High Flux Forward Osmosis Desalination. ACS Appl Mater Interfaces 8(7), 4561-4574.
Obaid, M., Ghouri, Z.K., Fadali, O.A., Khalil, K.A., Almajid, A.A. and Barakat, N.A.M. (2015a) Amorphous SiO2 NP-incorporated poly(vinylidene fluoride) electron spun nanofiber membrane for high flux forward osmosis desalination. ACS Appl Mater Interfaces 8, 4561-4574.
Obaid, M., Mohamed, H.O., Yasin, A.S., Fadali, O.A., Khalil, K.A., Kim, T. and Barakat, N.A.M. (2016b) A novel strategy for enhancing the electrospun PVDF support layer of thin-film composite forward osmosis membranes. RSC Adv. 6(104), 102762-102772.
Obaid, M., Tolba, G.M.K., Motlak, M., Fadali, O.A., Khalil, K.A., Almajid, A.A., Kim, B. and Barakat, N.A.M. (2015b) Effective polysulfone-amorphous SiO2 NPs electrospun nanofiber membrane for high flux oil/water separation. Chemical Engineering Journal 279, 631-638.
Oh, Y., Lee, S., Elimelech, M., Lee, S. and Hong, S. (2014) Effect of hydraulic pressure and membrane orientation on water flux and reverse solute flux in pressure assisted osmosis. Journal of Membrane Science 465, 159-166.
Oickle, A.M., Goertzen, S.L., Hopper, K.R., Abdalla, Y.O. and Andreas, H.A. (2010) Standardization of the Boehm titration: Part II. Method of agitation, effect of filtering and dilute titrant. Carbon 48(12), 3313-3322.
Ong, R.C. and Chung, T.-S. (2012) Fabrication and positron annihilation spectroscopy (PAS) characterization of cellulose triacetate membranes for forward osmosis. Journal of Membrane Science 394-395, 230-240.
Ong, R.C., Chung, T.-S., de Wit, J.S. and Helmer, B.J. (2015) Novel cellulose ester substrates for high performance flat-sheet thin-film composite (TFC) forward osmosis (FO) membranes. Journal of Membrane Science 473, 63-71.
Oren, Y. (2008) Capacitive deionization (CDI) for desalination and water treatment — past, present and future (a review). Desalination 228(1), 10-29.
Pan, S.-F., Dong, Y., Zheng, Y.-M., Zhong, L.-B. and Yuan, Z.-H. (2017) Self-sustained hydrophilic nanofiber thin film composite forward osmosis membranes: Preparation, characterization and application for simulated antibiotic wastewater treatment. Journal of Membrane Science 523, 205-215.
Pan, Y., Wang, W., Peng, C., Shi, K., Luo, Y. and Ji, X. (2014) Novel hydrophobic polyvinyl alcohol–formaldehyde foams for organic solvents absorption and effective separation. RSC Adv. 4(2), 660-669.

Park, M.J., Nisola, G.M., Vivas, E.L., Limjuco, L.A., Lawagon, C.P., Seo, J.G., Kim, H., Shon, H.K. and Chung, W.-J. (2016) Mixed matrix nanofiber as a flow-through membrane adsorber for continuous Li + recovery from seawater. Journal of Membrane Science 510, 141-154.
Peng, N., Widjojo, N., Sukitpaneenit, P., Teoh, M.M., Lipscomb, G.G., Chung, T.-S. and Lai, J.-Y. (2012) Evolution of polymeric hollow fibers as sustainable technologies: Past, present, and future. Progress in Polymer Science 37(10), 1401-1424.
Perreault, F., Tousley, M.E. and Elimelech, M. (2014) Thin-Film Composite Polyamide Membranes Functionalized with Biocidal Graphene Oxide Nanosheets. Environmental Science & Technology Letters 1(1), 71-76.
Phillip, W.A., J.S. Yong, M. Elimelech (2010) Reverse draw solute permeation in FO: Modeling and experiments. Environ Sci Technol 44, 5170-5176.
Phillip, W.A., Yong, J.S. and Elimelech, M. (2010) Reverse draw solute permeation in forward osmosis: Modeling and experiments. Environ Sci Technol 44, 5170-5176.
Phuntsho, S., Kim, J.E., Johir, M.A.H., Hong, S., Li, Z., Ghaffour, N., Leiknes, T. and Shon, H.K. (2016) Fertiliser drawn forward osmosis process: Pilot-scale desalination of mine impaired water for fertigation. Journal of Membrane Science 508, 22-31.
Puguan, J.M.C., Kim, H.-S., Lee, K.-J. and Kim, H. (2014) Low internal concentration polarization in forward osmosis membranes with hydrophilic crosslinked PVA nanofibers as porous support layer. Desalination 336, 24-31.
Qin, D., Liu, Z., Bai, H. and Sun, D.D. (2017) Three-dimensional architecture constructed from a graphene oxide nanosheet–polymer composite for high-flux forward osmosis membranes. Journal of Materials Chemistry A 5(24), 12183-12192.
Qin, D., Liu, Z., Delai Sun, D., Song, X. and Bai, H. (2015) A new nanocomposite forward osmosis membrane custom-designed for treating shale gas wastewater. Sci Rep 5, 14530.
Qiu, S., Wu, L., Pan, X., Zhang, L., Chen, H. and Gao, C. (2009) Preparation and properties of functionalized carbon nanotube/PSF blend ultrafiltration membranes. Journal of Membrane Science 342(1-2), 165-172.
Ramakrishna, S., Fujihara, K., Teo, W.-E., Lim, T.-C. and Ma, Z. (2005) An Introduction to Electrospinning and Nanofibers, World Scientific Publishing Co., New Jersey.
Rana, D. and Matsuura, T. (2010) Surface modifications for antifouling membranes. Chemical Reviews 110(4), 2448-2471.
Ren, J., Chowdhury, M.R., Qi, J., Xia, L., Huey, B.D. and McCutcheon, J.R. (2017) Relating osmotic performance of thin film composite hollow fiber membranes to support layer surface pore size. Journal of Membrane Science 540, 344-353.

Ren, J., O'Grady, B., de Jesus, G. and McCutcheon, J.R. (2016) Sulfonated polysulfone supported high performance thin film composite membranes for forward osmosis. Polymer 103, 486-497.
Sahebi, S. (2015) Developing thin film composite membranes for engineered osmosis processes, University of Technology Sydney, New South Wales, Australia.
Sahebi, S., Phuntsho, S., Tijing, L., Han, G., Han, D.S., Abdel-Wahab, A. and Shon, H.K. (2017) Thin-film composite membrane on a compacted woven backing fabric for pressure assisted osmosis. Desalination 406, 98-108.
Sahebi, S., Phuntsho, S., Woo, Y.C., Park, M.J., Tijing, L.D., Hong, S. and Shon, H.K. (2016) Effect of sulphonated polyethersulfone substrate for thin film composite forward osmosis membrane. Desalination 389, 129-136.
Sairam, M., Sereewatthanawut, E., Li, K., Bismarck, A. and Livingston, A.G. (2011) Method for the preparation of cellulose acetate flat sheet composite membranes for forward osmosis - Desalination using MgSO4 draw solution. Desalination 273, 299-307.
Setiawan, L., Wang, R., Li, K. and Fane, A.G. (2011) Fabrication of novel poly (amide–imide) forward osmosis hollow fiber membranes with a positively charged nanofiltration-like selective layer. Journal of Membrane Science 369(1), 196-205.
Setiawan, L., Wang, R., Li, K. and Fane, A.G. (2012) Fabrication and characterization of forward osmosis hollow fiber membranes with antifouling NF-like selective layer. Journal of Membrane Science 394-395, 80-88.
Shannon, M.A., Bohn, P.W., Elimelech, M., Georgiadis, J.G., Marinas, B.J. and Mayes, A.M. (2008a) Science and technology for water purification in the coming decades. Nature 452(7185), 301-310.
Shannon, M.A., Bohn, P.W., Elimelech, M., Georgiadis, J.G., Marinas, B.J. and Mayes, A.M. (2008b) Science and technology for water purification in the coming decades. Nature 452(7185), 301-310.
She, Q., Jin, X. and Tang, C.Y. (2012) Osmotic power production from salinity gradient resource by pressure retarded osmosis: Effects of operating conditions and reverse solute diffusion. Journal of Membrane Science 401-402, 262-273.
She, Q., Wei, J., Ma, N., Sim, V., Fane, A.G., Wang, R. and Tang, C.Y. (2016) Fabrication and characterization of fabric-reinforced pressure retarded osmosis membranes for osmotic power harvesting. Journal of Membrane Science 504, 75-88.
Shen, Y.-x., Saboe, P.O., Sines, I.T., Erbakan, M. and Kumar, M. (2014) Biomimetic membranes: A review. Journal of Membrane Science 454, 359-381.

Shi, L., Chou, S.R., Wang, R., Fang, W.X., Tang, C.Y. and Fane, A.G. (2011) Effect of substrate structure on the performance of thin-film composite forward osmosis hollow fiber membranes. Journal of Membrane Science 382(1), 116-123.
Shibuya, M., Yasukawa, M., Mishima, S., Tanaka, Y., Takahashi, T. and Matsuyama, H. (2017) A thin-film composite-hollow fiber forward osmosis membrane with a polyketone hollow fiber membrane as a support. Desalination 402, 33-41.
Shibuya, M., Yasukawa, M., Takahashi, T., Miyoshi, T., Higa, M. and Matsuyama, H. (2015) Effect of operating conditions on osmotic-driven membrane performances of cellulose triacetate forward osmosis hollow fiber membrane. Desalination 362, 34-42.
Shokrgozar Eslah, S., Shokrollahzadeh, S., Moini Jazani, O. and Samimi, A. (2017) Forward osmosis water desalination: Fabrication of graphene oxide-polyamide/polysulfone thin-film nanocomposite membrane with high water flux and low reverse salt diffusion. Separation Science and Technology 53(3), 573-583.
Shukla, A.K., Alam, J., Alhoshan, M., Dass, L.A. and Muthumareeswaran, M.R. (2017) Development of a nanocomposite ultrafiltration membrane based on polyphenylsulfone blended with graphene oxide. Sci Rep 7, 41976.
Skilhagen, S.E., Dugstad, J.E. and Aaberg, R.J. (2008) Osmotic power — power production based on the osmotic pressure difference between waters with varying salt gradients. Desalination 220(1-3), 476-482.
Song, X., Liu, Z. and Sun, D.D. (2011a) Nano gives the answer: breaking the bottleneck of internal concentration polarization with a nanofiber composite forward osmosis membrane for a high water production rate. Adv Mater 23(29), 3256-3260.
Song, X., Liu, Z. and Sun, D.D. (2011b) Nano gives the answer: Breaking the bottleneck of internal concentration polarization with a nanofiber composite forward osmosis membrane for a higher wate production rate. Adv Mater 23, 3256-3260.
Song, X., Liu, Z. and Sun, D.D. (2013) Energy recovery from concentrated seawater brine by thin-film nanofiber composite pressure retarded osmosis membranes with high power density. Energy & Environmental Science 6(4), 1199.
Song, X., Wang, L., Tang, C.Y., Wang, Z. and Gao, C. (2015) Fabrication of carbon nanotubes incorporated double-skinned thin film nanocomposite membranes for enhanced separation performance and antifouling capability in forward osmosis process. Desalination 369, 1-9.
Stankovich, S., Dikin, D.A., Dommett, G.H., Kohlhaas, K.M., Zimney, E.J., Stach, E.A., Piner, R.D., Nguyen, S.T. and Ruoff, R.S. (2006) Graphene-based composite materials. Nature 442(7100), 282-286.
Strathmann, H. (2001) Membrane separation processes: Current relevance and future opportunities. AIChE Journal 47(5), 1077-1087.

Su, J., Chung, T.-S., Helmer, B.J. and de Wit, J.S. (2012) Enhanced double-skinned FO membranes with inner dense layer for wastewater treatment and macromolecule recycle using sucrose as draw solute. Journal of Membrane Science 396, 92-100.
Su, J., Yang, Q., Teo, J.F. and Chung, T.-S. (2010) Cellulose acetate nanofiltration hollow fiber membranes for forward osmosis processes. Journal of Membrane Science 355(1-2), 36-44.
Sukitpaneenit, P. and Chung, T.-S. (2012a) High performance thin-film composite forward osmosis hollow fiber membranes with macrovoid-free and highly porous structure for sustainable water production. Environ Sci Technol 46(13), 7358-7365.
Sukitpaneenit, P. and Chung, T.S. (2012b) High performance thin-film composite forward osmosis hollow fiber membranes with macrovoid-free and highly porous structure for sustainable water production. Environ Sci Technol 46(13), 7358-7365.
Sun, S.P. and Chung, T.S. (2013) Outer-selective pressure-retarded osmosis hollow fiber membranes from vacuum-assisted interfacial polymerization for osmotic power generation. Environ Sci Technol 47(22), 13167-13174.
Sun, Y., Xue, L., Zhang, Y., Zhao, X., Huang, Y. and Du, X. (2014) High flux polyamide thin film composite forward osmosis membranes prepared from porous substrates made of polysulfone and polyethersulfone blends. Desalination 336, 72-79.
Tan, C.H. and Ng, H.Y. (2008) Modified models to predict flux behavior in forward osmosis in consideration of external and internal concentration polarizations. Journal of Membrane Science 324(1-2), 209-219.
Tan, C.H. and Ng, H.Y. (2013) Revised external and internal concentration polarization models to improve flux prediction in forward osmosis process. Desalination 309, 125-140.
Tang, C., Kwon, Y. and Leckie, J. (2007) Probing the nano- and micro-scales of reverse osmosis membranes—A comprehensive characterization of physiochemical properties of uncoated and coated membranes by XPS, TEM, ATR-FTIR, and streaming potential measurements. Journal of Membrane Science 287(1), 146-156.
Tang, C.Y., She, Q., Lay, W.C.L., Wang, R. and Fane, A.G. (2010) Coupled effects of internal concentration polarization and fouling on flux behavior of forward osmosis membranes during humic acid filtration. Journal of Membrane Science 354(1-2), 123-133.
Tian, E.L., Zhou, H., Ren, Y.W., Mirza, Z., Wang, X.Z. and Xiong, S.W. (2014a) Novel design of hydrophobic/hydrophilic interpenetrating network composite nanofibers for the support layer of forward osmosis membrane. Desalination 347, 207-214.
Tian, E.L., Zhou, H., Ren, Y.W., mirza, Z.a., Wang, X.Z. and Xiong, S.W. (2014b) Novel design of hydrophobic/hydrophilic interpenetrating network composite nanofibers for the support layer of forward osmosis membrane. Desalination 347, 207-214.

Tian, M., Qiu, C., Liao, Y., Chou, S. and Wang, R. (2013) Preparation of polyamide thin film composite forward osmosis membranes using electrospun polyvinylidene fluoride (PVDF) nanofibers as substrates. Separation and Purification Technology 118, 727-736.
Tian, M., Wang, R., Goh, K., Liao, Y. and Fane, A.G. (2015a) Synthesis and characterization of high-performance novel thin film nanocomposite PRO membranes with tiered nanofiber support reinforced by functionalized carbon nanotubes. Journal of Membrane Science 486, 151-160.
Tian, M., Wang, Y.-N. and Wang, R. (2015b) Synthesis and characterization of novel high-performance thin film nanocomposite (TFN) FO membranes with nanofibrous substrate reinforced by functionalized carbon nanotubes. Desalination 370, 79-86.
Tian, M., Wang, Y.-N., Wang, R. and Fane, A.G. (2017) Synthesis and characterization of thin film nanocomposite forward osmosis membranes supported by silica nanoparticle incorporated nanofibrous substrate. Desalination 401, 142-150.
Tijing, L.D., Choi, J.-S., Lee, S., Kim, S.-H. and Shon, H.K. (2014) Recent progress of membrane distillation using electrospun nanofibrous membrane. Journal of Membrane Science 453, 435-462.
Tiraferri, A., Yip, N.Y., Phillip, W.A., Schiffman, J.D. and Elimelech, M. (2011a) Relating performance of thin-film composite forward osmosis membranes to support layer formation and structure. Journal of Membrane Science 367(1-2), 340-352.
Tiraferri, A., Yip, N.Y., Phillip, W.A., Schiffman, J.D. and Elimelech, M. (2011b) Relating performance of thin-film composite forward osmosis membranes to support layer formation and structure. Journal of Membrane Science 367, 340-352.
Tiraferri, A., Yip, N.Y., Straub, A.P., Romero-Vargas Castrillon, S. and Elimelech, M. (2013) A method for the simultaneous determination of transport and structural parameters of forward osmosis membranes. Journal of Membrane Science 444, 523-538.
Tow, E.W., McGovern, R.K. and Lienhard V, J.H. (2015) Raising forward osmosis brine concentration efficiency through flow rate optimization. Desalination 366, 71-79.
Wang, H., Chung, T.-S. and Tong, Y.W. (2013a) Study on water transport through a mechanically robust Aquaporin Z biomimetic membrane. Journal of Membrane Science 445, 47-52.
Wang, H.L., Chung, T.-S., Tong, Y.W., Jeyaseelan, K., Armugam, A., Duong, H.H.P., Fu, F., Seah, H., Yang, J. and Hong, M. (2013b) Mechanically robust and highly permeable AquaporinZ biomimetic membranes. Journal of Membrane Science 434, 130-136.
Wang, K.Y., Chung, T.-S. and Amy, G. (2012a) Developing thin-film-composite forward osmosis membranes on the PES/SPSf substrate through interfacial polymerization. AIChE Journal 58(3), 770-781.

Wang, K.Y., Chung, T.-S. and Qin, J.-J. (2007) Polybenzimidazole (PBI) nanofiltration hollow fiber membranes applied in forward osmosis process. Journal of Membrane Science 300(1-2), 6-12.
Wang, K.Y., Ong, R.C. and Chung, T.-S. (2010a) Double-skinned forward osmosis membranes for reducing internal concentration polarization within the porous sublayer. Industrial & Engineering Chemistry Research 49(10), 4824-4831.
Wang, K.Y., Yang, Q., Chung, T.-S. and Rajagopalan, R. (2009) Enhanced forward osmosis from chemically modified polybenzimidazole (PBI) nanofiltration hollow fiber membranes with a thin wall. Chemical Engineering Science 64(7), 1577-1584.
Wang, R., Shi, L., Tang, C.Y., Chou, S., Qiu, C. and Fane, A.G. (2010b) Characterization of novel forward osmosis hollow fiber membranes. Journal of Membrane Science 355(1), 158-167.
Wang, R., Xu, C., Sun, J., Gao, L. and Lin, C. (2013c) Flexible free-standing hollow Fe3O4/graphene hybrid films for lithium-ion batteries. Journal of Materials Chemistry A 1(5), 1794.
Wang, X., Xu, J., Li, L., Li, H. and Yang, C. (2017) Thiourea grafted PVDF affinity membrane with narrow pore size distribution for Au (III) adsorption: Preparation, characterization, performance investigation and modeling. Chemical Engineering Journal 314, 700-713.
Wang, Y., Ou, R., Ge, Q., Wang, H. and Xu, T. (2013d) Preparation of polyethersulfone/carbon nanotube substrate for high-performance forward osmosis membrane. Desalination 330, 70-78.
Wang, Y., Ou, R., Wang, H. and Xu, T. (2015) Graphene oxide modified graphitic carbon nitride as a modifier for thin film composite forward osmosis membrane. Journal of Membrane Science 475, 281-289.
Wang, Z., Yu, H., Xia, J., Zhang, F., Li, F., Xia, Y. and Li, Y. (2012b) Novel GO-blended PVDF ultrafiltration membranes. Desalination 299, 50-54.
Wei, J., Qiu, C., Tang, C.Y., Wang, R. and Fane, A.G. (2011) Synthesis and characterization of flat-sheet thin film composite forward osmosis membranes. Journal of Membrane Science 372(1-2), 292-302.
Wei, R., Zhang, S., Cui, Y., Ong, R.C., Chung, T.-S., Helmer, B.J. and de Wit, J.S. (2015) Highly permeable forward osmosis (FO) membranes for high osmotic pressure but viscous draw solutes. Journal of Membrane Science 496, 132-141.
Widjojo, N., Chung, T.-S., Weber, M., Maletzko, C. and Warzelhan, V. (2011a) The role of sulphonated polymer and macrovoid-free structure in the support layer for thin-film composite (TFC) forward (FO) membranes. Journal of Membrane Science 383, 214-223.
Widjojo, N., Chung, T.-S., Weber, M., Maletzko, C. and Warzelhan, V. (2011b) The role of sulphonated polymer and macrovoid-free structure in the support layer for thin-film composite (TFC) forward osmosis (FO) membranes. Journal of Membrane Science 383(1-2), 214-223.

Widjojo, N., Chung, T.-S., Weber, M., Maletzko, C. and Warzelhan, V. (2013) A sulfonated polyphenylenesulfone (sPPSU) as the supporting substrate in thin film composite (TFC) membranes with enhanced performance for forward osmosis (FO). Chemical Engineering Journal 220, 15-23.
Wolf, P.H., Siverns, S. and Monti, S. (2005) UF membranes for RO desalination pretreatment. Desalination 182(1), 293-300.
Woo, Y.C., Tijing, L.D., Park, M.J., Yao, M., Choi, J.-S., Lee, S., Kim, S.-H., An, K.-J. and Shon, H.K. (2017) Electrospun dual-layer nonwoven membrane for desalination by air gap membrane distillation. Desalination 403, 187-198.
Wu, X., Field, R.W., Wu, J.J. and Zhang, K. (2017) Polyvinylpyrrolidone modified graphene oxide as a modifier for thin film composite forward osmosis membranes. Journal of Membrane Science 540, 251-260.
Xiao, P., Nghiem, L.D., Yin, Y., Li, X.-M., Zhang, M., Chen, G., Song, J. and He, T. (2015) A sacrificial-layer approach to fabricate polysulfone support for forward osmosis thin-film composite membranes with reduced internal concentration polarisation. Journal of Membrane Science 481, 106-114.
Xie, M., Lee, J., Nghiem, L.D. and Elimelech, M. (2015) Role of pressure in organic fouling in forward osmosis and reverse osmosis. Journal of Membrane Science 493, 748-754.
Xiong, J.Y., Cheng, Z.L., Wan, C.F., Chen, S.C. and Chung, T.-S. (2016) Analysis of flux reduction behaviors of PRO hollow fiber membranes: Experiments, mechanisms, and implications. Journal of Membrane Science 505, 1-14.
Xu, Z., Zhang, J., Shan, M., Li, Y., Li, B., Niu, J., Zhou, B. and Qian, X. (2014) Organosilane-functionalized graphene oxide for enhanced antifouling and mechanical properties of polyvinylidene fluoride ultrafiltration membranes. Journal of Membrane Science 458, 1-13.
Yan, H., Li, J., Fan, H., Ji, S., Zhang, G. and Zhang, Z. (2015a) Sonication-enhanced in situ assembly of organic/inorganic hybrid membranes: Evolution of nanoparticle distribution and pervaporation performance. Journal of Membrane Science 481, 94-105.
Yan, H., Miao, X., Xu, J., Pan, G., Zhang, Y., Shi, Y., Guo, M. and Liu, Y. (2015b) The porous structure of the fully-aromatic polyamide film in reverse osmosis membranes. Journal of Membrane Science 475, 504-510.
Yan, W., Wang, Z., Wu, J., Zhao, S., Wang, J. and Wang, S. (2016) Enhancing the flux of brackish water TFC RO membrane by improving support surface porosity via a secondary pore-forming method. Journal of Membrane Science 498, 227-241.
Yang, Q., Wang, K.Y. and Chung, T.-S. (2009a) Dual-layer hollow fibers with enhanced flux as novel forward osmosis membranes for water production. Environ Sci Technol 43(8), 2800-2805.

Yang, Q., Wang, K.Y. and Chung, T.-S. (2009b) A novel dual-layer forward osmosis membrane for protein enrichment and concentration. Separation and Purification Technology 69(3), 269-274.
Yasukawa, M., Mishima, S., Shibuya, M., Saeki, D., Takahashi, T., Miyoshi, T. and Matsuyama, H. (2015a) Preparation of a forward osmosis membrane using a highly porous polyketone microfiltration membrane as a novel support. Journal of Membrane Science 487, 51-59.
Yasukawa, M., Tanaka, Y., Takahashi, T., Shibuya, M., Mishima, S. and Matsuyama, H. (2015b) Effect of molecular weight of draw solute on water permeation in forward osmosis process. Industrial & Engineering Chemistry Research 54, 8239-8246.
Yeow, M.L., Liu, Y.T. and Li, K. (2004) Morphological Study of Poly (vinylidene fluoride) Asymmetric Membranes: Effect of the Solvent, Additive, and Dope Temperature. Journal of Applied Polymer Science 92, 1782-1789.
Yin, J. and Deng, B. (2015) Polymer-matrix nanocomposite membranes for water treatment. Journal of Membrane Science 479, 256-275.
Yip, N.Y. and Elimelech, M. (2014) Comparison of energy efficiency and power density in pressure retarded osmosis and reverse electrodialysis. Environ Sci Technol 48(18), 11002-11012.
Yip, N.Y., Tiraferri, A., Phillip, W.A., Schiffman, J.D. and Elimelech, M. (2010) High performance thin-film composite forward osmosis membrane. Environ Sci Technol 44, 3812-3818.
Yip, N.Y., Tiraferri, A., Phillip, W.A., Schiffman, J.D., Hoover, L.A., Kim, Y.C. and Elimelech, M. (2011a) Thin-film composite pressure retarded osmosis membranes for sustainable power generation from salinity gradients. Environmental Science & Technology 45(10), 4360-4369.
Yip, N.Y., Tiraferri, A., Phillip, W.A., Schiffman, J.D., Hoover, L.A., Kim, Y.C. and Elimelech, M. (2011b) Thin-film composite pressure retarded osmosis membranes for sustainable power generation from salinity gradients. Environ Sci Technol 45(10), 4360-4369.
Yong, J.S., Phillip, W.A. and Elimelech, M. (2012) Coupled reverse draw solute permeation and water flux in forward osmosis with neutral draw solutes. Journal of Membrane Science 392, 9-17.
Yoon, H., Baek, Y., Yu, J. and Yoon, J. (2013) Biofouling occurrence process and its control in the forward osmosis. Desalination 325, 30-36.
Yu, L., Zhang, Y., Zhang, B., Liu, J., Zhang, H. and Song, C. (2013) Preparation and characterization of HPEI-GO/PES ultrafiltration membrane with antifouling and antibacterial properties. Journal of Membrane Science 447, 452-462.

Yu, Y., Seo, S., Kim, I.-C. and Lee, S. (2011) Nanoporous polyethersulfone (PES) membrane with enhanced flux applied in forward osmosis process. Journal of Membrane Science 375(1), 63-68.
Yun, T., Kim, Y.-J., Lee, S., Hong, S. and Kim, G.I. (2014) Flux behavior and membrane fouling in pressure-assisted forward osmosis. Desalination and Water Treatment 52(4-6), 564-569.
Zeng, Z., Yu, D., He, Z., Liu, J., Xiao, F.X., Zhang, Y., Wang, R., Bhattacharyya, D. and Tan, T.T. (2016) Graphene Oxide Quantum Dots Covalently Functionalized PVDF Membrane with Significantly-Enhanced Bactericidal and Antibiofouling Performances. Sci Rep 6, 20142.
Zhang, C., HUang, M., Meng, L., Li, B. and Cai, T. (2017a) Electrospun polysulfone (PSf)/titanium dioxide (TiO2) nanocomposite fibers as substrates to prepare thin film forward osmosis membranes. Journal of Chemical Technology and Biotechnology 92(8), 2090-2097.
Zhang, L., She, Q., Wang, R., Wongchitphimon, S., Chen, Y. and Fane, A.G. (2016a) Unique roles of aminosilane in developing anti-fouling thin film composite (TFC) membranes for pressure retarded osmosis (PRO). Desalination 389, 119-128.
Zhang, M., Liu, R., Wang, Z., Zhao, B., Song, J., Park, M.J., Shon, H.K., Li, X.-M. and He, T. (2016b) Dehydration of forward osmosis membranes in treating high salinity wastewaters: Performance and implications. Journal of Membrane Science 498, 365-373.
Zhang, S., Fu, F. and Chung, T.-S. (2013) Substrate modifications and alcohol treatment on thin film composite membranes for osmotic power. Chemical Engineering Science 87, 40-50.
Zhang, S., Sukitpaneenit, P. and Chung, T.-S. (2014) Design of robust hollow fiber membranes with high power density for osmotic energy production. Chemical Engineering Journal 241, 457-465.
Zhang, S., Wang, K.Y., Chung, T.-S., Chen, H., Jean, Y.C. and Amy, G. (2010) Well-constructed cellulose acetate membranes for forward osmosis: Minimized internal concentration polarization with an ultra-thin selective layer. Journal of Membrane Science 360(1-2), 522-535.
Zhang, S., Wang, K.Y., Chung, T.-S., Jean, Y.C. and Chen, H. (2011) Molecular design of the cellulose ester-based forward osmosis membranes for desalination. Chemical Engineering Science 66(9), 2008-2018.
Zhang, X., Shen, L., Lang, W.-Z. and Wang, Y. (2017b) Improved performance of thin-film composite membrane with PVDF/PFSA substrate for forward osmosis process. Journal of Membrane Science.
Zhao, C., Xu, X., Chen, J. and Yang, F. (2013a) Effect of graphene oxide concentration on the morphologies and antifouling properties of PVDF ultrafiltration membranes. Journal of Environmental Chemical Engineering 1(3), 349-354.

Zhao, H., Wu, L., Zhou, Z., Zhang, L. and Chen, H. (2013b) Improving the antifouling property of polysulfone ultrafiltration membrane by incorporation of isocyanate-treated graphene oxide. Phys Chem Chem Phys 15(23), 9084-9092.
Zhao, S. and Zou, L. (2011a) Relating solution physicochemical properties to internal concentration polarization in forward osmosis. Journal of Membrane Science 379(1), 459-467.
Zhao, S., Zou, L. and Mulcahy, D. (2011b) Effects of membrane orientation on process performance in forward osmosis applications. Journal of Membrane Science 382(1), 308-315.
Zhao, S., Zou, L., Tang, C.Y. and Mulcahy, D. (2012) Recent developments in forward osmosis: Opportunities and challenges. Journal of Membrane Science 396, 1-21.
Zhou, Z., Lee, J.Y. and Chung, T.-S. (2014) Thin film composite forward-osmosis membranes with enhanced internal osmotic pressure for internal concentration polarization reduction. Chemical Engineering Journal 249, 236-245.
Zinadini, S., Zinatizadeh, A.A., Rahimi, M., Vatanpour, V. and Zangeneh, H. (2014) Preparation of a novel antifouling mixed matrix PES membrane by embedding graphene oxide nanoplates. Journal of Membrane Science 453, 292-301.
Zirehpour, A., Rahimpour, A., Seyedpour, F. and Jahanshahi, M. (2015) Developing new CTA/CA-based membrane containing hydrophilic nanoparticles to enhance the forward osmosis desalination. Desalination 371, 46-57.
Zirehpour, A., Rahimpour, A. and Ulbricht, M. (2017) Nano-sized metal organic framework to improve the structural properties and desalination performance of thin film composite forward osmosis membrane. Journal of Membrane Science 531, 59-67.
Zornoza, B., Tellez, C., Coronas, J., Gascon, J. and Kapteijn, F. (2013) Metal organic framework based mixed matrix membranes: An increasingly important field of research with a large application potential. Microporous and Mesoporous Materials 166, 67-78.
Zou, S., Gu, Y., Xiao, D. and Tang, C.Y. (2011) The role of physical and chemical parameters on forward osmosis membrane fouling during algae separation. Journal of Membrane Science 366(1), 356-362.
Zuo, J., Wang, Y. and Chung, T.-S. (2013) Novel organic–inorganic thin film composite membranes with separation performance surpassing ceramic membranes for isopropanol dehydration. Journal of Membrane Science 433, 60-71.